Control for quantum technologies at the nanoscale

Benjamin Rousseaux

Université Bourgogne Franche-Comté
Faculté des Sciences
Laboratoire Interdisciplinaire Carnot de Bourgogne

Control for quantum technologies at the nanoscale

Thesis presented by

Benjamin Rousseaux

to obtain the degree of

Doctor of Philosophy in Physics

Examining board:

Luis Martín-Moreno	Univ. Zaragoza	referee
Michael Fleischhauer	Univ. Kaiserslautern	referee
Axel Kuhn	Univ. Oxford	examiner
Zsolt Kis	Univ. Budapest	examiner
Alain Dereux	Univ. Dijon	examiner
Stéphane Guérin	Univ. Dijon	supervisor
Gérard Colas des Francs	Univ. Dijon	cosupervisor

Date of defense: Nov. 8th 2016

Laboratoire Interdisciplinaire Carnot de Bourgogne, UMR 6303 CNRS,
9 avenue Alain Savary, BP 47870, 21078 Dijon Cedex, France

Contents

Résumé

Le contrôle des émetteurs quantiques (atomes, molécules, quantum dots, etc.) et des interactions lumière-matière est une perspective majeure pour l'implémentation des systèmes tout-optiques et du traitement de l'information à l'échelle quantique. En général, ceci nécessite un régime de couplage fort entre les émetteurs et les modes photoniques, comme cela peut être réalisé avec une cavité optique à haut facteur de qualité, afin de contrôler efficacement la dynamique par le biais de l'électrodynamique en cavité (cQED).
L'intégration des principes de l'optique quantique à l'échelle nanométrique, via la plasmonique, a été envisagée sur l'hypothèse d'un régime de couplage fort entre des émetteurs quantiques et des plasmons-polaritons de surface (SPPs), dont le volume modal confiné transcende la limite de diffraction. De récents progrès ont montré la possibilité d'un tel régime de couplage fort, permettant le développement de la plasmonique quantique, où les plasmons-polaritons jouent le rôle de modes de cavité. Cependant, les applications de la plasmonique quantique apparaissent limitées en pratique à cause de la présence intrinsèque de nombreux modes dissipatifs, ce qui complique la description et l'interprétation de l'interaction et introduit une forte décohérence dans le système, en particulier dans le cas du couplage fort.
Ce travail présente une vue d'ensemble détaillée des concepts du contrôle quantique appliqués à plusieurs systèmes : pièges à ions, cavités optiques et plasmons-polaritons de surface. La première partie du manuscrit correspond à l'étude de processus adiabatiques dans le cas des pièges à ions et de l'électrodynamique en cavité, elle présente :

- Un résumé de l'information et du calcul quantiques, ainsi que le contrôle de systèmes quantiques par laser en régime adiabatique.
- Une démonstration de l'implémentation d'une porte quantique générale, en manipulant des ions piégés par laser.
- Une étude et une application des modèles de l'électrodynamique en cavité pour la génération d'états à un ou plusieurs photons sortant d'une cavité.

La deuxième partie détaille un formalisme décrivant la dynamique quantique d'émetteurs au voisinage de structures nanométriques et des résultats numériques montrant le régime de couplage fort, ainsi que le couplage d'émetteurs via des plasmons ; elle aborde plus spécifiquement :

- Le détail de la quantification du champ électromagnétique pour un milieu à couches sphériques.
- Le développement de modèles effectifs basés sur la quantification, dont nous mettons en exergue leur analogie avec les modèles cQED.
- La description de l'interaction de plasmons-polaritons localisés (LSPs) avec des émetteurs.
- Le couplage et l'intrication d'émetteurs par passage adiabatique via des modes plasmoniques d'une nanoparticule sphérique.

Abstract

Controlling quantum emitters (atoms, molecules, quantum dots, etc.), light, and its interactions is a key issue for implementing all-optical devices and information processing at the quantum level. This generally necessitates a strong coupling of emitters to photonic modes, as achieved by a high-Q cavity, for efficient manipulation of the atoms and field dynamics through cavity quantum electrodynamics (cQED).
The integration of the principles of quantum optics at the nanoscale in a plasmonic platform has been envisioned, on the basis of a possible strong coupling between a quantum emitter and the surface plasmon polaritons (SPPs) via their strong mode confinement. Recent progress showed the possibility to reach such a strong coupling regime, allowing the development of quantum plasmonics where a SPP mode takes the role of the cavity mode. However, its application appears notoriously limited in practical situations due to the intrinsic presence of numerous and lossy modes, which complicates the description and the interpretation of the interaction, and introduces strong decoherence in the system, in particular for strong coupling.
In this work, a detailed overview of quantum control applied to ion trapping, cQED, and plasmonics, is presented. The first part of the thesis is a study of adiabatic processes in trapped ion systems and cQED:

- We summarize quantum computation processes using quantum gates, and control using adiabatic laser pulses with atomic systems.
- We design arbitrary quantum gates with ions manipulated with laser pulses.
- Models for cQED are derived and applied for the production of photon states leaking from a cavity.

In the second part, we develop a formalism to describe the quantum dynamics of emitters close to nanoscale structures, and numerics showing the strong coupling regime and the coupling of emitters via plasmon modes. More specifically:

- We provide a general field quantization procedure for spherically layered systems.
- Effective models using the field quantization are derived, and we show they are analogous to cQED models.
- We describe the interaction of localized plasmons (LSPs) with quantum emitters.
- The coupling/entanglement of emitters by adiabatic passage through lossy plasmonic modes of a nanosphere is shown.

Part I

Introduction

Overview of quantum control in information processing and quantum optics

Quantum control has become an important tool over the last decades. The control of quantum processes and the manipulation of quantum states have many applications in atomic, molecular and condensed matter physics, as well as in optics, information processing and computation, and chemistry with aims of a selective control of chemical reactions.
Specifically, the manipulation of quantum electronic states using microwave radiation or lasers has been developing in all the mentioned fields. In this thesis, we focus on the fields of quantum information processing, quantum computation and quantum optics. Tools to develop robust, fast and efficient quantum control for the design of quantum gates, which are key elements of quantum computation, are presented. We underline, in particular, their physical implementation with trapped ions manipulated by laser pulses [1]. The robustness and efficiency of the novel construction for the arbitrary quantum gate presented here is ensured by the use of the stimulated Raman adiabatic passage (STIRAP), known for more than twenty-five years now [2–7]. Such Raman adiabatic techniques, in general, are an efficient tool for the control of quantum systems because they provide relatively high-fidelity population transfer and entanglement, due to the avoidance of lossy excited states, yet exploiting them through their coupling with the metastable initial and target states.
Control in quantum optics has also been developing over the last decades, in particular for the control of *flying qubits* carried by photons, in quantum key distribution (QKD), quantum cryptography [8], networking for distributed computation, communication and metrology. The photon is seen as the best candidate for the role of quantum information carrier, transmitting qubits from one node to the other. Nowadays, in most applications, photons in coherent states are being used to carry flying qubits. Deterministic single photons are better candidates as they show better entanglement and interference properties (crucial for quantum information and security protocols) than coherent states produced with low-intensity lasers. However, the experimental achievement of such single photon sources is still challenging. One key point is to control the node-photon interfacing so that the node can send, receive, store and release photonic quantum information. In addition, the control of quantum emitters, such as atoms, molecules, quantum dots and other artificial quantum systems, as well as the control of light and its interaction with emitters are key issues for implementing all-optical devices and information processing at the quantum level. The strong coupling of emitters with photonic modes, as it is achieved by a high quality factor cavity (high-Q cavity), is necessary for efficient manipulation of the atoms and field dynamics. The field of cavity quantum electrodynamics (cQED) provides understanding of the production of single or few-photon states from an optical cavity, and its interaction with single atoms [9]. We present an overview of this field, and detailed derivations of the models applicable to the control of the interaction of quantum light with atoms. Then, we propose a self-consistent theoretical basis, valid for leaky cavities and notably discuss the production of single and several photon states leaking out of a cavity.
Moreover, the description of leaky (but non-absorbing) cavities will be helpful for understanding the behaviour of lossy configurations, such as plasmonic systems investigated in the last part of this manuscript.

Towards quantum control in plasmonics

The interest of miniaturizing optical devices has grown since the 70s, but the size of optical components is limited by diffraction, around 0.5 μm. This is the case, for instance, with optical cavities, whose mode area must be significantly larger (at least seven orders of magnitude) than the absorption cross-section of the emitters they interact with. Low temperature experiments enables the absorption cross section of molecules to increase, then reaching a comparable size with a highly focused beam, hence reaching a satisfactory quantum efficiency, as almost all energy from the beam can be absorbed by the molecule.
Another strategy consists in the confinement of light in the subwavelength regime, as yielded by the field of plasmonics [10–13]. Plasmons are collective oscillations of the free electrons at the surface of a conductive medium. As they are a phenomenon of electric charge acceleration, they are associated to electromagnetic waves due to the oscillating electric field they generate. For this reason, one usually refers to plasmons as surface plasmon polaritons (SPPs). Plasmon modes are generally of two kinds: propagating SPP modes, and localized surface plasmons (LSPs). The integration of the principles of quantum optics at the nanoscale in a plasmonic platform has been envisioned, on the basis of a possible strong coupling between quantum emitters and SPPs, via their strong mode confinement in the subwavelength regime. Recent progress showed the possibility to reach strong coupling regime, allowing the development of *quantum plasmonics*, where a plasmon mode plays an analogous role as a cavity mode [14–27]. However, since the plasmon modes are intrinsically numerous and present strong losses due to the ohmic properties of conductive media, it appears notoriously complicated to describe and interpret their interaction with quantum emitters, and they introduce strong decoherence in the system. These drawbacks severely limit the applications for coherent manipulation of quantum emitters coupled to single plasmons at the nanoscale.
In this thesis, we solve these issues by introducing a novel approach for quantum plasmonics, including a full quantization scheme derived from the Green's tensor formalism, applying it to spherically layered media, and constructing effective models for the dynamics of SPPs coupled to quantum emitters. We show precisely how to calculate the emitter-field coupling constants from the geometry and arrangements of the system, the material properties of the dielectric bodies in it, and the positions of the quantum emitters. We provide a consistent guideline for creating a geometry-specific, mode-selective quantization relying on the Green's tensor of the system. The quantization is demonstrated through the example of a spherically layered, non-magnetic medium, with the aim of building models for quantum emitters coupled to metallic nanospheres. Nevertheless, it can be analogously extended to other types of geometries, with different symmetries. We construct, in a second step, effective models where the complete plasmonic coupling can then be interpreted as a multimode lossy cQED interaction. The potential of the derived effective models is shown in a last step, where we engineer a specific coherent manipulation, by laser pulses, of a pair of emitters coupled by LSPs, making full use of the coupling while circumventing the plasmonic losses. This is achieved by adapting the technique of STIRAP. The transfer happens via a connection to a *dark state*, immune to loss, thanks to adiabaticity usually reached for modest pulse durations and energies. The complete population transfer mediated by plasmons can be interpreted as a polariton propagating between the two networking emitters, while partial transfer creates high-fidelity entanglement between them.

Organization of the thesis, and reading guide

The body of the thesis is organized as follows. In part II we introduce the basic concepts of quantum control and novel results with applications in quantum information and computation, and quantum optics with cQED. It includes two chapters:

- A first chapter as a short introduction to quantum information processing, quantum control in the adiabatic limit, and the application of these concepts to trapped ions, which are excellent candidates for nodes in a quantum network, being addressable by laser beams and having been used to perform quantum algorithms. We also show a novel quantum gate construction based on the concept of *qudit*, and detail its physical implementation using two-shot STIRAP pulse sequences.

- A second chapter where we present in a self-consistent way the field of cavity QED, and applications of the models to the production of single and few-photon signals leaking from a cavity. This chapter is essential to the understanding of the thesis since it presents the most important concepts derived in quantum optics, which are used in the quantization procedure and effective models in quantum plasmonics derived in the following part.

Part III is designed as a route towards the application of quantum optics and control with surface plasmon polaritons. It is constructed in three chapters being mutually dependent:

- Chapter three presents an introduction to light-matter interaction at the nanoscale, and the mode-selective quantization procedure for spherically layered structures. The full quantization based on the Green's tensor formalism is presented and provides the basis of the following chapter.

- Chapter four details the construction of effective, cQED-comparable models starting from the mode-selective quantization procedure for spherically layered structures. The construction is done in two steps: the construction of an effective continuous model, and a discrete effective model structurally analogous to the alternative cQED model derived in chapter two.

- Chapter five presents the applications of effective models to quantum emitters coupled to a metallic nanoparticle (MNP), and in particular, when the emitters are manipulated by laser in a STIRAP pulse sequence.

A conclusion of this work as well as perspectives for future applications of the derived concepts is presented in part IV. We note that the first chapter can be read independently from the others. Parts II and III are also self-consistent, therefore they can be read independently. However, we underline the analogy between section 2.2 and chapter four, where the effective models are structurally the same.
Last but not least, this work, in its self-consistent approach, present numerous equations and expressions. Some important equations, in particular when they imply an important result, are boxed in the following way:

$$\boxed{\{\text{important result}\}.}$$

For an easier reading, we also regrouped long derivations as well as examples of general equations and models in appendices, at the end of every chapter.

Part II

Quantum control with trapped ions and optical cavities

Chapter 1

Trapped ions controlled by lasers and quantum information

Chapter overview

Objectives: This chapter presents quantum information and computation through the example of trapped ions. Important concepts are introduced, such as the adiabatic theorem, the control of ions by laser, and the design of quantum gates by adiabatic passage.

Guideline:

- Basic concepts of quantum information & quantum computation.
- Introduction to adiabatic techniques for the control of atoms by lasers.
- Presentation of the stimulated Raman adiabatic passage (STIRAP).
- Description of ions in a Paul trap, quantization of the vibrational modes, manipulation by laser.
- **keywords:** *qubit, quantum gate, adiabatic passage, ion trap, vibrational mode, center-of-mass mode, Lamb-Dicke regime, Householder reflection (HR), qudit, quantum Fourier transform (QFT)*

Results/novelty: Arbitrary qudit gate by adiabatic passage.

1.1 Quantum Information in the adiabatic limit

This chapter presents adiabatic techniques to build quantum gates, i.e. basic operations of quantum computation. These techniques have been shown to provide efficient control of population transfer between quantum states of atoms, molecules, and ions by laser pulses. More specifically, when the laser pulse area is large enough, the adiabatic limit is invoked and allows one to target eigenvectors subspaces of interest for the dynamics, e.g. metastable quantum states, which are less affected by decoherence.
This is of particular interest for quantum information and quantum computation [28, 29], where decoherence is the main adversary and introduces errors in the algorithms or the protocols. It is also possible, using these techniques, to reduce the number of operations needed to construct a given non-trivial quantum gate, as it is shown. To make the connection with a physical implementation of quantum computation, the formalism for trapped ions experiments is derived and the laser pulses configuration for the control of the latter is explained.
The chapter is organized as follows: in the first section we present the basic elements of quantum information and the adiabatic theorem in a general way; the second section presents the quantization of vibrational motion of ions in a Paul trap and the Hamiltonian of the system is derived to determine the adiabatic dynamics; the last section presents the novel construction of an arbitrary gate of dimension d, that can be implemented with a system of $d+1$ trapped ions.

1.1.1 Basic notions of quantum computing

The qubit

The classical theory of information developed in the twentieth century is based on the concept of *bit*, i.e. an information unit having two possible values: 0 or 1. An integer number can be represented as an ensemble of bits, and operations applied on them are called *logic gates*.
In the quantum information theory, the concept of bit is replaced by the *qubit*, or *quantum bit*. While a bit can have values 0 or 1 only, the qubit can be any quantum superposition of states $|0\rangle$ and $|1\rangle$, and its wavefunction has the general form:

$$|\psi\rangle = \mathrm{e}^{i\xi}\Big(\cos\frac{\theta}{2}|0\rangle + \mathrm{e}^{i\phi}\sin\frac{\theta}{2}|1\rangle\Big), \tag{1.1.1}$$

where ξ is an irrelevant global phase, and the state of the qubit is characterized by two angles: $0 \leqslant \theta \leqslant \pi$ defining the weights in the superposition state, and $0 \leqslant \phi < 2\pi$ being the relative phase. The state of a qubit is often represented as a point on the surface of a sphere, whose poles are $|0\rangle$ and $|1\rangle$. This representation is called the *Bloch sphere*, and is displayed in fig. 1.1.

Quantum gates and algorithms

When an operation is carried out on a qubit, its wavefunction is modified through a unitary transformation. This is another difference with classical computing, because most operations with classical bits are irreversible, as they are done with two bits for one output bit. The

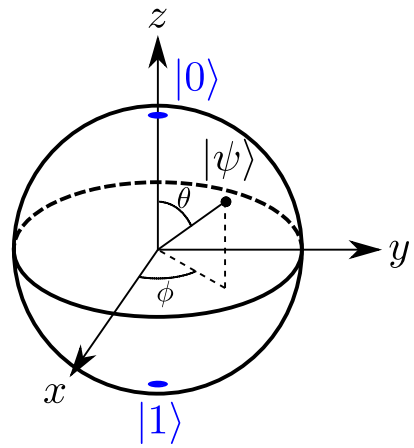

Figure 1.1: Bloch sphere representation of the qubit (1.1.1).

reversible transformation corresponds to the propagator of the time-dependent Schrödinger equation for the wavefunction $|\psi\rangle$, and for a transformation of duration T, we have:

$$|\psi(T)\rangle = \widehat{U}_T|\psi(t_0)\rangle, \tag{1.1.2}$$

where $|\psi(t_0)\rangle$ is the initial wavefunction. For the qubit, the transformation $\widehat{U}_T \equiv \widehat{U}(T+t_0, t_0)$ is a two by two matrix, and in practice its elements can be tuned to get a specific target transformation, which corresponds to a *quantum gate*. Thus, quantum gates are elementary transformation that can be applied to one or many qubits, and specific algorithms such as the Shor algorithm [30, 31], the Grover search algorithm [32], or the quantum Fourier transform (QFT) [28, 29] can be designed using sequences of quantum gates. An example of a single qubit quantum gate can be given by the NOT gate:

$$\widehat{U}_{\text{NOT}} = \begin{bmatrix} 0 & 1 \\ 1 & 0 \end{bmatrix}, \tag{1.1.3}$$

which swaps the two components of the qubit. Another important transformation is the phase gate:

$$\widehat{U}_\varphi = \begin{bmatrix} 1 & 0 \\ 0 & \mathrm{e}^{i\varphi} \end{bmatrix}, \tag{1.1.4}$$

which brings a relative phase φ between the two components. As a last example, we can mention the Hadamard gate:

$$\widehat{U}_H = \frac{1}{\sqrt{2}} \begin{bmatrix} 1 & 1 \\ 1 & -1 \end{bmatrix}. \tag{1.1.5}$$

This last gate corresponds to bringing the qubit in a superposition state. If the initial state is $|0\rangle$, for example, then the output state will be:

$$|\psi\rangle = \widehat{U}_H|0\rangle = \tfrac{1}{\sqrt{2}}\big(|0\rangle + |1\rangle\big). \tag{1.1.6}$$

In general, the synthesis of the whole space spanned by the single qubit propagator is parametrized with four real-valued angles $\alpha, \beta, \gamma, \delta$ [28]:

$$\widehat{U} = \mathrm{e}^{i\alpha} \begin{bmatrix} \mathrm{e}^{-i\beta/2} & 0 \\ 0 & \mathrm{e}^{i\beta/2} \end{bmatrix} \begin{bmatrix} \cos\frac{\gamma}{2} & -\sin\frac{\gamma}{2} \\ \sin\frac{\gamma}{2} & \cos\frac{\gamma}{2} \end{bmatrix} \begin{bmatrix} \mathrm{e}^{-i\delta/2} & 0 \\ 0 & \mathrm{e}^{i\delta/2} \end{bmatrix}. \tag{1.1.7}$$

Quantum gates are also designed to act on several qubits. The most famous example of multiple qubits gate is the *controlled-NOT* (cNOT) gate, operating on two qubits. While qubit 1 is in state $|0\rangle$, the cNOT operation leaves qubit 2 unchanged and while qubit 1 is in $|1\rangle$, it transforms qubit 2 with a NOT operation. In the product basis $\{|00\rangle, |01\rangle, |10\rangle, |11\rangle\}$ (where $|ij\rangle \equiv |i\rangle_1 |j\rangle_2$), the cNOT gate has the matrix form:

$$\widehat{U}_{\mathrm{cNOT}} = \begin{bmatrix} 1 & 0 & 0 & 0 \\ 0 & 1 & 0 & 0 \\ 0 & 0 & 0 & 1 \\ 0 & 0 & 1 & 0 \end{bmatrix}. \tag{1.1.8}$$

The most general quantum transformation in terms of qubit transformations is a unitary matrix operating in the 2^n-dimensional Hilbert space $\mathcal{H}^{\otimes n}$, where n is the number of qubits. A theorem states that *any* unitary transformation on $\mathcal{H}^{\otimes n}$ can be decomposed into a product of cNOT gates and single qubit gates (universal set of gates). Hence, all operations can be done with only one and two-qubit operations.

Operating on qubits leads to many interesting computation applications, yet nowadays it is still a challenge. The main obstacle to achieving effective quantum computing is decoherence. Indeed, quantum systems are very sensitive to their environment, and the spontaneous dissipation of energy brings errors in performed operations. The fragility of these processes imposes a good timing for the implementation of gates, and the faster they are, the least number of errors and the more efficient quantum computation will be achieved. Minimizing the number of operations is a reasonable way of overcoming decoherence effects. For instance, the quantum Fourier transform requires about $n^2/2$ operations for n qubits. In the last section, we show that gathering qubits in a single qudit with size $d = n/2$, the quantum Fourier transform can be implemented with at most d operations.

1.1.2 Adiabatic theorem

The adiabatic regime is characterized by specific dynamics for a quantum system, which we develop in this section. More precisely, we deal with a specific time scale T, the adiabatic limit arising when T tends to the infinity. In quantum information, the dynamics are described by the Schrödinger equation:

$$i\hbar \frac{\mathrm{d}|\Psi(t)\rangle}{\mathrm{d}t} = \widehat{H}(t)|\Psi(t)\rangle, \tag{1.1.9}$$

where $|\Psi(t)\rangle$ is the wavefunction of the system, and $\widehat{H}(t)$ its time-dependent Hamiltonian. The general solution of the Schrödinger equation reads:

$$|\Psi(t)\rangle = \widehat{U}(t, t_0)|\Psi(t_0)\rangle, \tag{1.1.10}$$

where $\widehat{U}(t,t_0)$ is the propagator of the wavefunction from the initial time t_0 to t. From equation (1.1.10), we have the requirement that $\widehat{U}(t_0,t_0) = \widehat{\mathbb{1}}$. Rewriting the Schrödinger equation in terms of propagator, and using the change of variables $s = t/T$, we get:

$$\frac{i\hbar}{T}\frac{\mathrm{d}\widehat{U}(s,s_0)}{\mathrm{d}s} = \widehat{H}(s)\widehat{U}(s,s_0), \tag{1.1.11}$$

rewriting $\widehat{U}(sT,s_0T)$ as $\widehat{U}(s,s_0)$ for simplicity. To specify the adiabatic regime, we need to define a basis of instantaneous eigenvectors $\{|\Phi_n^{(\alpha)}(s)\rangle\}$, with degeneracy index $\alpha = 0,...,d_n$ such that:

$$\widehat{H}(s)|\Phi_n^{(\alpha)}(s)\rangle = \lambda_n(s)|\Phi_n^{(\alpha)}(s)\rangle \tag{1.1.12a}$$

$$\langle\Phi_n^{(\alpha)}(t)|\Phi_m^{(\beta)}(t)\rangle = \delta_{nm}\delta_{\alpha\beta} \tag{1.1.12b}$$

$\lambda_n(s)$ being the instantaneous eigenvalue associated with $|\Phi_n^{(\alpha)}(s)\rangle$. We suppose that the eigenvectors are differentiable with respect to time, and we define the transformation:

$$\widehat{\mathcal{T}}(s) = \sum_{n,\alpha}|\Phi_n^{(\alpha)}(s)\rangle\langle\Phi_n^{(\alpha)}(s_0)|, \quad \widehat{U}(s,s_0) \to \widehat{\mathcal{U}}(s,s_0) := \widehat{\mathcal{T}}^\dagger(s)\widehat{U}(s,s_0)\widehat{\mathcal{T}}(s_0). \tag{1.1.13}$$

From this definition, we have $\widehat{\mathcal{T}}(s_0) = \widehat{\mathbb{1}}$. The columns of $\widehat{\mathcal{T}}(s)$ are the instantaneous eigenvectors $|\Phi_n^{(\alpha)}(s)\rangle$ expressed in the same basis $\{|\Phi_n^{(\alpha)}(s_0)\rangle\}$. The new propagator $\widehat{\mathcal{U}}(s,s_0)$ obeys also a Schrödinger equation:

$$\frac{i\hbar}{T}\frac{\mathrm{d}\widehat{\mathcal{U}}(s,s_0)}{\mathrm{d}s} = \widehat{\mathcal{H}}(s)\widehat{\mathcal{U}}(s,s_0), \tag{1.1.14}$$

with a new Hamiltonian $\widehat{\mathcal{H}}(s)$ that can be separated as:

$$\widehat{\mathcal{H}}(s) = \widehat{D}(s) - \frac{i\hbar}{T}\widehat{\mathcal{T}}^\dagger(s)\frac{\mathrm{d}\widehat{\mathcal{T}}(s)}{\mathrm{d}s} \tag{1.1.15a}$$

$$\widehat{D}(s) = \widehat{\mathcal{T}}^\dagger(s)\widehat{H}(s)\widehat{\mathcal{T}}(s). \tag{1.1.15b}$$

The transformed Hamiltonian $\widehat{D}(s)$ is diagonal in the initial eigenvector basis:

$$\widehat{D}(s) = \sum_n \lambda_n(s)\widehat{P}_n(s_0), \tag{1.1.16}$$

where $\widehat{P}_n(s_0) = \sum_\alpha |\Phi_n^{(\alpha)}(s_0)\rangle\langle\Phi_n^{(\alpha)}(s_0)|$ is a projector in the n-th subspace manifold of the eigenvector basis. We can write more explicitly the elements of the Hamiltonian $\widehat{\mathcal{H}}$ in two specific parts:

- The elements corresponding to the internal elements of the eigenvector subspace of eigenvalue $\lambda_n(s)$:

$$\langle\Phi_n^{(\alpha)}(s_0)|\widehat{\mathcal{H}}(s)|\Phi_n^{(\beta)}(s_0)\rangle = \lambda_n(s)\delta_{\alpha\beta} - \frac{i\hbar}{T}\langle\Phi_n^{(\alpha)}(s)|\frac{\mathrm{d}}{\mathrm{d}s}|\Phi_n^{(\beta)}(s)\rangle. \tag{1.1.17}$$

- The elements corresponding to couplings from a subspace to another (for $n \neq m$):

$$\langle \Phi_n^{(\alpha)}(s_0)|\widehat{\mathcal{H}}(s)|\Phi_m^{(\beta)}(s_0)\rangle = \frac{i\hbar}{T}\frac{\langle \Phi_n^{(\alpha)}(s)|\frac{\mathrm{d}\widehat{\mathcal{H}}}{\mathrm{d}s}|\Phi_m^{(\beta)}(s)\rangle}{\lambda_n(s)-\lambda_m(s)}. \tag{1.1.18}$$

The adiabatic limit is specified when $T \to \infty$. As a consequence, the coupling term between the subspaces (1.1.18), proportional to $1/T$, shall be much smaller than the energy difference $|\lambda_n(s) - \lambda_m(s)|$ between the subspaces. However, if the energy difference is of the same order of magnitude as the coupling term, the latter should be taken into account. This leads to the adiabaticity condition:

$$\boxed{|\lambda_n(s)-\lambda_m(s)| \gg \left|\frac{\hbar}{T}\frac{\langle \Phi_n^{(\alpha)}(s)|\frac{\mathrm{d}\widehat{\mathcal{H}}}{\mathrm{d}s}|\Phi_m^{(\beta)}(s)\rangle}{\lambda_n(s)-\lambda_m(s)}\right|,} \tag{1.1.19}$$

which can be formulated, in terms of the characteristic time scale:

$$T \gg \left|\hbar\frac{\langle \Phi_n^{(\alpha)}(s)|\frac{\mathrm{d}\widehat{\mathcal{H}}}{\mathrm{d}s}|\Phi_m^{(\beta)}(s)\rangle}{(\lambda_n(s)-\lambda_m(s))^2}\right|, \tag{1.1.20}$$

for all $\alpha, \beta, n, m \neq n$ and for all s. The adiabatic limit implying vanishing couplings between subspaces, the dynamics can be treated separately in each subspace (labelled n), in the initial eigenvector basis. The consequence is a splitting of the Schrödinger equation into many decoupled equations:

$$\frac{i\hbar}{T}\frac{\mathrm{d}\widehat{\mathcal{U}}_{\mathrm{a}}^{(n)}(s,s_0)}{\mathrm{d}s} = \widehat{\mathcal{H}}^{(n)}(s)\widehat{\mathcal{U}}_{\mathrm{a}}^{(n)}(s,s_0) \tag{1.1.21}$$

$$\widehat{\mathcal{H}}^{(n)}(s) = \widehat{P}_n(s_0)\widehat{\mathcal{H}}(s)\widehat{P}_n(s_0), \tag{1.1.22}$$

where each propagator $\widehat{\mathcal{U}}_{\mathrm{a}}^{(n)}(s,s_0)$ works in the n-th subspace with initial basis $\{|\Phi_n^{\alpha}(s_0)\rangle\}$. The total adiabatic propagator $\widehat{\mathcal{U}}_{\mathrm{a}}(s,s_0)$ working in the full basis writes then as a direct sum of all n-th subspaces propagators:

$$\widehat{\mathcal{U}}_{\mathrm{a}}(s,s_0) = \bigoplus_n \widehat{\mathcal{U}}_{\mathrm{a}}^{(n)}(s,s_0). \tag{1.1.23}$$

The propagator in the initial basis is obtained by inverting the transformation:

$$\widehat{U}_{\mathrm{a}}(s,s_0) = \widehat{\mathcal{T}}(s)\widehat{\mathcal{U}}_{\mathrm{a}}(s,s_0)\widehat{\mathcal{T}}^{\dagger}(s_0), \tag{1.1.24}$$

leading to the identity, known as the adiabatic theorem:

$$\widehat{P}_n(t)\widehat{U}_{\mathrm{a}}(t,t_0) = \widehat{U}_{\mathrm{a}}(t,t_0)\widehat{P}_n(t_0). \tag{1.1.25}$$

The theorem is stated as follow [33]:

Adiabatic theorem: If the instantaneous eigenvalues never cross, i.e. $|\lambda_n(t) - \lambda_m(t)| > \delta_0 \in \mathbb{R}\,\forall t$, then in the limit where the characteristic time $T \to \infty$ the subspaces generated by the instantaneous eigenvectors evolve independently from each other:

$$\lim_{T\to\infty} \widehat{P}_n(t)\widehat{U}(t,t_0) = \lim_{T\to\infty} \widehat{U}(t,t_0)\widehat{P}_n(t_0).$$

In a simpler case, where the eigenvalues are not degenerate, the Hamiltonian is entirely diagonal (whereas block-diagonal in the general case). The state of the system at time t is then, in the adiabatic limit:

$$|\Psi(t)\rangle = \sum_n \langle\Phi_n(t_0)|\Psi(t_0)\rangle \mathrm{e}^{-i(\phi_d^{(n)}(t)+\phi_B^{(n)}(t))}|\Phi_n(t)\rangle, \tag{1.1.26}$$

where $\phi_d^{(n)}(t)$ (dynamical phase) and $\phi_B^{(n)}(t)$ (geometric phase) are two time-dependent phases coming from the integration of (1.1.17):

$$\phi_d^{(n)}(t) = \frac{1}{\hbar}\int_{t_0}^{t} \mathrm{d}t'\lambda_n(t') \tag{1.1.27a}$$

$$\phi_B^{(n)}(t) = -i\int_{t_0}^{t} \mathrm{d}t'\langle\Phi_n(t')|\frac{\mathrm{d}}{\mathrm{d}t'}|\Phi_n(t')\rangle. \tag{1.1.27b}$$

The geometric phase can be removed locally by an appropriate choice of local phase of the eigenvectors. However, in a closed loop dynamics in the parameter space, the final phase differs in general with respect to the initial one, leading to a Berry phase (only dependent on the loop and the geometry of the parameter space, and not on the speed of the dynamics).
In this section the adiabatic theorem is derived for non-crossing eigenvalues in a finite dimensional Hilbert space [34–37]. The most general case of an infinite dimensional Hilbert space with possible crossing between the eigenvalues is treated in refs [34, 38–41].

1.1.3 Stimulated Raman adiabatic passage (STIRAP)

Raman processes [42] are three-state sequences of transitions where the final state is different from the initial state, after applying a pump field inducing radiative excitation. The final state can be higher in energy than the initial one, resulting in an emission line being to the red of the pump line, called *Stokes* line. If the final state is lower in energy than the initial one, then the line is called *anti-Stokes*. The interest of stimulated Raman processes is to provide coherent quantum states manipulation by using controlled laser (pump, Stokes and anti-stokes) fields. In the following, we denote by pump the laser field providing the excitation and by Stokes the field providing the final state, resulting in a two-photon process. We have displayed on fig. 1.2 the sketch of a three-level system manipulated by pump and Stokes laser fields. The pump field P with frequency ω_P produces excitation into the excited state $|e\rangle$ from the initial metastable (or ground) state $|g\rangle$, while the Stokes field S with frequency ω_S produces deexcitation into the other metastable state $|f\rangle$. The excited state $|e\rangle$ is lossy with a decay rate Γ. The rotating wave approximation (RWA) Hamiltonian for this system writes,

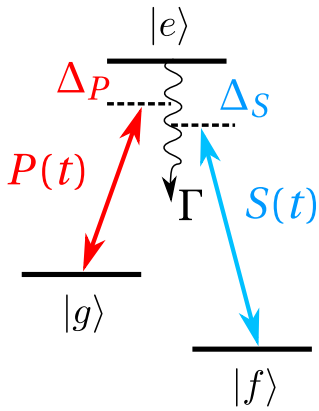

Figure 1.2: Three-level system with two ground metastable states $|g\rangle, |f\rangle$ coupled to a lossy excited state $|e\rangle$. Transition $|g\rangle \leftrightarrow |e\rangle$ is driven with a pump laser pulse $P(t)$ while transition $|f\rangle \leftrightarrow |e\rangle$ is driven with a Stokes laser pulse $S(t)$. Both laser controls are detuned with the transitions with detunings Δ_P, Δ_S, respectively. The losses of state $|e\rangle$ are modeled with a decay rate Γ.

in a matrix form (in unit of $\hbar$):

$$\widehat{H} = \begin{pmatrix} 0 & \frac{1}{2}\Omega_P \mathrm{e}^{-i\phi_P} & 0 \\ \frac{1}{2}\Omega_P \mathrm{e}^{i\phi_P} & \Delta_P - i\frac{\Gamma}{2} & \frac{1}{2}\Omega_S \mathrm{e}^{i\phi_S} \\ 0 & \frac{1}{2}\Omega_S \mathrm{e}^{-i\phi_S} & \Delta_P - \Delta_S \end{pmatrix}, \tag{1.1.28}$$

where the $\Omega_{P,S}$ are (time-dependent) Rabi frequencies associated with the pump (resp. Stokes) laser fields, $\Delta_P = \omega_{eg} - \omega_P$, $\Delta_S = \omega_{ef} - \omega_S$, and $\phi_{P,S}$ are phases suited to the "Λ" linkage. Using this Hamiltonian, different stimulated Raman processes are possible using different combination of pump-Stokes pulse sequences. The one in interest of this section has for motivation the efficient population transfer between $|g\rangle$ and $|f\rangle$, and is called *stimulated Raman adiabatic passage* (STIRAP) [2, 42–44]. It can be summarized in three points:

- **Pulse sequence**: for population initially in state $|g\rangle$, the Stokes field precedes the pump with a delay, and an overlap. This is called a *counter-intuitive pulse sequence*, as transfer population from $|g\rangle$ to $|f\rangle$ is achieved by turning on S first, and then P.
- **Two-photon resonance**: both fields should keep two-photon resonant detuning, that is $\Delta_P = \Delta_S \equiv \Delta$.
- **Adiabaticity**: the time length of the laser pulses should be adiabatic.

We notice that the Hamiltonian (1.1.28) is non-Hermitian due to the excited state's loss Γ. In the following, we consider the Hermitian part of the STIRAP Hamiltonian, for simplicity:

$$\widehat{H}_{\text{stirap}} = \begin{pmatrix} 0 & \frac{1}{2}\Omega_P \mathrm{e}^{-i\phi_P} & 0 \\ \frac{1}{2}\Omega_P \mathrm{e}^{i\phi_P} & \Delta & \frac{1}{2}\Omega_S \mathrm{e}^{i\phi_S} \\ 0 & \frac{1}{2}\Omega_S \mathrm{e}^{-i\phi_S} & 0 \end{pmatrix}, \tag{1.1.29}$$

which admits for instantaneous eigenvalues:

$$\lambda_0 = 0 \tag{1.1.30a}$$

$$\lambda_\pm(t) = \frac{1}{2}\left(\Delta \pm \sqrt{\Delta^2 + \Omega_P^2(t) + \Omega_S^2(t)}\right), \tag{1.1.30b}$$

and associated instantaneous eigenvectors:

$$|\mathbf{\Phi}_0(t)\rangle = \cos\theta(t)|g\rangle - \mathrm{e}^{i\phi}\sin\theta(t)|f\rangle \tag{1.1.31a}$$

$$|\Phi_+(t)\rangle = \sin\theta(t)\cos\varphi(t)|g\rangle + \mathrm{e}^{-i\phi_P}\sin\varphi(t)|e\rangle + \mathrm{e}^{i\phi}\cos\theta(t)\cos\varphi(t)|f\rangle \tag{1.1.31b}$$

$$|\Phi_-(t)\rangle = \sin\theta(t)\sin\varphi(t)|g\rangle - \mathrm{e}^{-i\phi_P}\cos\varphi(t)|e\rangle + \mathrm{e}^{i\phi}\cos\theta(t)\sin\varphi(t)|f\rangle, \tag{1.1.31c}$$

where the dynamical angles $\theta(t), \varphi(t)$ and the phase ϕ are defined as follow:

$$\tan\theta(t) = \frac{\Omega_P(t)}{\Omega_S(t)} \tag{1.1.32}$$

$$\tan\varphi(t) = \frac{2\lambda_+(t)}{\sqrt{\Omega_P^2(t) + \Omega_S^2(t)}} \tag{1.1.33}$$

$$\phi = \phi_P - \phi_S. \tag{1.1.34}$$

The eigenstate (1.1.31a) is important, because it has no component of the excited state $|e\rangle$, hence it is not affected by the latter's losses into spontaneous emission. For this reason, the eigenstate $|\mathbf{\Phi}_0(t)\rangle$ is called a *dark state*. Introducing the excited state's loss in the Hamiltonian leads to more complex expressions for $\lambda_\pm(t)$ and $|\Phi_\pm(t)\rangle$, but the dark state $|\mathbf{\Phi}_0(t)\rangle$ is not affected. We see from the expression of the eigenstates, and the initial condition $|\Psi(t_i)\rangle = |g\rangle$, that the mixing angle $\theta(t)$ varies from 0 to $\pi/2$ over time to achieve population transfer between $|g\rangle$ and $|f\rangle$. This implies, looking at (1.1.32), that:

$$\tan\theta(t_i) = 0$$
$$\tan\theta(t_f) \to +\infty,$$

at the beginning and the end of the process, which is achieved with the counter-intuitive pulse sequence. The dynamics of the STIRAP process are displayed on fig. 1.3. As can be seen in the dynamics, the overlap between the pulses is necessary to keep the adiabatic eigenvalues distant from each other, so that their difference remains much larger than the couplings between the dynamical subspaces (see equation (1.1.19)). The dynamics then stays in the adiabatic basis generated by $|\mathbf{\Phi}_0(t)\rangle, |\Phi_\pm(t)\rangle$. Moreover, the counter-intuitive sequence ensures that the wavefunction aligns with the dark state, so that we get the following time evolution:

$$\boxed{\begin{array}{c} |\Psi(t_i)\rangle = |\mathbf{\Phi}_0(t_i)\rangle = |g\rangle \\ \downarrow \\ |\Psi(t)\rangle = |\mathbf{\Phi}_0(t)\rangle \\ \downarrow \\ |\Psi(t_f)\rangle = |\mathbf{\Phi}_0(t_f)\rangle = -\mathrm{e}^{i\phi}|f\rangle. \end{array}}$$

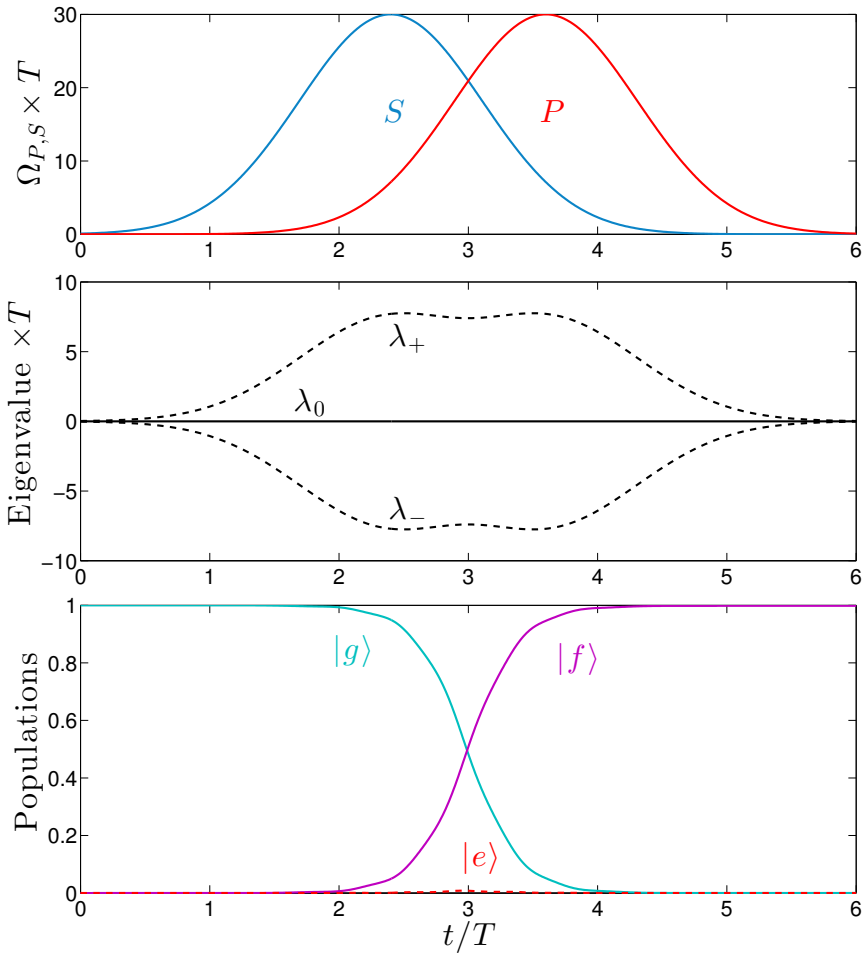

Figure 1.3: STIRAP dynamics for $\Delta = 0$. (upper pannel) Counter-intuitive sequence Rabi frequencies of the driving lasers versus time. The pulse shapes are chosen to be gaussians: $\Omega_{P,S}(t) = \Omega_0 e^{-((t\pm\tau)/T)^2}$, where τ is the time delay between the two pulses, and T is the pulse width. (middle pannel) Time-dependent adiabatic eigenvalues. (lower pannel) Populations of the different levels. Complete population transfer from $|g\rangle$ to $|f\rangle$ is achieved with very small population in the excited state $|e\rangle$.

The overall process brings a phase gain $\phi + \pi$, where the phase ϕ can be controlled precisely in experiments. The adiabaticity condition (1.1.20) for the STIRAP is:

$$|\dot{\theta}| \ll \left| \Omega(s) T \frac{\sin \varphi(s)}{\cos^2 \varphi(s)} \right| \tag{1.1.35a}$$

$$|\dot{\theta}| \ll \left| \Omega(s) T \frac{\cos \varphi(s)}{\sin^2 \varphi(s)} \right|, \tag{1.1.35b}$$

where $\dot{\theta} \equiv \frac{\mathrm{d}}{\mathrm{d}s}\theta(s)$, and $\Omega(s) = \sqrt{\Omega_P^2(s) + \Omega_S^2(s)}$. Two cases can be distinguished for deriving the adiabaticity condition:

- If the detuning is small, that is $\Delta \ll \Omega_0$, where Ω_0 is the maximal amplitude of the pump (or Stokes) Rabi frequencies, then the angle $\varphi(t)$ is close to $\pi/2$ and the condition (1.1.35b) is stronger than (1.1.35a). Using slow-varying derivatives $\dot{\Omega}_{P,S} \simeq \Omega_{P,S}/T$, we get the usual adiabaticity condition for the STIRAP:

$$\Omega_0 T \gg 1. \tag{1.1.36}$$

- If the detuning is big, that is $\Delta \gg \Omega_0$, we get analogously the large detuning adiabaticity condition for the STIRAP:

$$\Omega_0^2 T \gg \Delta. \tag{1.1.37}$$

The STIRAP technique is interesting because of its *robustness*, i.e. the fact that it does not depend strongly on the parameters' fluctuations. Only the variation of the mixing angle θ from 0 to $\pi/2$ is essential, including the adiabaticity condition through the pulses area $\Omega_0 T$. However, it does neither depend on a specific pulse shape nor on a specific pulse area. It is also not affected much by the detuning Δ, provided the corresponding adiabaticity condition. The spontaneous emission occuring while population goes into state $|e\rangle$, the STIRAP avoids it by negligibly populating it. If the dynamics are not perfectly adiabatic, the losses by spontaneous emission are negligible in the limit where the decay rate Γ is small, that is:

$$\Gamma \ll \Omega_0^2 T. \tag{1.1.38}$$

We remark that this condition does not prevent Γ to be larger than Ω_0, provided that $\Omega_0 T \gg 1$. We have presented the general concepts of quantum information and computation using quantum gates, as well as a general guideline for the manipulation of quantum systems in the adiabatic limit. We illustrated adiabatic processes with the example of the STIRAP. In the next sections, we focus on the application of such concepts with trapped ions, which are very good candidates for the design of quantum gates.

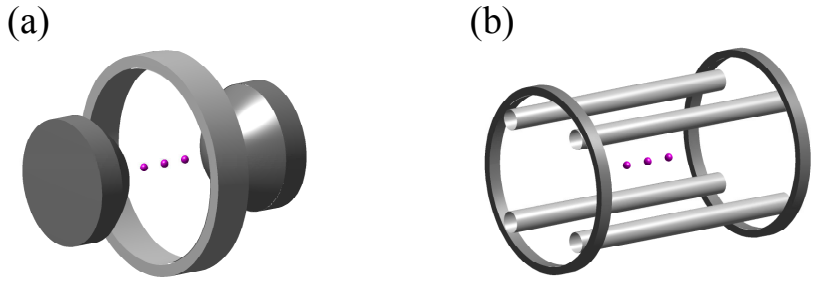

Figure 1.4: Two different geometries of Paul traps. Ions are trapped: (a) axially with two end cap electrodes, and laterally with a ring electrode (b) axially with two ring electrodes, and laterally with four rod electrodes.

1.2 Ion trap as a model for quantum information

In the previous section, we have presented some general conditions that allow robust control of quantum states. Here we discuss some practical applications for an ion trap, this device being a powerful configuration for quantum control.
An ion trap is a device designed to isolate and handle ions in a small region of space, using electromagnetic potentials configurations. Trapping a point-like particle with charge q at position $\mathbf{r}_0$ necessitates a potential extremum in all space directions, being minimal (resp. maximal) for $q > 0$ (resp. $q < 0$). If $U(\mathbf{r})$ is the potential and $q > 0$, this condition reads:

$$\left.\frac{\partial^2 U}{\partial \alpha^2}\right|_{\mathbf{r}=\mathbf{r}_0} > 0, \quad \alpha = x, y, z. \tag{1.2.1}$$

However, the Gauss theorem stating that the Laplacian of the potential is zero, it is not possible to design a static potential satisfying (1.2.1) in all directions simultaneously. A static potential can, at most, provide extrema in two spatial directions. In experiments, there are many kinds of traps that can fulfill (1.2.1), such as Penning or Paul traps. In a Penning trap, only static fields are involved: an electric potential confines the ion in a given direction, while a magnetic field oriented along the same direction traps the ion sidelong with Lorentz centripetal force. In our work, we focus on the Paul trap, which combines both static and oscillating fields. Many geometries exist for the different ion traps ; we study in this section the quadrupolar Paul trap.

1.2.1 Linear Paul trap - trapping of a single ion

The linear Paul trap is preferred in quantum information for its ability to isolate ions from external disturbances. There are two main geometries known in the literature: both of them are depicted in figure 1.4. We focus on the quadrupolar geometry (fig. 1.4 (b)), where the two ring electrodes provide a static axial trapping with potential $U_z(\mathbf{r})$, while the four rod

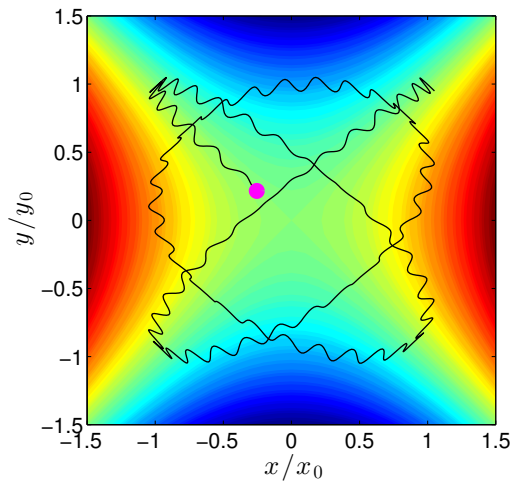

Figure 1.5: Trajectory of a single ion (solid line), in an oscillating quadrupolar potential (contour plot for $\omega t = 2k\pi$, k integer), for $a = 0.001$ and $b = 0.1$.

electrodes trap the ion in xy plane with a time-dependent potential $U_{xy}(\mathbf{r}, t)$. This oscillating potential:

$$U_{xy}(\mathbf{r}, t) = \frac{U_0 + V_0 \cos \Omega t}{2R^2}(x^2 - y^2) \tag{1.2.2}$$

is applied to two diagonal rods, while the two other ones are grounded. In the expression above, U_0 is a static potential, V_0 is the oscillation amplitude, Ω the frequency of the oscillations (in the RF regime), and R the distance from the z-axis to one rod electrode. The classical motion of an electric charge in a potential, given by $m\ddot{\mathbf{r}} = -q\nabla U(\mathbf{r}, t)$, when projected in the xy-plane, gives the system of equations:

$$\left[\frac{\mathrm{d}^2}{\mathrm{d}s^2} + a + 2b\cos 2s\right] \left\{ \begin{array}{c} x(t) \\ y(t) \end{array} \right\} = 0, \tag{1.2.3}$$

where:

$$s = \frac{\Omega t}{2}, \quad a = \frac{4qU_0}{mR^2\Omega^2}, \quad b = \frac{2qV_0}{mR^2\Omega^2}. \tag{1.2.4}$$

Equations (1.2.3) are called Mathieu equations. Adjusting R, Ω, U_0 and V_0, it is possible to write approximate solutions of the Mathieu equation, in the case $a \ll b^2 \ll 1$:

$$\boxed{\begin{aligned} x(t) &= x_0 \left[1 + \frac{b}{2}\cos \Omega t\right] \cos(\omega_x t + \phi_x) && \text{(1.2.5a)} \\ y(t) &= y_0 \left[1 - \frac{b}{2}\cos \Omega t\right] \cos(\omega_y t + \phi_y), && \text{(1.2.5b)} \end{aligned}}$$

where:

$$\omega_x = \frac{\Omega}{2}\sqrt{\frac{b^2}{2} + a}, \quad \omega_y = \frac{\Omega}{2}\sqrt{\frac{b^2}{2} - a}. \tag{1.2.6}$$

In figure 1.5, we show a single ion trajectory projected on the xy-plane, using the approximated solutions of the Mathieu equations.

1.2.2 Quantization of the vibrational modes

In quantum information, we consider an ensemble of ions as several qubits, which are coupled through the Coulomb interaction. The vibrational normal modes will be derived considering ideal lateral trapping, so that the motion is seen along the z-axis, where the ions are aligned as a 1D lattice. The potential energy of N identical linearly trapped ions is given by:

$$V = \sum_{j=1}^{N} \frac{1}{2} m\omega_z^2 z_j^2(t) + \sum_{j\neq k}^{N} \frac{q^2}{4\pi\epsilon_0} \frac{1}{|Z_j(t) - Z_k(t)|}, \tag{1.2.7}$$

where $Z_j(t) = Z_0^{(j)} + z_j(t)$ is the position of the j-th ion on the z-axis, m is the mass of the ion, ω_z is the oscillation frequency of the potential, q is the ion charge, and ϵ_0 the electric permittivity of the vacuum. The first term in the expression of the potential corresponds to the potential energy of the ions in the trap, considered as an approximation to be harmonic, with $\frac{1}{2}m\omega_z^2 z_r^2 \simeq \eta q U_z$, where U_z is the static potential applied to the electrodes, η a geometrical factor, and z_r the distance between the center of the trap and one electrode. The second term corresponds to the Coulomb interaction between ions. The Lagrangian reads:

$$L = \frac{1}{2}\sum_{j=1}^{N} m\dot{z}_j^2 - \frac{1}{2}\sum_{j,k=1}^{N} \left[\frac{\partial^2 V}{\partial Z_j \partial Z_k}\right]_{\mathbf{Z}=\mathbf{Z}_0} z_j z_k, \tag{1.2.8}$$

where the potential (1.2.7) is expanded in a Taylor series until the second order. $\mathbf{Z} = [Z_1, ..., Z_N]$ and $\mathbf{Z}_0 = [Z_0^{(1)}, ..., Z_0^{(N)}]$ are vectors containing all absolute and equilibrium positions of the ions, respectively, with $[\partial V/\partial z_j]_{\mathbf{Z}=\mathbf{Z}_0} = 0$. The Lagrange equation:

$$\frac{\mathrm{d}}{\mathrm{d}t}\frac{\partial L}{\partial \dot{z}_j} - \frac{\partial L}{\partial z_j} = 0 \tag{1.2.9}$$

leads to an eigenvalue equation, when solutions are written in the form $z_j(t) = C_j \mathrm{e}^{-i\omega t}$. This eigenvalue equation reads:

$$\det(\omega_z^2 \overline{\overline{V}} - \omega^2 \overline{\overline{\mathbb{1}}}_N) = 0, \tag{1.2.10}$$

where $\overline{\overline{V}}$ is a tensor of size $N \times N$ whose elements are $V_{jk} = \frac{1}{m\omega_z^2}\left[\frac{\partial^2 V}{\partial Z_j \partial Z_k}\right]_{\mathbf{Z}=\mathbf{Z}_0}$, and $\overline{\overline{\mathbb{1}}}_N$ is the corresponding identity tensor. The eigenvalues that are solutions of (1.2.10) are being written in the form $\nu_\alpha = \omega_z\sqrt{\mu_\alpha}$ where α is another index running from 1 to N, and μ_α is a so-called reduced eigenvalue, as it is satisfying:

$$\sum_{j=1}^{N} V_{jk} D_j^{(\alpha)} = \mu_\alpha D_k^{(\alpha)}, \tag{1.2.11}$$

with N eigenvectors $\mathbf{D}_\alpha$, chosen to be orthogonal and normalized:

$$\sum_{j=1}^{N} D_j^{(\alpha)} D_j^{(\beta)} = \delta_{\alpha\beta}. \tag{1.2.12}$$

The j-th ion's position can be expanded in this new basis:

$$z_j(t) = \sum_{\alpha=1}^{N} D_j^{(\alpha)} q_\alpha(t), \tag{1.2.13}$$

where $q_\alpha(t) = C_\alpha \mathrm{e}^{-i\nu_\alpha t}$. For example, if $N = 2$, we get two eigenvalues $\nu_1 = \omega_z$ and $\nu_2 = \omega_z\sqrt{3}$, each of them being associated to a specific vibrational mode. Mode 1 is known as the *center of mass* mode (COM), and mode 2 is known as the *breathing* mode. The COM mode is characterized by a collective motion where the velocity vectors of the ions are pointing in the same direction, whereas in the breathing mode case, the velocity vectors point in opposite directions. There are as many vibrational modes as there are ions, that is N, and the diagonalization of matrix $\overline{\overline{V}}$ leads to analytical results for $N \leqslant 3$; for more ions, the solutions of (1.2.10) can be determined numerically (see [1]). In ion trap quantum information, the vibrational modes must be quantized, corresponding to phonon modes. In practice, the experiment is realized under very low temperature regime (a few Kelvins) to avoid decoherence effects. However, this is not enough, and further cooling is required: it is convenient to use a combination of Doppler cooling and red sideband pumping to annihilate phonons. To quantize the vibrational modes, we replace z_j by its modal expansion (1.2.13) in the classical Hamiltonian $H = T + V$. Defining the momenta $p_\alpha = m\dot{q}_\alpha$, the Hamiltonian reads:

$$H = \sum_{\alpha=1}^{N} \left(\frac{p_\alpha^2}{2m} + \frac{1}{2} m\nu_\alpha^2 q_\alpha^2 \right). \tag{1.2.14}$$

Once we defined the conjugate variables (q_α, p_α), which obey the Hamilton equations, we replace them by operators acting on a Hilbert space, and provide a change of variables to express all observables in terms of creation/annihilation operators acting on a Fock space:

$$q_\alpha \;\rightarrow\; \widehat{q}_\alpha = \sqrt{\frac{\hbar}{2m\nu_\alpha}} \left(\widehat{a}_\alpha^\dagger + \widehat{a}_\alpha \right), \tag{1.2.15}$$

$$p_\alpha \;\rightarrow\; \widehat{p}_\alpha = i\sqrt{\frac{\hbar m\nu_\alpha}{2}} \left(\widehat{a}_\alpha^\dagger - \widehat{a}_\alpha \right), \tag{1.2.16}$$

where $(\widehat{q}_\alpha, \widehat{p}_\alpha)$ and $(\widehat{a}_\alpha, \widehat{a}_\alpha^\dagger)$ obey the commutation relations:

$$[\widehat{q}_\alpha, \widehat{p}_\beta] = i\hbar\delta_{\alpha\beta}, \quad [\widehat{a}_\alpha, \widehat{a}_\beta^\dagger] = \delta_{\alpha\beta}. \tag{1.2.17}$$

The quantum Hamiltonian for the vibrational motion in the trap is the classical one, where replaced all quantities by operators:

$$\boxed{\widehat{H}_{\text{vib}} = \sum_{\alpha=1}^{N} \hbar\nu_\alpha \left(\widehat{a}_\alpha^\dagger \widehat{a}_\alpha + \tfrac{1}{2} \right).} \tag{1.2.18}$$

Recalling the expression for the positions of the ions, we now write the quantized form:

$$\widehat{z}_j = \sum_{\alpha=1}^{N} \mathcal{K}_j^{(\alpha)} \sqrt{\frac{\hbar}{2m\omega_z}} \left(\widehat{a}_\alpha^\dagger + \widehat{a}_\alpha \right), \tag{1.2.19}$$

where $\mathcal{K}_j^{(\alpha)} = D_j^{(\alpha)} / \sqrt[4]{\mu_\alpha}$ is a factor that can be determined numerically for $N \geqslant 4$. In the following, we will consider only center-of-mass motion, that is $\alpha = 1$. We summarize the center-of-mass parameters in table 1.1.

Table 1.1: center-of-mass motion parameters

index	$\alpha = 1$
eigenvalue	$\mu_1 = 1$
frequency	$\nu_1 = \omega_z$
eigenvector component	$\mathcal{K}_j^{(1)} = 1/\sqrt{N}$

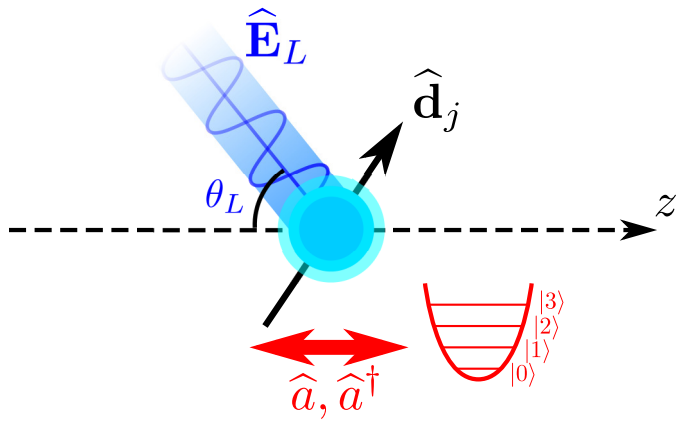

Figure 1.6: Single ion (labelled j), trapped on the axis z and driven by a laser field $\widehat{\mathbf{E}}_L(\widehat{z}_j, t)$, where $\widehat{z}_j$ is the quantized position of the ion. The laser beam is oriented with an angle $\theta_L = (\mathbf{k}_L, Oz)$. The excitation process leads to the creation and annihilation of quantized center-of-mass vibrational modes $\widehat{a}, \widehat{a}^\dagger$.

1.2.3 Manipulating ions by laser - Lamb-Dicke regime

The vibrational motion Hamiltonian (1.2.18) describes external states of the ions. Quantum information can be encoded in these states, but also in internal atomic states like the electronic excitations. All the states can be manipulated by addressing each ion with a laser beam. The laser beam is modeled by a monochromatic traveling wave:

$$\widehat{\mathbf{E}}_L(\widehat{z}_j, t) = \boldsymbol{\mathcal{E}}_L(t) \cos(\omega_L t - k_L \cos\theta_L \widehat{z}_j + \phi_j(\mathbf{k}_L)), \tag{1.2.20}$$

where $\boldsymbol{\mathcal{E}}_L(t) = \mathcal{E}_L(t)\boldsymbol{\epsilon}$ is a slow-varying envelope function times the polarization vector, ω_L is the frequency of the laser, k_L is the norm of the wavevector $\mathbf{k}_L = \frac{\omega_L}{c}\mathbf{n}$ ($\mathbf{n}$ being the unit vector pointing towards the direction of propagation of the field), θ_L is the angle between $\mathbf{k}_L$ and Oz, $\widehat{z}_j$ is the ion position operator and $\phi_j(\mathbf{k}_L) = \phi - k_L \cos\theta_L z_0^{(j)}$ is a phase factor. In the next steps, we consider only a single mode center-of-mass vibrational motion, so we drop the index α in (1.2.18), and the Hamiltonian is renormalized so that the zero-point energy responsible for the 1/2 factor in (1.2.18) is dropped as well. The full quantum Hamiltonian

for a single ion j is then given by:

$$\widehat{H}_j = \widehat{H}_0^{(j)} + \widehat{V}_j(t) \tag{1.2.21a}$$

$$\widehat{H}_0^{(j)} = \hbar\omega_0 \widehat{\sigma}_+^{(j)} \widehat{\sigma}_-^{(j)} + \hbar\nu \widehat{a}^\dagger \widehat{a} \tag{1.2.21b}$$

$$\widehat{V}_j(t) = -\widehat{\mathbf{d}}_j \cdot \widehat{\mathbf{E}}_L(\widehat{z}_j, t), \tag{1.2.21c}$$

where ω_0 is the transition frequency of the ion, and $\widehat{\mathbf{d}}_j = q\widehat{\mathbf{x}}_j$ is the transition dipole moment associated to the internal position operator $\widehat{\mathbf{x}}_j$ of the valence electron in the ion, q being the electron charge. The internal degrees of freedom of the ion are supposed to be a two-level structure, with a two-dimensional Hilbert space (with basis $\{|g_j\rangle, |e_j\rangle\}$) on which atomic operators like $\widehat{\sigma}_-^{(j)}$ act. The dipole operator can be "sandwiched" with the unit operator $\widehat{\mathbb{1}}_j = |e_j\rangle\langle e_j| + |g_j\rangle\langle g_j|$ and we get:

$$\widehat{\mathbf{d}}_j = \mathbf{d}_j \widehat{\sigma}_+^{(j)} + \mathbf{d}_j^* \widehat{\sigma}_-^{(j)}, \tag{1.2.22}$$

where $\mathbf{d}_j = \langle e_j|\widehat{\mathbf{d}}_j|g_j\rangle$, $\widehat{\sigma}_+^{(j)} = |e_j\rangle\langle g_j|$ and $\widehat{\sigma}_-^{(j)} = (\widehat{\sigma}_+^{(j)})^\dagger$. Writing the position operator $\widehat{z}_j$ in terms of the annihilation and creation operators $\widehat{a}, \widehat{a}^\dagger$ we get:

$$k_L \cos\theta_L \widehat{z}_j = \eta_j(\widehat{a}^\dagger + \widehat{a}), \tag{1.2.23}$$

where $\eta_j = k_L \cos\theta_L \mathcal{K}_j^{(1)} \sqrt{\frac{\hbar}{2m\nu}}$ is the Lamb-Dicke parameter associated with the j-th ion driven by a laser beam, whose wavevector has an angle θ_L with the trapping axis (see fig. 1.6). As only the center-of-mass mode is considered, we used the eigenvector component $\mathcal{K}_j^{(1)} = 1/\sqrt{N}$, which does not depend on the ion index j. As a consequence, the Lamb-Dicke parameter $\eta_j \equiv \eta_L$ will depend only on the laser parameters. To have a look at the energies of the states, we write the interaction picture of the Hamiltonian (1.2.21a):

$$\begin{aligned}\widehat{H}_j^{(I)}(t) &= \widehat{U}_{0,j}^\dagger(t,0)\widehat{H}_j(t)\widehat{U}_{0,j}(t,0) + i\hbar\frac{\mathrm{d}\widehat{U}_{0,j}^\dagger(t,0)}{\mathrm{d}t}\widehat{U}_{0,j}(t,0) \\ &= \widehat{U}_{0,j}^\dagger(t,0)\widehat{V}_j(t)\widehat{U}_{0,j}(t,0),\end{aligned} \tag{1.2.24a}$$

$$\widehat{U}_{0,j}(t,0) = \mathrm{e}^{-\frac{i}{\hbar}\widehat{H}_0^{(j)}t}. \tag{1.2.24b}$$

We see from the latter equations that the transformation applies only to the interaction part $V_j(t)$, as the term depending on the derivative of $\widehat{U}_{0,j}(t,0)$ with respect to time cancels with $H_0^{(j)}$, which is not affected. The interaction picture leads to a time-dependence of the operators:

$$\widehat{\sigma}_+^{(j)} \to \widehat{\sigma}_+^{(j)}\mathrm{e}^{i\omega_0 t} \tag{1.2.25}$$

$$\widehat{a} \to \widehat{a}\mathrm{e}^{-i\nu t}, \tag{1.2.26}$$

and writing the cosine function as a sum of exponentials in (1.2.20), we write:

$$\widehat{H}_j^{(I)}(t) = -(\mathbf{d}_j\widehat{\sigma}_+^{(j)}\mathrm{e}^{i\omega_0 t} + \mathbf{d}_j^*\widehat{\sigma}_-^{(j)}\mathrm{e}^{-i\omega_0 t}) \cdot \frac{\boldsymbol{\mathcal{E}}_L(t)}{2}\left(\mathrm{e}^{i\omega_L t}\mathrm{e}^{-i\eta_L(\widehat{a}^\dagger\mathrm{e}^{i\nu t} + \widehat{a}\mathrm{e}^{-i\nu t})}\mathrm{e}^{i\phi_j(\mathbf{k}_L)} + \text{h.c.}\right). \tag{1.2.27}$$

At this point, we invoke a rotating wave approximation (RWA), as fast-rotating terms in $\mathrm{e}^{\pm i(\omega_0+\omega_L)t}$ appear in the interaction, and are averaged out. We keep only the slow varying terms in $\mathrm{e}^{\pm i(\omega_0-\omega_L)t}$. Considering this approximation, we get:

$$\widehat{H}_j^{(I)}(t) = \frac{\hbar\Omega_j(t)}{2}\widehat{\sigma}_+^{(j)}\mathrm{e}^{i(\omega_0-\omega_L)t}\mathrm{e}^{i\eta_L(\widehat{a}^\dagger \mathrm{e}^{i\nu t}+\widehat{a}\mathrm{e}^{-i\nu t})} + \text{h.c.} \tag{1.2.28}$$

where $\Omega_j(t) := -\mathbf{d}_j \cdot \boldsymbol{\mathcal{E}}_L(t)\mathrm{e}^{-i\phi_j(\mathbf{k}_L)}/\hbar$ is the Rabi frequency associated with the laser field envelope. In this chapter, our aim is to derive a simple model, which can be easily manipulated to implement quantum processing techniques, as will be done in the next section. The work done in ref. [1] on the derivation of models for quantum processing with cold trapped ions is very complete, but a bit technical for this chapter, due to the $\mathrm{e}^{i\eta_L(\widehat{a}^\dagger \mathrm{e}^{i\nu t}+\widehat{a}\mathrm{e}^{-i\nu t})}$ term in the last expression. For simplicity, we consider that the spatial extent $Z_0 = \mathcal{K}_j^{(1)}\sqrt{\frac{\hbar}{2m\nu}}$ is much smaller than the laser wavelength. This approximation is called *Lamb-Dicke regime*, and involves the condition (see [1], appendix B):

$$\frac{\eta_L^2}{2} \ll 1. \tag{1.2.29}$$

Using the Baker-Campbell-Hausdorff formula: $\mathrm{e}^{\widehat{A}+\widehat{B}} = \mathrm{e}^{\widehat{A}}\mathrm{e}^{\widehat{B}}\mathrm{e}^{-\frac{1}{2}\widehat{A},\widehat{B}]}$, we write:

$$\begin{aligned}\mathrm{e}^{i\eta_L(\widehat{a}^\dagger \mathrm{e}^{i\nu t}+\widehat{a}\mathrm{e}^{-i\nu t})} &= \mathrm{e}^{-\frac{\eta_L^2}{2}}\left(\mathbb{1} + i\eta_L\widehat{a}^\dagger\mathrm{e}^{i\nu t} + \mathcal{O}(\eta_L^2)\right)\left(\mathbb{1} + i\eta_L\widehat{a}\mathrm{e}^{-i\nu t} + \mathcal{O}(\eta_L^2)\right)\\ &\approx \left(\mathbb{1} + i\eta_L\widehat{a}^\dagger\mathrm{e}^{i\nu t} + i\eta_L\widehat{a}\mathrm{e}^{-i\nu t}\right),\end{aligned} \tag{1.2.30}$$

and the interaction picture Hamiltonian becomes:

$$\boxed{\widehat{H}_j^{(I)}(t) = \frac{\hbar\Omega_j(t)}{2}\widehat{\sigma}_+^{(j)}\mathrm{e}^{i(\omega_0-\omega_L)t}\Big(\mathbb{1} + i\eta_L\widehat{a}^\dagger\mathrm{e}^{i\nu t} + i\eta_L\widehat{a}\mathrm{e}^{-i\nu t}\Big) + \text{h.c.}} \tag{1.2.31}$$

From this expression, we see three terms oscillating with three different frequencies. When the frequency of the laser is tuned to one of these terms the two others are fast-rotating and consequently are evinced from the dynamics. If $\omega_L \sim \omega_0$ the first term becomes slow-varying and corresponds to the *carrier* frequency: in the dynamics the laser controls the $|g\rangle \leftrightarrow |e\rangle$ for a given number state $|n\rangle$ for the vibrational motion. For $\omega_L \sim \omega_0 \pm \nu$, either the second or the third term becomes slow-varying, and those transitions correspond to the *blue* and *red sideband*, respectively. The blue sideband frequency drives the transitions $|g\rangle|n\rangle \leftrightarrow |e\rangle|n+1\rangle$, and the red sideband drives $|g\rangle|n+1\rangle \leftrightarrow |e\rangle|n\rangle$. A sketch representing the vibrational ladder and the possible transitions is displayed in fig. 1.7.

Excitation of a single center-of-mass mode

From the Hamiltonian (1.2.31), we can see that it is possible to manipulate both the internal and the vibrational states. Using different techniques of laser cooling, it is possible to bring the ions into the vacuum vibrational state $|0\rangle$, and start the dynamics from there. We focus here on how to excite a single center-of-mass vibrational mode using two laser beams: according to the previous derivation and fig. 1.7, we require a carrier and a red sideband control, which

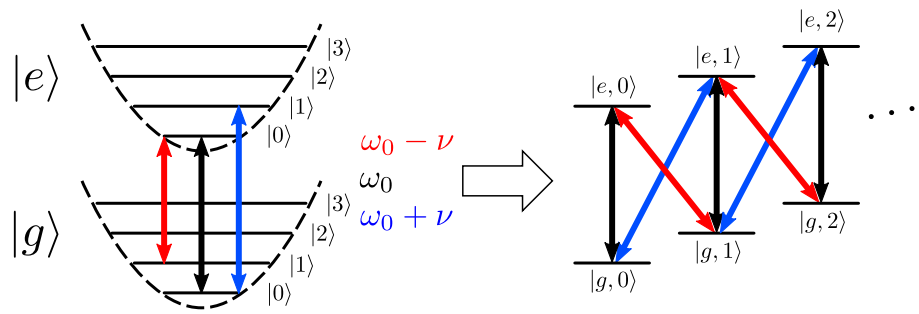

Figure 1.7: Two-level structure of the internal states of a single trapped ion, with the vibrational ladder associated with the creation/annihilation operators $\widehat{a}^\dagger, \widehat{a}$ of a COM mode. The states can be driven with three different frequencies corresponding to the *carrier* (ω_0), the *red sideband* ($\omega_0 - \nu$), and the *blue sideband* ($\omega_0 + \nu$). These three transitions are shown with black, red and blue double arrows, respectively. On the right, we display the level scheme in the dressed basis ($|i, n\rangle \equiv |i\rangle|n\rangle$ with $i = g, e$ and $n = 0, 1, 2...$).

can be done using two laser pulses whose frequencies approach ω_0 and $\omega_0 - \nu$, respectively. The coupling being assumed to be weak, we have therefore two Rabi frequencies associated with each laser (for simplicity we drop the index j as we manipulate only one ion): $\Omega_C(t)$ and $\Omega_R(t)$, with frequencies $\omega_C \sim \omega_0$ and $\omega_R \sim \omega_0 - \nu$. The Hamiltonian (1.2.31) back in the Schrödinger picture is then:

$$\widehat{H}(t) = \hbar\omega_0\widehat{\sigma}_+\widehat{\sigma}_- + \hbar\nu\widehat{a}^\dagger\widehat{a} + \left(\frac{\hbar\Omega_C(t)}{2}\widehat{\sigma}_+ \mathrm{e}^{-i\omega_C t} + \frac{\hbar\widetilde{\Omega}_R(t)}{2}\widehat{\sigma}_+\widehat{a}\mathrm{e}^{-i\omega_R t} + \mathrm{h.c.}\right), \tag{1.2.32}$$

where $\widetilde{\Omega}_R(t) = i\eta_R\Omega_R(t)$, η_R being the Lamb-Dicke parameter associated with the red sideband laser beam. Finally, we transform the Hamiltonian into a rotating frame defined by the operator:

$$\widehat{\mathcal{R}}(t) := \mathrm{e}^{-i\omega_C t\widehat{\sigma}_+\widehat{\sigma}_-}\mathrm{e}^{-i(\omega_R-\omega_C)t\widehat{a}^\dagger\widehat{a}}, \tag{1.2.33}$$

leading to:

$$\begin{aligned}\widehat{H}_{\mathcal{R}}(t) &= \widehat{\mathcal{R}}^\dagger(t)\widehat{H}(t)\widehat{\mathcal{R}}(t) + i\hbar\frac{\mathrm{d}\widehat{\mathcal{R}}^\dagger}{\mathrm{d}t}\widehat{\mathcal{R}}(t) \\ &= \hbar\Delta_C\widehat{\sigma}_+\widehat{\sigma}_- + \hbar(\Delta_C - \Delta_R)\widehat{a}^\dagger\widehat{a} + \left(\frac{\hbar\Omega_C(t)}{2}\widehat{\sigma}_+ + \frac{\hbar\widetilde{\Omega}_R(t)}{2}\widehat{\sigma}_+\widehat{a} + \mathrm{h.c.}\right),\end{aligned} \tag{1.2.34}$$

where we introduced the detunings $\Delta_C = \omega_0 - \omega_C$ and $\Delta_R = \omega_0 - \nu - \omega_R$, which should be small compared to the frequencies ω_0, ν. Taking the initial state to be:

$$|\psi(t_i)\rangle = |g, 0\rangle, \tag{1.2.35}$$

we can write the matrix form of the Hamiltonian in the rotating frame, in the single excitation basis $\{|g,0\rangle, |e,0\rangle, |g,1\rangle\}$:

$$\boxed{\widehat{H}_{\mathcal{R}}(t)/\hbar = \begin{pmatrix} 0 & \frac{1}{2}\Omega_C(t) & 0 \\ \frac{1}{2}\Omega_C^*(t) & \Delta_C & \frac{1}{2}\widetilde{\Omega}_R(t) \\ 0 & \frac{1}{2}\widetilde{\Omega}_R^*(t) & \Delta_C - \Delta_R \end{pmatrix},} \tag{1.2.36}$$

and we recognize the structure of the Raman Hamiltonian (1.1.28).

1.3 Building arbitrary gates by adiabatic passage

We show, in this section, the feasibility of arbitrary quantum gates using adiabatic techniques. It has been shown recently that a general SU(d) transformation can be implemented much more efficiently, scaling as d operations, than $d/2$ sequences of SU(2) transformations, scaling as d^2. The mathematical transformation involved in an arbitrary SU(d) transformation is called a *generalised Householder reflection* (HR). In a Hilbert space of dimension d, the generalised HR has the form [45]:

$$\widehat{M}(\chi;\varphi) = \widehat{\mathbb{1}} + (\mathrm{e}^{i\varphi} - 1)|\chi\rangle\langle\chi|, \tag{1.3.1}$$

where $\widehat{\mathbb{1}}$ is the identity operator, φ is a parametrizable phase, and $|\chi\rangle$ is a parametrizable vector belonging to the Hilbert space. This type of construction has been recently investigated for the qutrit [46]. A HR can remarkably result from the propagator in the degenerate manifold of a d-pod quantum system, which consists of d degenerate states coupled to a single common upper state by d simultaneous pulsed fields of well-defined detuning and areas [47]. This applies in particular in an ensemble of trapped ions in a linear Paul trap [48]. The quantum search algorithm can be, in principle, implemented without gates and circuits by such HR transformations [32,49,50]. On the other hand, concrete implementations of quantum information processing, and more generally of the control of quantum systems, suffers from the imperfection of the systems, of the lack of knowledge on the system, and of decoherence by the environment. In particular, the laser scheme proposed in references [45, 47] for the implementation of a HR transformation requires stringent conditions of detuning and pulse areas, which makes it difficult to implement in practice. It also leads to a significant population transfer in the lossy excited state. Thus robust techniques that, in addition, restrict the dynamics to decoherence-free subspaces, are desirable. Adiabatic passage techniques, and especially the ones that make use of dark states, such as the stimulated Raman adiabatic passage (STIRAP), are designed to overcome these issues [3–5]. STIRAP has been shown, for instance, to allow the transfer between arbitrary initial and final superpositions of states [6]. The extension of such results to the construction of a general gate is a much more difficult task since it requires to implement in a controlled way the propagator that produces an arbitrary SU(d) transformation. This has been solved only by adiabatic techniques to generate an arbitrary single-qubit gate [51], specific two-qubit gates [52–54], and a continuous version of

the Grover search algorithm [55–57].
We solve the above issue by proposing a controlled adiabatic scheme that implements an arbitrary SU(d) transformation. More precisely, we show how to generate any HR by a two-shot STIRAP. Such processes are then sequentially composed according to the factorisation of a SU(d) transformation into HRs. We show the remarkable property that the energy of the lasers is constant as a function of d to achieve the adiabatic synthesis. This implies a growth of the energy only as d for the implementation of an arbitrary SU(d) transformation. As an example, we show a numerical synthesis of the quantum Fourier transform on a quartit (i.e. a qudit with $d = 4$). We finally present a discussion for its practical implementation.

1.3.1 Householder reflections by adiabatic passage

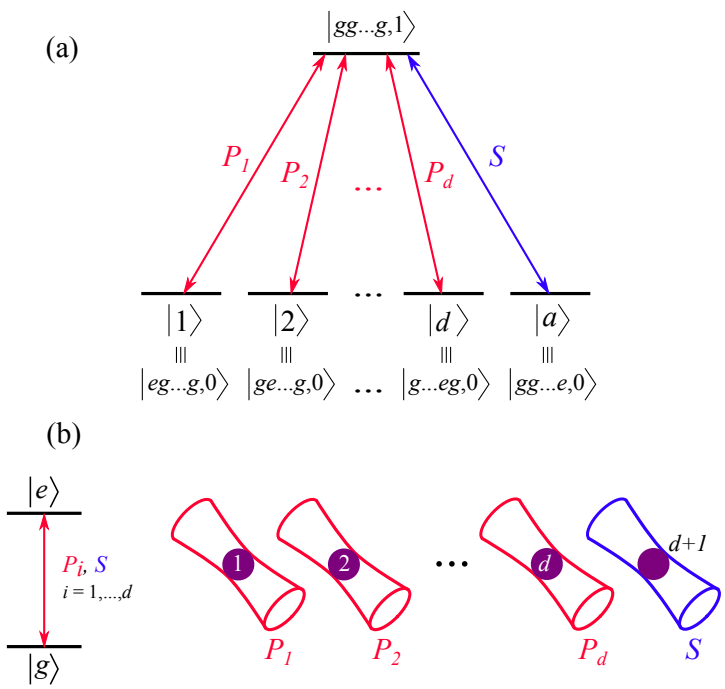

Figure 1.8: (a) Level scheme of the $(d+1)$-pod featuring the d states of the qudit (labeled from $|1\rangle$ to $|d\rangle$) and the ancillary state $|a\rangle$. The pump fields $\{P_1, P_2, ..., P_d\}$ couple the states of the qudit to an excited state, and a Stokes field S couples the ancillary to the excited state. (b) The states can be identified with multipartite states from $d+1$ trapped two-level ions through zero- and one-phonon states and individually coupled by the pump and Stokes fields, respectively.

We consider a $(d+1)$-pod system comprising $d+1$ ground states: the d states of the qudit, and an ancillary state. All of them are coupled to a common excited state by d pump lasers for the d first transitions, and a Stokes laser for the last one involving the ancillary state (see fig. 1.8). Such a quantum system can be implemented by $d+1$ ions in a linear Paul trap, generalizing the system described in the previous section for one ion (see equation (1.2.36)). The system is designed such that one laser pulse drives one ion using a vibrational red sideband transition through the Coulomb interaction between all ions. As can be seen on

fig. 1.8, the $d+1$ trapped ions and their center-of-mass quantized motion create a dressed state basis where:

- either one ion is in its excited state $|e_j\rangle$, and the vibrational motion is in a vacuum state $|0\rangle$,
- or all ions are in their ground states $|g_j\rangle$, and one vibrational quantum is excited: $|1\rangle$.

For notational simplicity, we write the dressed states in the form $\{|g_1\rangle \otimes ... \otimes |g_{j-1}\rangle \otimes |e_j\rangle \otimes |g_{j+1}\rangle \otimes ... \otimes |g_{d+1}\rangle\} \otimes |n\rangle \equiv |g...geg...g, n\rangle$, with $n = 0, 1$ being the number of vibrational quanta. The full basis contains $d+2$ elements and reads:

$$\{|gg...g, 1\rangle, |eg...g, 0\rangle, |ge...g, 0\rangle, ..., |gg...e, 0\rangle\}. \tag{1.3.2}$$

The one-phonon excitation state $|gg...g, 1\rangle$ is coupled to all other states by $d+1$ red sideband laser pulses: d of them are pumps and will be denoted $P_1, P_2, ..., P_d$, and the last one is a Stokes pulse, denoted S. All pump fields drive population of the defined qudit $\{|eg...g, 0\rangle, |ge...g, 0\rangle, ..., |g...eg, 0\rangle\} = \{|1\rangle, |2\rangle, ..., |d\rangle\}$ to the one-phonon state $|gg...g, 1\rangle$. The Stokes drives population of the ancillary state, that we denote $|gg...e, 0\rangle = |a\rangle$, with the same excited state. We rewrite the basis:

$$\{|a\rangle, |gg...g, 1\rangle, \underbrace{|1\rangle, |2, \rangle, ..., |d\rangle}_{\text{qudit}}\}. \tag{1.3.3}$$

The symbols P_j and S denote the Rabi frequency corresponding ton respectively, the pump fields j and the Stokes field with their respective transition moment.
The initial condition for the wavefunction is composed of any superposition of the first d ground states:

$$|\psi(t_i)\rangle \equiv |\psi_i\rangle = a_1|1\rangle + a_2|2\rangle + ... + a_d|d\rangle, \tag{1.3.4}$$

and the fields are designed such that the Stokes-pump field sequence, where all the pumps share a common pulse-shape dependence $P_0(t)$ (assuming that they are produced from a single source), drives all the population to the ancillary state $|a\rangle$ by STIRAP. The full RWA Hamiltonian written in basis (1.3.3) reads, in matrix form:

$$\widehat{H}(t) = \begin{pmatrix} 0 & S^*(t) & 0 & 0 & \dots & 0 \\ S(t) & \Delta_S & P_1^*(t) & P_2^*(t) & \dots & P_d^*(t) \\ 0 & P_1(t) & \Delta_S - \Delta_P & 0 & \dots & 0 \\ 0 & P_2(t) & 0 & \ddots & & \vdots \\ \vdots & \vdots & \vdots & & & \\ 0 & P_d(t) & 0 & \dots & & \Delta_S - \Delta_P \end{pmatrix}, \tag{1.3.5}$$

where $\Delta_S = \omega_S - \omega_0 + \nu$ and $\Delta_P = \omega_P - \omega_0 + \nu$. For the STIRAP to be achived, one requires a two-photon resonance, that is $\Delta_S = \Delta_P$, therefore the diagonal term $\Delta_S - \Delta_P$ must vanish. In the Hamiltonian (1.3.5), we can parametrize the pump fields $P_j(t)$ in amplitudes and phases, in the following manner:

$$\begin{pmatrix} P_1(t) \\ P_2(t) \\ \vdots \\ P_d(t) \end{pmatrix} = P_0(t) \begin{pmatrix} \chi_1 \\ \chi_2 \\ \vdots \\ \chi_d \end{pmatrix} \equiv P_0(t)|\chi\rangle, \tag{1.3.6}$$

where $P_0(t)$ is a common real time-dependence shape for the pump fields (assuming we use the same laser source), and $|\chi\rangle$ is the vector which parametrizes the phases and amplitudes of each component. As we will show, this $|\chi\rangle$ vector is the same as in the Householder reflection expression (1.3.1). Using these assumptions, we can find a $(d+1)$-fold basis $\{|a\rangle, |gg...g,1\rangle, |\chi\rangle, |\text{n.c.}_1\rangle, ..., |\text{n.c.}_{d-1}\rangle\}$ where the dynamics happen only in the 3-fold subspace $\{|a\rangle, |gg...g,1\rangle, |\chi\rangle\}$. The basis vectors $\{|\text{n.c.}_j\rangle\}$ are not coupled to $|gg...g,1\rangle$, therefore they correspond to a subspace where nothing is affected by the dynamics. This basis is found when we have defined a proper unitary, time-independent transformation $\widehat{T}$:

$$\widehat{T} = \begin{pmatrix} \mathbb{1}_2 & \mathbf{0}_{2\times d} \\ \mathbf{0}_{d\times 2} & \widehat{T}_d \end{pmatrix}, \quad \widehat{T}_d = \Big(|\chi\rangle, |\text{n.c.}_1\rangle, ..., |\text{n.c.}_{d-1}\rangle\Big), \tag{1.3.7}$$

which leaves $|a\rangle$ and $|gg...g,1\rangle$ unchanged while the qudit basis is being transformed into the χ-basis:

$$\{|1\rangle, |2\rangle, ..., |d\rangle\} \xrightarrow{\widehat{T}_d} \{|\chi\rangle, |\text{n.c.}_1\rangle, ..., |\text{n.c.}_{d-1}\rangle\}.$$

The general parametrization of $|\chi\rangle$ can be set defining angles θ_j such that $0 \leqslant \theta_j < \pi/2$ and $1 \leqslant j \leqslant d-1$, in the following way:

$$|\chi\rangle = \begin{pmatrix} \chi_1 = \cos\theta_1 \cos\theta_2 ... \cos\theta_{d-1} \\ \chi_2 = \sin\theta_1 \cos\theta_2 ... \cos\theta_{d-1} \mathrm{e}^{i\phi_2} \\ \chi_3 = \sin\theta_2 \cos\theta_3 ... \cos\theta_{d-1} \mathrm{e}^{i\phi_3} \\ \vdots \\ \chi_d = \sin\theta_{d-1} \mathrm{e}^{i\phi_d} \end{pmatrix}, \tag{1.3.8}$$

where ϕ_j are the relative phases of the pump fields P_j with respect to P_1 ($\phi_1 = 0$). The above expression also ensures that $\langle\chi|\chi\rangle = 1$, and one has to find the other components of the transformation $\widehat{T}_d$. This is achieved when we recall the unitary property $\widehat{T}_d^\dagger \widehat{T}_d = \widehat{\mathbb{1}}$ or, similarly:

$$\langle \text{n.c.}_j|\chi\rangle = 0 \tag{1.3.9a}$$

$$\langle \text{n.c.}_j|\text{n.c.}_k\rangle = \delta_{jk}. \tag{1.3.9b}$$

We complete the transformation $\widehat{T}_d$ by writing the remaining columns, given by the $|\text{n.c.}_j\rangle$:

$$|\text{n.c.}_j\rangle = \begin{pmatrix} \cos\theta_1 ... \cos\theta_{j-1} \sin\theta_j \\ \cos\theta_1 ... \sin\theta_{j-1} \sin\theta_j \mathrm{e}^{i\phi_2} \\ \vdots \\ \cos\theta_1 ... \cos\theta_{j-n} \sin\theta_{j-n+1} ... \sin\theta_j \mathrm{e}^{i\phi_n} \\ \vdots \\ \sin\theta_1 ... \sin\theta_j \mathrm{e}^{i\phi_j} \\ -\cos\theta_j \mathrm{e}^{i\phi_{j+1}} \\ \vec{0}_{d-(j+1)} \end{pmatrix}, \tag{1.3.10}$$

where $1 \leqslant n \leqslant j$ labels the components and $\vec{0}_{d-(j+1)}$ is a column of $d-(j+1)$ zeros. Projecting the Hamiltonian (1.3.5) in the new basis, corresponding to a Morris-Shore basis,

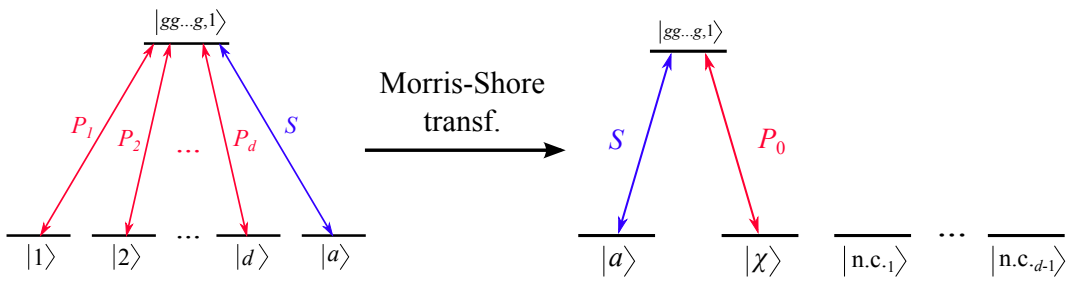

Figure 1.9: Sketch of the Morris-Shore transformation applied on the qudit basis $\{|1\rangle, ..., |d\rangle\}$. The transformation projects the full system into an effective Λ system in the basis $\{|a\rangle, |gg...g, 1\rangle, |\chi\rangle\}$. All states $|\text{n.c.}_j\rangle$ remain unaffected by the dynamics. This transformation can be applied when all the pump fields share a common pulse shape dependence.

we get:

$$\widehat{H}_{\text{MS}}(t) = \widehat{T}^\dagger \widehat{H}(t)\widehat{T} \equiv \begin{pmatrix} 0 & S^*(t) & 0 \\ S(t) & 0 & P_0(t) \\ 0 & P_0(t) & 0 \end{pmatrix}, \tag{1.3.11}$$

where we wrote the matrix form in the subspace $\{|a\rangle, |gg...g, 1\rangle, |\chi\rangle\}$, as there are zeros everywhere else. The Morris-Shore transformation leads to a new basis where the $(d+1)$-pod system becomes an effective three-level (or Λ) system, as shown in fig. 1.9.
The most general quantum gate can be synthesized by a product of, at most, d Householder reflections. Each of them is parametrized by angles $\theta_1, ..., \theta_{d-1}$ and phases $\phi_2, ..., \phi_d$ in vector $|\chi\rangle$, plus an extra phase φ:

$$\prod_{n=1}^{d} \widehat{M}_d(\chi_n; \varphi_n).$$

Each Householder reflection is built as follow:

- We start in the initial condition (1.3.4), and a first counter-intuitive Stokes-pump pulse sequence brings population from $|\chi\rangle$ to $|a\rangle$.
- After the first population transfer, a pump-Stokes pulse sequence brings back population from $|a\rangle$ to $e^{i\varphi}|\chi\rangle$, where a phase φ has been introduced with the second Stokes pulse, so that the overall transfer $|\chi\rangle \to e^{i\varphi}|\chi\rangle$ is achieved.

A sketch of the physical process leading to the Householder reflection is shown in fig. 1.10. When the process is over, the wavefunction $|\psi(t_f)\rangle \equiv |\psi_f\rangle$ is obtained by writing $|\psi_i\rangle$ in the Morris-Shore basis and replacing $|\chi\rangle$ by $e^{i\varphi}|\chi\rangle$. Identifying the initial state in the final expression, we can write the propagator $\widehat{U}(t_f, t_i)$ in the adiabatic limit:

$$\widehat{U}(t_f, t_i) = \begin{pmatrix} 1 + (e^{i\varphi} - 1)|\chi_1|^2 & (e^{i\varphi} - 1)\chi_1\chi_2 & \dots & (e^{i\varphi} - 1)\chi_1\chi_d \\ (e^{i\varphi} - 1)\chi_1^*\chi_2^* & 1 + (e^{i\varphi} - 1)|\chi_2|^2 & \dots & (e^{i\varphi} - 1)\chi_2\chi_d \\ \vdots & \vdots & \ddots & \vdots \\ (e^{i\varphi} - 1)\chi_1^*\chi_d^* & (e^{i\varphi} - 1)\chi_2^*\chi_d^* & \dots & 1 + (e^{i\varphi} - 1)|\chi_d|^2 \end{pmatrix} \equiv \widehat{M}_d(\chi; \varphi). \tag{1.3.12}$$

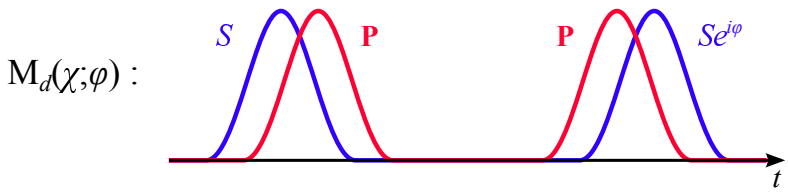

Figure 1.10: Pulse sequence with two consecutive STIRAPs generating the HR transformation $\widehat{M}_d(\chi;\varphi)$. Here the ensemble of the d pump fields $\mathbf{P} \equiv P_0|\chi\rangle$ is schematically represented by a single line. The second STIRAP is reversed with respect to the first one and contains the additional phase φ for the Stokes pulse.

We remark the importance of the phase φ introduced with the second Stokes pulse: if $\varphi = 0$, then $\widehat{M}_d(\chi;0) = \widehat{\mathbb{1}}$. For more details about how the Householder reflection synthesized by the two-shot STIRAP is derived, we refer to appendix 1.A, where for simplicity we expanded the derivation for a qubit ($d = 2$).
In practice, when we want to implement a specific quantum gate on a qudit, we have to proceed as follow:

- The most general quantum gate on a d-dimensional space being a product of, *at most*, d different HRs, the recipe for the factorisation of the desired gate into HRs has to be known. The parametrization will then be spanned on k ($1 \leqslant k \leqslant d$) Householder vectors $|\chi\rangle_\ell$ and phases φ_ℓ, $1 \leqslant \ell \leqslant k$.

- For each specific HR, one has to determine the angles $\theta_j,\ j = 1, ..., d-1$ that define the transformation (the phases ϕ_j are simply given by the phases of the components χ_j). One achieves this program using the relations from the components of $|\chi\rangle$:

$$\begin{aligned} \cos^2\theta_{d-1} &= |\chi_1|^2 + ... + |\chi_{d-1}|^2 \\ \cos^2\theta_{d-2}\cos^2\theta_{d-1} &= |\chi_1|^2 + ... + |\chi_{d-2}|^2 \\ &\vdots \\ \cos^2\theta_1 ... \cos^2\theta_{d-1} &= |\chi_1|^2. \end{aligned} \tag{1.3.13}$$

1.3.2 Quantum Fourier transform on a quartit and energy study

To illustrate the construction of Householder reflections to design arbitrary quantum gates, we show an implementation of a quantum Fourier transform (QFT), which is of great interest in quantum computing, especially in algorithms like the famous Shore factorization algorithm. The general qudit QFT is given by the unitary transformation:

$$\widehat{F}_d = \frac{1}{\sqrt{d}} \sum_{j,k=1}^{d} \mathrm{e}^{i\frac{2\pi(j-1)(k-1)}{d}} |j\rangle\langle k|. \tag{1.3.14}$$

Recipes of QFT have been shown with qubits [28, 29, 58], and recently with qudits, using Householder reflections [45, 46]. In this section, we apply the QFT on a quartit, or so to say

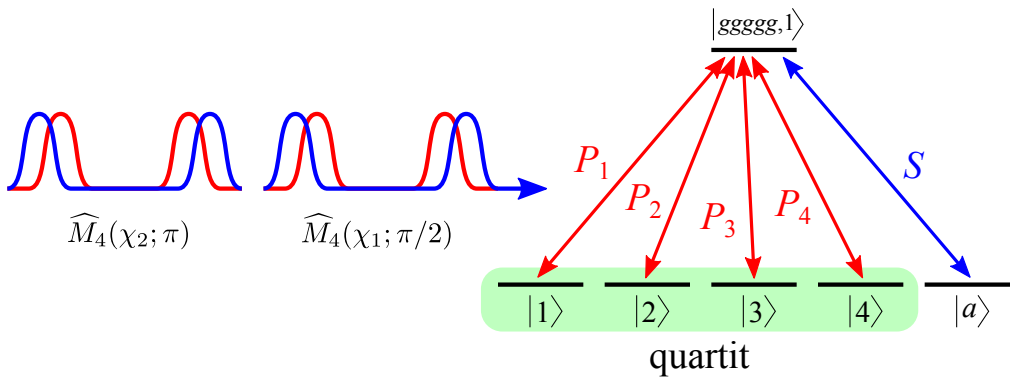

Figure 1.11: Quartit in a 5-pod system, manipulated by two-shot STIRAP Householder reflections to design a quartit QFT.

a qudit with $d = 4$. The matrix form of the QFT in the quartit basis $\{|1\rangle, |2\rangle, |3\rangle, |4\rangle\}$ reads:

$$\widehat{F}_4 = \frac{1}{2}\begin{pmatrix} 1 & 1 & 1 & 1 \\ 1 & i & -1 & -i \\ 1 & -1 & 1 & -1 \\ 1 & -i & -1 & i \end{pmatrix}. \tag{1.3.15}$$

This transformation is synthesized with two Householder reflections [45]:

$$\begin{aligned} &\widehat{F}_4 = \widehat{M}_4(\chi_2;\pi)\widehat{M}_4(\chi_1;\pi/2), \\ &|\chi_1\rangle = \frac{1}{\sqrt{2}}\begin{pmatrix} 0 \\ 1 \\ 0 \\ -1 \end{pmatrix}, \quad |\chi_2\rangle = \frac{1}{2}\begin{pmatrix} -1 \\ 1 \\ 1 \\ 1 \end{pmatrix}, \end{aligned} \tag{1.3.16}$$

each of them being parametrized with a specific pulse sequence whose characteristics are given by vectors $|\chi_1\rangle, |\chi_2\rangle$ and phases φ_1, φ_2. The quartit as a 5-pod system being manipulated by two-shot STIRAPs to get Householder reflections is displayed in fig. 1.11.

The QFT can be described in two steps, each of them describing the physical implementation of one Householder reflection:

- The first HR: $\widehat{M}_4(\chi_1;\pi/2)$. The parametrization of $|\chi_1\rangle$ shows that, for pumps, only P_2 and P_4 are turned on during this process, each time having a phase difference of π between them. The second Stokes pulse should have a phase difference of $\pi/2$ with the first one.

- The second HR: $\widehat{M}_4(\chi_2;\pi)$. This time all pumps are on, and P_1 must have a π phase difference with all other pulses. The second Stokes should also have a phase difference of π with the first one.

We solved the Schrödinger equation with this specific pulse sequence, and displayed the results on figure 1.12. The dynamics are being focused on the propagator solution of the Schrödinger equation:

$$i\hbar\frac{\mathrm{d}}{\mathrm{d}t}\widehat{U}(t,t_i) = \widehat{H}(t)\widehat{U}(t,t_i), \tag{1.3.17}$$

as we are interested in the gate obtained at the end of the process. Such a computation must be independent of the initial state, that is:

$$\widehat{U}(t_i, t_i) = \widehat{\mathbb{1}}. \tag{1.3.18}$$

The third graph shown in fig. 1.12 is a calculation comparing the elements of $\widehat{U}(t, t_i)$ and the target propagator $\widehat{F}_4$. The quantity being evaluated is the infidelity, as a matrix dimensionless distance, defined as:

$$||\widehat{U}_4(t, t_i) - \widehat{F}_4|| = \mathrm{Tr}\left\{\left(\widehat{U}(t, t_i) - \widehat{F}_4\right)^\dagger \left(\widehat{U}(t, t_i) - \widehat{F}_4\right)\right\}. \tag{1.3.19}$$

The infidelity vanishing means that $\widehat{U}_4(t, t_i)$, being the propagator projected on the quartit subspace, is strictly equal to $\widehat{F}_4$, which is achieved in the end of the second Householder reflection. The number of non-simultaneous pulses to reach the quartit QFT is 8. For a qudit, the generalized quantum gate requires in general $4d$ non-simultaneous pulses, as d HRs are in general required.

We study below, as a function of d, the total fluence of the amplitude of the laser fields (that is, its time integrated pulse area), which is proportional to the total Rabi frequency fluence:

$$F_E = \int_{-\infty}^{+\infty} \mathrm{d}t \left(|S(t)| + \sum_{j=1}^{d} |P_j(t)|\right), \tag{1.3.20}$$

and the laser intensity fluence, corresponding to the laser energy (per unit area), proportional to the fluence F_I of the mean square pump Rabi frequency and the square Stokes Rabi frequency:

$$F_I = \int_{-\infty}^{+\infty} \mathrm{d}t \left(|S(t)|^2 + |P_0(t)|^2\right). \tag{1.3.21}$$

From the effective Hamiltonian (1.3.11), we immediately conclude that the process does not depend on d. This means the remarkable property that the energy (F_I) required to achieve by adiabatic passage a single HR operation *does not depend on d*. This result is shown numerically in fig. 1.13, where we have determined, for random HR (constructed from a random normalized vector $|\chi\rangle$ and taking $\varphi = \pi$), the peak amplitude of $P_0(t)$ from which the infidelity $||\widehat{U}_d(t, t_i) - \widehat{M}_d(\chi; \pi)||$ goes below the accuracy 10^{-4}. On the other hand, we anticipate the total Rabi frequency fluence F_E to be bounded by a function growing as $\sqrt{d}$ for large d, since the adiabaticity criterium is given by the area $P_{0,\mathrm{peak}}T \gg 1$, with $P_{0,\mathrm{peak}}$ the peak amplitude of $P_0(t)$ and taking $S_{\mathrm{peak}} \sim P_{0,\mathrm{peak}}$. We have indeed:

$$S_{\mathrm{peak}} + \sum_{j=1}^{d} P_{j,\mathrm{peak}} = S_{\mathrm{peak}} + P_{0,\mathrm{peak}} \sum_{j=1}^{d} \chi_j \leqslant S_{\mathrm{peak}} + P_{0,\mathrm{peak}}\sqrt{d}. \tag{1.3.22}$$

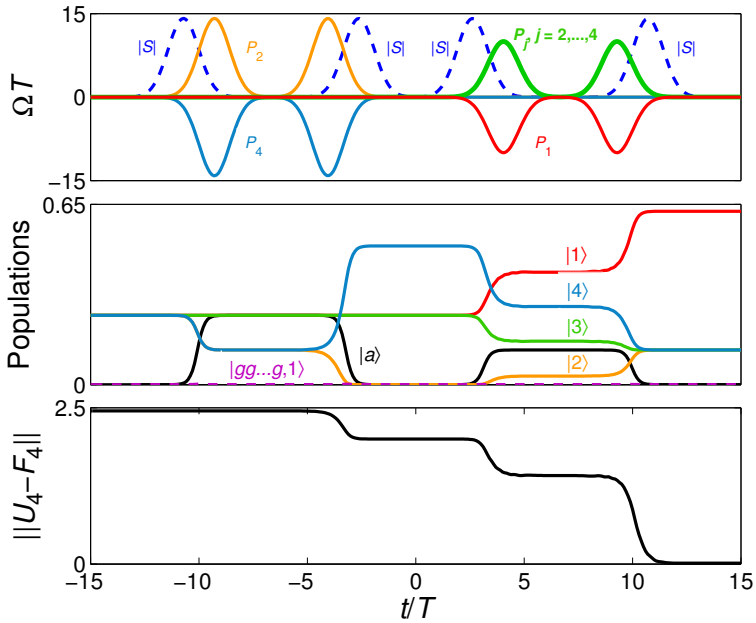

Figure 1.12: Numerical simulation of the quantum Fourier transform on a quartit in a 5-pod system with two HRs. Upper: the dimensionless Rabi frequencies associated with the pump and Stokes fields. The sequence of the pump and Stokes lasers allows the implementation of the two required HRs, $\widehat{M}_4(\chi_1;\pi/2)$, where only the pumps P_2 and P_4 are on, and next $\widehat{M}_4(\chi_2;\pi)$, where all the pumps are on [according to equation (1.3.16)]. All pulses are of shape $\mathrm{e}^{-(t/T)^2}$ and the time delays between Stokes and pumps are all $T/1.4$. Middle: Dynamics of the 5-pod system during the process for the particular initial condition $|\psi_i\rangle = \frac{1}{2}(|1\rangle + i|2\rangle + |3\rangle + |4\rangle)$. Lower: Infidelity as dimensionless distance $||\widehat{U}_4(t,t_i) - \widehat{F}_4||$ between the propagator $\widehat{U}_4(t,t_i)$ (projected in the space defining the quartit states) and the quartit QFT $\widehat{F}_4$.

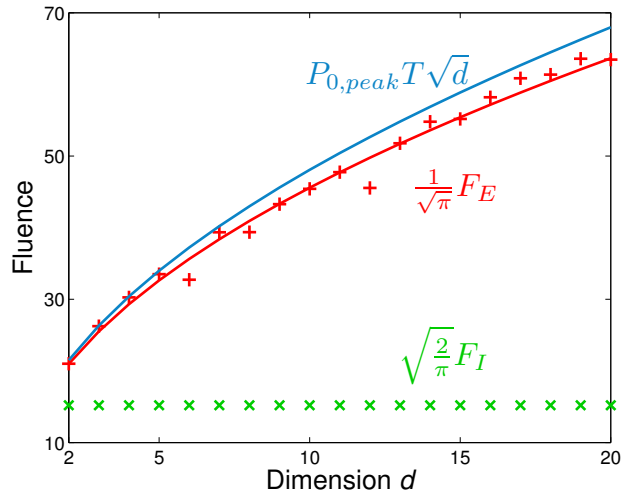

Figure 1.13: Normalized square Rabi frequency fluence F_I proportional to the energy per area unit (green crosses, in units of $1/T$) and normalized Rabi frequency fluence F_E proportional to the laser field amplitude fluence (crosses, dimensionless, fitted by the bent solid red line) required to synthesize numerically a random HR with an infidelity below 10^{-4} as a function of the dimension d. For simplicity, only the pump fields have been considered in the present calculation. The curve fitting F_E and the normalized Rabi frequency fluences are bounded by $P_{0,\text{peak}}T\sqrt{d}$.

Summary

In conclusion, we have summarized the basic concepts of quantum information and quantum computation, expanded the formalism of adiabaticity with the Schrödinger equation when manipulating single atoms or ions by laser pulses, and detailed the physical implementation of such processes with the example of ions in a Paul trap. Lastly, we proposed a new technique to perform an arbitrary quantum gate on a qudit, which is synthesized with d Householder reflections at most. In the case of the Fourier transform, this is promising because this algorithm requires $n^2/2$ operations if done on a set of n qubits, but viewing the latter as a single qudit of dimension $d = 2n$, the number of operations is reduced to d.
We have shown that a double STIRAP can be used to produce a single Householder reflection, which acts as a phase gate in the space $\{|a\rangle, |\chi\rangle\}$. It has been recently shown that a phase gate can be used directly in the space $\{|\chi\rangle, |gg...g, 1\rangle\}$ if non-negligible population in the excited state is allowed [59].

Appendix

1.A Derivation of the Householder reflection for a qubit

We derive the Householder reflection transformation for a qubit, which shows in a simple way how the general propagator is obtained. Generalization to higher dimensional qudits is straightforward. The Hamiltonian and the transformation in the basis $\{|a\rangle, |ggg, 1\rangle, |1\rangle, |2\rangle\}$ are:

$$\widehat{H}(t) = \begin{pmatrix} 0 & S^*(t) & 0 & 0 \\ S(t) & 0 & P_1^*(t) & P_2^*(t) \\ 0 & P_1(t) & 0 & 0 \\ 0 & P_2(t) & 0 & 0 \end{pmatrix}, \quad \widehat{T} = \begin{pmatrix} 1 & 0 & 0 & 0 \\ 0 & 1 & 0 & 0 \\ 0 & 0 & \cos\theta & \sin\theta \\ 0 & 0 & \sin\theta \mathrm{e}^{i\phi} & -\cos\theta \mathrm{e}^{i\phi} \end{pmatrix}. \tag{1.A.1}$$

Here, the parametrization is done so that $\left\{ \begin{array}{c} P_1(t) \\ P_2(t) \end{array} \right\} = P_0(t)|\chi\rangle \equiv P_0(t) \left\{ \begin{array}{c} \cos\theta \\ \sin\theta \mathrm{e}^{i\phi} \end{array} \right\}$. From the arbitrary initial state:

$$|\psi_i\rangle = a_1|1\rangle + a_2|2\rangle, \tag{1.A.2}$$

we reach a final state where the $|\chi\rangle$ component acquires a phase factor $\mathrm{e}^{i\varphi}$. We need to write the qubit vector components $\{|1\rangle, |2\rangle\}$ in terms of $\{|\chi\rangle, |\text{n.c.}\rangle\}$, which is done by inverting the transformation $\widehat{T}_2$:

$$\left\{ \begin{array}{l} |\chi\rangle = \widehat{T}_2|1\rangle \\ |\text{n.c.}\rangle = \widehat{T}_2|2\rangle \end{array} \right. \xrightarrow{\text{inversion}} \left\{ \begin{array}{l} |1\rangle = \widehat{T}_2^\dagger|\chi\rangle = \cos\theta|\chi\rangle + \sin\theta|\text{n.c.}\rangle \\ |2\rangle = \widehat{T}_2^\dagger|\text{n.c.}\rangle = \mathrm{e}^{-i\phi}\Big(\sin\theta|\chi\rangle - \cos\theta|\text{n.c.}\rangle\Big) \end{array} \right. . \tag{1.A.3}$$

Writing the initial and final states in the new basis, we get:

$$\begin{array}{c} |\psi_i\rangle = a_1\Big(\cos\theta|\chi\rangle + \sin\theta|\text{n.c.}\rangle\Big) + a_2\mathrm{e}^{-i\phi}\Big(\sin\theta|\chi\rangle - \cos\theta|\text{n.c.}\rangle\Big) \\ \Big\downarrow \text{HR: } |\chi\rangle \to \mathrm{e}^{i\varphi}|\chi\rangle \\ |\psi_f\rangle = a_1\Big(\cos\theta\mathrm{e}^{i\varphi}|\chi\rangle + \sin\theta|\text{n.c.}\rangle\Big) + a_2\mathrm{e}^{-i\phi}\Big(\sin\theta\mathrm{e}^{i\varphi}|\chi\rangle - \cos\theta|\text{n.c.}\rangle\Big) \end{array}, \tag{1.A.4}$$

and writing the final state in the original basis, one obtains:

$$\begin{aligned} |\psi_f\rangle = &\Big(a_1(\cos^2\theta\mathrm{e}^{i\varphi} + \sin^2\theta) + a_2\mathrm{e}^{-i\phi}\sin\theta\cos\theta(\mathrm{e}^{i\varphi} - 1)\Big)|1\rangle \\ &+ \Big(a_1\mathrm{e}^{i\phi}\sin\theta\cos\theta(\mathrm{e}^{i\varphi} - 1) + a_2(\mathrm{e}^{i\varphi}\sin^2\theta + \cos^2\theta)\Big)|2\rangle. \end{aligned} \tag{1.A.5}$$

The propagator is obtained by writing this result in a matrix form, and using the identity $\sin^2\theta + \cos^2\theta = 1$:

$$|\psi_f\rangle = \begin{pmatrix} 1 + (\mathrm{e}^{i\varphi} - 1)\cos^2\theta & (\mathrm{e}^{i\varphi} - 1)\sin\theta\cos\theta\mathrm{e}^{-i\phi} \\ (\mathrm{e}^{i\varphi} - 1)\sin\theta\cos\theta\mathrm{e}^{i\phi} & 1 + (\mathrm{e}^{i\varphi} - 1)\sin^2\theta \end{pmatrix} \begin{pmatrix} a_1 \\ a_2 \end{pmatrix} = \widehat{U}(t_f, t_i)|\psi_i\rangle, \tag{1.A.6}$$

retrieving the expression for the Householder reflection $\widehat{U}(t_f, t_i) \equiv \widehat{M}_2(\chi; \varphi)$, for $|\chi\rangle = \cos\theta|1\rangle + \sin\theta\mathrm{e}^{i\phi}|2\rangle$.

Chapter 2

Quantum optics with atoms in cavities

Chapter overview

Objectives: In this chapter, we explore quantum optics in the field of cavity quantum electrodynamics (cQED). Starting from the general field quantization procedure, we follow the construction of the cavity field, whose losses are modeled with a reservoir coupling. We also present an alternative derivation of the atom-field effective model, and results for the generation of single and few-photon states leaking from a cavity.

Guideline:

- Canonical quantization in a lossless dielectric medium.
- Study of the one-dimensional cavity system: response function, photon flux, master equation.
- Alternative derivation of the effective atom-cavity model with global field operators.
- Study of the output field with one and two Λ-atoms inside a cavity.
- **keywords:** *canonical quantization, cavity, eigenmode equation, response function, input-output relations, photon flux, spontaneous emission, single photon, photon state.*

Results/novelty: Production of photon states from multiple Λ-atoms in a cavity.

2.1 Model for cavity quantum electrodynamics (cQED) with imperfect mirrors

The quantization procedure for the electromagnetic modes of a perfect cavity is, nowadays, well known. The quantization leads to a set of discrete normal modes with annihilation and creation operators assigned to each of them. The wave functions associated with those modes are the solutions of the one-dimensional Helmholtz equation, with zero boundary conditions at the positions of the mirrors: the result is a set of sine functions with different discrete frequencies $\omega_n = n\frac{\pi c}{\ell}$, where ℓ is the length of the one-dimensional cavity.

The conventional way to describe a cavity field must, however, take losses via imperfect (yet not absorbing) mirrors into account. Deriving models that are closer to real experiments, having imperfect mirrors has its own interest, since it allows to transfer photons from the cavity to propagating modes. In this work we will consider that one mirror is perfect while the other is not in order to identify a unique channel for leaking photons. The procedure usually adopted describes the damping of the radiation field in the cavity with a phenomenological system-reservoir approach [60, 61], where the cavity system is described by a set of quantized harmonic oscillators associated to the discrete modes the cavity would have in the absence of damping. The reservoir is another set of quantized harmonic oscillators associated with the continuum of external free-space modes. It is often assumed that the coupling strength between cavity and outside modes is independent of the frequency, leading to a Markovian damping. The input-output relations, which relate in principle the outside field to the intra-cavity field, are also based on this property. However, it has been shown by Dutra and Nienhuis that this property is valid up to the first order in the transmission coefficient $|\underline{t}|$, based on the derivation of the phenomenological Hamiltonian from first principles [62, 63]. It allows one to obtain an explicit expression for the coupling strength. They show that the phenomenological Hamiltonian is valid up to the first order transmission of the leaking mirror, i.e. it is well justified for high-Q cavities. We present this approach in this section, the approximations it involves and derive its consequences on the input-output formulation. We also show that it allows one to characterize the leaking photon by including the Poynting vector to this formulation.

In section 2.2, we will focus on another way of deriving effective models for cQED and show that it is consistent with the derivation of Dutra and Nienhuis, since it leads to the effective Hamiltonian up to the first order in the transmission $|\underline{t}|$. This description will be used to link cQED and plasmonic QED, studied in the next part of the thesis. Indeed, the input-output description is valid for high-Q cavities, but in the case of plasmons the quality factor is low. This requires stepping back to the global field description and building the effective model from this starting point. As we show the equivalence of the input-output and the global field approaches, this paves the way for cQED-like description of quantum plasmonics.

The chapter is organized as follows:

- In the first section we present the general field quantization, and its application to a one-dimensional cavity and spontaneous emission in a homogeneous medium. The global field operators are introduced, and we provide a description of the input-output equivalence, i.e. the decomposition of the global field into a perfect cavity field coupled to a set of continuous reservoir operators. We base the derivation of the photon flux and the master equation on the input-output approach.

- The second section is an alternative derivation of the atom-cavity field model, based on the coupling between the atom and the global field operators. We show the equivalence of this derivation with the input-output model, which is useful as the plasmonic system will be studied under the structure of this alternative derivation.
- The last section presents results on the control of photon wavepackets leaking from a cavity, with the use of single and multiple atoms coupled to a cavity field.

2.1.1 Quantization of the electromagnetic field

In this section we derive the quantization of the electromagnetic field in a linear, passive medium. The standard quantization procedure is slightly tricky because unlike atoms, the electromagnetic field is a continuous distribution of harmonic oscillators. A single harmonic oscillator is quantized by writing the canonical variables q, p and substituting them by operators $\widehat{q}, \widehat{p}$ acting on a well-defined Hilbert space $L_2(\mathbb{R}, \mathrm{d}q)$. An infinite collection of harmonic oscillators would then bring a total Hilbert space as an infinite tensor product of $L_2(\mathbb{R}, \mathrm{d}q)$, and since $\mathrm{d}^\infty q$ is not a well-defined Lebesgue measure, the total space would not be defined either [64]. The difficulty with the definition of the Hilbert space is avoided by reformulating the theory in a well-defined Fock space, which is isomorphic to $L_2(\mathbb{R}^N, \mathrm{d}^N q)$ for models with finite degrees of freedom N. Another difficulty arises due to the electromagnetic field transversality constraint $\boldsymbol{\nabla} \cdot \mathbf{A} = 0$ (in a homogeneous medium), leading to the canonical variables $\mathbf{A}, \boldsymbol{\Pi}$ not being independent. The redundancy is removed by making a canonical change of variables such that in the new coordinate system, the constraint is automatically satisfied.

We start the quantization procedure by writing Maxwell's equations for an inhomogeneous lossless dielectric medium [65, 66]:

$$\boldsymbol{\nabla} \cdot (\epsilon(\mathbf{r})\mathbf{E}) = 0 \tag{2.1.1}$$

$$\boldsymbol{\nabla} \times \mathbf{E} = -\frac{\partial \mathbf{B}}{\partial t} \tag{2.1.2}$$

$$\boldsymbol{\nabla} \cdot \mathbf{B} = 0 \tag{2.1.3}$$

$$\boldsymbol{\nabla} \times \mathbf{B} = \mu_0 \epsilon(\mathbf{r}) \frac{\partial \mathbf{E}}{\partial t}, \tag{2.1.4}$$

where $\epsilon(\mathbf{r}) = \epsilon_0 \epsilon_r(\mathbf{r})$ is the dielectric function of the medium. As usual we define the vector potential $\mathbf{A}$:

$$\mathbf{B} = \boldsymbol{\nabla} \times \mathbf{A}, \tag{2.1.5}$$

$$\mathbf{E} = -\frac{\partial \mathbf{A}}{\partial t} - \nabla \phi, \tag{2.1.6}$$

where ϕ is the scalar electric potential. Combining Maxwell's equations and the generalized Coulomb gauge:

$$\boldsymbol{\nabla} \cdot (\epsilon(\mathbf{r})\mathbf{A}) = 0, \tag{2.1.7a}$$

$$\phi = 0, \tag{2.1.7b}$$

we find the propagation equation for the vector potential:

$$\left(\frac{\partial^2}{\partial t^2} + \frac{c^2}{\epsilon_r(\mathbf{r})}\boldsymbol{\nabla}\times\boldsymbol{\nabla}\times\right)\mathbf{A} = 0. \tag{2.1.8}$$

At this point we make the change of variables $\mathbf{A}' = \sqrt{\epsilon_r(\mathbf{r})}\mathbf{A}$ in order to get a Hermitian and self-adjoint operator acting on the field variable, and write the latter equation as a Hamiltonian system. The propagation equation turns into:

$$\left(\frac{\partial^2}{\partial t^2} + \boldsymbol{\Omega}^2\right)\mathbf{A}' = 0, \tag{2.1.9}$$

where we define the Hermitian operator $\boldsymbol{\Omega} := (\boldsymbol{\Xi}^\dagger\boldsymbol{\Xi})^{1/2}$, with $\boldsymbol{\Xi} = c\boldsymbol{\nabla}\times\frac{1}{\sqrt{\epsilon_r}}$. The next step consists in defining a canonically conjugate variable $\boldsymbol{\Pi}'$ such that the pair $(\mathbf{A}', \boldsymbol{\Pi}')$ forms a Hamiltonian system. This is done in appendix 2.A, where all the steps of the quantization procedure are detailed. The field variables $(\mathbf{A}', \boldsymbol{\Pi}')$ are then expressed as linear combinations of complex eigenfunctions $\boldsymbol{\Phi}_\kappa$ forming a complete orthonormal basis, satisfying the transversality constraint:

$$\boldsymbol{\nabla}\cdot(\epsilon\boldsymbol{\Phi}_\kappa) = 0. \tag{2.1.10}$$

The latter must satisfies the eigenmode equation:

$$\boxed{\boldsymbol{\Omega}^2\boldsymbol{\Phi}_\kappa = \omega_\kappa^2\boldsymbol{\Phi}_\kappa,} \tag{2.1.11}$$

where ω_κ is the frequency associated to the normal mode labelled κ. Using the basis that satisfies the constraints, we go to a new set of canonical, constraint-free variables with a map $(\mathbf{A}', \boldsymbol{\Pi}') \mapsto (\underline{q}, \underline{p})$. The latter are quantized using the principle of correspondence, and this leads to the expressions of the quantized field variables in terms of the eigenfunctions $\boldsymbol{\Phi}_\kappa$, the eigenvalues ω_κ, and the creation/annihilation operators $\widehat{a}_\kappa^\dagger, \widehat{a}_\kappa$:

$$\widehat{\mathbf{A}}'(\mathbf{r}) = \sum_\kappa \sqrt{\frac{\hbar}{2\omega_\kappa}}\Big(\boldsymbol{\Phi}_\kappa(\mathbf{r})\widehat{a}_\kappa + \boldsymbol{\Phi}_\kappa^*(\mathbf{r})\widehat{a}_\kappa^\dagger\Big) \tag{2.1.12a}$$

$$\widehat{\boldsymbol{\Pi}}'(\mathbf{r}) = -i\sum_\kappa \sqrt{\frac{\hbar\omega_\kappa}{2}}\Big(\boldsymbol{\Phi}_\kappa(\mathbf{r})\widehat{a}_\kappa - \boldsymbol{\Phi}_\kappa^*(\mathbf{r})\widehat{a}_\kappa^\dagger\Big), \tag{2.1.12b}$$

where the creation/annihilation pairs are linear combinations of the quantized versions of $(\underline{q}, \underline{p})$ (see appendix 2.A). The corresponding electric field is given by:

$$\widehat{\mathbf{E}}(\mathbf{r}) = -\frac{1}{\sqrt{\epsilon_r(\mathbf{r})}}\boldsymbol{\Pi}'(\mathbf{r}), \tag{2.1.13}$$

and the quantum Hamiltonian of the electromagnetic field is finally expressed as:

$$\boxed{\widehat{H} = \frac{1}{2}\sum_\kappa \hbar\omega_\kappa\Big(\widehat{a}_\kappa^\dagger\widehat{a}_\kappa + \widehat{a}_\kappa\widehat{a}_\kappa^\dagger\Big).} \tag{2.1.14}$$

Quantization in a box and large box limit

In this paragraph, we first check that the global field operator, needed to describe the properties of leaky cavities is consistent with the standard field quantization for the vacuum (or a homogeneous medium), derived using the large box limit. In a finite box of volume V with zero boundary conditions for the electric field, there is a discrete number of possible $\mathbf{k}$-vectors. Therefore, we can replace the general index κ and its summation by $\mathbf{k}$ and a polarization index $\lambda = 1, 2$. The Hamiltonian then assumes the form:

$$\widehat{H} = \sum_{\mathbf{k},\lambda} \hbar\omega_k \Big(\widehat{a}^\dagger_{\mathbf{k},\lambda} \widehat{a}_{\mathbf{k},\lambda} + \tfrac{1}{2} \Big), \tag{2.1.15}$$

where the field operators obey the commutation relations:

$$\big[\widehat{a}_{\mathbf{k},\lambda}, \widehat{a}^\dagger_{\mathbf{k}',\lambda'}\big] = \delta_{\mathbf{k}\mathbf{k}'}\delta_{\lambda\lambda'} \tag{2.1.16a}$$

$$\big[\widehat{a}_{\mathbf{k},\lambda}, \widehat{a}_{\mathbf{k}',\lambda'}\big] = \big[\widehat{a}^\dagger_{\mathbf{k},\lambda}, \widehat{a}^\dagger_{\mathbf{k}',\lambda'}\big] = 0. \tag{2.1.16b}$$

The electric field is expressed in terms of the annihilation/creation operators. In the vacuum, for example, the mode functions $\mathbf{\Phi}_{\mathbf{k},\lambda}(\mathbf{r})$ reduce to $\frac{1}{\sqrt{V}}\boldsymbol{\epsilon}_{\mathbf{k},\lambda}\mathrm{e}^{i\mathbf{k}\cdot\mathbf{r}}$, with $\boldsymbol{\epsilon}_{\mathbf{k},\lambda}$ being the field polarization unit vector, and the electric field reads:

$$\widehat{\mathbf{E}}(\mathbf{r}) = i \sum_{\mathbf{k},\lambda} \sqrt{\frac{\hbar\omega_k}{2\epsilon_0 V}} \boldsymbol{\epsilon}_{\mathbf{k},\lambda} \Big(\mathrm{e}^{i\mathbf{k}\cdot\mathbf{r}} \widehat{a}_{\mathbf{k},\lambda} - \mathrm{e}^{-i\mathbf{k}\cdot\mathbf{r}} \widehat{a}^\dagger_{\mathbf{k},\lambda} \Big), \tag{2.1.17}$$

where $\omega_k = |\mathbf{k}|c$. In the absence of boundaries, we write the large box limit, leading to a 3-dimensional integral over $\mathbf{k}$:

$$\sum_{\mathbf{k},\lambda} \longrightarrow \frac{V}{(2\pi)^3} \sum_{\lambda} \int \mathrm{d}^3 k. \tag{2.1.18}$$

The resulting integral leads to operators and mode functions written in units of $\sqrt{V/(2\pi)^3}$:

$$\widehat{a}_{\mathbf{k},\lambda} \longrightarrow \widehat{b}_{\mathbf{k},\lambda} = \sqrt{\tfrac{V}{(2\pi)^3}}\widehat{a}_{\mathbf{k},\lambda} \tag{2.1.19}$$

$$\mathbf{\Phi}_{\mathbf{k},\lambda}(\mathbf{r}) \longrightarrow \mathbf{\Psi}_{\mathbf{k},\lambda}(\mathbf{r}) = \sqrt{\tfrac{V}{(2\pi)^3}}\mathbf{\Phi}_{\mathbf{k},\lambda}(\mathbf{r}), \tag{2.1.20}$$

where the mode functions are orthonormal to each other: $\langle \mathbf{\Psi}_{\mathbf{k},\lambda}, \mathbf{\Psi}_{\mathbf{k}',\lambda'} \rangle = \delta(\mathbf{k} - \mathbf{k}')\delta_{\lambda\lambda'}$. The commutation relations are then:

$$\big[\widehat{b}_{\mathbf{k},\lambda}, \widehat{b}^\dagger_{\mathbf{k}',\lambda'}\big] = \delta(\mathbf{k} - \mathbf{k}')\delta_{\lambda\lambda'} \tag{2.1.21a}$$

$$\big[\widehat{b}_{\mathbf{k},\lambda}, \widehat{b}_{\mathbf{k}',\lambda'}\big] = \big[\widehat{b}^\dagger_{\mathbf{k},\lambda}, \widehat{b}^\dagger_{\mathbf{k}',\lambda'}\big] = 0. \tag{2.1.21b}$$

Finally, we write the Hamiltonian and the conjugate fields $\mathbf{A}', \mathbf{\Pi}'$ in the large box limit:

$$\boxed{\begin{aligned} \widehat{H} &= \sum_{\lambda=1,2} \int \mathrm{d}^3 k \hbar\omega_k \Big(\widehat{b}^\dagger_{\mathbf{k},\lambda} \widehat{b}_{\mathbf{k},\lambda} + \tfrac{1}{2} \Big) && (2.1.22) \\ \widehat{\mathbf{A}}'(\mathbf{r}) &= \sum_{\lambda=1,2} \int \mathrm{d}^3 k \sqrt{\frac{\hbar}{2\omega_k}} \Big(\mathbf{\Psi}_{\mathbf{k},\lambda}(\mathbf{r}) \widehat{b}_{\mathbf{k},\lambda} + \mathbf{\Psi}^*_{\mathbf{k},\lambda}(\mathbf{r}) \widehat{b}^\dagger_{\mathbf{k},\lambda} \Big) && (2.1.23) \\ \widehat{\mathbf{\Pi}}'(\mathbf{r}) &= -i \sum_{\lambda=1,2} \int \mathrm{d}^3 k \sqrt{\frac{\hbar\omega_k}{2}} \Big(\mathbf{\Psi}_{\mathbf{k},\lambda}(\mathbf{r}) \widehat{b}_{\mathbf{k},\lambda} - \mathbf{\Psi}^*_{\mathbf{k},\lambda}(\mathbf{r}) \widehat{b}^\dagger_{\mathbf{k},\lambda} \Big), && (2.1.24) \end{aligned}}$$

2.1.2 The one-dimensional cavity field

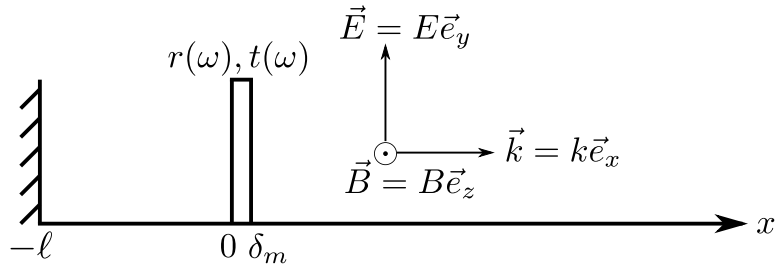

Figure 2.1: Sketch of a 1D cavity made of two planar mirrors facing each other. The left mirror is perfect ($\underline{\mathrm{r}} = -1, \underline{\mathrm{t}} = 0$) and the right mirror is a thin semi-transparent layer.

We consider two mirrors facing each other, a perfect one placed at position $x_{\mathrm{pm}} = -\ell$ and a semi-transparent and non-absorbing one placed at position $x_{\mathrm{stm}} = 0$. We first restrict the system to a one-dimensional model where only linearly polarized fields are taken into account. As depicted on fig. 2.1, the electric field is polarized along the y-axis, the magnetic field along the z-axis, and the wave vector is chosen to point in the direction of the positive x coordinates. The electromagnetic field is determined by solving the eigenmode equation (2.1.11) (also known as the general Helmholtz equation):

$$\left(\frac{\partial^2}{\partial x^2} + \epsilon_r(x)k^2\right)\Phi(x,\omega) = 0, \tag{2.1.25}$$

where $\epsilon_r(x)$ is the space-dependent relative permittivity, $k = \omega/c$ and $\Phi(x,\omega)$ is the field eigenfunction (here being scalar). The semi-transparent mirror is modeled by a medium of thickness δ_m and refractive index n such that:

$$\epsilon_r(x) = \begin{cases} 1 & \text{if } -\ell \leqslant x < 0,\ x \geqslant \delta_m \\ n^2 & \text{if } 0 \leqslant x < \delta_m, \end{cases} \tag{2.1.26}$$

and the reflection and transmission coefficients $\underline{\mathrm{r}}(\omega), \underline{\mathrm{t}}(\omega)$ of the mirror must fulfill the general relations:

$$|\underline{\mathrm{r}}(\omega)|^2 + |\underline{\mathrm{t}}(\omega)|^2 = 1, \tag{2.1.27a}$$

$$\underline{\mathrm{r}}^*(\omega)\underline{\mathrm{t}}(\omega) + \underline{\mathrm{t}}^*(\omega)\underline{\mathrm{r}}(\omega) = 0. \tag{2.1.27b}$$

By writing equations (2.1.27), we do not consider losses by absorption in the mirror. The treatment of ohmic losses will be addressed in chapters 3-4, where lossy structured materials are considered. However, we are interested in the process of cavity losses as a leakage of the modes outside the cavity. In general, the reflection/transmission coefficients depend on ω because of the thickness δ_m and the index of the mirror's material:

$$\underline{\mathrm{r}}(\omega) = r_m \mathrm{e}^{-i\frac{\omega}{c}\delta_m} \frac{\exp\left[i2n\delta_m\omega/c\right] - 1}{1 - r_m^2 \exp[i2n\delta_m\omega/c]}, \tag{2.1.28a}$$

$$\underline{\mathrm{t}}(\omega) = \frac{(1 - r_m^2)\exp\left[i(n-1)\delta_m\omega/c\right]}{1 - r_m^2 \exp\left[i2n\delta_m\omega/c\right]}, \tag{2.1.28b}$$

$$r_m = \frac{n-1}{n+1}. \tag{2.1.28c}$$

Equations (2.1.28) are derived from (2.1.25), using the different boundary conditions for the field, and eventually the global mode function for the vector potential, reads [67, 68]:

$$\Phi(x,\omega) = \frac{1}{\sqrt{2\pi c\mathcal{A}}} \begin{cases} -2i\mathrm{e}^{i\frac{\omega}{c}\ell}\mathcal{T}(\omega)\sin\left[\frac{\omega}{c}(x+\ell)\right] & \text{if } -\ell \leqslant x < 0 \\ -\mathrm{e}^{-i\frac{\omega}{c}x} - \mathrm{e}^{i\frac{\omega}{c}x}\left[\underline{\mathrm{r}}(\omega) - \underline{\mathrm{t}}(\omega)\mathrm{e}^{i2\frac{\omega}{c}L}\mathcal{T}(\omega)\right] & \text{if } x \geqslant \delta_m, \end{cases} \tag{2.1.29}$$

where $\mathcal{A}$ is the mode area corresponding to the surface of one mirror, and we have introduced the cavity response function:

$$\mathcal{T}(\omega) = \frac{\underline{\mathrm{t}}(\omega)}{1 + \underline{\mathrm{r}}(\omega)\mathrm{e}^{i2\frac{\omega}{c}L}}, \quad L = \ell + \delta_m. \tag{2.1.30}$$

As can be seen in (2.1.29), we have not written the expression of $\Phi(x,\omega)$ inside the semi-transparent mirror, since we are interested in the field inside the cavity to describe the coupling with atoms, and in the field outside to determine measured quantities like the Poynting vector. The semi-transparent mirror is seen as a purely passive dielectric layer, described by the coefficients (2.1.28).
The theoretical limit of a perfect cavity is recovered when $n \to \infty$ (i.e. $r_m \to 1$), giving $\underline{\mathrm{r}}(\omega) \to -\mathrm{e}^{-i\frac{\omega}{c}\delta_m}$ and $\underline{\mathrm{t}}(\omega) \to 0$. If we take additionally $\frac{\omega}{c}\delta_m \ll 1$, then $\underline{\mathrm{r}}(\omega) \to -1$. In practice, to ensure high reflectivity, the mirror is made of a complicated dielectric multi-slab configuration (coating of thin layers). Whatever the mode structure is inside the semi-transparent mirror, equations (2.1.27), (2.1.29) and (2.1.30) (where $L \approx \ell$, i.e. neglecting the thickness of the mirror) are general with $\underline{\mathrm{r}}(\omega) \to -1$ and $\underline{\mathrm{t}}(\omega) \to 0$ for a perfect mirror.

High-quality resonator limit

We focus on the expression of the cavity response function (2.1.30), which is shown to have a Lorentzian structure in appendix 2.B. We underline the nuance between what we call *Lorentzian structure* and the fact that $\mathcal{T}(\omega)$ can be a sum of Lorentzian functions. Indeed, in appendix 2.B we show the exact result:

$$|\mathcal{T}(\omega)|^2 = \sum_{m=-\infty}^{+\infty} \frac{c}{2L} \frac{\gamma(\omega)}{\left(\omega - \widetilde{\omega}_m(\omega)\right)^2 + \left(\frac{\gamma(\omega)}{2}\right)^2}, \tag{2.1.31a}$$

$$\gamma(\omega) = -\frac{c}{L}\ln|\underline{\mathrm{r}}(\omega)|, \tag{2.1.31b}$$

$$\widetilde{\omega}_m(\omega) = m\frac{\pi c}{L} + \frac{c}{2L}\big(\pi - \phi_r(\omega)\big), \tag{2.1.31c}$$

where $\phi_r(\omega) = \arg(\underline{\mathrm{r}}(\omega))$, and the Lorentzian structure (2.1.31a) can be approximated as a discrete sum of Lorentzian functions only if $\underline{\mathrm{r}}(\omega)$ is slow-varying in ω for the range of frequencies considered, i.e. the eigenfrequencies ω_n of the perfect cavity case. This condition can be achieved when the reflection coefficient modulus is close to 1 (as shown in fig. 2.2) and more generally when the reflection coefficient is sufficiently flat in frequency, i.e. does not vary significantly over the width of the Lorentzian. In this case one can indeed make a

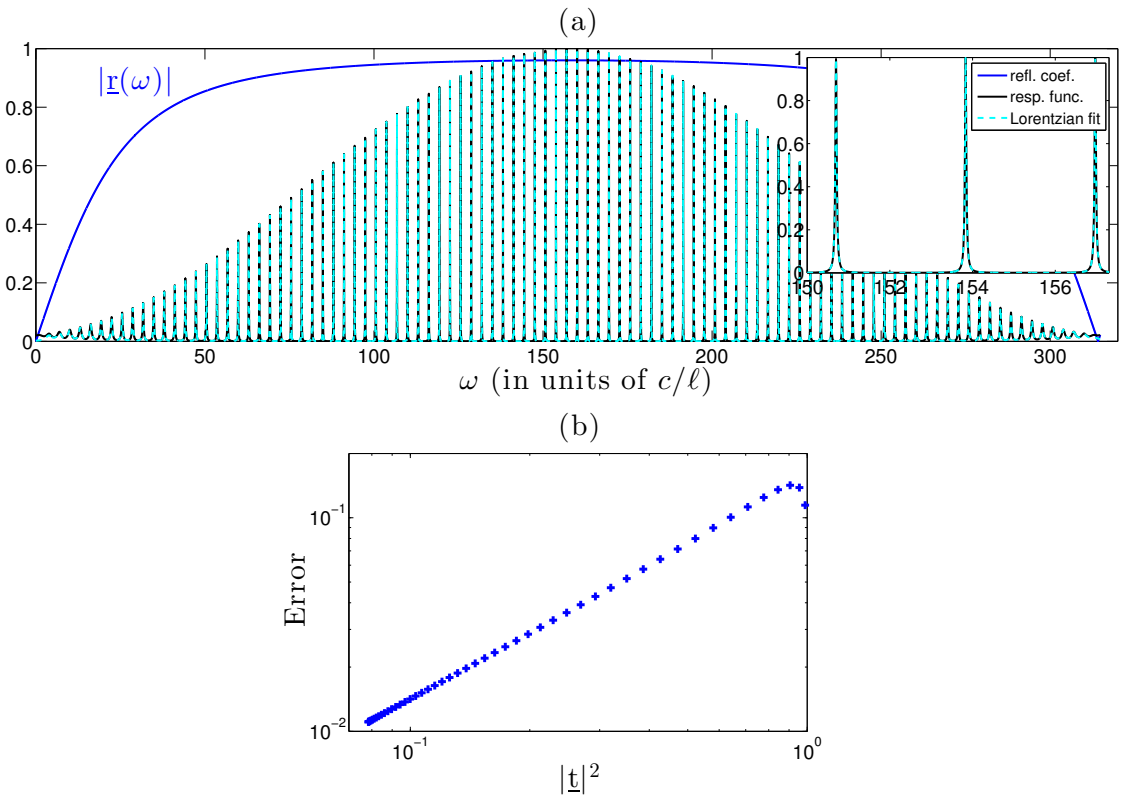

Figure 2.2: (a) Absolute value of the reflection coefficient $\underline{r}(\omega)$ (2.1.28a) with $r_m = 0.75$ (dark blue line). Corresponding square modulus cavity response function $|\mathcal{T}(\omega)|^2$ (2.1.30), normalized with its maximal value (black line), and its approximative representation as a sum of Lorentzian lineshapes $L_m(\omega)$ (equation (2.1.31a) with $\underline{r}(\omega) \simeq \underline{r}(\omega_m)$), also normalized with the maximal value of $|\mathcal{T}(\omega)|^2$ (dashed blue line). (b) Error between the full response function and the Lorentzian fit, as a function of $|\underline{t}|^2$. The error is defined as $1 - \langle \mathcal{T}, L_m \rangle$, where the scalar product is the integral over ω of the response function times the Lorentzian fit, in a bandwidth taken around a resonance $\widetilde{\omega}_m$.

further approximation:

$$|\mathcal{T}(\omega)|^2 \approx \sum_{m=-\infty}^{+\infty} L_m(\omega); \quad L_m(\omega) = \frac{c}{2L}\frac{\Gamma_m}{\left(\omega - \widetilde{\omega}_m\right)^2 + \left(\frac{\Gamma_m}{2}\right)^2}, \tag{2.1.32a}$$

$$\Gamma_m = \gamma(\omega_m), \tag{2.1.32b}$$

$$\widetilde{\omega}_m = m\frac{\pi c}{L} + \frac{c}{2L}\big(\pi - \phi_r(\omega_m)\big). \tag{2.1.32c}$$

The approximation made in (2.1.32) is analyzed numerically and is shown in fig. 2.2 (b). We refer to this Lorentzian behaviour in section 2.2, where we use it to derive an alternative quantization procedure. For now, we follow the procedure derived in [62, 63], to justify the choice of the known phenomenological cQED Hamiltonian, where we separate creation and annihilation operators into two kinds:

- The intra-cavity discrete operators $\widehat{c}_n, \widehat{c}_n^\dagger$, corresponding to a set of quantized harmonic oscillators for a perfect cavity, isolated from the environment. Every mode n is characterized by the eigenfrequency $\omega_n = n\frac{\pi c}{\ell}$, and they are obtained applying the zero boundary condition for the electric field at the positions of the two mirrors.

- The output continuous mode (or reservoir mode) operators $\widehat{b}(\omega), \widehat{b}^\dagger(\omega)$, corresponding to the outside of the cavity, applying the zero boundary condition to a single perfect mirror at position $x = 0$, and solving the Helmholtz equation for free space.

With this scheme, the losses of the cavity field into the outside free space are modeled with a coupling parameter $\kappa_n(\omega)$ between the two fields, and the phenomenological Hamiltonian reads:

$$\widehat{H} = \widehat{H}_0 + \widehat{V}, \tag{2.1.33a}$$

$$\widehat{H}_0 = \sum_{n=1}^{+\infty} \hbar\omega_n\left(\widehat{c}_n^\dagger\widehat{c}_n + \tfrac{1}{2}\right) + \int_0^{+\infty} \mathrm{d}\omega\hbar\omega\left(\widehat{b}^\dagger(\omega)\widehat{b}(\omega) + \tfrac{1}{2}\right), \tag{2.1.33b}$$

$$\widehat{V} = i\hbar\sum_{n=1}^{+\infty}\int_0^{+\infty}\mathrm{d}\omega\left(\kappa_n(\omega)\widehat{b}^\dagger(\omega)\widehat{c}_n - \kappa_n^*(\omega)\widehat{c}_n^\dagger\widehat{b}(\omega)\right). \tag{2.1.33c}$$

The complete Hamiltonian (2.1.22) with the global operators $\widehat{a}(\omega), \widehat{a}^\dagger(\omega)$ can be compared to the latter one, which is valid for $\underline{\mathrm{r}}(\omega) \equiv \underline{\mathrm{r}}$ and $\underline{\mathrm{r}} \sim -1$. To do so, we write the electric and magnetic fields for the perfect cavity case, and compare them to the global field. As a result, we get the expression of $\widehat{c}_n$ and $\widehat{b}(\omega)$ as functions of $\widehat{a}(\omega), \widehat{a}^\dagger(\omega)$:

$$\widehat{c}_n = \int_0^{+\infty}\mathrm{d}\omega\big(\alpha_{n,-}^*(\omega)\widehat{a}(\omega) - \alpha_{n,+}(\omega)\widehat{a}^\dagger(\omega)\big) \tag{2.1.34}$$

$$\widehat{b}(\omega) = \int_0^{+\infty}\mathrm{d}\omega'\big(\beta_-^*(\omega,\omega')\widehat{a}(\omega') - \beta_+(\omega,\omega')\widehat{a}^\dagger(\omega')\big), \tag{2.1.35}$$

where the functions $\alpha_{n,\pm}(\omega), \beta_{\pm}(\omega,\omega')$ are properly chosen to fulfill the transformation (see references [62,63]). The latter expressions hold, but inverting them to get the global operator:

$$\begin{aligned}\widehat{a}(\omega) = &\sum_{n=1}^{+\infty}\left(\alpha_{n,-}(\omega)\widehat{c}_n + \alpha_{n,+}(\omega)\widehat{c}_n^\dagger\right)\\ &+\int_0^{+\infty}\mathrm{d}\omega'\left(\beta_-(\omega,\omega')\widehat{b}(\omega') + \beta_+(\omega,\omega')\widehat{b}^\dagger(\omega')\right),\end{aligned} \tag{2.1.36}$$

is not possible without an approximation. Indeed, $\widehat{c}_n, \widehat{c}_n^\dagger, \widehat{b}(\omega)$ and $\widehat{b}^\dagger(\omega)$ form a complete set of operators for the Fock space spanned by $\widehat{a}(\omega), \widehat{a}^\dagger(\omega)$ when the difference between the actual values of the inside and the outside field on the boundaries $x = 0$, $x = \delta_m$ is negligible. It can be shown that this difference is small for a highly reflective mirror ($\underline{r} \sim -1$). For instance, if one can write:

$$\underline{\mathrm{r}} = -\sqrt{1 - |\underline{\mathrm{t}}|^2}, \tag{2.1.37}$$

where $|\underline{\mathrm{t}}|^2 \ll 1$, then the inversion (2.1.36) holds up to the first order in $|\underline{\mathrm{t}}|$.
Another important feature is the cavity-exterior coupling function, which expresses [62,67]:

$$\kappa_n(\omega) = -\frac{|\underline{\mathrm{t}}|}{2}\sqrt{\frac{c}{\pi L}}\mathrm{e}^{-i\frac{\omega}{c}L}\frac{\sin\left[(\omega-\omega_n)\frac{L}{c}\right]}{(\omega-\omega_n)\frac{L}{c}}. \tag{2.1.38}$$

There is one single reservoir for the cavity field, described by the operators $\widehat{b}(\omega), \widehat{b}^\dagger(\omega)$. However, the cavity-reservoir coupling splits into many functions $\kappa_n(\omega)$, each centered around a resonance ω_n, with a finite width $\pi c/L$. It can be shown that this finite width leads to non-Markovian dynamics for the cavity mode operators $\widehat{c}_n$ in general, but in the case of a high-Q resonator, the cavity-reservoir coupling varies slowly compared to the intra-cavity field strength $|\mathcal{T}(\omega)|^2$, whose width Γ_n is then much smaller than $\pi c/L$. In that limit, the Markov approximation is valid.

A consequence of (2.1.38) is that, for a given mode, overlaps between its assigned reservoir coupling function and the neighboring mode resonances might happen. The high-Q limit prevents the overlaps because the reservoir coupling is far much smaller with a neighboring reservoir mode than with its own reservoir. However, when the quality factor Q decreases, this approach fails and one must consider the global shape of the reservoir, instead of writing the Hamiltonian (2.1.33). A more global approach is going to be of interest later in the manuscript, when studying the lossy plasmons coupled to quantum emitters. This derivation is also presented for cQED in section 2.2.

2.1.3 Three-level atoms in a cavity

The production of quantum light can be achieved with the use of attenuated laser sources. With low intensity lasers, one can design non-classical light beams, and nowadays such systems are being commercialized for quantum key distribution (QKD), using the horizontal and vertical polarization of anti-bunched photons as flying qubits [8]. With such non-classical sources, portable devices have been developed. The production of controlled single or N-photon states allows to generate entanglement and interference between them, hence quantum information and high security protocols for QKD.

Experiments with single quantum emitters, such as atoms, placed in an optical cavity showed anti-bunched and indistinguishable single photon signals [69]. Hence, we require models for understanding the interaction between single or few atoms with a quantized cavity field. Moreover, three-level atoms trapped in a cavity can be controlled by laser pulses (in the transverse direction with respect to the cavity axis), enabling the control of the single photon time envelope [70–73].
We derive the full Hamiltonian for N identical three-level atoms in a single leaky cavity mode. The atoms have a ground $|g\rangle$, a metastable$|f\rangle$ and an excited state $|e\rangle$, forming a set that we denote by $\mathcal{A}_N$. They are coupled to the linearly polarized cavity field, of volume V and frequency ω_c, through the atomic transition $|f\rangle \leftrightarrow |e\rangle$ of frequency ω_{ef} and dipole moment modulus d_{ef}, with the coupling factor (positioned at a maximum of the coupling):

$$g = \sqrt{\frac{\omega_c}{\hbar\epsilon_0 V}} d_{ef}. \tag{2.1.39}$$

It is assumed that g is constant for each atom. It is also assumed that the j-th atom is addressable with a laser field:

$$\mathbf{E}_j(t) = \mathcal{E}_j(t)\boldsymbol{\epsilon}_L \cos(\omega_L t + \varphi), \tag{2.1.40}$$

where $\mathcal{E}_j(t)$ is the field envelope, $\boldsymbol{\epsilon}_L$ is the field polarization, and ω_L the frequency of the laser field. For simplicity, we choose the laser polarization to be aligned with the dipole moment of the atom, and we write the (assumed real) pulse-shaped Rabi frequency of the laser:

$$\Omega_j(t) = -\frac{d_{eg}\mathcal{E}_j(t)}{2\hbar}, \tag{2.1.41}$$

on the transition $|g\rangle \leftrightarrow |e\rangle$ of frequency ω_{eg} and dipole moment d_{eg}. We also consider a two-photon resonance, that is we take the laser detuning $\Delta_L = \omega_{eg} - \omega_L$ being equal to the atom cavity detuning $\Delta_c = \omega_{ef} - \omega_c$. This leads to the identity $\omega_{gf} = \omega_c - \omega_L$. A sketch of the described system is shown in fig. 2.3, where we also displayed the intrinsic vacuum decay rates Γ_a of the individual atoms, and the cavity decay rate Γ_c.

The cavity field (denoted $\mathcal{C}$) and the output reservoir (denoted $\mathcal{R}_c$) are modeled with the Hamiltonian (2.1.33), where we drop the sum since we select a single mode (the other modes being too far from the atomic transition):

$$\widehat{H}_{\text{cav}} = \hbar\omega_c \widehat{c}^\dagger \widehat{c} + \int_0^{+\infty} \mathrm{d}\omega\, \hbar\omega\, \widehat{b}_\omega^\dagger \widehat{b}_\omega + i\hbar \int_0^{+\infty} \mathrm{d}\omega \Big(\kappa_c(\omega)\widehat{b}_\omega^\dagger \widehat{c} - \kappa_c^*(\omega)\widehat{c}^\dagger \widehat{b}_\omega\Big), \tag{2.1.42}$$

where $\kappa_c(\omega)$ is the cavity-output field coupling corresponding to (2.1.38), and we have chosen a compact notation $\widehat{b}(\omega) \to \widehat{b}_\omega$. To describe the atoms $\mathcal{A}_N$ and their decay outside of the cavity, we assume that they are all coupled to a three-dimensional reservoir $\mathcal{R}_\mathcal{F}$ featuring all the wave vectors $\mathbf{k}$ and the two corresponding transverse polarization vectors $\boldsymbol{\epsilon}_{\mathbf{k},\lambda}$ labelled with $\lambda = 1, 2$. For brevity of the derivation, we simplify the model considering the spontaneous emission only on the $|e\rangle \leftrightarrow |f\rangle$ transition. We further justify this simplification with the fact that, in practice, the degradation of the photon generation by the spontaneous emission is due to the $|e\rangle \leftrightarrow |f\rangle$ transition, since it removes the atoms from the pump cycle [74]. The

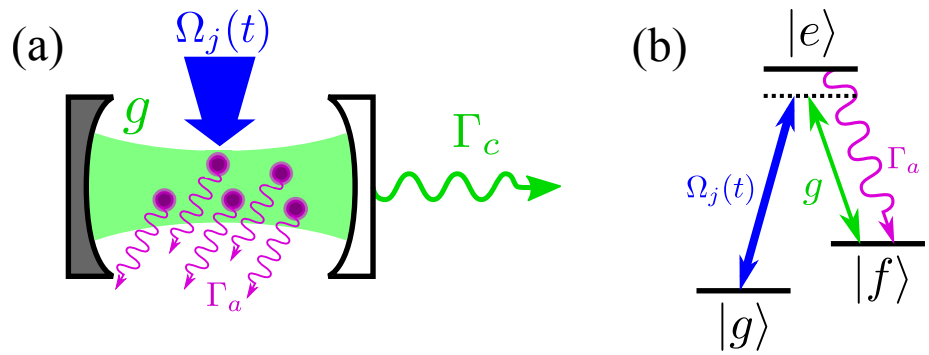

Figure 2.3: Representation of the cQED system: (a) N atoms in a cavity with atom-cavity coupling g, individual atomic decay rate Γ_a and decay rate Γ_c for the cavity field through the right (semi-transparent) mirror. The j-th atom is driven by a laser pulse of Rabi frequency $\Omega_j(t)$. (b) Three-level (or "Λ") linkage pattern of a single atom: transition $|g\rangle \leftrightarrow |e\rangle$ is driven with the laser pulse $\Omega_j(t)$ while transition $|f\rangle \leftrightarrow |e\rangle$ is coupled with the atom-cavity coupling g.

laser driven atoms and the vacuum reservoir modes are modeled with the RWA Hamiltonian:

$$\widehat{H}_{\rm at}(t) = \hbar \sum_{j=1}^{N} \Big(\Delta \widehat{\sigma}_{ee}^{(j)} + \Omega_j(t) \big(\widehat{\sigma}_{ge}^{(j)} + \widehat{\sigma}_{eg}^{(j)} \big) \Big) + \sum_{\lambda} \int {\rm d}^3 k \, \hbar \omega_k \, \widehat{b}_{\mathbf{k},\lambda}^{\dagger} \widehat{b}_{\mathbf{k},\lambda} + i\hbar\sqrt{N} \sum_{\lambda} \int {\rm d}^3 k \Big(g_{\mathbf{k},\lambda} \widehat{b}_{\mathbf{k},\lambda}^{\dagger} \widehat{\sigma} - g_{\mathbf{k},\lambda}^{*} \widehat{\sigma}^{\dagger} \widehat{b}_{\mathbf{k},\lambda} \Big) \quad (2.1.43)$$

with $\Delta = \Delta_L$, the atomic operators $\widehat{\sigma}_{k\ell}^{(j)} = (|k\rangle\langle\ell|)^{(j)}$ for the j-th atom, the collective atomic operator for transition $|e\rangle \leftrightarrow |f\rangle$:

$$\widehat{\sigma} = \frac{1}{\sqrt{N}} \sum_{j=1}^{N} \widehat{\sigma}_{fe}^{(j)}, \quad (2.1.44)$$

and the atom-field coupling for the outside mode $(\mathbf{k}, \lambda)$:

$$g_{\mathbf{k},\lambda} = -\sqrt{\frac{\omega_k}{2(2\pi)^3 \hbar \epsilon_0}} \mathbf{d}_{ef} \cdot \boldsymbol{\epsilon}_{\mathbf{k},\lambda}. \quad (2.1.45)$$

We used for $\widehat{H}_{\rm at}(t)$ the rotating frame defined by the unitary operator:

$$\widehat{U}_{\rm RW}(t) = \exp\Big[i\omega_L t \sum_{j=1}^{N} \widehat{\sigma}_{ee}^{(j)} + i\omega_{fg} t \sum_{j=1}^{N} \widehat{\sigma}_{ff}^{(j)} \Big]. \quad (2.1.46)$$

The last part of the Hamiltonian is the atom-cavity coupling:

$$\widehat{H}_{AC} = \hbar g \sqrt{N} \Big(\widehat{c}^{\dagger} \widehat{\sigma} + \widehat{\sigma}^{\dagger} \widehat{c} \Big), \quad (2.1.47)$$

and the Hamiltonian for the full system $\mathcal{A}_N \oplus \mathcal{C} \oplus \mathcal{R}_c \oplus \mathcal{R}_{\mathcal{F}}$ in the Schrödinger picture reads:

$$\boxed{\widehat{H}(t) = \widehat{H}_{\text{at}}(t) + \widehat{H}_{\text{cav}} + \widehat{H}_{AC}.} \tag{2.1.48}$$

The cavity and reservoir mode operators satisfy the commutation relations:

$$\left[\widehat{c}, \widehat{c}^\dagger\right] = 1 \tag{2.1.49a}$$

$$\left[\widehat{b}_\omega, \widehat{b}^\dagger_{\omega'}\right] = \delta(\omega - \omega') \tag{2.1.49b}$$

$$\left[\widehat{b}_{\mathbf{k},\lambda}, \widehat{b}^\dagger_{\mathbf{k}',\lambda'}\right] = \delta(\mathbf{k} - \mathbf{k}')\delta_{\lambda\lambda'}. \tag{2.1.49c}$$

We are going to derive the dynamics of the atoms-cavity system $\mathcal{S} = \mathcal{A}_N \oplus \mathcal{C}$, coupled to the reservoir $\mathcal{R} = \mathcal{R}_c \oplus \mathcal{R}_{\mathcal{F}}$. Our aim is to control the production of outgoing photons leaking from the cavity by driving specifically the atoms in the cavity, using external laser fields. The effective model is derived in two steps: first we define the outgoing photon flux which is connected to the quantum average of the Heisenberg time evolution of the cavity field number operator $\widehat{c}^\dagger\widehat{c}$. Next we derive a master equation of the system $\mathcal{S}$ by eliminating the reservoir degrees of freedom, which will allow the calculation of the quantum averages.

Equations of motion for the operators

Let $\widehat{X}$ be an arbitrary time-independent Schrödinger picture operator acting on the whole Hilbert space corresponding to the atoms, the cavity field, and the external reservoir: $\mathcal{H}_{\mathcal{S}} \otimes \mathcal{H}_{\mathcal{R}}$. The Heisenberg picture operator $\widehat{X}^{(H)}(t)$ is obtained using the propagator of the (here time-dependent) Schrödinger picture Hamiltonian $\widehat{H}(t)$:

$$\widehat{X}^{(H)}(t) = \widehat{U}^\dagger(t, t_0)\widehat{X}\widehat{U}(t, t_0), \tag{2.1.50a}$$

$$i\hbar\frac{\partial}{\partial t}\widehat{U}(t, t_0) = \widehat{H}(t)\widehat{U}(t, t_0). \tag{2.1.50b}$$

The Heisenberg equation provides the time evolution of the Heisenberg picture operator $\widehat{X}^{(H)}(t)$ through the equation:

$$\frac{\mathrm{d}\widehat{X}^{(H)}}{\mathrm{d}t} = -\frac{i}{\hbar}\left[\widehat{X}^{(H)}(t), \widehat{H}^{(H)}(t)\right], \tag{2.1.51}$$

where $\widehat{H}^{(H)}(t)$ is the Heisenberg picture operator of the Hamiltonian $\widehat{H}(t)$. From now on, we drop the superscript (H) of the Heisenberg picture operators for readability, and they will appear as $\widehat{X}^{(H)}(t) \equiv \widehat{X}(t)$, except if they are already time dependent in the Schrödinger picture (like the Hamiltonian). The Heisenberg-Langevin equations of motion for the reservoir operators and the cavity field operator are then:

$$\boxed{\begin{aligned} \dot{\widehat{b}}_\omega &= -i\omega\widehat{b}_\omega(t) + \kappa_c(\omega)\widehat{c}(t), && (2.1.52a)\\ \dot{\widehat{b}}_{\mathbf{k},\lambda} &= -i\omega_k\widehat{b}_{\mathbf{k},\lambda}(t) + g_{\mathbf{k},\lambda}\sqrt{N}\widehat{\sigma}(t), && (2.1.52b)\\ \dot{\widehat{c}} &= -i\omega_c\widehat{c}(t) - \int_0^{+\infty}\mathrm{d}\omega\,\kappa_c^*(\omega)\widehat{b}_\omega(t) - ig\sqrt{N}\widehat{\sigma}(t). && (2.1.52c)\end{aligned}}$$

2.1.4 Cavity input-output relation and photon flux

Integrating equation (2.1.52a) from the initial time t_0 to t, we define the integrated field operator, propagated to the position $z > 0$ of the detector:

$$\begin{aligned}\widehat{b}(z,t) &= \frac{1}{\sqrt{2\pi}}\int_0^{+\infty} \mathrm{d}\omega\, \widehat{b}_\omega(t)\mathrm{e}^{i\omega\frac{z}{c}} \\ &= \widehat{b}_{\mathrm{in}}\left(t-\tfrac{z}{c}\right) + \int_{t_0}^{t}\mathrm{d}t'\widehat{c}(t')\int_0^{+\infty}\mathrm{d}\omega\frac{\kappa_c(\omega)}{\sqrt{2\pi}}\mathrm{e}^{-i\omega(t-t_0-t')}\mathrm{e}^{i\omega\frac{z}{c}},\end{aligned} \tag{2.1.53}$$

with the *input* operator, defined as:

$$\widehat{b}_{\mathrm{in}}\left(t-\tfrac{z}{c}\right) = \frac{1}{\sqrt{2\pi}}\int_0^{+\infty}\mathrm{d}\omega\widehat{b}_\omega(t_0)\mathrm{e}^{-i\omega(t-t_0-\frac{z}{c})}, \tag{2.1.54}$$

corresponding to the solution of (2.1.52a) without the cavity mode. Consequently, we evaluate the following integral:

$$\begin{aligned}\mathcal{I} &= \int_0^{+\infty}\mathrm{d}\omega\frac{\kappa_c(\omega)}{\sqrt{2\pi}}\mathrm{e}^{-i\omega(t-t')}\mathrm{e}^{i\omega\frac{z}{c}} \\ &= -\frac{|\underline{t}|}{2\pi}\sqrt{\frac{c}{2L}}\int_0^{+\infty}\mathrm{d}\omega\frac{\sin[(\omega-\omega_c)\frac{L}{c}]}{(\omega-\omega_c)\frac{L}{c}}\mathrm{e}^{-i\omega(\frac{L}{c}-\frac{z}{c})}\mathrm{e}^{-i\omega(t-t')},\end{aligned} \tag{2.1.55}$$

where, for simplicity we set $t_0 = 0$. We introduce the variables $\widetilde{\omega} = \omega - \omega_c$ and $\widetilde{\tau} = t - t' - \frac{z}{c} + \frac{L}{c}$, and assume:

$$\int_0^{+\infty}\mathrm{d}\omega \to \int_{-\omega_c}^{+\infty}\mathrm{d}\widetilde{\omega} \approx \int_{-\infty}^{+\infty}\mathrm{d}\widetilde{\omega}, \tag{2.1.56}$$

as ω_c is very large compared to the width of the sinc function. We write now the integral:

$$\mathcal{I} = -\frac{|\underline{t}|}{2\pi}\sqrt{\frac{c}{2L}}\mathrm{e}^{-i\omega_c\widetilde{\tau}}\int_{-\infty}^{+\infty}\mathrm{d}\widetilde{\omega}\,\mathrm{e}^{-i\widetilde{\omega}\widetilde{\tau}}\mathrm{sinc}[\widetilde{\omega}\tfrac{L}{c}], \tag{2.1.57}$$

where we recognize the Fourier transform of the sinc function, which is computed using:

$$\int_{-\infty}^{+\infty}\mathrm{d}\widetilde{\omega}\,\mathrm{e}^{-i\widetilde{\omega}\widetilde{\tau}}\mathrm{sinc}[\widetilde{\omega}\tfrac{L}{c}] = \frac{\pi c}{2L}\Big(\mathrm{sgn}(\widetilde{\tau}+\tfrac{L}{c}) - \mathrm{sgn}(\widetilde{\tau}-\tfrac{L}{c})\Big). \tag{2.1.58}$$

Using the relation $\mathrm{sgn}(x) = 2\Theta(x) - 1$, where $\Theta(x)$ is the Heaviside step function, we find that the integral reads:

$$\mathcal{I} = -\frac{|\underline{t}|c}{2L}\sqrt{\frac{c}{2L}}\mathrm{e}^{-i\omega_c\widetilde{\tau}}\Big(\Theta(\widetilde{\tau}+\tfrac{L}{c}) - \Theta(\widetilde{\tau}-\tfrac{L}{c})\Big), \tag{2.1.59}$$

and back to the integrated operator, we have the following expression:

$$\begin{aligned}\widehat{b}(t-\tfrac{z}{c}) - \widehat{b}_{\mathrm{in}}(t-\tfrac{z}{c}) = -|\underline{t}|\sqrt{\frac{c}{2L}}\int_0^t \mathrm{d}t'\widehat{c}(t')\mathrm{e}^{-i\omega_c(t-t'-\frac{z}{c}+\frac{L}{c})} \\ \times\frac{c}{2L}\Big(\Theta(t-t'-\tfrac{z}{c}+\tfrac{2L}{c}) - \Theta(t-t'-\tfrac{z}{c})\Big).\end{aligned} \tag{2.1.60}$$

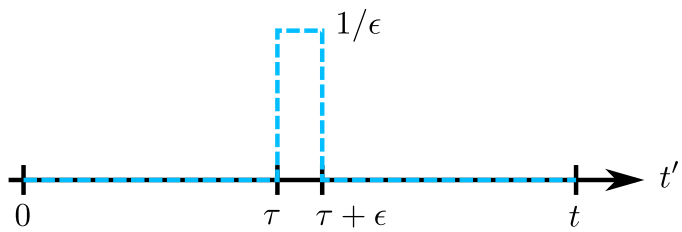

Figure 2.4: Rectangle function $\frac{1}{\epsilon}\big(\Theta(\tau)-\Theta(\tau+\epsilon)\big)$.

The integrand of the time integral is a function multiplied with a rectangle function $\frac{c}{2L}\big(\Theta(t-t'-\frac{z}{c}+\frac{2L}{c})-\Theta(t-t'-\frac{z}{c})\big)$ of width $2L/c$ (see fig. 2.4). The latter is equal to $-c/2L$ between $t-\frac{z}{c}$ and $t-\frac{z}{c}+\frac{2L}{c}$, and zero elsewhere. With the hypothesis of non-resolved time of flight $\epsilon = 2L/c$, the dynamics happens on a time scale which is much larger. Hence, we have $|t-\frac{z}{c}| \gg \epsilon$. In the integral, we can take the limit $\epsilon \to 0^+$ of the rectangle function, whose area is 1:

$$\lim_{\epsilon\to 0^+}\frac{1}{\epsilon}\Big(\Theta(t-t'-\tfrac{z}{c}+\epsilon)-\Theta(t-t'-\tfrac{z}{c})\Big)=\delta(t-t'-\tfrac{z}{c}). \tag{2.1.61}$$

Finally, replacing in the integral we get, for $z > 2L$:

$$\widehat{b}(t-\tfrac{z}{c})-\widehat{b}_{\text{in}}(t-\tfrac{z}{c})=|\underline{t}|\sqrt{\frac{c}{2L}}\widehat{c}(t-\tfrac{z}{c}). \tag{2.1.62}$$

This calculation is justified since for $z > 0$, and $t' \in [0,t]$, the inequality $0 < t-\frac{z}{c}-t' < t$ holds. In the cavity response function, the decay rate Γ_c is $|\underline{t}|^2 c/2L$ in the high quality resonator limit. Hence, we write:

$$\boxed{\widehat{b}(t-\tfrac{z}{c})-\widehat{b}_{\text{in}}(t-\tfrac{z}{c})=\sqrt{\Gamma_c}\widehat{c}(t-\tfrac{z}{c}),} \tag{2.1.63}$$

which is the input-output formula. We also underline that the "Markov approximation" relation: $2\pi|\kappa_c(\omega_c)|^2 = \Gamma_c$ is retrieved, with the use of (2.1.38), and that the result is not well-defined when $0 \leqslant z \leqslant 2L$.

Poynting vector and photon flux

Measurements are done with a photodetector, at position z. The observable we are interested in is the averaged photon flux, which we derive here. The energy carried by the photons leaking from the cavity can be characterized by the Poynting vector operator in the Heisenberg picture [76], where we have assumed a propagation with increasing z and the cavity emitter at position $z = 0$ (see fig. 2.5). We define an observable corresponding to the Poynting vector:

$$\widehat{S}(z,t)=\frac{\hbar}{2\pi\mathcal{A}}\int_0^{+\infty}\mathrm{d}\omega\int_0^{+\infty}\mathrm{d}\omega'\sqrt{\omega\omega'}\,\widehat{b}^\dagger_\omega(t)\widehat{b}_{\omega'}(t)\mathrm{e}^{-i(\omega-\omega')\frac{z}{c}}, \tag{2.1.64}$$

with the use of the quantized electric and magnetic fields [77–79] and $\mathcal{A}$ is the area of the free field modes. The time dependence of the Poynting vector arises from the Heisenberg

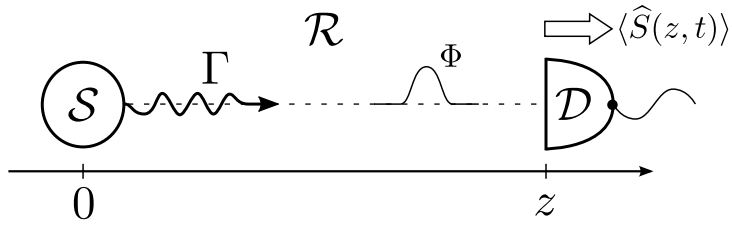

Figure 2.5: Sketch of the photodetection process: the source system $\mathcal{S}$ emits a photon with decay rate Γ at position 0, towards a detector $\mathcal{D}$ at a position z through the reservoir $\mathcal{R}$. The photon flux Φ is measured using the data on the averaged quantum Poynting vector $\langle\widehat{S}(z,t)\rangle$.

picture operators $\widehat{b}_\omega(t)$, that we get from the integration of equation (2.1.52a), as it was done precedingly for the integrated reservoir operators. The photodetection process is related with the quantum average of Poynting vector flux, as depicted in fig. 2.5, hence we are interested in computing the following expression:

$$\begin{aligned}\left\langle\widehat{S}(z,t)\right\rangle &= \langle\psi(0)|\widehat{S}(z,t)|\psi(0)\rangle \\ &= \left(\sqrt{\frac{\hbar}{2\pi\mathcal{A}}}\int_0^{+\infty}\mathrm{d}\omega\sqrt{\omega}\ \mathrm{e}^{-i\omega\frac{z}{c}}\langle\psi(0)|\widehat{b}^\dagger_\omega(t)\right)\left(\sqrt{\frac{\hbar}{2\pi\mathcal{A}}}\int_0^{+\infty}\mathrm{d}\omega\sqrt{\omega}\ \mathrm{e}^{i\omega\frac{z}{c}}\widehat{b}_\omega(t)|\psi(0)\rangle\right),\end{aligned} \tag{2.1.65}$$

where $|\psi(0)\rangle$ is the initial time field wavefunction for the system and the exterior. We see from the latter expression that we have to evaluate only one integral in ω and then write the scalar product with itself to get the average Poynting vector. Moreover, the initial time wavefunction is chosen to be the vacuum state for the exterior: $|\psi(0)\rangle = |\psi_{\mathcal{S}}(0), \mathbf{0}\rangle$, therefore all terms containing $\widehat{b}_\omega(0)$ will vanish since $\widehat{b}_\omega(0)|\mathbf{0}\rangle = 0$.
The integration of (2.1.52a) then leads to the following integral, where we exchange the order of the time and the frequency integrals:

$$\begin{aligned}|\mathcal{I}_S(t)\rangle &= \sqrt{\frac{\hbar}{2\pi\mathcal{A}}}\int_0^{+\infty}\mathrm{d}\omega\sqrt{\omega}\ \mathrm{e}^{i\omega\frac{z}{c}}\widehat{b}_\omega(t)|\psi(0)\rangle \\ &= -\frac{|\underline{t}|}{2\pi}\sqrt{\frac{\hbar c}{2\mathcal{A}L}}\int_0^t \mathrm{d}t'\widehat{c}(t')\int_0^{+\infty}\mathrm{d}\omega\sqrt{\omega}\kappa_c(\omega)\mathrm{e}^{-i\omega\left(t-t'-\frac{z}{c}+\frac{L}{c}\right)}|\psi(0)\rangle.\end{aligned} \tag{2.1.66}$$

We notice that the frequency integral factor is very similar to expression (2.1.55) derived in the preceding section, the only difference being a $\sqrt{\omega}$ factor in the integrand. Therefore, we use the same change of variables as was done for the calculation of (2.1.55), leading to the Fourier transform:

$$\int_{-\infty}^{+\infty}\mathrm{d}\widetilde{\omega}\sqrt{\widetilde{\omega}+\omega_c}\mathrm{e}^{-i\widetilde{\omega}\widetilde{\tau}}\mathrm{sinc}[\widetilde{\omega}\tfrac{L}{c}] = \sqrt{\omega_c}\frac{\pi c}{L}\Big(\Theta(\widetilde{\tau}+\tfrac{L}{c})-\Theta(\widetilde{\tau}-\tfrac{L}{c})\Big), \tag{2.1.67}$$

where we have used the expression of the coupling (2.1.38) and the approximation (2.1.56). Using the limit $\epsilon \to 0^+$ where $\epsilon = 2L/c$, as was done above, a delta function appears in the time integral, leading to the result (valid for $z > 0$):

$$|\mathcal{I}_S(t)\rangle = -\sqrt{\frac{\hbar\omega_c\Gamma_c}{\mathcal{A}}}\ \widehat{c}\big(t-\tfrac{z}{c}\big)|\psi(0)\rangle. \tag{2.1.68}$$

The quantum average of the Poynting vector is finally:

$$\left\langle \widehat{S}(z,t)\right\rangle = \langle \mathcal{I}_S(t)|\mathcal{I}_S(t)\rangle = \frac{\hbar\omega_c\Gamma_c}{\mathcal{A}}\langle\psi(0)|\widehat{c}^\dagger\big(t-\tfrac{z}{c}\big)\widehat{c}\big(t-\tfrac{z}{c}\big)|\psi(0)\rangle. \tag{2.1.69}$$

For a given state, the amount of energy going through the field mode area $\mathcal{A}$ during the time $\mathrm{d}t$ is the quantum average of the flux of the Poynting vector:

$$\mathcal{A}\langle\widehat{S}(z,t)\rangle\mathrm{d}t = \hbar\omega_c\Gamma_c\big\langle\widehat{c}^\dagger\big(t-\tfrac{z}{c}\big)\widehat{c}\big(t-\tfrac{z}{c}\big)\big\rangle\mathrm{d}t. \tag{2.1.70}$$

Normalizing by $\hbar\omega_c$, we get the averaged number of photons $\mathrm{d}n(z,t) = \Gamma_c\big\langle\widehat{c}^\dagger\big(t-\frac{z}{c}\big)\widehat{c}\big(t-\frac{z}{c}\big)\big\rangle\mathrm{d}t$ going through the mode area during $\mathrm{d}t$, defining the photon flux:

$$\boxed{\Phi\left(t-\tfrac{z}{c}\right) = \frac{\mathrm{d}n}{\mathrm{d}t}\left(t-\tfrac{z}{c}\right) = \Gamma_c\big\langle\,\widehat{c}^\dagger\left(t-\tfrac{z}{c}\right)\widehat{c}\left(t-\tfrac{z}{c}\right)\big\rangle.} \tag{2.1.71}$$

This key result shows that one can determine the flux from the quantum average of the dynamics of the cavity photon number in the Heisenberg picture [72]. Later in this chapter, we derive the effective master equation reduced to the system $\mathcal{S}$ which is used to calculate the flux (2.1.71).
We have derived the key quantity to describe the absorption of a photon by a photodetector. In the next subsection, we treat the atomic spontaneous emission process.

2.1.5 Heisenberg treatment of spontaneous emission

Having derived the effective Heisenberg operator for the transmission of the field through the semi-transparent mirror, we may now derive, at $z = 0$, the integrated field operator corresponding to the transverse three-dimensional reservoir:

$$\widehat{b}_{\mathcal{F}}(t) = \sum_\lambda \int \mathrm{d}^3k\, g^*_{\mathbf{k},\lambda}\widehat{b}_{\mathbf{k},\lambda}(t). \tag{2.1.72}$$

This operator models the dynamics of the spontaneous emission of the transition $|e\rangle \leftrightarrow |f\rangle$, corresponding to the emission of photons outside of the cavity mode. We formally integrate equation (2.1.52b) to get:

$$\widehat{b}_{\mathbf{k},\lambda}(t) = \mathrm{e}^{-i\omega_k(t-t_0)}\widehat{b}_{\mathbf{k},\lambda}(t_0) + g_{\mathbf{k},\lambda}\sqrt{N}\int_{t_0}^{t}\mathrm{d}t'\widehat{\sigma}(t')\mathrm{e}^{-i\omega_k(t-t_0-t')}. \tag{2.1.73}$$

Inserting this result in the definition of the integrated field operator yields:

$$\widehat{b}_{\mathcal{F}}(t) = \widehat{b}_{\mathcal{F},\mathrm{in}}(t) + \sqrt{N}\sum_\lambda\int \mathrm{d}^3k\,|g_{\mathbf{k},\lambda}|^2\int_{t_0}^{t}\mathrm{d}t'\widehat{\sigma}(t')\mathrm{e}^{-i\omega_k(t-t_0-t')} \tag{2.1.74a}$$

$$\widehat{b}_{\mathcal{F},\mathrm{in}}(t) = \sum_\lambda\int \mathrm{d}^3k\, g^*_{\mathbf{k},\lambda}\widehat{b}_{\mathbf{k},\lambda}(t_0)\mathrm{e}^{-i\omega_k(t-t_0)}, \tag{2.1.74b}$$

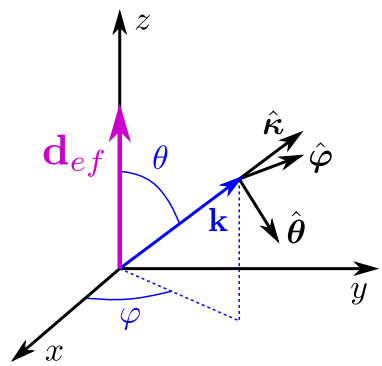

Figure 2.6: Transition dipole moment $\mathbf{d}_{ef} = d_{ef}\hat{\mathbf{z}}$ of a single atom. The $\mathbf{k}$-vector is represented in spherical coordinates with the unit vectors $(\hat{\boldsymbol{\kappa}}, \hat{\boldsymbol{\theta}}, \hat{\boldsymbol{\varphi}})$, and has an angle θ with the dipole moment.

and exchanging the order of the two integrals, we write:

$$\widehat{b}_{\mathcal{F}}(t) = \widehat{b}_{\mathcal{F},\text{in}}(t) + \sqrt{N}\int_{t_0}^{t} \mathrm{d}t'\widehat{\sigma}(t')\mathcal{I}(t-t') \tag{2.1.75a}$$

$$\mathcal{I}(t-t') = \sum_{\lambda}\int \mathrm{d}^3k\,|g_{\mathbf{k},\lambda}|^2 \mathrm{e}^{-i\omega_k(t-t_0-t')}. \tag{2.1.75b}$$

We evaluate the integral $\mathcal{I}(t-t')$ using the expression of the atom-field coupling (2.1.45):

$$\mathcal{I}(t-t') = \frac{1}{2(2\pi)^3\hbar\epsilon_0}\sum_{\lambda}\int \mathrm{d}^3k\,\omega_k|\mathbf{d}_{ef}\cdot\boldsymbol{\epsilon}_{\mathbf{k},\lambda}|^2\mathrm{e}^{-i\omega_k(t-t_0-t')}. \tag{2.1.76}$$

For simplicity, we choose the dipole moment $\mathbf{d}_{ef}$ to be aligned with the z-axis, as depicted in fig. 2.6. Using the law of cosines, we write the scalar product:

$$\sum_{\lambda=1,2}|\mathbf{d}_{ef}\cdot\boldsymbol{\epsilon}_{\mathbf{k},\lambda}|^2 = d_{ef}^2(1-\cos^2\theta), \tag{2.1.77}$$

and expanding the three-dimensional integral over $\mathbf{k}$ in spherical coordinates, the angular part in $\mathcal{I}(t-t')$ factorizes and becomes:

$$\int_0^{2\pi}\mathrm{d}\varphi\int_0^{\pi}\mathrm{d}\theta\sin\theta(1-\cos^2\theta) = \frac{8\pi}{3}. \tag{2.1.78}$$

The integrated operator assumes now a simpler form:

$$\widehat{b}_{\mathcal{F}}(t) = \widehat{b}_{\mathcal{F},\text{in}}(t) + \sqrt{N}\frac{d_{ef}^2}{6\pi^2\hbar\epsilon_0 c^3}\int_{t_0}^{t}\mathrm{d}t'\widehat{\sigma}(t')\int_0^{+\infty}\mathrm{d}\omega_k\,\omega_k^3\mathrm{e}^{-i\omega_k(t-t_0-t')}, \tag{2.1.79}$$

where the integrals are evaluated using a the rotating frame $\widehat{\sigma}(t') \to \widetilde{\sigma}(t')\mathrm{e}^{-i\omega_{ef}t'}$ and the change of variables $\Delta_k = \omega_k - \omega_{ef}$. The integral over Δ_k runs from $-\omega_{ef}$ to $+\infty$, but we allow the extension of the lower bound to $-\infty$ since ω_{ef} is large. Moreover, this integral has a

large contribution around ω_{ef} and negligible contribution far away from this frequency, hence it can be approximated with a Dirac delta function:

$$\int_{-\infty}^{+\infty} \mathrm{d}\Delta_k (\Delta_k + \omega_{ef})^3 \mathrm{e}^{-i\Delta_k(t-t_0-t')} \approx 2\pi\omega_{ef}^3 \delta(t - t_0 - t'). \tag{2.1.80}$$

Finally, replacing the latter in the integrated operator formula yields:

$$\boxed{\widehat{b}_{\mathcal{F}}(t) = \widehat{b}_{\mathcal{F},\mathrm{in}}(t) + \sqrt{N}\frac{\Gamma_a}{2}\widehat{\sigma}(t),} \tag{2.1.81}$$

where Γ_a is the atomic vacuum decay rate corresponding to spontaneous emission with transition $|e\rangle \leftrightarrow |f\rangle$:

$$\Gamma_a = \frac{d_{ef}^2 \omega_{ef}^3}{3\hbar\pi\epsilon_0 c^3}. \tag{2.1.82}$$

2.1.6 Master equation

To compute the dynamics of the atom-cavity system, and therefore get the time-dependent photon flux, we have to derive the master equation. We recall for completeness the standard way to derive it, as done in refs. [75, 80–82]. Let $\widehat{X}_{\mathcal{S}}$ be an arbitrary operator acting on the inside cavity field and the atomic Hilbert spaces. The Heisenberg picture of an arbitrary operator reads:

$$\widehat{X}_{\mathcal{S}}(t) = \widehat{U}^\dagger(t,t_0)\widehat{X}_{\mathcal{S}}\widehat{U}(t,t_0), \quad \widehat{X}_{\mathcal{S}} \text{ acting on } \mathcal{H}_{\mathcal{S}} = \mathcal{H}_{\mathcal{A}_N} \otimes \mathcal{H}_{\mathcal{C}}. \tag{2.1.83}$$

The Heisenberg time evolution of this operator is described by the equation (we drop the time argument t for readability):

$$\begin{aligned}\dot{\widehat{X}}_{\mathcal{S}} = -\frac{i}{\hbar}\big[\widehat{X}_{\mathcal{S}}, \widehat{H}_{\mathcal{S}}^{(H)}\big] + \int_0^{+\infty} \mathrm{d}\omega \left(\kappa_c(\omega)\widehat{b}_\omega^\dagger\big[\widehat{X}_{\mathcal{S}}, \widehat{c}\big] - \kappa_c^*(\omega)\big[\widehat{X}_{\mathcal{S}}, \widehat{c}^\dagger\big]\widehat{b}_\omega\right) \\ + \sqrt{N}\sum_\lambda \int \mathrm{d}^3k \left(g_{\mathbf{k},\lambda}\widehat{b}_{\mathbf{k},\lambda}^\dagger\big[\widehat{X}_{\mathcal{S}}, \widehat{\sigma}\big] - g_{\mathbf{k},\lambda}^*\big[\widehat{X}_{\mathcal{S}}, \widehat{\sigma}^\dagger\big]\widehat{b}_{\mathbf{k},\lambda}\right),\end{aligned} \tag{2.1.84}$$

where $\widehat{H}_{\mathcal{S}}^{(H)} \equiv \widehat{H}_{\mathcal{S}}^{(H)}(t) = \widehat{U}^\dagger(t,t_0)\widehat{H}_{\mathcal{S}}(t)\widehat{U}(t,t_0)$ is the Heisenberg picture system Hamiltonian whose Schrödinger picture is also time-dependent due to the laser fields:

$$\widehat{H}_{\mathcal{S}}(t) = \widehat{H}_A(t) + \widehat{H}_C + \widehat{H}_{AC} \tag{2.1.85a}$$

$$\widehat{H}_A(t) = \hbar\sum_{j=1}^N \left(\Delta\widehat{\sigma}_{ee}^{(j)} + \Omega_j(t)\big(\widehat{\sigma}_{ge}^{(j)} + \widehat{\sigma}_{eg}^{(j)}\big)\right) \tag{2.1.85b}$$

$$\widehat{H}_C = \hbar\omega_c\widehat{c}^\dagger\widehat{c}, \tag{2.1.85c}$$

and $\widehat{H}_{AC}$ is given in (2.1.47). We now insert the integrated Heisenberg operator (2.1.81) derived in the preceding section into the equation of motion, and in the second term on the

right hand side of equation (2.1.84), we insert the formal integration of equation (2.1.52a) to evaluate the integral:

$$\int_0^{+\infty} \mathrm{d}\omega\ \kappa_c^*(\omega)\widehat{b}_\omega(t) = \widehat{b}'_{\mathrm{in}}(t) + \mathcal{I}(t) \tag{2.1.86a}$$

$$\widehat{b}'_{\mathrm{in}}(t) = \int_0^{+\infty} \mathrm{d}\omega\ \kappa_c^*(\omega)\widehat{b}_\omega(0)\mathrm{e}^{-i\omega t} \tag{2.1.86b}$$

$$\mathcal{I}(t) = \int_0^t \mathrm{d}t'\widehat{c}(t') \int_0^{+\infty} \mathrm{d}\omega|\kappa_c(\omega)|^2\mathrm{e}^{-i\omega(t-t')} \tag{2.1.86c}$$

We note that the introduced $\widehat{b}'_{\mathrm{in}}(t)$ is a different definition from the input expression (2.1.54) for $z = 0$, as here it is integrated jointly with the coupling $\kappa_c(\omega)$. The integral that is met is similar to the previous (2.1.55) ($t_0 = 0$ here), the only difference being that we have replace $\kappa_c(\omega)$ by its square modulus. We have also exchanged the order of the time and frequency integrals. In an analogous way, we write the frequency integral:

$$\mathcal{I}'(\widetilde{\tau}) = \frac{\Gamma_c}{2\pi}\mathrm{e}^{-i\omega_c\widetilde{\tau}} \int_{-\infty}^{+\infty} \mathrm{d}\widetilde{\omega}\, \mathrm{e}^{-i\widetilde{\omega}\widetilde{\tau}}\mathrm{sinc}^2[\widetilde{\omega}\tfrac{L}{c}], \tag{2.1.87}$$

where we used the variables $\widetilde{\omega} = \omega - \omega_c$ and $\widetilde{\tau} = t - t' + \frac{L}{c}$. This time, we have to evaluate the Fourier transform of the sinc^2 function, which is a triangular function:

$$\int_{-\infty}^{+\infty} \mathrm{d}\widetilde{\omega}\, \mathrm{e}^{-i\widetilde{\omega}\widetilde{\tau}}\mathrm{sinc}^2[\widetilde{\omega}\tfrac{L}{c}] = \frac{c}{L}\mathrm{tri}\left(\frac{\widetilde{\tau}c}{2\pi L}\right), \tag{2.1.88}$$

and the triangular function is defined through ($T > 0$):

$$\mathrm{tri}\left(\frac{t}{T}\right) = \begin{cases} 1 - |t|/T & \text{if } |t| \leqslant T \\ 0 & \text{elsewhere} \end{cases}. \tag{2.1.89}$$

Hence, we have now:

$$\mathcal{I}'(\widetilde{\tau}) = \frac{\Gamma_c}{2\pi}\mathrm{e}^{-i\omega_c\widetilde{\tau}}\frac{c}{L}\mathrm{tri}\left(\frac{\widetilde{\tau}c}{2\pi L}\right), \tag{2.1.90}$$

and we must now integrate it over time, through the original integral:

$$\mathcal{I}(t) = \Gamma_c \int_0^t \mathrm{d}t'\widehat{c}(t')\mathrm{e}^{-i\omega_c(t-t'+\frac{\epsilon}{2})}\frac{1}{\pi\epsilon}\mathrm{tri}\left(\frac{t-t'+\frac{\epsilon}{2}}{\pi\epsilon}\right), \tag{2.1.91}$$

where we used $\epsilon = 2L/c$. Taking the limit $\epsilon \to 0^+$, we have to integrate function $\widehat{c}(t')\mathrm{e}^{-i\omega_c(t-t'+\frac{\epsilon}{2})}$ over a very narrow time domain $[t - \pi\epsilon, t + \pi\epsilon]$ corresponding to the triangle function, which approaches the Dirac delta function:

$$\lim_{\epsilon\to 0^+}\frac{1}{\pi\epsilon}\mathrm{tri}\left(\frac{t-t'+\frac{\epsilon}{2}}{\pi\epsilon}\right) = \delta(t-t'). \tag{2.1.92}$$

The initial triangle function being centered on $t + \frac{\epsilon}{2}$, taking the limit leads to a Dirac delta function centered on t. However, this leads to the strange result (see, e.g. [67]):

$$\int_0^t \mathrm{d}t'\varphi(t')\delta(t-t') = ? \tag{2.1.93}$$

To overcome this, we underline that the triangle function, centered around t, is then half-integrated. As a consequence, and because the triangular function is symmetric in time, we can extend the upper bound of the integral to $+\infty$, as $\mathrm{tri}((t-t'+\frac{\epsilon}{2})/\pi\epsilon)=0$ when $t'>t+\pi\epsilon$, and divide the integral by two, as we now integrate over the whole triangle. Then, taking the limit $\epsilon\to 0^+$:

$$\begin{aligned}\mathcal{I}(t) &= \Gamma_c \lim_{\epsilon\to 0^+}\int_0^t \mathrm{d}t'\widehat{c}(t')\mathrm{e}^{-i\omega_c(t-t'+\frac{\epsilon}{2})}\frac{1}{\pi\epsilon}\mathrm{tri}\left(\frac{t-t'+\frac{\epsilon}{2}}{\pi\epsilon}\right)\\ &= \frac{\Gamma_c}{2}\int_0^{+\infty}\mathrm{d}t'\widehat{c}(t')\mathrm{e}^{-i\omega_c(t-t')}\delta(t-t')\\ &= \frac{\Gamma_c}{2}\widehat{c}(t),\end{aligned} \tag{2.1.94}$$

which is the expected result. Equation (2.1.84) then turns into:

$$\begin{aligned}\dot{\widehat{X}}_{\mathcal{S}} = -\frac{i}{\hbar}\big[\widehat{X}_{\mathcal{S}},\widehat{H}_{\mathcal{S}}^{(H)}\big] + \mathcal{D}_{\mathrm{in}}^{\dagger}\big[\widehat{X}_{\mathcal{S}}\big] + N\Gamma_a\Big(\widehat{\sigma}^{\dagger}\widehat{X}_{\mathcal{S}}\widehat{\sigma} - \tfrac{1}{2}\widehat{X}_{\mathcal{S}}\widehat{\sigma}^{\dagger}\widehat{\sigma} - \tfrac{1}{2}\widehat{\sigma}^{\dagger}\widehat{\sigma}\widehat{X}_{\mathcal{S}}\Big)\\ + \Gamma_c\Big(\widehat{c}^{\dagger}\widehat{X}_{\mathcal{S}}\widehat{c} - \tfrac{1}{2}\widehat{X}_{\mathcal{S}}\widehat{c}^{\dagger}\widehat{c} - \tfrac{1}{2}\widehat{c}^{\dagger}\widehat{c}\widehat{X}_{\mathcal{S}}\Big),\end{aligned} \tag{2.1.95}$$

with $\mathcal{D}_{\mathrm{in}}^{\dagger}\big[\widehat{X}_{\mathcal{S}}\big] = \sqrt{N}\big(\widehat{b}_{\mathcal{F},\mathrm{in}}^{\dagger}\big[\widehat{X}_{\mathcal{S}},\widehat{\sigma}\big] - \big[\widehat{X}_{\mathcal{S}},\widehat{\sigma}^{\dagger}\big]\widehat{b}_{\mathcal{F},\mathrm{in}}\big) + \widehat{b}_{\mathrm{in}}'^{\dagger}\big[\widehat{X}_{\mathcal{S}},\widehat{c}\big] - \big[\widehat{X}_{\mathcal{S}},\widehat{c}^{\dagger}\big]\widehat{b}_{\mathrm{in}}'$ being the initial field reservoir contribution. From this expression, we get to the master equation by transforming it to the Schrödinger picture. To do so, we define the expectation value of $\widehat{X}_{\mathcal{S}}$:

$$\big\langle\widehat{X}_S\big\rangle(t) = \mathrm{Tr}_S\Big\{\widehat{X}_S\widehat{\varrho}_S(t)\Big\} = \mathrm{Tr}\Big\{\widehat{X}_S(t)\widehat{\varrho}(t_0)\Big\}, \tag{2.1.96}$$

where $\widehat{\varrho}(t_0)=\widehat{\varrho}_{\mathcal{S}}(t_0)\otimes\widehat{\varrho}_{\mathcal{R}}(t_0)$ is the complete density operator and $\widehat{\varrho}_S(t)=\mathrm{Tr}_R\{\widehat{\varrho}(t)\}$ is the reduced density operator describing $\mathcal{S}$ with partial trace $\mathrm{Tr}_R\{\cdot\}$ eliminating the degrees of freedom corresponding to the reservoir. We here assume that the reservoir is initially a vacuum state $\widehat{\varrho}_{\mathcal{R}}(t_0)\equiv|\mathbf{0}\rangle\langle\mathbf{0}|$ such that $\mathcal{D}_{\mathrm{in},t}^{\dagger}[\cdot]$ cancels out in average. Finally, averaging equation (2.1.84), using (2.1.96), the cyclic property of the trace, and the property $\forall A\ \mathrm{Tr}\{AB\}=\mathrm{Tr}\{AC\}\Leftrightarrow B=C$, we find the Lindblad master equation for $\widehat{\varrho}_{\mathcal{S}}(t)$:

$$\boxed{\begin{aligned}\frac{\mathrm{d}}{\mathrm{d}t}\widehat{\varrho}_{\mathcal{S}}(t) = -\frac{i}{\hbar}[\widehat{H}_{\mathcal{S}}(t),\widehat{\varrho}_{\mathcal{S}}(t)] + N\Gamma_a\Big(\widehat{\sigma}\widehat{\varrho}_S(t)\widehat{\sigma}^{\dagger} - \tfrac{1}{2}\{\widehat{\sigma}^{\dagger}\widehat{\sigma},\widehat{\varrho}_S(t)\}\Big)\\ + \Gamma_c\Big(\widehat{c}\widehat{\varrho}_S(t)\widehat{c}^{\dagger} - \tfrac{1}{2}\{\widehat{c}^{\dagger}\widehat{c},\widehat{\varrho}_{\mathcal{S}}(t)\}\Big),\end{aligned}} \tag{2.1.97}$$

where, here, all Schrödinger system operators $\widehat{\sigma},\widehat{c}$ are time-independent. If several cavities are considered, where the output of one cavity is fed into that of the next cavity, the systems can be "cascaded" [70,75,81]. In the following sections, we assume that the atoms are strongly coupled to the cavity mode and neglect for simplicity the transverse decay: $\Gamma_a\ll g,\Gamma_c$.

2.2 An alternative derivation of the cQED effective model

Starting from the general quantization procedure developed in section 2.1.1, we derive an alternative form of the effective model corresponding to Hamiltonian (2.1.33). In the preceding

sections, we quantized the global field and derived effective perfect cavity field operators $\widehat{c}_n, \widehat{c}_n^\dagger$ coupled to a flat reservoir whose excitations are toggled by $\widehat{b}(\omega), \widehat{b}^\dagger(\omega)$, and lastly we described the interaction of the inside cavity field with atoms. The field in and out of the cavity must match at the boundaries, and it does in the high-Q limit when we consider first order series expansion in $|\underline{\mathrm{t}}|^2$. The alternative derivation we present here is different in the order of the procedure steps: we start with the global field operators $\widehat{a}(\omega), \widehat{a}^\dagger(\omega)$ corresponding to the classical mode $\Phi(x,\omega)$ given by equation (2.1.29), and describe its interaction with a single atom when it is placed inside of the cavity.

2.2.1 Atom-field interaction

The global field operator, considering a rectilinear polarization, has the form:

$$\widehat{E}(x) = i\int_0^{+\infty} \mathrm{d}\omega \sqrt{\frac{\hbar\omega}{2\epsilon_0}}\Big(\Phi(x,\omega)\widehat{a}(\omega) - \Phi^*(x,\omega)\widehat{a}^\dagger(\omega)\Big). \tag{2.2.1}$$

We recall that the mode function $\Phi(x,\omega)$ satisfies the eigenvalue equation (2.1.11), and as it is also normalized it verifies:

$$\langle \Phi(\omega), \Phi(\omega')\rangle = \delta(\omega-\omega'). \tag{2.2.2}$$

Operators $\widehat{a}(\omega), \widehat{a}^\dagger(\omega)$ then have the commutation relations:

$$\big[\widehat{a}(\omega), \widehat{a}^\dagger(\omega')\big] = \delta(\omega-\omega'), \tag{2.2.3a}$$

$$\big[\widehat{a}(\omega), \widehat{a}(\omega')\big] = \big[\widehat{a}^\dagger(\omega), \widehat{a}^\dagger(\omega')\big] = 0. \tag{2.2.3b}$$

For notational preference we choose to write the mode function as a sum of two terms, corresponding to the inside ($-\ell \leqslant x < 0$) and the outside field ($x \geqslant \delta_m$) [see (2.1.29)]:

$$\Phi(x,\omega) = \Phi_{\mathrm{in}}(x,\omega) + \Phi_{\mathrm{out}}(x,\omega), \tag{2.2.4a}$$

$$\Phi_{\mathrm{in}}(x,\omega) = \frac{-2i}{\sqrt{2\pi c\mathcal{A}}}\chi_{[-\ell,0]}(x)\sin\big[\tfrac{\omega}{c}(x+\ell)\big]\mathrm{e}^{i\frac{\omega}{c}\ell}\mathcal{T}(\omega), \tag{2.2.4b}$$

$$\Phi_{\mathrm{out}}(x,\omega) = \frac{-1}{\sqrt{2\pi c\mathcal{A}}}\Theta(x-\delta_m)\Big(\mathrm{e}^{-i\frac{\omega}{c}x} + \mathrm{e}^{i\frac{\omega}{c}x}\big[\underline{\mathrm{r}}(\omega) - \underline{\mathrm{t}}(\omega)\mathrm{e}^{i2\frac{\omega}{c}L}\mathcal{T}(\omega)\big]\Big), \tag{2.2.4c}$$

where we introduced a characteristic function $\chi_{[-\ell,0]}(x) = 1$ for $x \in [-\ell, 0]$, 0 otherwise, and a Heaviside function. In the high-Q limit, the cavity response function behaves as a sum of Lorentzians whose widths Γ_m are much smaller than the spacing $\Delta\omega = \pi c/L$ between the resonance frequencies. Up to a global phase depending on the optical path $n\delta_m$ in the semi-transparent mirror [68], the cavity response function reads, in this limit [see (2.1.32)]:

$$\mathcal{T}(\omega) = \sum_m \mathcal{T}_m(\omega) = \sum_m \sqrt{\frac{c}{2L}}\frac{\sqrt{\Gamma_m}}{\omega - \widetilde{\omega}_m + i\frac{\Gamma_m}{2}} + \mathcal{O}(|\underline{\mathrm{t}}|^2), \tag{2.2.5}$$

where $L = \ell + \delta_m \approx \ell$ as $\delta_m \ll \ell$. The mode-selective response functions $\mathcal{T}_m(\omega)$, in regard of (2.1.32), have the property:

$$\mathcal{T}_m^*(\omega)\mathcal{T}_{m'}(\omega) = \delta_{mm'}|\mathcal{T}_m(\omega)|^2. \tag{2.2.6}$$

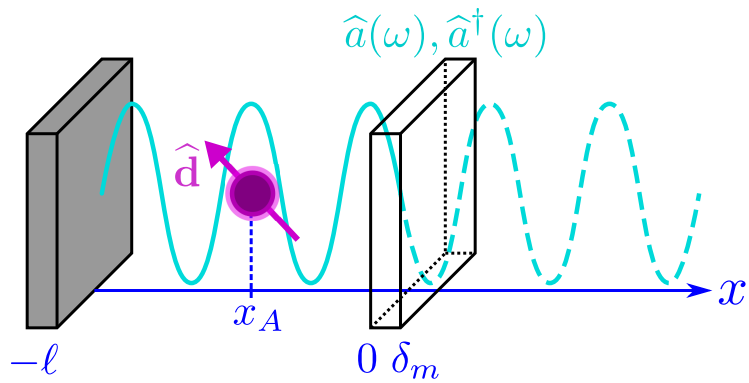

Figure 2.7: Single atom placed in an one-dimensional cavity. The field is quantized fully and operators $\widehat{a}(\omega), \widehat{a}^\dagger(\omega)$ annihilate (resp. create) optical modes $\Phi(x,\omega)$ corresponding to equation (2.1.29) in the full space. The dipole moment $\widehat{\mathbf{d}}$ of the atom positioned at $-\ell < x_A < 0$ has an angle θ with the electric field.

The decomposition of $\mathcal{T}(\omega)$ leads to a mode-selective decomposition of the field mode function inside the cavity:

$$\Phi_{\text{in}}(x,\omega) = \sum_m \Phi_{m,\text{in}}(x,\omega), \tag{2.2.7a}$$

$$\Phi_{m,\text{in}}(x,\omega) = \frac{-i}{\sqrt{\pi \mathcal{A} L}} \chi_{[-\ell,0]}(x) \mathrm{e}^{i\frac{\omega}{c}\ell} \sin\left[\tfrac{\omega}{c}(x+\ell)\right] \frac{\sqrt{\Gamma_m}}{\omega - \widetilde{\omega}_m + i\frac{\Gamma_m}{2}}. \tag{2.2.7b}$$

We consider a single atom placed inside the cavity, at position $-\ell < x_A < 0$, as depicted in fig. 2.7. The interaction between the field and the single two-level atom is described by the dipolar coupling term:

$$\widehat{V} = -\widehat{d}\widehat{E}(x_A), \tag{2.2.8}$$

where $\widehat{d} = d\widehat{\sigma}_+ + d^*\widehat{\sigma}_-$ is the projection of the transition dipole moment on the field polarization direction, with $\widehat{\sigma}_+ = |e\rangle\langle g|$ and $\widehat{\sigma}_- = |g\rangle\langle e|$. The electric field is picked at the position of the atom, therefore it has the form:

$$\widehat{E}(x_A) = \sum_m \int_0^{+\infty} \mathrm{d}\omega \sqrt{\frac{\hbar\omega}{2\epsilon_0}} \Big(\Phi_{m,\text{in}}(x_A,\omega)\widehat{a}(\omega) - \Phi^*_{m,\text{in}}(x_A,\omega)\widehat{a}^\dagger(\omega) \Big). \tag{2.2.9}$$

The interaction Hamiltonian then reads, after having removed the fast-rotating terms (RWA):

$$\widehat{V} = i\hbar \sum_m \int_0^{+\infty} \mathrm{d}\omega \Big(\eta_m(\omega)\widehat{\sigma}_+\widehat{a}(\omega) - \eta^*_m(\omega)\widehat{a}^\dagger(\omega)\widehat{\sigma}_- \Big), \tag{2.2.10a}$$

$$\eta_m(\omega) = i\sqrt{\frac{\omega}{\hbar\epsilon_0 \mathcal{A} L}} d \mathrm{e}^{i\frac{\omega}{c}\ell} \sin\left[\tfrac{\omega}{c}(x_A+\ell)\right] \sqrt{\frac{\Gamma_m}{2\pi}} \frac{1}{\omega - \widetilde{\omega}_m + i\frac{\Gamma_m}{2}}, \tag{2.2.10b}$$

where we have introduced the mode-selective coupling $\eta_m(\omega)$, which corresponds to the interaction between the atom and a single Lorentzian cavity mode m. Over the width Γ_m

of a single Lorentzian, ω is close to $\widetilde{\omega}_m$ and varies very slowly, therefore the mode-selective coupling is further approximated as:

$$\eta_m(\omega) \approx i\sqrt{\frac{\widetilde{\omega}_m}{\hbar\epsilon_0 \mathcal{A}L}} d e^{i\frac{\omega}{c}\ell} \sin\left[\tfrac{\omega}{c}(x_A+\ell)\right] \sqrt{\frac{\Gamma_m}{2\pi}} \frac{1}{\omega - \widetilde{\omega}_m + i\frac{\Gamma_m}{2}}. \tag{2.2.11}$$

Finally, the full atom-field Hamiltonian reads:

$$\boxed{\begin{aligned}\widehat{H} = \hbar\omega_0 \widehat{\sigma}_+\widehat{\sigma}_- + \int_0^{+\infty} \mathrm{d}\omega\, \hbar\omega\, \widehat{a}^\dagger(\omega)\widehat{a}(\omega) \\ + i\hbar \sum_m \int_0^{+\infty} \mathrm{d}\omega \Big(\eta_m(\omega)\widehat{\sigma}_+\widehat{a}(\omega) - \eta_m^*(\omega)\widehat{a}^\dagger(\omega)\widehat{\sigma}_-\Big),\end{aligned}} \tag{2.2.12}$$

where ω_0 is the transition frequency of the two-level atom.

2.2.2 Mode-selective quantum dynamics and effective Hamiltonian

From the Hamiltonian of the atom-field system, we get the dynamics with the time-dependent Schrödinger equation. The atom is coupled to m structured reservoirs with the coupling (2.2.11), and the structure of each reservoir leads to effective dynamics. If the coupling is very weak (e.g. if the cavity volume is large) the atom must have a similar behavior as in the vacuum: it should decay spontaneously with a modified decay rate depending on the atom-field coupling (Purcell effect). However, to describe such a process one needs to introduce a three-dimensional reservoir, because the atom emits photons in all directions. We focus here on the strong coupling regime (small cavity volume) such that the atomic decay rate is small compared to the inverse of the characteristic interaction time T_S:

$$\gamma_0 T_S \ll 1. \tag{2.2.13}$$

In that limit, the space can be decomposed into one direction along the cavity axis and two other transverse directions to account for the modified spontaneous emission of the atom [80]. This leads to a one-dimensional model for the atom-cavity interaction. For the spontaneous emission, we usually use the same value as the one in the full three-dimensional reservoir. Here we limit the calculation for the one-dimensional cavity model. Another remark about the characteristic interaction time is that its inverse must be small compared to the system's characteristic transition frequencies:

$$\omega_S T_S \gg 1. \tag{2.2.14}$$

In the atom-cavity problem, ω_S is either ω_0 or the resonance frequency of the cavity mode interacting with the atom. With this condition, the RWA argument is valid and the atom can absorb only a single photon. Therefore, the dynamics of the system can be confined to the vacuum state and the single excitation manifold for the Fock space associated to the field. We denote the one-photon excitation with the ket notation:

$$\widehat{a}^\dagger(\omega)|\mathbf{0}\rangle = |1_\omega\rangle \tag{2.2.15a}$$

$$\widehat{a}(\omega)|1_{\omega'}\rangle = \delta(\omega-\omega')|\mathbf{0}\rangle, \tag{2.2.15b}$$

where $|\mathbf{0}\rangle = |00...0\rangle$ is the vacuum state and $|1_\omega\rangle = |00...1_\omega...0\rangle$ is a single excitation state at frequency ω. We expand the interaction picture wavefunction of the atom-field system as:

$$|\psi(t)\rangle = \int_0^{+\infty} \mathrm{d}\omega\, c_{g,1}(\omega,t)\mathrm{e}^{-i\omega t}|g\rangle|1_\omega\rangle + c_{e,\mathbf{0}}(t)\mathrm{e}^{-i\omega_0 t}|e\rangle|\mathbf{0}\rangle, \tag{2.2.16}$$

and the Schrödinger equation leads to the coupled equations of motion of the coefficients:

$$\dot{c}_{g,1}(\omega) = -\sum_m \eta_m^*(\omega)\mathrm{e}^{i(\omega-\omega_0)t}c_{e,\mathbf{0}}(t), \tag{2.2.17a}$$

$$\dot{c}_{e,\mathbf{0}} = \sum_m \int_0^{+\infty} \mathrm{d}\omega\, \eta_m(\omega)\mathrm{e}^{-i(\omega-\omega_0)t}c_{g,1}(\omega,t). \tag{2.2.17b}$$

In order to trace out the continuous degrees of freedom from the dynamics, we define the integrated, mode-selective probability amplitude:

$$\boxed{c_{g,1}^{(m)}(t) := \frac{1}{g_m}\int_0^{+\infty} \mathrm{d}\omega\, \eta_m(\omega)\mathrm{e}^{-i(\omega-\omega_0)t}c_{g,1}(\omega,t).} \tag{2.2.18}$$

The denominator g_m is introduced as a normalization constant. We shall write the time derivative of the mode-selective coefficient, using the property:

$$\eta_m^*(\omega)\eta_{m'}(\omega) = \delta_{mm'}|\eta_m(\omega)|^2, \tag{2.2.19}$$

which is a consequence of equation (2.2.6), and we get the equation of motion for the m-th mode, using the integration of (2.2.17a) and inverting the order of time and frequency integrations:

$$\begin{aligned}\dot{c}_{g,1}^{(m)} = \dot{c}_{g,1}^{(m,0)} &- \frac{1}{g_m}\int_0^{+\infty}\mathrm{d}\omega|\eta_m(\omega)|^2 c_{e,\mathbf{0}}(t) \\ &+ \frac{i}{g_m}\int_0^t \mathrm{d}t' c_{e,\mathbf{0}}(t')\int_0^{+\infty}\mathrm{d}\omega|\eta_m(\omega)|^2(\omega-\omega_0)\mathrm{e}^{-i(\omega-\omega_0)(t-t')},\end{aligned} \tag{2.2.20}$$

where we introduce the time derivative of the initial time term defined as follows:

$$c_{g,1}^{(m,0)}(t) := \frac{1}{g_m}\int_0^{+\infty} \mathrm{d}\omega\, \eta_m(\omega)\mathrm{e}^{-i(\omega-\omega_0)t}c_{g,1}(\omega,0). \tag{2.2.21}$$

Two integrals appear in (2.2.20), which are to be evaluated using complex contour methods derived in appendix 2.C:

$$\mathcal{I} = \int_0^{+\infty}\mathrm{d}\omega|\eta_m(\omega)|^2, \tag{2.2.22a}$$

$$\mathcal{I}' = \int_0^{+\infty}\mathrm{d}\omega|\eta_m(\omega)|^2(\omega-\omega_0)\mathrm{e}^{-i(\omega-\omega_0)(t-t')}. \tag{2.2.22b}$$

These integrals can be decomposed in three parts, with different exponential factors implying integration either in the upper half plane or the lower half plane. The poles $z_\pm = \pm i\frac{\Gamma_m}{2}$ are

given by the widths of the Lorentzians. The result of appendix 2.C is, in the limit $\Gamma_m \ll \widetilde{\omega}_m$:

$$\mathcal{I} = \frac{\widetilde{\omega}_m |d|^2}{2\hbar\epsilon_0 \mathcal{A} L}\Big(1 - \mathrm{e}^{-\Gamma_m \frac{x_A+\ell}{c}} \cos\big[2\tfrac{\widetilde{\omega}_m}{c}(x_A+\ell)\big]\Big) \tag{2.2.23}$$

$$\mathcal{I}' = h_m\Big(\widetilde{\Delta}_m - i\frac{\Gamma_m}{2}\Big)\mathrm{e}^{-i\left(\widetilde{\Delta}_m - i\frac{\Gamma_m}{2}\right)(t-t')}, \tag{2.2.24}$$

where $\widetilde{\Delta}_m = \widetilde{\omega}_m - \omega_0$ is the atom-cavity mode detuning and the function h_m has the following expression:

$$h_m = \frac{\widetilde{\omega}_m |d|^2}{2\hbar\epsilon_0 \mathcal{A} L}\Big(1 - \cos\big[2\tfrac{\widetilde{\omega}_m}{c}(x_A+\ell)\big]\cosh\big[\Gamma_m \tfrac{x_A+\ell}{c}\big] - i\sin\big[2\tfrac{\widetilde{\omega}_m}{c}(x_A+\ell)\big]\sinh\big[\Gamma_m \tfrac{x_A+\ell}{c}\big]\Big). \tag{2.2.25}$$

In the expressions of $\mathcal{I}$ and h_m, we find products of slow and fast-varying factors. The slow-varying ones are in $\Gamma_m \frac{x_A+\ell}{c}$ and the fast ones are in $2\frac{\widetilde{\omega}_m}{c}(x_a+\ell)$, as we have $\Gamma_m \ll \widetilde{\omega}_m$. The Lorentzian width Γ_m, when the semi-transparent mirror transmission $|\underline{t}|^2$ in the vicinity of the resonance is small, is expressed using a Taylor series expansion (from equation (2.1.32)):

$$\Gamma_m = -\frac{c}{L}\ln\Big[\sqrt{1-|\underline{t}|^2}\Big] = \frac{c}{2L}\Big(|\underline{t}|^2 + \mathcal{O}(|\underline{t}|^4)\Big). \tag{2.2.26}$$

The integral $\mathcal{I}$ and the function h_m must correspond to the square modulus of the atom-cavity mode coupling g_m, introduced before to normalize the mode-selective probability amplitude $c_{g,1}^{(m)}$. We show below that this is the case when we expand the slow-varying factors in Taylor series up to the first order in $|\underline{t}|$. The argument $\Gamma_m \frac{x_A+\ell}{c}$ is of the order of $|\underline{t}|^2$ as we see in (2.2.26). We write the Taylor expansions:

$$\mathrm{e}^{-\Gamma_m \frac{x_A+\ell}{c}} = 1 + \mathcal{O}(|\underline{t}|^2) \tag{2.2.27a}$$

$$\cosh\big[\Gamma_m \tfrac{x_A+\ell}{c}\big] = 1 + \mathcal{O}(|\underline{t}|^2) \tag{2.2.27b}$$

$$\sinh\big[\Gamma_m \tfrac{x_A+\ell}{c}\big] = \mathcal{O}(|\underline{t}|^2). \tag{2.2.27c}$$

In this limit, both $\mathcal{I}$ and h_m are equal up to an error of the order of $|\underline{t}|^2$ and correspond to $|g_m|^2$:

$$|g_m|^2 = \frac{\widetilde{\omega}_m |d|^2}{\hbar\epsilon_0 \mathcal{A} L}\sin^2\big[\tfrac{\widetilde{\omega}_m}{c}(x_A+\ell)\big] + \mathcal{O}(|\underline{t}|^2), \tag{2.2.28}$$

where we used the identity $\sin^2 a = \frac{1}{2}(1-\cos 2a)$. The atom-cavity mode coupling g_m is found to be the same as if we had a perfect cavity, up to a factor in $\mathcal{O}(|\underline{t}|^2)$. Its expression is found when writing the perfect cavity Hamiltonian with zero boundary conditions at the mirrors:

$$\boxed{g_m = \sqrt{\frac{\widetilde{\omega}_m}{\hbar\epsilon_0 \mathcal{A} L}}\, d\, \mathrm{e}^{i\frac{\widetilde{\omega}_m}{c}\ell}\sin\big[\tfrac{\widetilde{\omega}_m}{c}(x_A+\ell)\big].} \tag{2.2.29}$$

We can now rewrite the equation of motion (2.2.20):

$$\dot{c}_{g,1}^{(m)} = \dot{c}_{g,1}^{(m,0)} - g_m^* c_{e,\mathbf{0}}(t) + i g_m^* \int_0^t \mathrm{d}t' c_{e,\mathbf{0}}(t')\Big(\widetilde{\Delta}_m - i\frac{\Gamma_m}{2}\Big)\mathrm{e}^{-i\left(\widetilde{\Delta}_m - i\frac{\Gamma_m}{2}\right)(t-t')}. \tag{2.2.30}$$

With the definition (2.2.18) and the formal integration of equation (2.2.17a), we show that:

$$c_{g,1}^{(m)}(t) - c_{g,1}^{(m,0)}(t) = -g_m^* \int_0^t \mathrm{d}t' c_{e,\mathbf{0}}(t') \mathrm{e}^{-i\left(\widetilde{\Delta}_m - i\frac{\Gamma_m}{2}\right)(t-t')}, \tag{2.2.31}$$

where another integral appears, and is evaluated with a treatment which is analogous to appendix 2.C:

$$\int_0^{+\infty} \mathrm{d}\omega |\eta_m(\omega)|^2 \mathrm{e}^{-i(\omega-\omega_0)(t-t')} = |g_m|^2 \mathrm{e}^{-i\left(\widetilde{\Delta}_m - i\frac{\Gamma_m}{2}\right)(t-t')}. \tag{2.2.32}$$

Replacing (2.2.31) in the equation of motion, we finally get:

$$\dot{c}_{g,1}^{(m)} = \dot{c}_{g,1}^{(m,0)} - g_m^* c_{e,\mathbf{0}}(t) - i\left(\widetilde{\Delta}_m - i\frac{\Gamma_m}{2}\right)\left(c_{g,1}^{(m)}(t) - c_{g,1}^{(m,0)}(t)\right). \tag{2.2.33}$$

This equation is valid for all possible initial conditions. However, we will limit the Hilbert space to a subspace containing the excited atom state $|e, \mathbf{0}\rangle$ and the single excitation of a cavity mode. The latter is defined using an analogous definition as (2.2.18) in terms of operators:

$$\boxed{\widehat{a}_m := \frac{1}{g_m} \int_0^{+\infty} \eta_m(\omega) \widehat{a}(\omega).} \tag{2.2.34}$$

Using the commutation relations (2.2.3) and the property (2.2.19), we find easily the commutation relations:

$$\left[\widehat{a}_m, \widehat{a}_{m'}^\dagger\right] = \delta_{mm'}, \tag{2.2.35a}$$

$$\left[\widehat{a}_m, \widehat{a}_{m'}\right] = \left[\widehat{a}_m^\dagger, \widehat{a}_{m'}^\dagger\right] = 0. \tag{2.2.35b}$$

The application of operator $\widehat{a}_m^\dagger$ on the vacuum state creates the single cavity mode excitation:

$$\widehat{a}_m^\dagger |\mathbf{0}\rangle = |1_m\rangle, \tag{2.2.36a}$$

$$\widehat{a}_m |1_{m'}\rangle = \delta_{mm'} |\mathbf{0}\rangle. \tag{2.2.36b}$$

Writing the initial condition being any superposition state:

$$|\psi(0)\rangle = \alpha |e, \mathbf{0}\rangle + \sum_m \beta_m |g, 1_m\rangle, \tag{2.2.37}$$

with $|\alpha|^2 + \sum_m |\beta_m|^2 = 1$, which corresponds to $c_{g,1}(\omega, 0) = \sum_m \beta_m \frac{\eta_m^*(\omega)}{g_m^*}$, we find that the set of equations of motion for the probability amplitudes is:

$$\boxed{\begin{aligned} \dot{c}_{g,1}^{(m)} &= -g_m^* c_{e,\mathbf{0}}(t) - i\left(\widetilde{\Delta}_m - i\frac{\Gamma_m}{2}\right) c_{g,1}^{(m)}(t), && (2.2.38a) \\ \dot{c}_{e,\mathbf{0}} &= \sum_m g_m c_{g,1}^{(m)}(t). && (2.2.38b) \end{aligned}}$$

These probability amplitudes correspond to the effective unnormalized wavefunction:

$$|\bar{\psi}(t)\rangle = c_{e,\mathbf{0}}(t) + \sum_m c_{g,1}^{(m)}(t)|g, 1_m\rangle, \tag{2.2.39}$$

with, in the simplified basis $\{|e, \mathbf{0}\rangle, |g, 1_m\rangle\}$, the non-Hermitian Hamiltonian in matrix form:

$$\boxed{\widehat{H}_{\text{eff}} = \begin{pmatrix} 0 & -ig_m^* \\ ig_m & \widetilde{\Delta}_m - i\frac{\Gamma_m}{2} \end{pmatrix}.} \tag{2.2.40}$$

We remark that the coupling is taken up to the first order in $|\underline{t}|$, while the (imaginary) loss is taken up to the second order in $|\underline{t}|$, corresponding to the lowest order different from zero. Finally, we can write the effective Hamiltonian back from the rotating frame, via the transformation:

$$\widehat{\mathcal{R}}(t) = \mathrm{e}^{i\omega_0 t\left(\widehat{\sigma}_+\widehat{\sigma}_- + \sum_m \widehat{a}_m^\dagger \widehat{a}_m\right)}, \tag{2.2.41}$$

leading to:

$$\boxed{\begin{aligned} \widehat{H}_{\text{eff}} = \hbar\omega_0\widehat{\sigma}_+\widehat{\sigma}_- + \sum_m \left(\hbar\widetilde{\omega}_m - i\hbar\frac{\Gamma_m}{2}\right)\widehat{a}_m^\dagger\widehat{a}_m \\ + i\hbar\sum_m \left(g_m\widehat{\sigma}_+\widehat{a}_m - g_m^*\widehat{a}_m^\dagger\widehat{\sigma}_-\right). \end{aligned}} \tag{2.2.42}$$

This Hamiltonian describes the dynamics of the 1D atom-cavity mode system, therefore, as the atomic transition is considered nearly resonant to a single cavity mode m, the sum can be dropped. Since it is non-Hermitian, the energy leaves this system as t increases. This leakage corresponds to the escape of photons through the semi-transparent mirror. This effective model is found as well using the master equation formalism (2.1.97) derived earlier from the Hamiltonian (2.1.33). Indeed, when writing the master equation in the product basis (as will be done in the next section), the dynamics is decomposed into a leaking part equivalent to the Schrödinger equation with Hamiltonian (2.2.42), and another part collecting the energy loss of the preceding one. The first part corresponds to the atom-cavity mode system, while the other one corresponds to the photon leakage. Therefore, the effective model we have just derived is enough to get the dynamics of the atom in the cavity. The output field is found when writing the Poynting vector in terms of the output reservoir operators $\widehat{b}(\omega), \widehat{b}^\dagger(\omega)$, which depend on the perfect cavity operators $\widehat{c}, \widehat{c}^\dagger$ (see equation (2.1.71)), shown to be equivalent to $\widehat{a}_m, \widehat{a}_m^\dagger$.

Such a derivation is very useful for the understanding of strong coupling regime and quantum emitter interactions with plasmons, as will be seen in chapter 4, where we build effective models for quantum emitters coupled to spherically layered media.

In the next section, however, we require the output field information, therefore we will use the usual cQED model with the master equation (2.1.97).

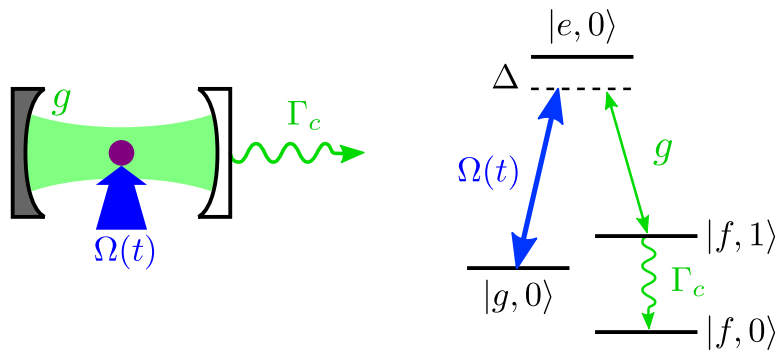

Figure 2.8: Atom-field interaction in the cavity: (left panel) a single Λ-atom is driven by an external classical laser field of Rabi frequency $\Omega(t)$, and a quantized cavity field with coupling strength g. (right panel) The fields are in two-photon resonance, the one-photon detuning is Δ. Initially the atom is in the ground state $|g\rangle$. In the course of the excitation process, one photon is taken from the laser field and transferred to the cavity, and eventually leaks out of the cavity, through the semi-transparent mirror, with decay rate Γ_c.

2.3 Production of photon states with atoms in a cavity

2.3.1 Single photons with one atom in a cavity

We derive from the preceding analysis the model for the generation of a single photon using a leaking cavity containing one atom driven by a pulsed laser of Rabi frequency $\Omega(t)$. The production of a single photon in such a system has been demonstrated with an atom flying through the cavity in a resonant stimulated Raman adiabatic passage configuration [71, 83] and for a trapped ion in a cavity [74]. We show that a large cavity detuning and a large leakage rate allows the direct and simple control of the photon temporal shape.
In a dressed basis, one denotes states $|i\rangle|n\rangle \equiv |i,n\rangle$ with i labelling the atomic states and n is the number state in the cavity. We assume an initial condition with zero photon in the cavity, and the basis splits into four relevant dressed states (see fig. 2.8):

$$\big\{|g,0\rangle, |e,0\rangle, |f,1\rangle, |f,0\rangle\big\}. \tag{2.3.1}$$

The dynamics is described by the Lindblad equation derived in the preceding sections:

$$\dot{\widehat{\varrho}} = -\frac{i}{\hbar}\big[\widehat{H}_S(t), \widehat{\varrho}(t)\big] + \Gamma_c\Big(\widehat{c}\,\widehat{\varrho}(t)\widehat{c}^\dagger - \tfrac{1}{2}\big\{\widehat{c}^\dagger\widehat{c}, \widehat{\varrho}(t)\big\}\Big), \tag{2.3.2}$$

where the brackets $\big\{\widehat{A}, \widehat{B}\big\} = \widehat{A}\widehat{B} + \widehat{B}\widehat{A}$ denote the anticommutator between two operators. The Lindblad equation can be written in another form:

$$\dot{\widehat{\varrho}} = -\frac{i}{\hbar}\Big(\widehat{H}_{\rm nh}(t)\widehat{\varrho}(t) - \widehat{\varrho}(t)\widehat{H}^\dagger_{\rm nh}(t)\Big) + \Gamma_c\widehat{c}\,\widehat{\varrho}(t)\widehat{c}^\dagger, \tag{2.3.3a}$$

$$\widehat{H}_{\rm nh}(t) = \widehat{H}_S(t) - i\hbar\frac{\Gamma_c}{2}\,\widehat{c}^\dagger\widehat{c}, \tag{2.3.3b}$$

where we introduce a non-Hermitian dissipative Hamiltonian $\widehat{H}_{\mathrm{nh}}$. Expressed in the dressed basis (2.3.1), the non-Hermitian Hamiltonian reads:

$$\widehat{H}_{\mathrm{nh}}(t)/\hbar = \left(\begin{array}{ccc|c} 0 & \Omega(t) & 0 & 0 \\ \Omega(t) & \Delta & g & 0 \\ 0 & g & -i\frac{\Gamma_c}{2} & 0 \\ \hline 0 & 0 & 0 & 0 \end{array}\right) = \begin{pmatrix} \mathbf{A}(t) & \mathbf{0}_{31} \\ \mathbf{0}_{13} & 0 \end{pmatrix}, \tag{2.3.4}$$

where we have highlighted the block $\mathbf{A}(t)$ in which the atom dynamics is happening, and $\mathbf{0}_{nm}$ is a $n \times m$ matrix containing zeros everywhere. Separating the blocks $\mathbf{A}$ and $\{0\}$ (the second one corresponding to the state $|f,0\rangle$), we write the density matrix in the following form:

$$\widehat{\varrho}(t) = \begin{pmatrix} \boldsymbol{\varrho}_{AA}(t) & \boldsymbol{\varrho}_{A0}(t) \\ \boldsymbol{\varrho}_{0A}(t) & \varrho_{00}(t) \end{pmatrix}. \tag{2.3.5}$$

Rewriting equation (2.3.3a) and choosing the initial condition such that $\boldsymbol{\varrho}_{A0}(t_i) = \boldsymbol{\varrho}_{0A}(t_i) = \mathbf{0}$, we get a set of two equations which are solved sequently:

$$\dot{\boldsymbol{\varrho}}_{AA} = -i\Big(\mathbf{A}(t)\boldsymbol{\varrho}_{AA}(t) - \boldsymbol{\varrho}_{AA}(t)\mathbf{A}^{\dagger}(t)\Big), \tag{2.3.6a}$$

$$\dot{\varrho}_{00} = \Gamma_c \langle f,1|\boldsymbol{\varrho}_{AA}(t)|f,1\rangle. \tag{2.3.6b}$$

With the initial condition chosen to be:

$$|\psi(t_i)\rangle = |g,0\rangle, \tag{2.3.7}$$

the dynamics of this system of equations is described in two steps:

- We solve equation (2.3.6a), which is a time-dependent Schrödinger equation with losses, since $\mathbf{A}$ is non-Hermitian:
$$i\frac{\mathrm{d}|\psi_A\rangle}{\mathrm{d}t} = \mathbf{A}(t)|\psi_A(t)\rangle, \tag{2.3.8}$$
where $|\psi_A(t)\rangle = c_{g,0}(t)|g,0\rangle + c_{e,0}(t)|e,0\rangle + c_{f,1}(t)|f,1\rangle$. As the cavity is going to decay in $|f,0\rangle$ when the state reaches $|f,1\rangle$, the total population of $|\psi_A(t)\rangle$ decreases over time.

- Rewriting equation (2.3.6b) in terms of state population $P_{i,n}(t) = \langle i,n|\widehat{\varrho}(t)|i,n\rangle$, we get:
$$\dot{P}_{f,0} = \Gamma_c P_{f,1}(t), \tag{2.3.9}$$
and this equation shows that the losses are collected in the population of $|f,0\rangle$, closing the whole system with the completeness:
$$\sum_{i,n} P_{i,n}(t) = 1. \tag{2.3.10}$$

The population of $|f,0\rangle$ is obtained by integrating $P_{f,1}(t)$ over time, and the dynamics is solved with equation (2.3.8). To calculate the photon flux, we use equation (2.1.71) and the definition of the average $\langle\widehat{A}\rangle = \mathrm{Tr}\{\widehat{A}\widehat{\varrho}\}$:

$$\Phi(t) = \frac{\mathrm{d}n}{\mathrm{d}t} = \Gamma_c P_{f,1}(t), \tag{2.3.11a}$$

$$n(t) = \int_{t_i}^{t} \mathrm{d}t'\Phi(t') = \Gamma_c \int_{t_i}^{t} \mathrm{d}t' P_{f,1}(t'). \tag{2.3.11b}$$

We see from the latter equation and (2.3.9) that the average photon number is identical to $P_{f,0}(t)$. The direct control of the production of a leaking single photon can be achieved with an adiabatic elimination of the excited state $|e,0\rangle$ [42], i.e. with a large one-photon detuning and a bad cavity regime:

$$\Delta \gg \Omega(t), g \tag{2.3.12a}$$

$$\Gamma_c \gg G(t), \frac{g^2}{\Delta}, \tag{2.3.12b}$$

where $G(t) = -g\Omega(t)/\Delta$ is the effective Raman coupling. Those two conditions combined lead to the adiabatic elimination of the state $|f,1\rangle$. Writing (2.3.8) for each coefficient, we get:

$$i\dot{c}_{g,0} = \Omega(t)c_{e,0}(t) \tag{2.3.13a}$$

$$i\dot{c}_{e,0} = \Omega(t)c_{g,0}(t) + \Delta c_{e,0}(t) + gc_{f,1}(t) \tag{2.3.13b}$$

$$i\dot{c}_{f,1} = gc_{e,0}(t) - i\tfrac{\Gamma_c}{2}c_{f,1}(t), \tag{2.3.13c}$$

and in the large detuning limit, the adiabatic elimination is done setting $\dot{c}_{e,0} = 0$, which is equivalent to averaging the fast oscillations of $c_{e,0}(t)$:

$$c_{e,0}(t) \simeq -\left(\frac{\Omega(t)}{\Delta}c_{g,0}(t) + \frac{g}{\Delta}c_{f,1}(t)\right). \tag{2.3.14}$$

The system of equations for the coefficients then reduces to:

$$i\dot{c}_{g,0} = S_L(t)c_{g,0}(t) + G(t)c_{f,1}(t) \tag{2.3.15a}$$

$$i\dot{c}_{f,1} = G(t)c_{g,0}(t) + \left(S_c - i\tfrac{\Gamma_c}{2}\right)c_{f,1}(t), \tag{2.3.15b}$$

where we introduced the Stark shifts $S_L(t) = -\Omega^2(t)/\Delta$ and $S_c = -g^2/\Delta$ caused respectively by the laser pulse and the cavity field. The last step of the adiabatic elimination is brought with condition (2.3.12b), which leads to $\dot{c}_{f,1} = 0$ and:

$$c_{f,1}(t) \simeq -\frac{G(t)}{S_c - i\frac{\Gamma_c}{2}}c_{g,0}(t) \simeq i\frac{2G(t)}{\Gamma_c}c_{g,0}(t). \tag{2.3.16}$$

As a consequence, only one equation of motion remains and it is integrated to determine $c_{g,0}(t)$:

$$c_{g,0}(t) = \mathrm{e}^{i\zeta(t)}\mathrm{e}^{-\frac{\theta(t)}{2}}, \tag{2.3.17a}$$

$$\zeta(t) = \int_{t_i}^{t} \mathrm{d}t'\, S_L(t'), \tag{2.3.17b}$$

$$\theta(t) = \int_{t_i}^{t} \mathrm{d}t' \frac{4G^2(t')}{\Gamma_c}. \tag{2.3.17c}$$

For any g, Δ, Γ_c and $\Omega(t)$ fulfilling conditions (2.3.12), we have solved the dynamics and, using both relation (2.3.16) and (2.3.11a), the time shape of the photon flux is:

$$\Phi(t) = \dot{\theta}\,\mathrm{e}^{-\theta(t)}. \tag{2.3.18}$$

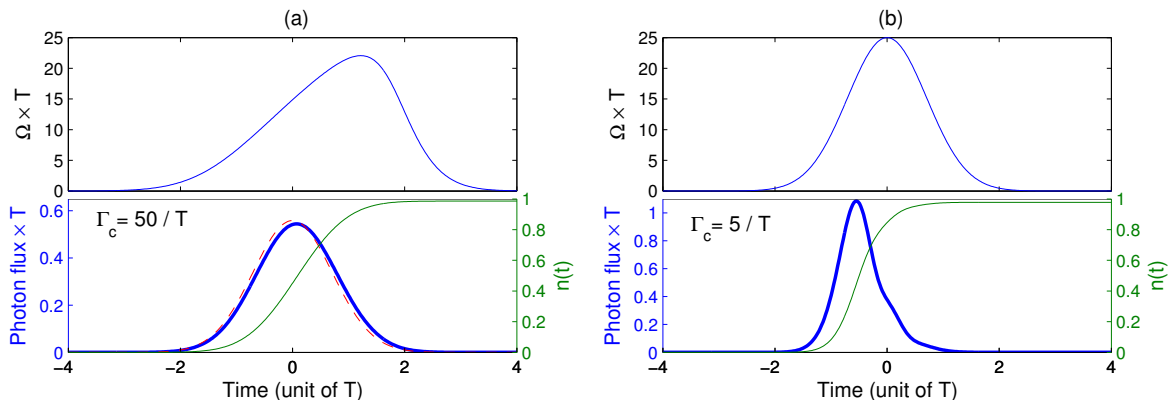

Figure 2.9: (a) Rabi frequency $\Omega(t)T$ (2.3.20) with $(g, \Gamma_c, \Delta) \times T = (25, 50, 100)$ and $\eta = 0.99$, determined from the desired Gaussian shape flux $\Phi(t)$ (2.3.21) [desired (dashed line) and numerical from the original model (2.3.8) (thick line)] of the single photon through the semi-transparent mirror (in units of T); number of outgoing photons $n(t)$ (2.3.11b) during the process (thin line). (b) Same calculation done for $\Gamma_c = 5/T$ and a chosen Rabi frequency $\Omega(t) = \Omega_0 \exp[-(t/T)^2]$, $\Omega_0 T = 25$.

An interesting feature from this analytic form of the photon flux is the possibility of reverse-engineering the process and to tailor a desired photon flux by deriving explicitly the corresponding laser pulse shape $\Omega(t)$, given g, Δ and Γ_c. This is achieved by determining $\theta(t)$ from (2.3.18):

$$\theta(t) = -\ln\left[1 - \int_{t_i}^{t} \mathrm{d}t' \Phi(t')\right], \tag{2.3.19}$$

and using the definition of $\theta(t)$ (2.3.17c), the laser Rabi frequency is obtained by differentiating the latter equation:

$$\Omega(t) = \frac{\Delta\sqrt{\Gamma_c}}{2g}\sqrt{\frac{\Phi(t)}{1 - \int_{t_i}^{t} \mathrm{d}t' \Phi(t')}}. \tag{2.3.20}$$

We remark that this definition of the Rabi frequency can diverge at large times. To prevent it, we introduce an efficiency parameter $\eta < 1$, which ensures that $\Omega(t \to +\infty) = 0$ when $\Phi(t \to +\infty) = 0$ [69]. Numerical results are shown for two different parameter sets. The first result, displayed on fig. 2.9a, is a plot of the Rabi frequency (2.3.20) when we chose a Gaussian probability shape for the single photon flux:

$$\Phi(t) = \frac{\eta}{T\sqrt{\pi}} \mathrm{e}^{-(t/T)^2}, \qquad \int_{-\infty}^{+\infty} \mathrm{d}t' \Phi(t') = \eta, \tag{2.3.21}$$

where T is the width of the flux. We have also set $\eta = 0.99$ such that the Rabi frequency needed to get $\Phi(t)$ does not diverge, and we obtain $\max_t G(t) \approx 5.5/T \ll \Gamma_c = 50/T$ as required. The resulting photon flux is checked numerically by calculating it from the solution of the Schrödinger equation (2.3.8) without applying the adiabatic elimination, with the Rabi frequency (2.3.20). The numerical photon flux closely follows the desired shape as expected. Other more complex forms can be investigated through (2.3.20) such as the ones obtained by the resonant process with flying atoms in [69].

Figure 2.9b shows a different situation in which the cavity has a better effective quality factor,

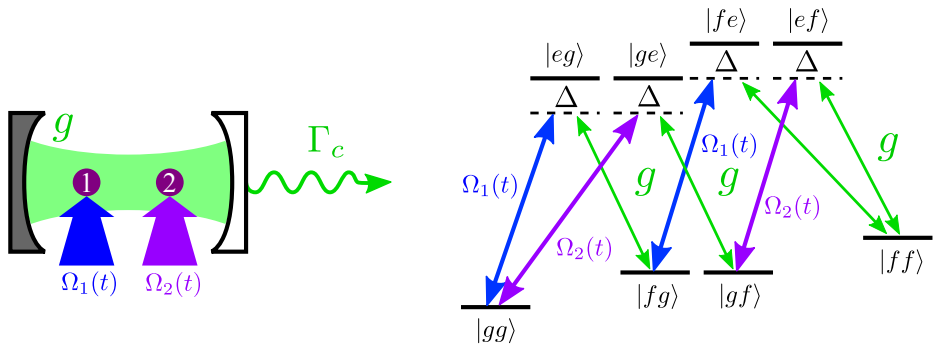

Figure 2.10: Atom-field interaction in the cavity: (left panel) two Λ-atoms driven by two external classical laser fields of Rabi frequency $\Omega_{1,2}(t)$ with the one-photon detuning Δ, and a quantized cavity field with coupling strength g. (right panel) 2-atom-cavity system. The states $|i\rangle_1 \otimes |j\rangle_2 \equiv |ij\rangle$ with $i, j = g, e, f$ form a basis for atoms 1 and 2.

and as a consequence the second adiabatic elimination (2.3.12b) cannot be made. In that case we do not reverse-engineer the process, and we chose the Rabi frequency of the laser pulse as a Gaussian function. The decay rate is taken to be smaller than in the preceding calculation: $\Gamma_c = 5/T \approx \max_t G(t) = 6.25/T$. The leakage of the single photon occurs earlier and faster due to the earlier peak and the different shape of the Rabi frequency. The better quality of the cavity leads to a deformation of the tail of the photonic shape, since the emitted photon still has time to interact with the atom before leaving the cavity.

2.3.2 Single and two-photon states with two atoms in a cavity

We present a numerical study of the outgoing photon flux when the cavity field interacts with two laser-driven atoms. The aim of this section is to describe in a precise way the nature of the outgoing two-photon state. The generation of an N-photon state has been investigated using, for instance, the Zeeman sublevels of a single alkali atom [72].
We consider the system shown in fig. 2.10: we assume that each atom (labelled 1 and 2) can be driven independently by two Rabi frequencies $\Omega_1(t)$ and $\Omega_2(t)$. The atom-cavity coupling g for the transition $|e\rangle \leftrightarrow |f\rangle$ allows the production of photons in the cavity mode leaking outside with decay rate Γ_c. We proceed as for the case of one atom and consider a large detuning. Stark shifts proportional to $\Omega_j^2(t)/\Delta$ and g^2/Δ appear from the elimination of the excited states, but the second condition of a leaking cavity make them negligible in the dynamics, since they are of the same order of magnitude as the effective Raman coupling strength $G_j(t) = -g\Omega_j(t)/\Delta$. We summarize the double adiabatic elimination conditions by the following relations:

$$\Delta \gg \Omega_j(t), g \tag{2.3.22a}$$
$$\Gamma_c \gg G_j(t). \tag{2.3.22b}$$

The effective dressed basis derived from the adiabatic eliminations is:

$$\{\underbrace{|gg,0\rangle, |fg,1\rangle, |gf,1\rangle, |ff,2\rangle}_{A}, \underbrace{|fg,0\rangle, |gf,0\rangle, |ff,1\rangle}_{B} \underbrace{|ff,0\rangle}_{\{0\}}\}, \tag{2.3.23}$$

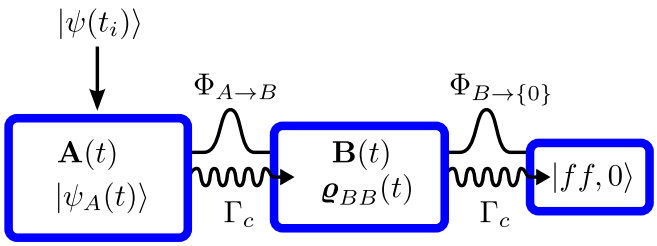

Figure 2.11: Dynamical map of a two-atom system driven by two laser fields and trapped in a cavity. The dynamics splits into three blocks [from left to right, A, B and $\{0\}$ see (2.3.24)] leaking from one to another with decay rate Γ_c. Eventually, all population ends up in state $|ff,0\rangle$ (block $\{0\}$).

where $|ij,n\rangle \equiv |i\rangle\otimes|j\rangle\otimes|n\rangle$, i,j label the atomic states g,e,f and $n=0,1,2$ label the photon number states. The effective non-Hermitian Hamiltonian in this basis is:

$$\widehat{H}_{\rm ad}(t) = \left(\begin{array}{cccc|ccc|c} 0 & G_1(t) & G_2(t) & 0 & 0 & 0 & 0 & 0 \\ G_1(t) & -i\frac{\Gamma_c}{2} & 0 & G_2(t) & 0 & 0 & 0 & 0 \\ G_2(t) & 0 & -i\frac{\Gamma_c}{2} & G_1(t) & 0 & 0 & 0 & 0 \\ 0 & G_2(t) & G_1(t) & -i\Gamma_c & 0 & 0 & 0 & 0 \\ \hline 0 & 0 & 0 & 0 & 0 & 0 & G_2(t) & 0 \\ 0 & 0 & 0 & 0 & 0 & 0 & G_1(t) & 0 \\ 0 & 0 & 0 & 0 & G_2(t) & G_1(t) & -i\frac{\Gamma_c}{2} & 0 \\ \hline 0 & 0 & 0 & 0 & 0 & 0 & 0 & 0 \end{array}\right)$$
$$= \begin{pmatrix} \mathbf{A}(t) & \mathbf{0}_{43} & \mathbf{0}_{41} \\ \mathbf{0}_{34} & \mathbf{B}(t) & \mathbf{0}_{31} \\ \mathbf{0}_{14} & \mathbf{0}_{13} & 0 \end{pmatrix}, \tag{2.3.24}$$

where we have recognized the block-diagonal structure and called the two big blocks $\mathbf{A}(t)$ and $\mathbf{B}(t)$. We denote by A, B and $\{0\}$ the three blocks of the dynamics, each one corresponding to a subspace in the effective basis (2.3.23). The system density matrix may be expanded as:

$$\widehat{\varrho} = \begin{pmatrix} \boldsymbol{\varrho}_{AA} & \boldsymbol{\varrho}_{AB} & \boldsymbol{\varrho}_{A0} \\ \boldsymbol{\varrho}_{BA} & \boldsymbol{\varrho}_{BB} & \boldsymbol{\varrho}_{B0} \\ \boldsymbol{\varrho}_{0A} & \boldsymbol{\varrho}_{0B} & \varrho_{00} \end{pmatrix}, \tag{2.3.25}$$

and, as in the preceding section, the initial condition is taken in block A. The off-diagonal blocks are then always empty: $\boldsymbol{\varrho}_{AB}(t) = \boldsymbol{\varrho}_{A0}(t) = \boldsymbol{\varrho}_{B0}(t) = \mathbf{0}$ and due to the strong cavity leakage, the dynamics flows from block to block as described in fig. 2.11. The dynamics is given by the Lindblad effective equation (2.3.3a), which can be reformulated with a non-Hermitian Schrödinger equation (2.3.8) for block A. In the limit of strong leakage, one can solve this equation analytically. The dynamics for the B block features a Schrödinger equation with a probability source:

$$\dot{\boldsymbol{\varrho}}_{BB} = -i\Big(\mathbf{B}(t)\boldsymbol{\varrho}_{BB}(t) - \boldsymbol{\varrho}_{BB}(t)\mathbf{B}^\dagger(t)\Big) + \underbrace{\Gamma_c\mathbf{C}\boldsymbol{\varrho}_{AA}(t)\mathbf{C}^\dagger}_{\text{prob. source term}}, \tag{2.3.26}$$

with

$$\mathbf{C} = \begin{pmatrix} 0 & 1 & 0 & 0 \\ 0 & 0 & 1 & 0 \\ 0 & 0 & 0 & \sqrt{2} \end{pmatrix}. \tag{2.3.27}$$

We need the solution $\boldsymbol{\varrho}_{AA}(t) = |\psi_A(t)\rangle\langle\psi_A(t)|$ from (2.3.8) to get the source term and solve (2.3.26). In the Redfield representation, this equation becomes:

$$\dot{\vec{\varrho}}_{BB} = -i\Big(\mathbf{B}(t) \otimes \mathbb{1}_B - \mathbb{1}_B \otimes \mathbf{B}^\dagger(t)\Big)\vec{\varrho}_{BB}(t) + \Gamma_c \vec{Y}(t), \tag{2.3.28}$$

where $\vec{\varrho}_{BB}(t)$ corresponds to the column form of the density matrix $\boldsymbol{\varrho}_{BB}(t)$ associated to block B, and $\vec{Y}(t)$ is the Redfield representation of the source term. This equation is of the form:

$$\dot{\vec{X}} = \mathbf{M}(t)\vec{X}(t) + \vec{Y}(t), \tag{2.3.29}$$

which is solvable numerically with a good precision (see appendix 2.D). The outgoing photon flux is calculated as in the preceding section, and reads:

$$\begin{aligned} \Phi(t) &= \Gamma_c \sum_{n>0} n P_{ij,n}(t) \\ &= \Phi_{A\to B}(t) + \Phi_{B\to\{0\}}(t), \end{aligned} \tag{2.3.30}$$

where $\Phi_{A\to B}(t) = \Phi_{fg,1}(t) + \Phi_{gf,1}(t) + \Phi_{ff,2}(t)$ describes the emission of a single photon from block A to block B, and $\Phi_{B\to\{0\}}(t) = \Phi_{ff,1}(t)$ corresponds to the emission of a single photon from B to $\{0\}$. Here, $P_{ff,2}(t)$ can be neglected with regard to (2.3.22b). One finds that the photon flux is a sum of partial photon fluxes as suggested in (2.3.30), each one corresponding to the production of a single photon. Figure 2.12 show the photon fluxes, for Gaussian pulse shapes:

$$\Omega_1(t) = \Omega_0 \mathrm{e}^{-\left(\frac{t-t_0-\tau}{T}\right)^2}, \quad \Omega_2(t) = \Omega_0 \mathrm{e}^{-\left(\frac{t-t_0+\tau}{T}\right)^2}, \tag{2.3.31}$$

where τ is the time delay between the laser pulses and T is the time duration of a pulse. The fluxes are determined numerically for the following two cases: (i) a sequence of laser pulses (laser 1 is switched on before laser 2), and (ii) simultaneous laser pulses. The partial flux $\Phi_{ff,2}(t)$ is seen to be negligible, and in the first case we obtain $\Phi_{A\to B}(t) \approx \Phi_{fg,1}(t)$. The two photons are produced one by one with a time delay corresponding to τ, and each photon results from a leakage from block to block. In fig. 2.12b, however, the photons are not generated separately, and the resulting two-photon state is not a Fock state. In the following section, we describe how to characterize the photonic state in the case of general one and two-photon states.

2.3.3 Characterization of the outgoing two-photon state

Knowing the photon flux from the previous calculations, we must provide a good description of the outgoing photonic state. We proceed in two steps:

- We write the general form of single and two-photon states, and we match it with the photon flux. The matching results in a fit, whose parameters help to fully determine the state function.
- We study the unnormalized second-order correlation function $G^{(2)}(t,\tau)$, whose shape provides information about the photonic state.

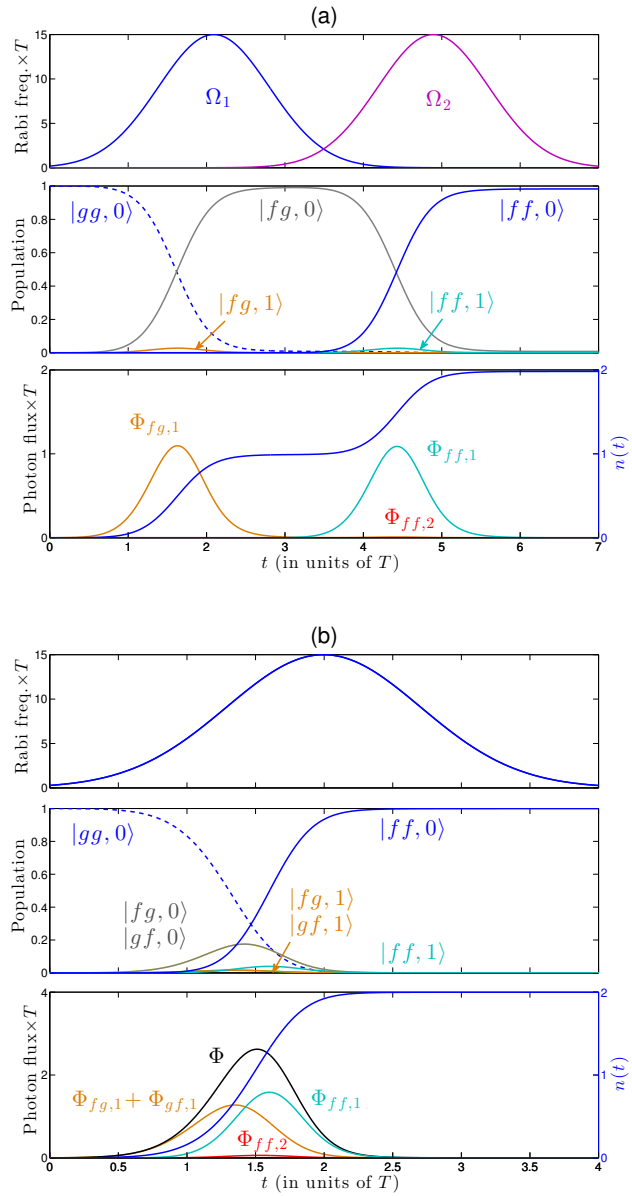

Figure 2.12: (a) (upper panel) Rabi frequencies (in units of T) of delay $2\tau = 2.8T$. (middle panel) Populations in the dressed basis for $(\Omega_0, \Delta, g, \Gamma_c) \times T = (15, 100, 40, 40)$. (lower panel) Outgoing photon flux $\Phi = \Phi_{fg,1} + \Phi_{ff,1} + \Phi_{ff,2}$ (in units of T) and outgoing photon number $n(t)$ (dark blue). (b) Same as in (a) but for $\Omega_1(t) = \Omega_2(t) \equiv \Omega(t)$.

One and multi-mode representation

According to reference [84, 85], general one and two-photon states $|1_\phi\rangle, |2_\Psi\rangle$ can be fully characterized from the knowledge of a function $\phi(\omega)$ for the single photon and a two-variable

function $\Psi(\omega_1, \omega_2)$, both defined in the frequency domain:

$$|1_\phi\rangle = \widehat{a}_\phi^\dagger|\mathbf{0}\rangle, \quad \widehat{a}_\phi^\dagger := \int_0^{+\infty} \mathrm{d}\omega\, \phi(\omega)\widehat{b}^\dagger(\omega), \tag{2.3.32}$$

$$|2_\Psi\rangle = \frac{1}{\mathcal{N}_2}\int_0^{+\infty} \mathrm{d}\omega_1 \mathrm{d}\omega_2 \Psi(\omega_1, \omega_2)\widehat{b}^\dagger(\omega_1)\widehat{b}^\dagger(\omega_2)|\mathbf{0}\rangle, \tag{2.3.33}$$

where $\mathcal{N}_2$ is a normalization factor, and $\widehat{b}^\dagger(\omega)$ is a creation operator for a photon in the mode ω, outside of the cavity. In the time domain, the same states can be written equivalently:

$$|1_\phi\rangle = \widehat{a}_\phi^\dagger|\mathbf{0}\rangle, \quad \widehat{a}_\phi^\dagger := \int_{-\infty}^{+\infty} \mathrm{d}t\, \widetilde{\phi}(t)\widehat{b}^\dagger(t), \tag{2.3.34a}$$

$$|2_\Psi\rangle = \frac{1}{\mathcal{N}_2}\int_{-\infty}^{+\infty} \mathrm{d}t_1 \mathrm{d}t_2 \widetilde{\Psi}(t_1, t_2)\widehat{b}^\dagger(t_1)\widehat{b}^\dagger(t_2)|\mathbf{0}\rangle. \tag{2.3.34b}$$

where we introduce the one and two-time Fourier transforms of $\phi(\omega), \Psi(\omega_1, \omega_2)$, respectively:

$$\widetilde{\phi}(t) = \frac{1}{2\pi}\int_0^{+\infty} \mathrm{d}\omega \phi(\omega)\mathrm{e}^{-i\omega t}, \tag{2.3.35a}$$

$$\widetilde{\Psi}(t_1, t_2) = \frac{1}{(2\pi)^2}\int_0^{+\infty} \mathrm{d}\omega_1 \mathrm{d}\omega_2 \Psi(\omega_1, \omega_2)\mathrm{e}^{-i(\omega_1 t_1 + \omega_2 t_2)}, \tag{2.3.35b}$$

and, considering the preceding functions to be square-integrable and normalized, the two-photon normalization factor is shown to be:

$$\mathcal{N}_2 = 1 + \int_{-\infty}^{+\infty} \mathrm{d}t_1 \mathrm{d}t_2 \widetilde{\Psi}(t_1, t_2)\widetilde{\Psi}^*(t_2, t_1). \tag{2.3.36}$$

In the following, we make the connection between $\widetilde{\Psi}(t_1, t_2)$ and the photon flux in the vacuum:

$$\Phi(t) := \left\langle \widehat{b}^\dagger(t)\widehat{b}(t)\right\rangle = \langle 2_\Psi|\, \widehat{b}^\dagger(t)\widehat{b}(t)|2_\Psi\rangle. \tag{2.3.37}$$

Using equation (2.3.35b) with the expression of the flux, we show that it splits into a sum of two partial fluxes of the form:

$$\Phi(t) = \Phi_1(t) + \Phi_2(t), \tag{2.3.38a}$$

$$\Phi_1(t) = \frac{1}{\mathcal{N}_2}\int_{-\infty}^{+\infty} \mathrm{d}t' \left(\widetilde{\Psi}^*(t, t') + \widetilde{\Psi}^*(t', t)\right) \widetilde{\Psi}(t, t'), \tag{2.3.38b}$$

$$\Phi_2(t) = \frac{1}{\mathcal{N}_2}\int_{-\infty}^{+\infty} \mathrm{d}t' \left(\widetilde{\Psi}^*(t, t') + \widetilde{\Psi}^*(t', t)\right) \widetilde{\Psi}(t', t). \tag{2.3.38c}$$

The expression for the photon flux derived here can be used to recover the photon number, by integration over time t. We see from the latter expression that the integrated partial fluxes both provide a single photon number, that is:

$$\int_{-\infty}^{+\infty} \mathrm{d}t\, \Phi_{1,2}(t) = 1, \tag{2.3.39}$$

which naturally brings a two-photon number for the total flux. However, we have to pay attention to the meaning of the partial fluxes $\Phi_{1,2}$. Their time integral being one does not mean that they carry one single photon, whose general state representation is given by equation (2.3.34a).

Well-separated single photon fluxes

The flux of a single photon is given, using the commutation relation $\left[\widehat{b}(t), \widehat{b}^\dagger(t')\right] = \delta(t-t')$ and the temporal function $\widetilde{\phi}(t)$:

$$\Phi_{\rm sp}(t) = \langle 1_\phi | \widehat{b}^\dagger(t)\widehat{b}(t) | 1_\phi \rangle = |\widetilde{\phi}(t)|^2. \tag{2.3.40}$$

If two single photons are emitted with a time delay τ such that $\tau \gg T_{\rm sp}$ where $T_{\rm sp}$ is a characteristic pulse width for a single photon, then the two photon state function can be written as:

$$\widetilde{\Psi}(t_1, t_2) = \widetilde{\phi}_1(t_1)\widetilde{\phi}_2(t_2), \tag{2.3.41}$$

where $\widetilde{\phi}_{1,2}(t)$ are the temporal functions of the first and second single photons, respectively. Those two functions respect $\widetilde{\phi}_1(t)\widetilde{\phi}_2(t) = 0$ for all t, since the single photons are well separated. As a consequence, we have $\mathcal{N}_2 = 1$ and the partial photon fluxes (2.3.38) become simply:

$$\Phi_{1,2}(t) = |\widetilde{\phi}_{1,2}(t)|^2. \tag{2.3.42}$$

As a consequence, the state (2.3.34b) can be written as two orthogonal single photon states:

$$|2_\Psi\rangle \equiv |1_{\phi_1}\rangle |1_{\phi_2}\rangle, \tag{2.3.43a}$$

$$\langle 1_{\phi_1} | 1_{\phi_2} \rangle = \int_{-\infty}^{+\infty} {\rm d}t\, \widetilde{\phi}_1^*(t)\widetilde{\phi}_2(t) = 0. \tag{2.3.43b}$$

General two-photon Fock state

A Fock state with two photons in the same mode has a temporal function which must be factorizable into two identical functions:

$$\widetilde{\Psi}_{2F}(t_1, t_2) = \widetilde{\phi}(t_1)\widetilde{\phi}(t_2), \tag{2.3.44}$$

such that the general two-photon state (2.3.34b) can take the form:

$$|2_\phi\rangle = \frac{\left(\widehat{a}_\phi^\dagger\right)^2}{\sqrt{2!}} |\mathbf{0}\rangle. \tag{2.3.45}$$

The criteria on producing a two-photon Fock state is then to have the partial photon fluxes (2.3.38) overlapping completely:

$$\Phi_1(t) = \Phi_2(t) = |\widetilde{\phi}(t)|^2. \tag{2.3.46}$$

Outgoing two-photon state with two atoms in a cavity

We analyze the results showed in fig. 2.12: for the case (a), we have two non-overlapping partial photon fluxes, each carrying one single photon. The outgoing photon state is then $|1_{\phi_1}\rangle|1_{\phi_2}\rangle$, where:

$$\widetilde{\phi}_1(t) \equiv \widetilde{\phi}(t), \tag{2.3.47}$$

$$\widetilde{\phi}_2(t) = \widetilde{\phi}(t + \tau_L), \tag{2.3.48}$$

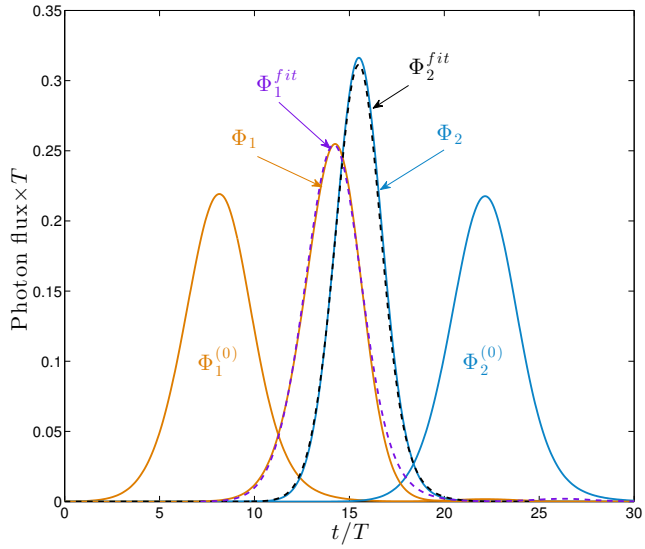

Figure 2.13: Photon flux fit (dashed lines) of the paritally overlapping photon fluxes ($\Phi_1 = \Phi_{fg,1} + \Phi_{gf,1}, \Phi_2 = \Phi_{ff,1}$ in fig. 2.12b), using non overlapping flux shapes ($\Phi_1^{(0)} = \Phi_{fg,1}, \Phi_2^{(0)} = \Phi_{ff,1}$ in fig. 2.12a).

τ_L being the delay between the two single photons, corresponding to the delay between the laser pulses. The wavefunction of this state can be fully determined from the partial fluxes:

$$|\widetilde{\Psi}^{(0)}(t_1, t_2)| = \sqrt{\mathcal{N}_2}\sqrt{\Phi_1^{(0)}(t_1)\Phi_2^{(0)}(t_2)}, \tag{2.3.49}$$

where we have labelled the wavefunction and the partial fluxes with a superscript (0) to specify that they don't overlap. For the case displayed on fig. 2.12b, the partial photon fluxes overlap. To determine the wavefunction, we assume the form:

$$|\widetilde{\Psi}(t_1, t_2)| = \sqrt{\mathcal{N}_2}\sqrt{\Phi_1(t_1)\Phi_2(t_2)}, \tag{2.3.50}$$

where:

$$\Phi_j\left(\frac{t}{T_j}\right) \approx \frac{T_j^{(0)}}{T_j}\Phi_j^{(0)}\left(\frac{t+\tau_j}{T_j^{(0)}}\right), \quad i = 1, 2 \tag{2.3.51}$$

with $\Phi_1 = \Phi_{fg,1} + \Phi_{gf,1}$, $\Phi_2 = \Phi_{ff,1}$ taken from fig. 2.12b and $\Phi_1^{(0)} = \Phi_{fg,1}, \Phi_2^{(0)} = \Phi_{ff,1}$ from fig. 2.12a. The coefficients $T_j^{(0)}, T_j$ and τ_j are adapted to satisfy at best (2.3.51). The results are shown in fig. 2.13. We can observe very close shapes between the exact and fitted fluxes. This allows the characterization with a good accuracy of the two-photon state in fig. 2.12 by a state of the form (2.3.34b) with (2.3.50).

Second-order correlation function

The autocorrelation function, or second-order correlation function, is a measurement performed by a Handbury-Brown-Twiss setup, and characterizes the quantum behavior of light,

such as single photon sources, squeezed light, or coherent states. We study the behavior of the unnormalized second-order correlation function $G^{(2)}(t,\tau)$ associated with the outgoing field of the cavity:

$$G^{(2)}(t,\tau) = \big\langle \widehat{c}^\dagger(t)\widehat{c}^\dagger(t+\tau)\widehat{c}(t+\tau)\widehat{c}(t)\big\rangle. \tag{2.3.52}$$

The two-time second order correlation function is not defined in the Schrödinger picture, because of the two time arguments. We apply the quantum regression theorem to compute numerically this function [86]. Using the propagator $\widehat{U}(t,t_0)$ of the system and the environment, and considering the Markov approximation, one finds:

$$\begin{aligned} G^{(2)}(t,\tau) &= \mathrm{Tr}_S\big\{\widetilde{\Lambda}(t+\tau,t)\widehat{c}\widehat{\varrho}(t)\widehat{c}^\dagger\big\} \\ &= \mathrm{Tr}_S\big\{\widehat{c}^\dagger\widehat{c}\,\Lambda(t+\tau,t)\big\}, \end{aligned} \tag{2.3.53}$$

with $\Lambda(t+\tau,t), \widetilde{\Lambda}(t+\tau,t)$ being defined as follows:

$$\Lambda(t+\tau,t) = \mathrm{Tr}_R\big\{\widehat{U}(t+\tau,t)\widehat{c}\widehat{\varrho}(t)\widehat{c}^\dagger\widehat{\varrho}_R\widehat{U}^\dagger(t+\tau,t)\big\}, \tag{2.3.54}$$

$$\widetilde{\Lambda}(t+\tau,t) = \mathrm{Tr}_R\big\{\widehat{U}(t+\tau,t)\widehat{c}^\dagger\widehat{c}\widehat{U}^\dagger(t+\tau,t)\widehat{\varrho}_R\big\}. \tag{2.3.55}$$

As can be seen from equation (2.3.53), we have the identity:

$$\mathrm{Tr}_S\big\{\widetilde{\Lambda}(t+\tau,t)\widehat{c}\widehat{\varrho}(t)\widehat{c}^\dagger\big\} = \mathrm{Tr}_S\big\{\widehat{c}^\dagger\widehat{c}\,\Lambda(t+\tau,t)\big\}, \tag{2.3.56}$$

and this identity still stands if $\widehat{c}\widehat{\varrho}(t)\widehat{c}^\dagger$ is replaced by $\widehat{\varrho}(t)$, leading to:

$$\begin{aligned} \mathrm{Tr}_S\big\{\widetilde{\Lambda}(t+\tau,t)\widehat{\varrho}(t)\big\} &= \mathrm{Tr}_S\big\{\widehat{c}^\dagger\widehat{c}\,\widehat{\varrho}(t)\big\} \\ &= \big\langle\widehat{c}^\dagger(t+\tau)\widehat{c}(t+\tau)\big\rangle. \end{aligned} \tag{2.3.57}$$

We have to compute the density operator propagated to $t+\tau$:

$$\frac{\mathrm{d}}{\mathrm{d}\tau}\widehat{\varrho}(t+\tau) = \mathcal{L}(t+\tau)\widehat{\varrho}(t+\tau), \tag{2.3.58a}$$

$$\mathcal{L}(t)\widehat{\varrho}(t) = -\frac{i}{\hbar}\big[\widehat{H}_S(t),\widehat{\varrho}(t)\big] + \Gamma_c\Big(\widehat{c}\widehat{\varrho}(t)\widehat{c}^\dagger - \tfrac{1}{2}\big\{\widehat{c}^\dagger\widehat{c},\widehat{\varrho}(t)\big\}\Big), \tag{2.3.58b}$$

and we write the solution of this equation:

$$\widehat{\varrho}(t+\tau) = V(t+\tau,t)\widehat{\varrho}(t). \tag{2.3.59}$$

Using bot equations (2.3.54) and (2.3.58a), we find that the same equation applies to $\Lambda(t+\tau,t)$:

$$\frac{\mathrm{d}}{\mathrm{d}\tau}\Lambda(t+\tau,t) = \mathcal{L}(t+\tau)\Lambda(t+\tau), \tag{2.3.60}$$

and as a consequence, the solution writes:

$$\begin{aligned} \Lambda(t+\tau,t) &= V(t+\tau,t)\Lambda(t,t) \\ &= V(t+\tau,t)\widehat{c}\widehat{\varrho}(t)\widehat{c}^\dagger. \end{aligned} \tag{2.3.61}$$

We display the unnormalized two-time second order correlation function in fig. 2.14. In this calculation, we chose a reference time t_{peak} corresponding to the peaked value of the total photon flux, and we propagated the solution of the master equation $\Lambda(t_{\mathrm{peak}}+\tau,t_{\mathrm{peak}})$ to get the results. The figure shows a small bump due to the coincidences at zero delays ($\tau=0$), indicating that the probability of a joint generation of two photons is higher than any other delayed generation of two single photons. However, regarding the sum over all possible delays, this probability is very small.

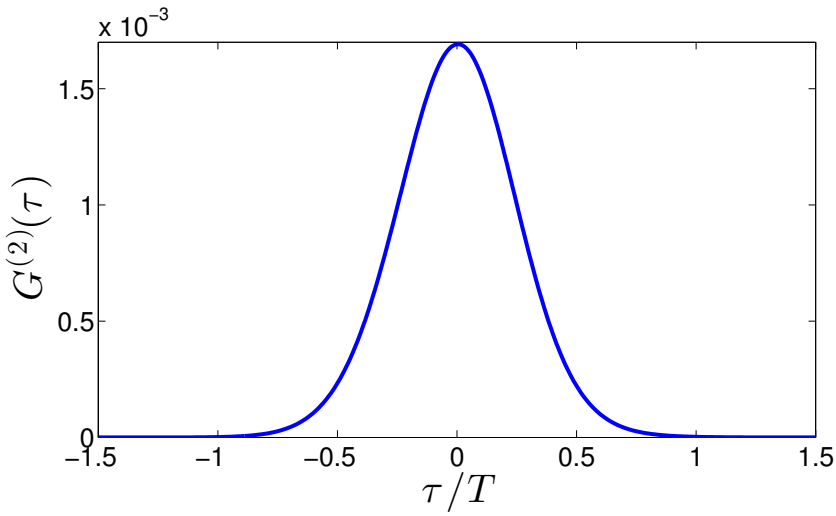

Figure 2.14: Unnormalized two-time second-order correlation function $G^{(2)}(t_{\text{peak}}, \tau) \equiv G^{(2)}(\tau)$, with respect to the reference time t_{peak} corresponding to the maximum of $\Phi(t)$.

Summary

We have presented a general study of cavity QED concepts, and derived the models associated with them. An application for the production of photon states leaking from a cavity was shown. In the next part, we transpose the concept of cQED to quantum plasmonics. Optical cavities are usually understood in the high-Q limit, but in the case of plasmons we have to consider low-Q systems. Nevertheless, the transposition of the concepts is still possible in terms of the structure of the effective models, as is shown in chapter 4.

Appendix

2.A Canonical quantization of the electromagnetic field in a dielectric medium

In this appendix, we derive the quantization procedure step by step, starting from the propagation equation (2.1.8). Using the new variable $\mathbf{A}' = \sqrt{\epsilon_r(\mathbf{r})}\mathbf{A}$, the propagation equation has the form:

$$\left(\frac{\partial^2}{\partial t^2} + \mathbf{\Omega}^2\right)\mathbf{A}' = 0, \tag{2.A.1}$$

where we define the Hermitian operator $\mathbf{\Omega} := (\mathbf{\Xi}^\dagger\mathbf{\Xi})^{1/2}$, with $\mathbf{\Xi} = c\boldsymbol{\nabla} \times \frac{1}{\sqrt{\epsilon_r}}$. To show the hermiticity of this operator, one can write operator $\mathbf{\Xi}$ as a matrix in Cartesian coordinates:

$$\mathbf{\Xi} = c\begin{pmatrix} 0 & -\partial_z & \partial_y \\ \partial_z & 0 & -\partial_x \\ -\partial_y & \partial_x & 0 \end{pmatrix}\frac{1}{\sqrt{\epsilon_r}}, \tag{2.A.2}$$

where we used the simplified notation $\partial_x \equiv \frac{\partial}{\partial x}$. Recalling that $(\partial_x)^\dagger = -\partial_x$, we find the operator $\mathbf{\Xi}^\dagger\mathbf{\Xi}$ to be Hermitian. The operator $\mathbf{\Xi}^\dagger\mathbf{\Xi}$ is positive by construction, so its square root is well-defined. The next step consists in defining a canonical conjugate variable $\mathbf{\Pi}'$ such that the pair $(\mathbf{A}', \mathbf{\Pi}')$ forms a Hamiltonian system:

$$\frac{\partial \mathbf{\Pi}'}{\partial t} = -\frac{\partial \mathcal{H}}{\partial \mathbf{A}'} \tag{2.A.3}$$

$$\frac{\partial \mathbf{A}'}{\partial t} = \frac{\partial \mathcal{H}}{\partial \mathbf{\Pi}'}, \tag{2.A.4}$$

with the Hamiltonian density:

$$\mathcal{H} = \frac{1}{2}\Big(\mathbf{\Pi}' \cdot \mathbf{\Pi}' + \mathbf{A}' \cdot \mathbf{\Omega}^2\mathbf{A}'\Big). \tag{2.A.5}$$

The Hamiltonian is obtained when integrating the latter over $\mathbf{r}$. Equations (2.A.3) to(2.A.5) lead indeed to (2.A.1). To relate $\mathbf{\Pi}'$ to a physical quantity, we connect (2.A.4) with (2.1.6) via:

$$\mathbf{\Pi}' = -\sqrt{\epsilon_r(\mathbf{r})}\mathbf{E}. \tag{2.A.6}$$

The Hamiltonian cannot be quantized directly using the principle of correspondence because the canonical variables have to satisfy the constraint given by the generalized Coulomb gauge (2.1.7). To get rid of the constraint, we introduce a coordinate in the complex phase space $\mathcal{P}_{\mathbb{C}}\{\mathbf{A}', \mathbf{\Pi}'\}$ spanned by $(\mathbf{A}', \mathbf{\Pi}')$:

$$\mathbf{Z} = \frac{1}{\sqrt{2\hbar}}\Big(\mathbf{\Omega}^{1/2}\mathbf{A}' + i\mathbf{\Omega}^{-1/2}\mathbf{\Pi}'\Big), \tag{2.A.7}$$

and we consider an orthonormal basis of complex functions $\{\mathbf{\Phi}_\kappa\}$ with the scalar product:

$$\langle \mathbf{\Phi}_\kappa, \mathbf{\Phi}_{\kappa'}\rangle = \int_V \mathrm{d}^3r\, \mathbf{\Phi}^*_\kappa(\mathbf{r}) \cdot \mathbf{\Phi}_{\kappa'}(\mathbf{r}) = \delta_{\kappa\kappa'}, \tag{2.A.8}$$

where κ is a label denoting the classical mode, and the total number N of normal modes is finite. These mode functions must fulfill the constraint (2.1.7): $\boldsymbol{\nabla} \cdot (\epsilon \boldsymbol{\Phi}_\kappa) = 0$ and we represent the phase space coordinate in this basis:

$$\mathbf{Z} = \sum_\kappa a_\kappa \boldsymbol{\Phi}_\kappa. \tag{2.A.9}$$

Doing so, we unravel a new map leading to another phase space where a_κ is the coordinate. Combining all modes in a vector $\underline{a} = (a_{\kappa_1}, ..., a_{\kappa_N})$, we write:

$$\underline{a} = \frac{1}{\sqrt{2\hbar}} \Big(\bar{\Omega}^{1/2} \underline{q} + i \bar{\Omega}^{-1/2} \underline{p} \Big), \tag{2.A.10}$$

where we introduced the mode representation of $\boldsymbol{\Omega}$ with the matrix elements:

$$\bar{\Omega}_{\kappa\kappa'} = \langle \boldsymbol{\Phi}_\kappa, \boldsymbol{\Omega} \boldsymbol{\Phi}_{\kappa'} \rangle. \tag{2.A.11}$$

By writing the coordinate in the mode representation, we get the map $(\mathbf{A}', \boldsymbol{\Pi}') \mapsto (\underline{q}, \underline{p})$, which is a canonical transformation, and the new coordinates $(\underline{q}, \underline{p})$ are free of constraints, therefore independent. The principle of correspondence is now possible and we replace the canonical operators by operators:

$$q_\kappa \mapsto \widehat{q}_\kappa \text{ (operator of multiplication by } q_\kappa), \qquad p_\kappa \mapsto \widehat{p}_\kappa := -i\hbar \frac{\partial}{\partial q_\kappa}, \tag{2.A.12}$$

with the commutation relations:

$$\big[\widehat{q}_\kappa, \widehat{q}_{\kappa'}\big] = \big[\widehat{p}_\kappa, \widehat{p}_{\kappa'}\big] = 0 \tag{2.A.13a}$$

$$\big[\widehat{q}_\kappa, \widehat{p}_{\kappa'}\big] = i\hbar \delta_{\kappa\kappa'}. \tag{2.A.13b}$$

The phase space coordinate becomes the annihilation operator with the related commutation relation:

$$\underline{z} \mapsto \underline{\widehat{a}} := \frac{1}{\sqrt{2\hbar}} \Big(\bar{\Omega}^{1/2} \underline{\widehat{q}} + i \bar{\Omega}^{-1/2} \underline{\widehat{p}} \Big), \qquad \big[\widehat{a}_\kappa, \widehat{a}^\dagger_{\kappa'}\big] = \delta_{\kappa\kappa'}. \tag{2.A.14}$$

The original variables corresponding to the field can be expressed as linear combinations of the creation and annihilation operators when writing the inverse relations:

$$\widehat{\mathbf{A}}'(\mathbf{r}) = \sqrt{\frac{\hbar}{2}} \sum_\kappa \boldsymbol{\Omega}^{-1/2} \Big(\boldsymbol{\Phi}_\kappa(\mathbf{r}) \widehat{a}_\kappa + \boldsymbol{\Phi}^*_\kappa(\mathbf{r}) \widehat{a}^\dagger_\kappa \Big) \tag{2.A.15a}$$

$$\widehat{\boldsymbol{\Pi}}'(\mathbf{r}) = -i \sqrt{\frac{\hbar}{2}} \sum_\kappa \boldsymbol{\Omega}^{1/2} \Big(\boldsymbol{\Phi}_\kappa(\mathbf{r}) \widehat{a}_\kappa - \boldsymbol{\Phi}^*_\kappa(\mathbf{r}) \widehat{a}^\dagger_\kappa \Big). \tag{2.A.15b}$$

In the previous derivation, the mode functions $\boldsymbol{\Phi}_\kappa$ have to satisfy the constraint and the boundary conditions. We consider them to be eigenmodes (or normal modes) of the frequency operator:

$$\boldsymbol{\Omega}^2 \boldsymbol{\Phi}_\kappa = \omega_\kappa^2 \boldsymbol{\Phi}_\kappa, \tag{2.A.16}$$

where ω_κ is the frequency associated to the normal mode labelled κ. The frequency operator being positive, its square root is defined and we write the observables in terms of the eigenvalues ω_κ:

$$\widehat{\mathbf{A}}'(\mathbf{r}) = \sum_\kappa \sqrt{\frac{\hbar}{2\omega_\kappa}} \Big(\mathbf{\Phi}_\kappa(\mathbf{r}) \widehat{a}_\kappa + \mathbf{\Phi}_\kappa^*(\mathbf{r}) \widehat{a}_\kappa^\dagger \Big) \tag{2.A.17a}$$

$$\widehat{\mathbf{\Pi}}'(\mathbf{r}) = -i \sum_\kappa \sqrt{\frac{\hbar\omega_\kappa}{2}} \Big(\mathbf{\Phi}_\kappa(\mathbf{r}) \widehat{a}_\kappa - \mathbf{\Phi}_\kappa^*(\mathbf{r}) \widehat{a}_\kappa^\dagger \Big). \tag{2.A.17b}$$

Appendix

2.B Lorentzian structure of the cavity spectral response function

In this section we derive the Lorentzian structure of the cavity response function (2.1.30):

$$\mathcal{T}(\omega) = \frac{\underline{\mathrm{t}}(\omega)}{1 + \underline{\mathrm{r}}(\omega)\mathrm{e}^{i2\frac{\omega}{c}L}}. \tag{2.B.1}$$

For simplicity, we do not write the dependence in ω of $\underline{\mathrm{r}}$ and $\underline{\mathrm{t}}$ in the calculation, and we use the complex notation $\underline{\mathrm{r}} = |\underline{\mathrm{r}}|\mathrm{e}^{i\phi_r}$. Writing the square modulus of $\mathcal{T}(\omega)$, and using (2.1.27a) we get:

$$\begin{aligned} |\mathcal{T}(\omega)|^2 &= \frac{1 - |\underline{\mathrm{r}}|^2}{|1 + |\underline{\mathrm{r}}|\mathrm{e}^{i\phi}|^2} \\ &= 1 - \frac{|\underline{\mathrm{r}}|\mathrm{e}^{i\phi}}{1 + |\underline{\mathrm{r}}|\mathrm{e}^{i\phi}} - \frac{|\underline{\mathrm{r}}|\mathrm{e}^{-i\phi}}{1 + |\underline{\mathrm{r}}|\mathrm{e}^{-i\phi}}, \end{aligned} \tag{2.B.2}$$

where $\phi = \phi_r + 2\frac{\omega}{c}L$. Using the geometric series formula:

$$\sum_{n=1}^{+\infty} q^n = \frac{q}{1-q}, \quad |q| < 1, \tag{2.B.3}$$

we can write the two last terms of the above expression in terms of discrete sums:

$$\begin{aligned} |\mathcal{T}(\omega)|^2 &= 1 + \sum_{n=1}^{+\infty} |\underline{\mathrm{r}}|^n \left(\mathrm{e}^{in(\phi+\pi)} + \mathrm{e}^{-in(\phi+\pi)}\right) \\ &= \sum_{n=-\infty}^{+\infty} |\underline{\mathrm{r}}|^{|n|}\mathrm{e}^{in(\phi+\pi)}. \end{aligned} \tag{2.B.4}$$

Having the expression of $|\mathcal{T}(\omega)|^2$ in terms of a single discrete sum where n runs from $-\infty$ to $+\infty$, we invoke the Poisson summation formula [87]:

$$\begin{aligned} \sum_{n=-\infty}^{+\infty} f(n) &= \sum_{m=-\infty}^{+\infty} \int_{-\infty}^{+\infty} \mathrm{d}x\, f(x)\mathrm{e}^{-i2\pi m x} \\ &= \sum_{m=-\infty}^{+\infty} \widetilde{f}(m), \end{aligned} \tag{2.B.5}$$

$\widetilde{f}(y) = \mathcal{F}_y[f(x)]$ being the Fourier transform of $f(x)$. We apply it to the function:

$$f(x) = |\underline{\mathrm{r}}|^{|x|}\mathrm{e}^{ix(\phi\pm\pi)} = \exp\Big(|x|\ln|\underline{\mathrm{r}}| + ix(\phi \pm \pi)\Big), \tag{2.B.6}$$

and we use the following identity to compute the Fourier transform:

$$\begin{aligned}\mathcal{F}_y\left[\mathrm{e}^{i2\pi y_0 x}\mathrm{e}^{-a|x|}\right] &= \mathcal{F}_{y-y_0}\left[\mathrm{e}^{-a|x|}\right] \\ &= \frac{2a}{\big(2\pi(y-y_0)\big)^2 + a^2}.\end{aligned} \tag{2.B.7}$$

Finally, the Fourier transform reads:

$$\widetilde{f}(m) = \frac{-2\ln|\underline{\mathrm{r}}|}{\big(2\pi m - (2\frac{\omega}{c}L - \phi_r + \pi)\big)^2 + (\ln|\underline{\mathrm{r}}|)^2}, \tag{2.B.8}$$

and multiplying both the numerator and the denominator by $(c/2L)^2$ we find the Lorentzian structure of the cavity spectral response function:

$$|\mathcal{T}(\omega)|^2 = \sum_{m=-\infty}^{+\infty} \frac{c}{2L}\frac{\gamma(\omega)}{\big(\omega - \widetilde{\omega}_m(\omega)\big)^2 + \left(\frac{\gamma(\omega)}{2}\right)^2}, \tag{2.B.9a}$$

$$\gamma(\omega) = -\frac{c}{L}\ln|\underline{\mathrm{r}}(\omega)|, \tag{2.B.9b}$$

$$\widetilde{\omega}_m(\omega) = m\frac{\pi c}{L} + \frac{c}{2L}\big(\pi - \phi_r(\omega)\big). \tag{2.B.9c}$$

Appendix

2.C Complex plane integration of the atom-field coupling

The integrals (2.2.22) are evaluated here. We recall the expression of the square modulus of the atom-field coupling:

$$|\eta_m(\omega)|^2 = \frac{\widetilde{\omega}_m |d|^2}{\hbar\epsilon_0 \mathcal{A} L} \sin^2\left[\tfrac{\omega}{c}(x_A+\ell)\right] \frac{\Gamma_m}{2\pi} \frac{1}{(\omega-\widetilde{\omega}_m)^2 + \left(\frac{\Gamma_m}{2}\right)^2}. \tag{2.C.1}$$

The $\sin^2$ function can be split into three terms:

$$\sin^2\left[\tfrac{\omega}{c}(x_A+\ell)\right] = \frac{1}{2}\left(1 - \frac{\mathrm{e}^{i2\frac{\omega}{c}(x_A+\ell)} + \mathrm{e}^{-i2\frac{\omega}{c}(x_A+\ell)}}{2}\right), \tag{2.C.2}$$

leading to three integral parts that have to be calculated separately. The first terms leads simply to the integral:

$$\begin{aligned}\mathcal{I}_0 &= \frac{\widetilde{\omega}_m |d|^2}{2\hbar\epsilon_0 \mathcal{A} L} \underbrace{\int_{-\widetilde{\omega}_m}^{+\infty} \mathrm{d}\Delta \, \frac{\Gamma_m}{2\pi} \frac{1}{\Delta^2 + \left(\frac{\Gamma_m}{2}\right)^2}}_{1 \text{ for } \widetilde{\omega}_m \to +\infty} \\ &= \frac{\widetilde{\omega}_m |d|^2}{2\hbar\epsilon_0 \mathcal{A} L},\end{aligned} \tag{2.C.3}$$

where we introduced the change of variables $\Delta = \omega - \widetilde{\omega}_m$ and extended the lower bound of the integral to $-\infty$, as we consider the limit $\Gamma_m \ll \widetilde{\omega}_m$. The two other integrals, corresponding to the exponential terms in (2.C.2), are:

$$\mathcal{I}_\pm = \frac{\widetilde{\omega}_m |d|^2}{4\hbar\epsilon_0 \mathcal{A} L} \mathrm{e}^{\pm i2\frac{\widetilde{\omega}_m}{c}(x_A+\ell)} \int_{-\infty}^{+\infty} \mathrm{d}\Delta \, \frac{\Gamma_m}{2\pi} \frac{\mathrm{e}^{\pm i2\frac{\Delta}{c}(x_A+\ell)}}{\Delta^2 + \left(\frac{\Gamma_m}{2}\right)^2}. \tag{2.C.4}$$

These integrals have to be done in the complex plane, using a proper contour (see fig. 2.15). To do so we define the complex functions:

$$f_\pm(z) = \frac{\Gamma_m}{2\pi} \frac{\mathrm{e}^{\pm i2\frac{z}{c}(x_A+\ell)}}{z^2 + \left(\frac{\Gamma_m}{2}\right)^2}. \tag{2.C.5}$$

The exponentials of the complex variable z lead to an integration in the positive half-plane for $f_+(z)$ and the negative half-plane for $f_-(z)$ (see fig. 2.15), because $x_A + \ell > 0$ and we require that the half-circle integrals vanish when $|z| \to +\infty$, such that we can use the residue theorem:

$$\begin{aligned}\int_{-\infty}^{+\infty} \mathrm{d}\Delta \, f_\pm(\Delta) &= \oint_C \mathrm{d}z f_\pm(z) \\ &= \pm 2\pi i \, \mathrm{Res}_{z=z_\pm} f_\pm(z),\end{aligned} \tag{2.C.6}$$

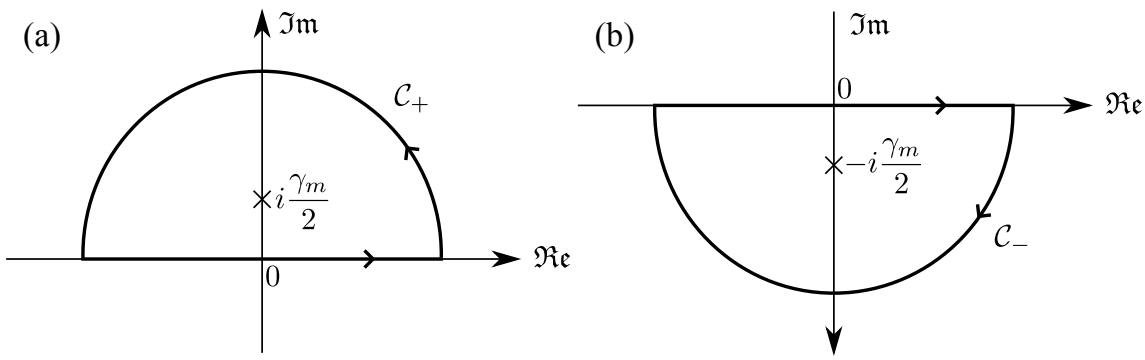

Figure 2.15: Half-plane contour integration in the complex plane for the integrals (a) $\mathcal{I}_+$ and (b) $\mathcal{I}_-$ (see (2.C.4)).

where $z_\pm = \pm i\frac{\Gamma_m}{2}$ are the poles of the functions $f_\pm(z)$. Their denominators can be factorized as $(z - z_\pm)(z + z_\pm)$, and the residues lead to:

$$\int_{-\infty}^{+\infty} \mathrm{d}\Delta\, f_\pm(\Delta) = \mathrm{e}^{-\Gamma_m \frac{x_A+\ell}{c}}. \tag{2.C.7}$$

As a result, we get the two integrals:

$$\mathcal{I}_\pm = \frac{\widetilde{\omega}_m |d|^2}{4\hbar\epsilon_0 \mathcal{A} L} \mathrm{e}^{\pm i 2\frac{\widetilde{\omega}_m}{c}(x_A+\ell)} \mathrm{e}^{-\Gamma_m \frac{x_A+\ell}{c}}, \tag{2.C.8}$$

and summing all three integrals as $\mathcal{I} = \mathcal{I}_0 - (\mathcal{I}_+ + \mathcal{I}_-)$ we get the integrated atom-field coupling:

$$\boxed{\int_0^{+\infty} \mathrm{d}\omega |\eta_m(\omega)|^2 = \frac{\widetilde{\omega}_m |d|^2}{2\hbar\epsilon_0 \mathcal{A} L} \left(1 - \mathrm{e}^{-\Gamma_m \frac{x_A+\ell}{c}} \cos\left[2\frac{\widetilde{\omega}_m}{c}(x_A+\ell)\right]\right).} \tag{2.C.9}$$

Another integral has to be calculated in (2.2.20):

$$\mathcal{I}' = \int_0^{+\infty} \mathrm{d}\omega |\eta_m(\omega)|^2 (\omega - \omega_0) \mathrm{e}^{-i(\omega-\omega_0)(t-t')}, \quad t - t' > 0. \tag{2.C.10}$$

Its integration, if analogous to the previous procedure, is slightly tricky and involves a coarse-graining approximation. The complex function to integrate has the same poles, but the exponential factor is more complicated:

$$f'_\pm(z) = \frac{\Gamma_m}{2\pi} \frac{z + \widetilde{\Delta}_m}{z^2 + \left(\frac{\Gamma_m}{2}\right)^2} \mathrm{e}^{-iz\left(t-t' \mp \frac{2(x_A+\ell)}{c}\right)}, \tag{2.C.11}$$

where we have introduced the atom-cavity mode detuning $\widetilde{\Delta}_m = \widetilde{\omega}_m - \omega_0$. The integral splits in three parts, due to the square sine function, and the three integrals are:

$$\mathcal{I}'_0 = \frac{\widetilde{\omega}_m |d|^2}{2\hbar\epsilon_0 \mathcal{A} L} \mathrm{e}^{-i\widetilde{\Delta}_m(t-t')} \int_{-\infty}^{+\infty} \mathrm{d}\Delta \frac{\Gamma_m}{2\pi} \frac{\Delta + \widetilde{\Delta}_m}{\Delta^2 + \left(\frac{\Gamma_m}{2}\right)^2} \mathrm{e}^{-i\Delta(t-t')} \tag{2.C.12a}$$

$$\mathcal{I}'_\pm = \frac{\widetilde{\omega}_m |d|^2}{4\hbar\epsilon_0 \mathcal{A} L} \mathrm{e}^{-i\widetilde{\Delta}_m(t-t')} \mathrm{e}^{\pm i\frac{\widetilde{\omega}_m}{c}(x_A+\ell)} \int_{-\infty}^{+\infty} \mathrm{d}\Delta f'_\pm(\Delta). \tag{2.C.12b}$$

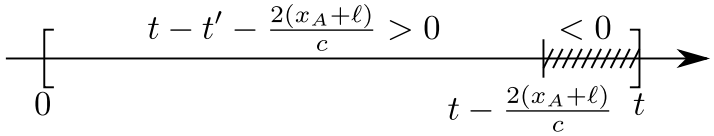

Figure 2.16: Positive and negative domains of the exponential argument in (2.C.11).

The first integral $\mathcal{I}'_0$ is trivial and is done in the lower half-plane, where the exponential doesn't diverge as $t - t' > 0$. For $\mathcal{I}'_+$ there is a possibility in the exponential term that $t - t' - \frac{2(x_A+\ell)}{c}$ is negative (see fig. 2.16), whereas $t - t' + \frac{2(x_A+\ell)}{c}$ is always positive in $\mathcal{I}'_-$. The integral over time can then be split into a positive and negative part:

$$\int_0^t \mathrm{d}t' = \int_0^{t-\frac{2(x_A+\ell)}{c}} \mathrm{d}t' + \int_{t-\frac{2(x_A+\ell)}{c}}^t \mathrm{d}t'. \tag{2.C.13}$$

However, the second part provides very little contribution due to the non-resolved time-of-flight timescale. Indeed, $\frac{2(x_A+\ell)}{c}$ is of the order of this timescale $T_{\mathrm{fl}} = \ell/c$, which is much smaller than the typical timescale in which the system evolves. As a consequence, we drop the second integral and one has:

$$\int_0^t \mathrm{d}t' \approx \int_0^{t-\frac{2(x_A+\ell)}{c}} \mathrm{d}t', \quad t - t' - \frac{2(x_A+\ell)}{c} > 0. \tag{2.C.14}$$

Therefore, all integrals are done in the lower half-plane and we get:

$$\mathcal{I}'_0 = \frac{\widetilde{\omega}_m |d|^2}{2\hbar\epsilon_0 \mathcal{A} L}\Big(\widetilde{\Delta}_m - i\frac{\Gamma_m}{2}\Big)\mathrm{e}^{-i\left(\widetilde{\Delta}_m - i\frac{\Gamma_m}{2}\right)(t-t')} \tag{2.C.15a}$$

$$\mathcal{I}'_\pm = \frac{\widetilde{\omega}_m |d|^2}{4\hbar\epsilon_0 \mathcal{A} L}\Big(\widetilde{\Delta}_m - i\frac{\Gamma_m}{2}\Big)\mathrm{e}^{-i\left(\widetilde{\Delta}_m - i\frac{\Gamma_m}{2}\right)(t-t')}\mathrm{e}^{\pm i\frac{\widetilde{\omega}_m}{c}(x_A+\ell)}\mathrm{e}^{\pm\Gamma_m\frac{x_A+\ell}{c}}. \tag{2.C.15b}$$

Summing them all, we finally get:

$$\begin{aligned}\mathcal{I}' &= \int_0^{+\infty} \mathrm{d}\omega |\eta_m(\omega)|^2(\omega - \omega_0)\mathrm{e}^{-i(\omega-\omega_0)(t-t')} \\ &= h_m\Big(\widetilde{\Delta}_m - i\frac{\Gamma_m}{2}\Big)\mathrm{e}^{-i\left(\widetilde{\Delta}_m - i\frac{\Gamma_m}{2}\right)(t-t')},\end{aligned} \tag{2.C.16}$$

where:

$$h_m = \frac{\widetilde{\omega}_m |d|^2}{2\hbar\epsilon_0 \mathcal{A} L}\Big(1 - \cos\left[2\tfrac{\widetilde{\omega}_m}{c}(x_A+\ell)\right]\cosh\left[\Gamma_m\tfrac{x_A+\ell}{c}\right] - i\sin\left[2\tfrac{\widetilde{\omega}_m}{c}(x_A+\ell)\right]\sinh\left[\Gamma_m\tfrac{x_A+\ell}{c}\right]\Big). \tag{2.C.17}$$

Appendix

2.D Numerical solution of $\dot{\vec{X}}(t) = \mathbf{M}(t)\vec{X}(t) + \vec{Y}(t)$

We solve numerically the equation:

$$\left(\frac{\mathrm{d}}{\mathrm{d}t} - \mathbf{M}(t)\right)\vec{X}(t) = \vec{Y}(t), \tag{2.D.1}$$

where $\vec{X}$ and $\vec{Y}$ are two columns of same dimension, and $\mathbf{M}$ is a matrix. The general solution of (2.D.1) is:

$$\vec{X}(t) = \mathrm{e}^{\int_{t_0}^{t}\mathrm{d}t'\mathbf{M}(t')}\vec{X}(t_0) + \int_{t_0}^{t}\mathrm{d}t'\mathrm{e}^{\int_{t'}^{t}\mathrm{d}t''\mathbf{M}(t'')}\vec{Y}(t'). \tag{2.D.2}$$

The numerical solution of (2.D.1) is obtained while discretizing time into small intervals. Thus, the full timespan T is cut into N time steps, each of them having a duration $\Delta t \equiv \varepsilon$. Knowing $\vec{X}$ at time t_n, we get it at time t_{n+1}:

$$\vec{X}(t_{n+1}) = \vec{X}(t_n) + \int_{t_n}^{t_{n+1}}\mathrm{d}t'\mathbf{M}(t')\vec{X}(t') + \int_{t_n}^{t_{n+1}}\mathrm{d}t'\vec{Y}(t'). \tag{2.D.3}$$

We get a good approximation of this expression when taking trapezoid integrals, i.e. taking values of $\vec{X}$, $\vec{Y}$, $\mathbf{M}$ in $t_{n+\frac{1}{2}}$ rather than in t_n:

$$\vec{X}(t_{n+1}) = \vec{X}(t_n) + \varepsilon\mathbf{M}(t_{n+\frac{1}{2}})\vec{X}(t_{n+\frac{1}{2}}) + \varepsilon\vec{Y}(t_{n+\frac{1}{2}}) + \mathcal{O}(\varepsilon^3). \tag{2.D.4}$$

$\vec{X}(t_{n+\frac{1}{2}})$ writes explicitly:

$$\vec{X}(t_{n+\frac{1}{2}}) = \vec{X}(t_n) + \frac{\varepsilon}{2}\frac{\mathrm{d}\vec{X}(t_n)}{\mathrm{d}t} + \mathcal{O}(\varepsilon^2) \tag{2.D.5a}$$

$$= \vec{X}(t_n) + \frac{\varepsilon}{2}\mathbf{M}(t_n)\vec{X}(t_n) + \frac{\varepsilon}{2}\vec{Y}(t_n) + \mathcal{O}(\varepsilon^2). \tag{2.D.5b}$$

The error between t_n and $t_{n+\frac{1}{2}}$ is of the order of ε:

$$\mathbf{M}(t_n) = \mathbf{M}(t_{n+\frac{1}{2}}) + \mathcal{O}(\varepsilon) \tag{2.D.6}$$

$$\vec{Y}(t_n) = \vec{Y}(t_{n+\frac{1}{2}}) + \mathcal{O}(\varepsilon), \tag{2.D.7}$$

and equation (2.D.5b) becomes:

$$\vec{X}(t_{n+\frac{1}{2}}) = \vec{X}(t_n) + \frac{\varepsilon}{2}\mathbf{M}(t_{n+\frac{1}{2}})\vec{X}(t_n) + \frac{\varepsilon}{2}\vec{Y}(t_{n+\frac{1}{2}}) + \mathcal{O}(\varepsilon^2). \tag{2.D.8}$$

Thus we can replace $X(t_{n+\frac{1}{2}})$ in (2.D.4) and write:

$$\vec{X}(t_{n+1}) = \left(\mathbb{1} + \varepsilon\mathbf{M}(t_{n+\frac{1}{2}}) + \frac{\varepsilon}{2}\mathbf{M}^2(t_{n+\frac{1}{2}})\right)\vec{X}(t_n) + \varepsilon\left(\mathbb{1} + \frac{\varepsilon}{2}\mathbf{M}(t_{n+\frac{1}{2}})\right)\vec{Y}(t_{n+\frac{1}{2}}) + \mathcal{O}(\varepsilon^3). \tag{2.D.9}$$

The factors in front of $\vec{X}(t_n)$ and $\vec{Y}(t_{n+\frac{1}{2}})$ can be identified as Taylor series of exponential functions up to the third and second order, respectively. The error is then of the order of ε^3, and we write finally:

$$\boxed{\vec{X}(t_{n+1}) = \mathrm{e}^{\varepsilon \mathbf{M}(t_{n+\frac{1}{2}})}\vec{X}(t_n) + \varepsilon \mathrm{e}^{\frac{\varepsilon}{2}\mathbf{M}(t_{n+\frac{1}{2}})}\vec{Y}(t_{n+\frac{1}{2}}) + \mathcal{O}(\varepsilon^3).} \tag{2.D.10}$$

The number of operations being $N = T/\varepsilon$, the total error corresponds to $\mathcal{O}(\varepsilon^2)$.

Part III

Quantum control of emitters coupled to plasmons

Chapter 3

Mode-selective quantization procedure in a spherically layered medium

Chapter overview

Objectives: In this chapter we present the basic concepts of light-matter interactions at the nanoscale, developing a quantum plasmonics approach. We notably quantize localized surface plasmons supported by a metallic spherical particle, with particular attention devoted to the dissipation process. Finally, we express the full Hamiltonian describing the interaction between emitters and plasmonic particles, that will serve as a basis for the derivation of effective models presented in the next chapter.

Guideline:

- Concepts of light-matter interaction at the nanoscale.
- Introduction to plasmonics and quantum plasmonics.
- Quantum approach with metallic nanospheres.
- Mode-selective field quantization for spherically layered systems.
- **keywords:** *nano-optics, plasmons, absorption cross section, surface plasmon polariton (SPP), localized surface plasmon (LSP), quantum emitter, Purcell factor, strong coupling regime, metallic nanosphere, mode expansion, spherical vector harmonics, Green's tensor, field quantization.*

Results/novelty: Mode-selective quantization and multimodal effective models for spherically layered systems.

3.1 Light-emitter interactions and quantum plasmonics

3.1.1 Nano-optics and plasmonics

For more than two decades, nanoscience and nanotechnology have been regrouping physics, chemistry, biology, and other fields to reduce the size of systems, for a better understanding of phenomena as well as for the improvement of diverse processes. In micro-electronics, the integration of a maximum number of components on chip has lead to component sizes approaching 30 nm. The bandwidth of these components, however, does not exceed a few GHz, while photonics has brought accessible THz bandwidths. For this reason, the interest in miniaturizing optical devices has grown since the 70s, but the size of the optical components is limited by the diffraction limit, around 0.5 μm.
Confining light in the subwavelength regime opened the opportunity of probing matter at the nanoscale. To get an idea of the light-matter interaction efficiency in a quantitative way, we can introduce the cross section: for a fluorescent molecule, the absorption cross section at room temperature is of the order of $\sigma_{\text{abs}} \sim 10^{-20}$ m^2. A beam of light in the visible regime can be focused at best around $(\lambda/2)^2 \sim 10^{-13}$ m^2, which is seven orders of magnitude larger than the molecule cross section. This mismatch reveals the challenges to overcome to obtain comparable surfaces.
There are several strategies to increase the efficiency of interaction between light and molecules. It is possible to increase the cross section of the molecule at very low temperature ($T < 10$ K): $\sigma_{\text{abs}} \to 3\frac{\lambda^2}{2\pi}$, so that it can absorb almost all the energy of a focused beam. Increasing the time of interaction is also another way of increasing the coupling: placing a molecule in a high-Q micro-cavity accelerates its spontaneous emission rate. The light can also be confined to dimensions comparable to the size of the molecule: working beyond the diffraction limit is possible in near-field optics or using plasmonic structures. In this thesis, we focus on plasmonics and connect it with quantum control methods to access effective models, which are analogous to cavity QED models.

Plasmons

Plasmons are collective oscillations of free electrons localized at the surface of a metallic structure. The oscillatory motion of charges is associated with electromagnetic waves, which are confined at the surface of the structure. Modes resulting from the coupling of an electromagnetic wave and free charges from the metal are called surface plasmon polaritons (SPP). These modes are of two kinds: we distinguish propagating SPP modes, that can guide light on a few dozens of micrometers, from localized surface plasmons (LSP) arising with nanoparticles. LSP do not propagate, yet they confine the electromagnetic field in three dimensions. Both aspects of plasmons are displayed in fig. 3.1, with two examples: the excitation of a propagating SPP at the surface of a metallic layer covering a prism, and localized plasmons behaving as dipole antennas with spherical nanoparticles. In both cases the confinement of the plasmon is in the subwavelength regime. However this is achieved at the price of large ohmic losses in the metal. For instance a delocalized plasmon cannot propagate over a few micrometer decades. Similarly, the dipole moment of a metallic nanoparticle lifetime is of the order of 10 fs.
The confinement of light in the subwavelength regime leads to a strong field intensity in the

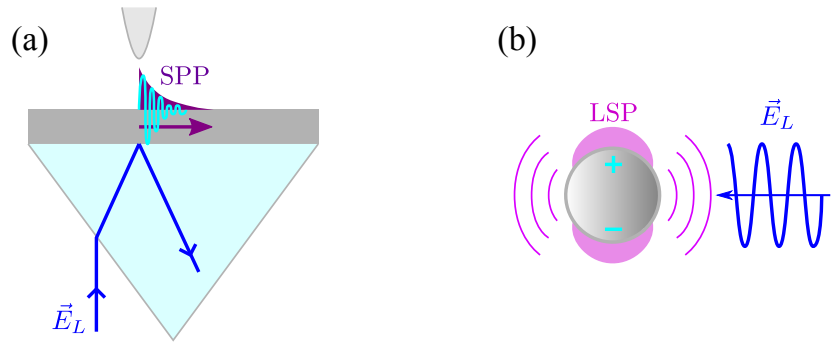

Figure 3.1: Surface plasmon polaritons in two schemes: (a) the excitation of a propagating plasmon at the surface of a metallic layer on a prism, excited with a laser beam; (b) the excitation of a dipolar plasmonic mode around a spherical nanoparticle. The plasmon is confined around the particle, and aligns with the excitation field in a two-lobe energy pattern. Reciprocally, the dipolar mode also radiates in the far field.

vicinity of the plasmonic structures, and such behavior has been used for applications such as bio-chemical sensors by surface plasmon resonance, or plasmonic waveguides for integrated photonics. The latter application allows both miniaturization and large bandwidth, making a compromise between micro-electronics and photonics.
Other applications such as plasmonic probes for near field optics can be mentioned [88]. To access subwavelength dimensions, a metallic nanoparticle is placed at the tip of an AFM probe and scatters the field efficiently. This enables enhanced surface spectroscopy, control of the fluorescence emission or Raman scattering by nanoscale monitoring of the probe-surface distance. In the following, we focus on the quantum control of nano-emitters and the interaction between light and plasmonic systems.

3.1.2 Nano-emitters near plasmonic structures

In the strategy of light confinement using plasmonic structures, the understanding of light-matter interactions at the nanoscale is crucial. Plasmons are confined on subwavelength scales, therefore they can be exploited via their interaction with very small light sources, such as quantum dots, N-V centers in diamond, or single molecules. Such nano-emitters, or *quantum emitters* therefore exchange energy with plasmonic modes, which present $\sim$ 10 fs lifetime. This opens the door to ultrafast nanophotonics.
From the point of view of a single emitter, the presence of plasmons opens new decay channels (through LSP modes) leading to the enhancement of the spontaneous emission process [89–91]. This effect is known as the *Purcell effect* and is often modeled as a single cavity mode interacting with quantum emitters. The key quantity is called *Purcell factor* and corresponds to the ratio between the modified decay rate Γ of the emitter near the plasmonic structure and the vacuum decay rate γ_0.
In the following, we consider a single emitter coupled to a cavity mode to derive the Purcell factor and show the use of this quantity. This opens the door to ultrafast nanophotonics [92].

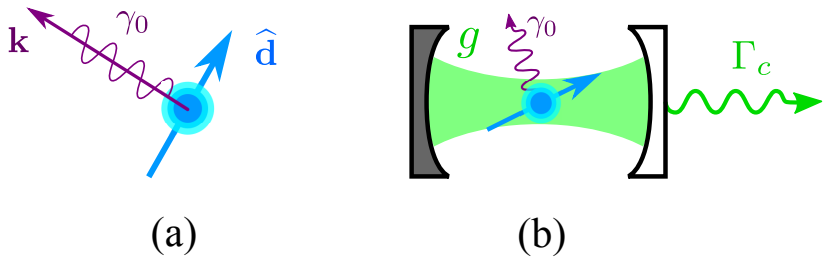

Figure 3.2: (a) A single atom in the vacuum: when emitting a photon, the atom decays to its ground state with decay rate γ_0, accounting for all possible direction along the wavevector $\mathbf{k}$ of the emitted photon. (b) An atom is placed in a cavity, and its transition coupled to the cavity field with coupling constant g. The cavity field leaks into outside vacuum modes with decay rate Γ_c (see chapter 2).

Emitter in a cavity - Purcell factor

The emission of light from a single emitter depends on its environment. The emission rate (or decay rate) corresponding to the emission is given by Fermi's golden rule:

$$\Gamma = \frac{2\pi}{\hbar^2} \sum_{\mathbf{k}} |\langle g, 1_{\mathbf{k}}|\widehat{\mathbf{d}} \cdot \widehat{\mathbf{E}}(\mathbf{r}_A)|e, \mathbf{0}\rangle|^2 \delta(\omega_0 - \omega_k), \tag{3.1.1}$$

where $\widehat{\mathbf{d}} = \mathbf{d}|e\rangle\langle g| + \text{H.c.}$ is the transition dipole operator of the emitter and $\widehat{\mathbf{E}}(\mathbf{r}_A)$ is the electric field operator at the position $\mathbf{r}_A$ of the emitter. In the vacuum, the quantized field is written using (2.A.17b), (2.A.6) and replacing the global index $\kappa \to (\mathbf{k}, \lambda)$, where $\mathbf{k}$ is the wavevector and $\lambda = 1, 2$ labels the polarization component. Hence the field is:

$$\widehat{\mathbf{E}}_{\text{vac}}(\mathbf{r}) = i \sum_{\mathbf{k},\lambda} \sqrt{\frac{\hbar\omega_k}{2\epsilon_0 V}} \boldsymbol{\epsilon}_\lambda \left(\widehat{a}_{\mathbf{k},\lambda} \mathrm{e}^{-i\mathbf{k}\cdot\mathbf{r}} - \widehat{a}^\dagger_{\mathbf{k},\lambda} \mathrm{e}^{i\mathbf{k}\cdot\mathbf{r}} \right). \tag{3.1.2}$$

Writing the continuous limit $\frac{1}{V}\sum_{\mathbf{k},\lambda} \to \sum_\lambda \frac{1}{(2\pi)^3} \int \mathrm{d}^3\mathbf{k}$ and replacing in the expression for the decay rate, we find the vacuum decay rate:

$$\gamma_0 = \frac{d^2\omega_0^3}{3\hbar\pi\epsilon_0 c^3}. \tag{3.1.3}$$

When placing the emitter in a different environment, e.g. a cavity (see fig. 3.2), its effective decay rate increases, since the confinement of the field increases the time of interaction between the emitter and a cavity mode. We can consider the cQED RWA Hamiltonian (2.2.42) for one cavity mode:

$$\widehat{H} = \hbar\left(\omega_0 - i\frac{\gamma_0}{2}\right)\widehat{\sigma}_+\widehat{\sigma}_- + \hbar\left(\omega_c - i\frac{\Gamma_c}{2}\right)\widehat{c}^\dagger\widehat{c} + \hbar\left(g\widehat{\sigma}_+\widehat{c} + g^*\widehat{c}^\dagger\widehat{\sigma}_-\right), \tag{3.1.4}$$

where we added the spontaneous emission as a non-Hermitian diagonal term for the emitter. We can remark that this model, derived in the preceding chapter, is one-dimensional, hence it cannot describe spontaneous emission, which is a three-dimensional process. To build such a model, one would have to consider a 3D cavity (e.g. two plane mirrors separated by a

distance ℓ) [93]. Another remark can be made about the vacuum decay rate in the presence of a planar cavity: if at least one of the mirrors is perfect ($r_m = -1$), then the decay rate γ_0 can be modified if the emitter's distance x_A to the mirror is subwavelength. For microcavities that is not the case because such distances are below the diffraction limit, and in general we choose the position of the emitter so that it is many wavelengths distant from the mirrors:

$$x_A \sim \frac{\ell}{2} \gg \lambda_0. \tag{3.1.5}$$

If this condition is true, then the decay rate for the emitter is given by (3.1.3). To study the modification of the decay due to the cavity field, we need to derive the dynamics of the excited state of the emitter in the presence of the cavity, for the case when the emitter-cavity coupling is weak ($g \ll \Gamma_c$). In the strong coupling regime ($g \gtrsim \Gamma_c$), Rabi oscillations arise and the decaying property is set by the cavity decay. The initial condition being the excited state for the emitter and the vacuum for the cavity field, the Hamiltonian may be represented in the matrix form:

$$\widehat{H}/\hbar = \begin{pmatrix} -i\frac{\gamma_0}{2} & g \\ g^* & \Delta - i\frac{\Gamma_c}{2} \end{pmatrix}. \tag{3.1.6}$$

where $\Delta = \omega_c - \omega_0$. The wavefunction is expanded in the basis:

$$|\psi(t)\rangle = c_{e,\mathbf{0}}(t)|e,\mathbf{0}\rangle + c_{g,1}(t)|g,1\rangle, \tag{3.1.7}$$

where $|j,n\rangle \equiv |j\rangle \otimes |n\rangle$ with $j = e, g$ and $n = \mathbf{0}, 1$. The Schrödinger equation leads to the equations of motion:

$$i\dot{c}_{e,\mathbf{0}} = -i\frac{\gamma_0}{2}c_{e,\mathbf{0}}(t) + gc_{g,1}(t) \tag{3.1.8a}$$

$$i\dot{c}_{g,1} = g^* c_{e,\mathbf{0}}(t) + \left(\Delta - i\frac{\Gamma_c}{2}\right)c_{g,1}(t). \tag{3.1.8b}$$

In the weak coupling regime, we can adiabatically eliminate the excited state and set $\dot{c}_{g,1} \sim 0$ since $\Gamma_c \gg g$. The $c_{g,1}(t)$ coefficient then follows the dynamics of the excited state and we get:

$$c_{g,1}(t) \approx -\frac{g^*}{\Delta - i\frac{\Gamma_c}{2}}c_{e,\mathbf{0}}(t), \tag{3.1.9}$$

and the system of two equations reduces to the single one:

$$i\dot{c}_{e,\mathbf{0}} = -\left(i\frac{\gamma_0}{2} + \frac{|g|^2}{\Delta - i\frac{\Gamma_c}{2}}\right)c_{e,\mathbf{0}}(t). \tag{3.1.10}$$

Finally, we write the solution of (3.1.10) as:

$$\boxed{\begin{aligned} c_{e,\mathbf{0}}(t) &= c_{e,\mathbf{0}}(0)\mathrm{e}^{i\delta\omega t}\mathrm{e}^{-\frac{\Gamma}{2}t}, && (3.1.11a)\\ \delta\omega &= \frac{|g|^2\Delta}{\Delta^2 + \left(\frac{\Gamma_c}{2}\right)^2}, && (3.1.11b)\\ \Gamma &= \gamma_0 + \frac{|g|^2\Gamma_c}{\Delta^2 + \left(\frac{\Gamma_c}{2}\right)^2}, && (3.1.11c) \end{aligned}}$$

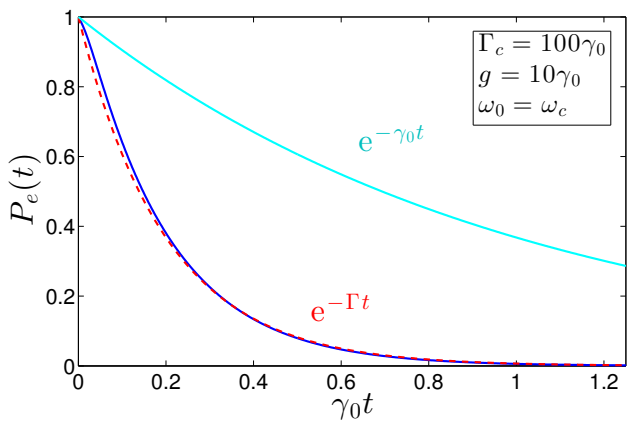

Figure 3.3: Probability of the excited state versus time of a two-level emitter initially in $|e, \mathbf{0}\rangle$ in the vacuum (light blue line) and in a cavity (dark blue line), obtained by the numerical solution of eq. (3.1.8) with $c_{e,\mathbf{0}}(0) = 1$. A comparison with the function $e^{-\Gamma t}$ with Γ corresponding to expression (3.1.11c) is done (red dashed line). Here $g \ll \Gamma_c$ and we chose zero detuning.

where $\delta\omega$ is a frequency shift induced by the cavity and Γ is the effective decay rate of the emitter. This solution retrieves the probability of excitation $P_{e,\mathbf{0}}(t) = P_{e,\mathbf{0}}(0)e^{-\Gamma t}$, and we see that the decay rate Γ of the emitter is increased with a term depending on the emitter-cavity coupling g, the cavity decay Γ_c and the detuning Δ. We call *Purcell factor* this additional term scaled by the vacuum decay rate:

$$F_P = \frac{|g|^2\Gamma_c}{\gamma_0\left[(\omega_c - \omega_0)^2 + \left(\frac{\Gamma_c}{2}\right)^2\right]} = \frac{\Gamma - \gamma_0}{\gamma_0}. \tag{3.1.12}$$

We display a graph of the dynamics of a two-level emitter coupled to a cavity field on fig. 3.3. The cavity coupling g can be expressed as (see e.g. equation (2.2.29) in chapter 2):

$$g = \sqrt{\frac{\omega_c}{2\hbar\epsilon_0 V}}\mathbf{d}\cdot\mathbf{\Phi}_{\text{cav}}(x_A), \tag{3.1.13}$$

where $\mathbf{d} = d\mathbf{n}$ is the transition dipole moment, V is the mode volume and $\mathbf{\Phi}_{\text{cav}}(x_A)$ is the mode spatial dependence of the cavity field at the position x_A of the emitter. Using the free-space decay rate expression (3.1.3) and the definition of the quality factor $Q = \omega_c/\Gamma_c$, we get the well-known expression of the Purcell factor:

$$\boxed{F_P = \frac{3}{4\pi^2}\,\lambda_0^3\,\frac{Q}{V}\,\frac{|\mathbf{n}\cdot\mathbf{\Phi}_{\text{cav}}(x_A)|^2}{1 + 4Q^2\left(\frac{\omega_c-\omega_0}{\omega_c}\right)^2}.} \tag{3.1.14}$$

We have retrieved the Q/V factor, and here we derived the Purcell factor for an emitter in the vacuum. If the emitter is embedded in a passive dielectric medium of index n_b, the above expression should be divided by n_b^3. The Purcell factor depends only on the cavity parameters and the frequency of the emitter transition, and is therefore a key parameter to design optical microcavities.

The Q/V ratio emphasizes that light-matter interactions can be controlled by adjusting either the mode lifetime through the Q factor (cQED approach), or the mode confinement V (quantum plasmonics approach). It is indeed possible to adapt this expression to plasmonics [90, 91]. This established a link between cQED and quantum plasmonics, and motivates the work presented in this chapter, devoted to deriving an exact model that transposes cQED concepts to quantum plasmonics.
For the derivation of the Purcell factor, we have considered the weak coupling regime approximation, therefore the plasmonic structure is here seen as a perturbation for the single emitter. To investigate the *strong* coupling regime, one has to go a step further and seek information in resonance fluorescence spectra. The vacuum Rabi splitting observed in the spectrum of a plasmonic structure coupled to emitters is a signature of the strong coupling regime [17, 18, 21–23, 25, 26].

3.1.3 Localized plasmons and nanoparticles

In general, the interaction of quantum emitters with plasmonic structures can be classified in two branches corresponding to the two main classes of plasmons: propagating SPPs and LSPs. In the first case, different groups are studying the interaction of emitters with plasmonic waveguides, as well as the coupling and the entanglement of emitters mediated by SPPs [11, 17, 101, 102].
In the thesis, we focus on the interaction of emitters with LSPs. The localized plasmon modes are observed with metallic nanoparticles whose size range is below the subwavelength regime [16, 18, 21–24, 26, 89, 103–105].
Nanoparticles can be of different shapes, but in general the study focuses on spherical or ellipsoidal nanoparticles. Other types of particles, such as nanoprisms, are examined experimentally because their geometries show strong light confinement [26].
Metal nanospheres are a widely chosen subject because the electromagnetic field can be expanded analytically with this geometry, and this provides benchmark models to study the interaction of emitters with LSPs. For this reason, we choose to expand the field quantization for spherically layered media in the following sections. In the next chapter, we derive the quantum effective models that we use for such systems, and we apply these models for the study of emitters near a metal nanosphere in the last chapter.

Plasmonic modes of a metal nanosphere

The optical response of a metal nanosphere of arbitrary size is exactly described by the Mie expansion of the particle plasmonic modes. This leads to the analytical expression for the metal nanosphere modes, which will be presented later.
Before discussing in details the quantum description of the emitter-field interaction, it is worthwhile to understand the dipole-nanosphere coupling in the classical approach. This allows to show the excitation of metal nanosphere modes by a single emitter and also introduces the Green's tensor that is used in the quantum description. The electric field at point $\mathbf{r}$ resulting from a dipole source placed at $\mathbf{r}_d$ is given by [88]:

$$\mathbf{E}(\mathbf{r}) = \omega^2 \mu_0 \bar{\bar{\mathbf{G}}}(\mathbf{r}, \mathbf{r}_d)\mathbf{d}, \tag{3.1.15}$$

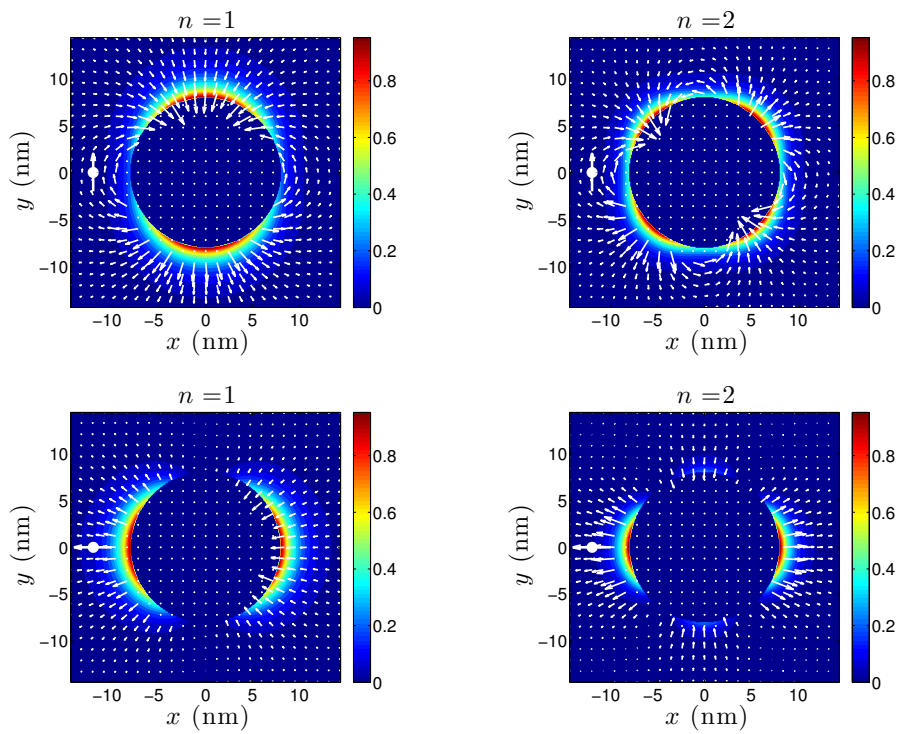

Figure 3.4: Normalized exterior field intensity (filled contour plot) and electric field (arrows) in the vicinity of a point-like quantum emitter (white circle) and a metallic nanosphere of radius $R = 8$ nm. On the left, we show the dipolar mode ($n = 1$), and on the right we show the quadrupolar mode (n=2). Upper panels: the dipole $\mathbf{d}$ is oriented along $\hat{\boldsymbol{\phi}}$. Lower panels: the dipole is oriented along $\hat{\boldsymbol{r}}$.

where ω is the angular frequency, μ_0 the magnetic permeability of the vacuum, $\bar{\bar{\mathbf{G}}}(\mathbf{r}, \mathbf{r}_d)$ the Green's tensor at the observation point $\mathbf{r}$ considering the source located at $\mathbf{r}_d$, and $\mathbf{d}$ is the dipole moment of the source. If we consider the scattered field of a metallic nanosphere, the Green's tensor can be decomposed as a sum over the index n of mode-selective terms $\bar{\bar{\mathbf{G}}}_n(\mathbf{r}, \mathbf{r}_d)$, and therefore the electric field also splits as an infinite sum of modes, each one associated to a specific plasmonic mode:

$$\mathbf{E}(\mathbf{r}) = \mathbf{E}_1(\mathbf{r}) + \mathbf{E}_2(\mathbf{r}) + ... = \sum_{n=1}^{+\infty} \mathbf{E}_n(\mathbf{r}). \tag{3.1.16}$$

The first mode, corresponding to $n = 1$ is called the *dipole* mode, due to its two-lobe spatial structure. The second one is the *quadrupole* mode, with four lobes, the third one is the *hexapole* mode, and so on. We show the two first modes of the scattered field in fig. 3.4, where we computed the external scattering for a dipole located 4 nm away from the surface of a silver sphere of radius $R = 8$ nm. Depending on the dipole orientation and oscillation frequency, we observe the excitation of different LSP modes. We note also that a LSP mode of order n presents a $2n + 1$ degeneracy (later labelled with index m), so that different mode profiles can be observed for the same number n. We study with more details the mode structure of nanospheres (resonances, decay rates...) in chapter 5.

3.2 Mode expansion in a spherically layered medium

In order to quantize the electromagnetic field for spherical metal nanoparticles, we derive the classical mode expansion of a spherically layered system. The initial steps of the method follow the scheme presented in refs. [94, 95]. We start with Maxwell's equations, where we introduce a charge and current density source term ρ_N and $\mathbf{j}_N$, respectively, usually called "noise polarization" and "noise current" in the literature. They are needed in order to later construct creation and annihilation operators for elementary excitations. Maxwell's equations read, in Fourier space:

$$\boldsymbol{\nabla} \cdot (\epsilon_0 \epsilon(\mathbf{r}, \omega) \mathbf{E}(\mathbf{r}, \omega)) = \rho_N(\mathbf{r}, \omega) \tag{3.2.1a}$$

$$\boldsymbol{\nabla} \times \mathbf{E}(\mathbf{r}, \omega) = i\omega \mathbf{B}(\mathbf{r}, \omega) \tag{3.2.1b}$$

$$\boldsymbol{\nabla} \cdot \mathbf{B}(\mathbf{r}, \omega) = 0 \tag{3.2.1c}$$

$$\boldsymbol{\nabla} \times \mathbf{B}(\mathbf{r}, \omega) = \mu_0 \mathbf{j}_N(\mathbf{r}, \omega) - i\frac{\omega}{c^2}\epsilon(\mathbf{r}, \omega)\mathbf{E}(\mathbf{r}, \omega). \tag{3.2.1d}$$

The noise charge and the noise current densities are expressed in terms of the noise polarization:

$$\rho_N(\mathbf{r}, \omega) = -\boldsymbol{\nabla} \cdot \mathbf{P}_N(\mathbf{r}, \omega) \tag{3.2.2}$$

$$\mathbf{j}_N(\mathbf{r}, \omega) = -i\omega \mathbf{P}_N(\mathbf{r}, \omega), \tag{3.2.3}$$

the latter showing up as a small fluctuation in the polarization in Fourier space:

$$\mathbf{P}(\mathbf{r}, \omega) = \epsilon_0(\epsilon(\mathbf{r}, \omega) - 1)\mathbf{E}(\mathbf{r}, \omega) + \mathbf{P}_N(\mathbf{r}, \omega). \tag{3.2.4}$$

We write the wave propagation equation for the electric field, with the noise current as a source term:

$$\boldsymbol{\nabla} \times \boldsymbol{\nabla} \times \mathbf{E}(\mathbf{r}, \omega) - \frac{\omega^2}{c^2}\epsilon(\mathbf{r}, \omega)\mathbf{E}(\mathbf{r}, \omega) = i\omega \mathbf{j}_N(\mathbf{r}, \omega). \tag{3.2.5}$$

The solution of this equation expresses in terms of the Green's tensor of the system:

$$\mathbf{E}(\mathbf{r}, \omega) = i\omega\mu_0 \int \mathrm{d}^3 r' \overline{\overline{\mathbf{G}}}(\mathbf{r}, \mathbf{r}', \omega)\, \mathbf{j}_N(\mathbf{r}', \omega), \tag{3.2.6}$$

and the Green's tensor must satisfy the Maxwell-Helmholtz equation:

$$\boldsymbol{\nabla} \times \boldsymbol{\nabla} \times \overline{\overline{\mathbf{G}}}(\mathbf{r}, \mathbf{r}', \omega) - \frac{\omega^2}{c^2}\epsilon(\mathbf{r}, \omega)\overline{\overline{\mathbf{G}}}(\mathbf{r}, \mathbf{r}', \omega) = \overline{\overline{\delta}}(\mathbf{r} - \mathbf{r}'), \tag{3.2.7}$$

where $\overline{\overline{\delta}}(\mathbf{r}-\mathbf{r}') = \overline{\overline{\mathbb{1}}}\delta(\mathbf{r}-\mathbf{r}')$. In order to construct a class of operators which separately create or annihilate excitations in arbitrary modes of a system, we must take into account the geometry.

3.2.1 Spherical vector harmonics and orthogonality relations

In this section we summarize the mathematical tools for layered systems with spherical symmetry, following refs. [96, 97]. The derivation of the mode expansion is done here for a spherically layered system: we consider N spherical layers of arbitrary different dielectric indices,

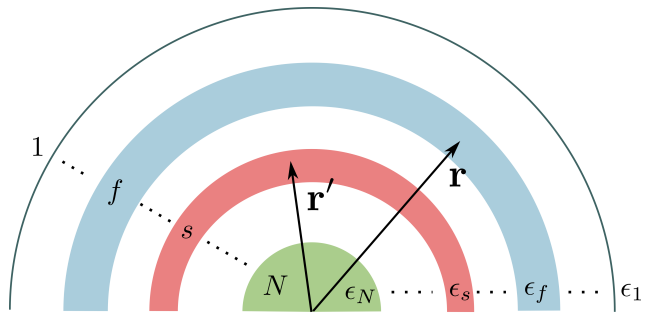

Figure 3.5: Structure of a spherically N-layered medium, where the material properties are piecewise homogeneous between individual layer interfaces. The source, located at $\mathbf{r}'$, belongs to the layer labelled s, and the observation point $\mathbf{r}$ is contained in the layer f where the field is measured.

all centered around the origin. The system is shown in fig. 3.5. The Green's tensor can be expanded in the tensorial basis obtained from a well chosen set of harmonic vector functions. These functions serve the technical purpose of fulfilling the boundary conditions, and using this expansion enables one to efficiently describe and handle intrinsic resonances with proper indices, as will be seen further in the derivation. In order to get the vector functions suitable for the multilayered system, we first solve the scalar Helmholtz equation:

$$\left(\nabla^2 + q^2\right)\psi(\mathbf{r}, q) = 0, \tag{3.2.8}$$

where $q \geqslant 0$ is a parameter having the dimension of the wave number. The solutions of this equation can be expressed in terms of the spherical harmonic eigenfunctions [96–98]:

$$\psi_{nm^{e}_{o}}(\mathbf{r}, q) = z_n(qr)P_n^m(\cos\theta)\begin{matrix}\cos\\ \sin\end{matrix}(m\phi), \tag{3.2.9}$$

with n, m being discrete harmonic indices, e and o refer to even and odd solutions in ϕ, respectively, z_n denoting a Bessel or Hankel function depending on the boundary conditions, and P_n^m are the associated Legendre polynomials labelled with the harmonic indices. The function z_n can be either a spherical Bessel or a spherical Hankel function depending on regularization requirements based on the boundary conditions. The vector harmonics used for the expansion of the Green's tensor are constructed as:

$$\mathbf{M}_{nm^{e}_{o}}(\mathbf{r}, q) = \boldsymbol{\nabla} \times \left(\psi_{nm^{e}_{o}}(\mathbf{r}, q)\mathbf{r}\right) \tag{3.2.10}$$

$$\mathbf{N}_{nm^{e}_{o}}(\mathbf{r}, q) = \frac{1}{q}\boldsymbol{\nabla} \times \boldsymbol{\nabla} \times \left(\psi_{nm^{e}_{o}}(\mathbf{r}, q)\mathbf{r}\right) \tag{3.2.11}$$

$$\mathbf{L}_{nm^{e}_{o}}(\mathbf{r}, q) = \boldsymbol{\nabla}\psi_{nm^{e}_{o}}(\mathbf{r}, q). \tag{3.2.12}$$

$\mathbf{M}(\mathbf{r}, q)$ and $\mathbf{N}(\mathbf{r}, q)$ are continuous-spectrum eigenvectors of:

$$\boldsymbol{\nabla} \times \boldsymbol{\nabla} \times \mathbf{K}(\mathbf{r}, q) = q^2\mathbf{K}(\mathbf{r}, q), \tag{3.2.13}$$

with eigenvalue q^2, and $\mathbf{L}(\mathbf{r}, q)$ spans the eigenvectors of the latter equation with eigenvalue 0. We show that the spherical vector harmonics form a complete basis that is orthogonal, but

not normalized. Using (3.2.9) and the expressions of the vector harmonics, we expand them as:

$$\mathbf{M}_{nm^e_o}(\mathbf{r},q) = \mp\frac{m}{\sin\theta} z_n(qr) P_n^m(\cos\theta) \begin{matrix}\sin\\ \cos\end{matrix} (m\phi)\hat{\boldsymbol{\theta}} - z_n(qr)\frac{\mathrm{d}P_n^m(\cos\theta)}{\mathrm{d}\theta} \begin{matrix}\cos\\ \sin\end{matrix} (m\phi)\hat{\boldsymbol{\phi}} \tag{3.2.14}$$

$$\begin{aligned}\mathbf{N}_{nm^e_o}(\mathbf{r},q) &= \frac{n(n+1)}{qr} z_n(qr) P_n^m(\cos\theta) \begin{matrix}\cos\\ \sin\end{matrix} (m\phi)\hat{\boldsymbol{r}} \\ &+ \frac{1}{qr}\frac{\mathrm{d}\big(rz_n(qr)\big)}{\mathrm{d}r}\left[\frac{\mathrm{d}P_n^m(\cos\theta)}{\mathrm{d}\theta} \begin{matrix}\cos\\ \sin\end{matrix} (m\phi)\hat{\boldsymbol{\theta}} \mp \frac{m}{\sin\theta} P_n^m(\cos\theta) \begin{matrix}\sin\\ \cos\end{matrix} (m\phi)\hat{\boldsymbol{\phi}}\right]\end{aligned} \tag{3.2.15}$$

$$\begin{aligned}\mathbf{L}_{nm^e_o}(\mathbf{r},q) &= \frac{\mathrm{d}z_n(qr)}{\mathrm{d}r} P_n^m(\cos\theta) \begin{matrix}\cos\\ \sin\end{matrix} (m\phi)\hat{\boldsymbol{r}} \\ &+ \frac{z_n(qr)}{r}\frac{\mathrm{d}P_n^m(\cos\theta)}{\mathrm{d}\theta} \begin{matrix}\cos\\ \sin\end{matrix} (m\phi)\hat{\boldsymbol{\theta}} \mp \frac{mz_n(qr)}{r\sin\theta} P_n^m(\cos\theta) \begin{matrix}\sin\\ \cos\end{matrix} (m\phi)\hat{\boldsymbol{\phi}},\end{aligned} \tag{3.2.16}$$

where we used the notation $\hat{\boldsymbol{r}}, \hat{\boldsymbol{\theta}}, \hat{\boldsymbol{\phi}}$ for the three unit vectors in spherical coordinates. To ease the readability while deriving the orthogonality relations, we introduce the notation:

$$\int \mathrm{d}^3r\, \mathbf{K}^*(\mathbf{r},q)\cdot\mathbf{K}'(\mathbf{r},q') = \langle\mathbf{K}(q)|\mathbf{K}'(q')\rangle, \tag{3.2.17}$$

where $\mathbf{K}, \mathbf{K}'$ are any of the three vector harmonics $\mathbf{M}, \mathbf{N}, \mathbf{L}$. The first part of the orthogonality relations is:

$$\langle\mathbf{K}_{nmp}(q)|\mathbf{K}'_{n'm'p'}(q')\rangle = 0 \text{ if } \mathbf{K}\neq\mathbf{K}', \tag{3.2.18}$$

$p, p' = e, o$ being indices associated with the parity. Taking the same class of vector harmonics, there is an orthogonality in the harmonic indices and in the parameter q. We choose a solution that is regular around the origin, i.e. the spherical Bessel function of the first kind:

$$z_n(qr) = j_n(qr), \tag{3.2.19}$$

and this should be true for the Nth layer, which contains the origin. The orthogonality relations, for $\mathbf{K} = \mathbf{K}'$, are:

$$\langle\mathbf{M}_{nm^e_o}(q)|\mathbf{M}_{n'm'^e_o}(q')\rangle = \langle\mathbf{N}_{nm^e_o}(q)|\mathbf{N}_{n'm'^e_o}(q')\rangle = Q_{nm}(q)\frac{1\pm\delta_{m0}}{2}\delta_{nn'}\delta_{mm'}\delta(q-q') \tag{3.2.20a}$$

$$\langle\mathbf{L}_{nm^e_o}(q)|\mathbf{L}_{n'm'^e_o}(q')\rangle = Q_{nm}(q)\frac{1\pm\delta_{m0}}{2n(n+1)}\delta_{nn'}\delta_{mm'}\delta(q-q'), \tag{3.2.20b}$$

where the upper sign on the right hand side refers to the scalar product of the even functions and the lower one to the odd ones, and:

$$Q_{nm}(q) = \frac{2\pi^2 n(n+1)(n+m)!}{q^2(2n+1)(n-m)!}. \tag{3.2.21}$$

We note that choosing a Hankel function of the first kind: $z_n(qr) = h_n^{(1)}(qr)$, leads to similar orthogonality relations, the only difference being a factor of 2 in the normalization constants. Due to the layered nature of the system, we will also encounter the situation of q being a function of the radius r:

$$q \to q(r).$$

In this case, the orthogonality relations become:

$$\langle \mathbf{M}_{nm^{e}_{o}}(q)|\mathbf{M}_{n'm'^{e}_{o}}(q')\rangle = \langle \mathbf{N}_{nm^{e}_{o}}(q)|\mathbf{N}_{n'm'^{e}_{o}}(q')\rangle = S_{nn'}(q,q')Q_{nm}(q)\frac{1\pm\delta_{m0}}{2}\delta_{nn'}\delta_{mm'} \quad (3.2.22a)$$

$$\langle \mathbf{L}_{nm^{e}_{o}}(q)|\mathbf{L}_{n'm'^{e}_{o}}(q')\rangle = S_{nn'}(q,q')Q_{nm}(q)\frac{1\pm\delta_{m0}}{2n(n+1)}\delta_{nn'}\delta_{mm'} \quad (3.2.22b)$$

$$S_{nn'}(q,q') = \int_0^{+\infty} \mathrm{d}r\, r^2\, z_n\big(q(r)r\big) z_{n'}\big(q'(r)r\big). \quad (3.2.22c)$$

However, this leaves the orthogonality between the spherical indices n, n' and m, m' intact.

3.2.2 Green's tensor expansion

The Green's tensor of a general N-layered spherical system (see fig. 3.5) is given by:

$$\bar{\bar{\mathbf{G}}}(\mathbf{r},\mathbf{r}',\omega) = \bar{\bar{\mathbf{G}}}_0(\mathbf{r},\mathbf{r}',\omega)\delta_{fs} + \bar{\bar{\mathbf{G}}}_S(\mathbf{r},\mathbf{r}',\omega), \quad (3.2.23)$$

where f is the index of the layer wherein the field point $\mathbf{r}$ is located, and the source point $\mathbf{r}'$ is contained in layer s. When $\mathbf{r}$ and $\mathbf{r}'$ are in the same layer, a term $\bar{\bar{\mathbf{G}}}_0(\mathbf{r},\mathbf{r}',\omega)$ that accounts for direct propagation between the source and the field point is added, while in general there is a single term $\bar{\bar{\mathbf{G}}}_S(\mathbf{r},\mathbf{r}',\omega)$ resulting from the scattering on the surrounding layers.
We expand the Green's tensor in the tensorial basis of spherical vector harmonics, in order to fulfill the boundary conditions on the layer interfaces:

$$\bar{\bar{\mathbf{G}}}(\mathbf{r},\mathbf{r}',\omega) = \sum_{p=e,o}\sum_{n=0}^{+\infty}\sum_{m=0}^{n} \bar{\bar{\mathbf{G}}}_{nmp}(\mathbf{r},\mathbf{r}',\omega). \quad (3.2.24)$$

Here, the expansion terms contain both $\bar{\bar{\mathbf{G}}}_0$ and $\bar{\bar{\mathbf{G}}}_S$ parts, and they have the general form:

$$\bar{\bar{\mathbf{G}}}_{nmp}(\mathbf{r},\mathbf{r}',\omega) = \frac{1}{k_s^2}\delta_{fs}\bar{\bar{\delta}}_{nmp}(\mathbf{r}-\mathbf{r}') + \sum_{j,k=0,1}\big[\mathcal{A}^{(jk)}_{nmp}(\omega)\mathbf{M}^{(j)}_{nmp}(\mathbf{r},k_f)\otimes\mathbf{M}^{(k)}_{nmp}(\mathbf{r}',k_s) + \mathcal{B}^{(jk)}_{nmp}(\omega)\mathbf{N}^{(j)}_{nmp}(\mathbf{r},k_f)\otimes\mathbf{N}^{(k)}_{nmp}(\mathbf{r}',k_s)\big], \quad (3.2.25)$$

where we have used the compact coefficients $\mathcal{A}^{(jk)}_{nmp}(\omega), \mathcal{B}^{(jk)}_{nmp}(\omega)$, which are chosen so that the boundary conditions are fulfilled. Moreover, if $f = s$, they contain terms of the direct contribution $\bar{\bar{\mathbf{G}}}_0$ as well. A detailed derivation is shown in appendix 3.A. The Dirac delta introduced in the latter expression is used to unravel the singular term in $\bar{\bar{\mathbf{G}}}_0$, and reads:

$$\bar{\bar{\delta}}_{nmp}(\mathbf{r}-\mathbf{r}') = \int_0^{+\infty}\mathrm{d}q\, C_{nm}(q)\Big(\mathbf{N}^{(0)}_{nmp}(\mathbf{r},q)\otimes\mathbf{N}^{(0)}_{nmp}(\mathbf{r}',q) + n(n+1)\mathbf{L}^{(0)}_{nmp}(\mathbf{r},q)\otimes\mathbf{L}^{(0)}_{nmp}(\mathbf{r}',q)\Big)_{\hat{\boldsymbol{r}}\otimes\hat{\boldsymbol{r}}}, \quad (3.2.26)$$

with the coefficient:

$$C_{nm}(q) = \frac{q^2(2n+1)(n-m)!}{\pi^2 n(n+1)(n+m)!(1+\delta_{m0})}. \quad (3.2.27)$$

This expansion obeys:

$$\sum_{nmp} \overline{\overline{\delta}}_{nmp}(\mathbf{r}-\mathbf{r}') = \delta(\mathbf{r}-\mathbf{r}')\hat{\boldsymbol{r}} \otimes \hat{\boldsymbol{r}}. \tag{3.2.28}$$

We note that the integral contains the tensorial product of the *radial* components of $\mathbf{N}$ and $\mathbf{L}$ only. The indices j and k can assume the values 0 and 1, meaning that for the radial function $z_n(qr)$ in (3.2.9) we use a spherical Bessel, or a spherical Hankel function of the first kind, respectively. All the layers are piecewise homogeneous, thus:

$$k_{f,s} = \frac{\omega}{c}\sqrt{\epsilon_{f,s}}, \tag{3.2.29}$$

where $\epsilon_{f,s}$ is the relative electric permittivity corresponding to layers f, s respectively. Recalling the field expression (3.2.6), we create a similar expansion for the noise current as well, so that instead of having a globally defined $\mathbf{j}_N$, we can manage separate currents labelled by the mode expansion indices n, m and the parity p:

$$\mathbf{j}_N(\mathbf{r},\omega) = \sum_{p=e,o}\sum_{n=0}^{+\infty}\sum_{m=0}^{n} \mathbf{j}_N^{(nmp)}(\mathbf{r},\omega). \tag{3.2.30}$$

The noise current is the variable that, in the next section, will be replaced by an operator by a correspondence principle. Nevertheless, this variable is not normalized; hence, we define the fundamental dynamical variables:

$$\mathbf{f}_{nmp}(\mathbf{r},\omega) = \frac{1}{\omega}\sqrt{\frac{\pi}{\hbar\epsilon_0\epsilon''(\mathbf{r},\omega)}}\mathbf{j}_N^{(nmp)}(\mathbf{r},\omega), \tag{3.2.31}$$

where $\epsilon''(\mathbf{r},\omega)$ is the imaginary part of the relative electric permittivity. Writing the expansion in the vector spherical harmonics:

$$\mathbf{f}_{nmp}(\mathbf{r},\omega) = \int_0^{+\infty} \mathrm{d}q \left[a_{nmp}(\omega,q)\mathbf{M}_{nmp}^{(0)}(\mathbf{r},q) + b_{nmp}(\omega,q)\mathbf{N}_{nmp}^{(0)}(\mathbf{r},q) + c_{nmp}(\omega,q)\mathbf{L}_{nmp}^{(0)}(\mathbf{r},q)\right]. \tag{3.2.32}$$

With this expansion, we represent each noise current term on the subspace spanned by the basis functions belonging to the respective n and m indices. The choice of Bessel functions for $z_n(qr)$ in the vector harmonics is justified because it yields an orthogonal, complete set of vectorial functions, which are regular at the origin. Now substituting (3.2.24) and (3.2.30) into (3.2.6), we get:

$$\mathbf{E}(\mathbf{r},\omega) = i\omega\mu_0 \sum_{\bar{n}}\sum_{\bar{n}'} \int \mathrm{d}^3r' \overline{\overline{\mathbf{G}}}_{\bar{n}}(\mathbf{r},\mathbf{r}',\omega)\,\mathbf{j}_N^{(\bar{n}')}(\mathbf{r}',\omega), \tag{3.2.33}$$

where we have grouped the harmonic and parity indices as $\bar{n} = n, m, p$. Using the relations (3.2.25) and (3.2.30) in the latter, applying the identity:

$$(\mathbf{a}\otimes\mathbf{b})\cdot\mathbf{c} = \mathbf{a}(\mathbf{b}\cdot\mathbf{c}), \tag{3.2.34}$$

and the orthogonality relations, the expression of the field simplifies into:

$$\boxed{\mathbf{E}(\mathbf{r},\omega) = i\omega\mu_0 \sum_{\bar{n}} \int \mathrm{d}^3r' \bar{\bar{\mathbf{G}}}_{\bar{n}}(\mathbf{r},\mathbf{r}',\omega)\, \mathbf{j}_N^{(\bar{n})}(\mathbf{r}',\omega).} \tag{3.2.35}$$

Because of the spherical symmetry of the system, $\epsilon(\mathbf{r},\omega) \equiv \epsilon(r,\omega)$ depends only radially on $\mathbf{r}$. The orthogonality relations (3.2.22) ensure that the harmonic index terms do not cross, and thus we have assigned independent noise currents to each of the harmonic terms of the Green's tensor.

3.3 Mode-selective quantization

3.3.1 Field quantization

To quantize the combined field-matter system in a way that creation/annihilation operators toggle excitations corresponding to individual harmonic orders, we take the quantization scheme of refs [94, 100] as a starting point, and then define new operators in relation to it.
In the last section, we have introduced the dynamical variable $\mathbf{f}(\mathbf{r},\omega)$ being the normalized noise current:

$$\mathbf{j}_N(\mathbf{r},\omega) = \omega\sqrt{\frac{\hbar\epsilon_0\epsilon''(\mathbf{r},\omega)}{\pi}}\mathbf{f}(\mathbf{r},\omega). \tag{3.3.1}$$

Using the correspondence principle, we replace this classical quantity by an operator acting on a Fock space:

$$\mathbf{f}(\mathbf{r},\omega) \mapsto \widehat{\mathbf{f}}(\mathbf{r},\omega).$$

The action of the creation operator on the vacuum state $|\mathbf{0}\rangle$ creates the single excitation state:

$$|\mathbf{1}(\mathbf{r},\omega)\rangle = \widehat{\mathbf{f}}^\dagger(\mathbf{r},\omega)|\mathbf{0}\rangle, \tag{3.3.2}$$

that is, the Fock space of a single excitation is spanned with three subspaces, each corresponding to a component of the vector operator $\widehat{\mathbf{f}}^\dagger(\mathbf{r},\omega)$. The components obey the following bosonic commutation relations:

$$\left[\widehat{f}_i(\mathbf{r},\omega), \widehat{f}_j^\dagger(\mathbf{r}',\omega')\right] = \delta_{ij}\delta(\mathbf{r}-\mathbf{r}')\delta(\omega-\omega') \tag{3.3.3a}$$

$$\left[\widehat{f}_i(\mathbf{r},\omega), \widehat{f}_j(\mathbf{r}',\omega')\right] = \left[\widehat{f}_i^\dagger(\mathbf{r},\omega), \widehat{f}_j^\dagger(\mathbf{r}',\omega')\right] = 0. \tag{3.3.3b}$$

The electric field operator can be written using (3.2.6) and (3.3.1), as:

$$\boxed{\widehat{\mathbf{E}}(\mathbf{r},\omega) = i\sqrt{\frac{\hbar}{\pi\epsilon_0}}\frac{\omega^2}{c^2}\int \mathrm{d}^3r' \sqrt{\epsilon''(\mathbf{r}',\omega)}\bar{\bar{\mathbf{G}}}(\mathbf{r},\mathbf{r}',\omega)\,\widehat{\mathbf{f}}(\mathbf{r}',\omega),} \tag{3.3.4}$$

and the Hamiltonian of the electromagnetic field coupled with the medium is obtained using the Fano diagonalisation procedure [95]:

$$\boxed{\widehat{H}_F = \int \mathrm{d}^3r \int_0^{+\infty} \mathrm{d}\omega\hbar\omega\, \widehat{\mathbf{f}}^\dagger(\mathbf{r},\omega)\cdot\widehat{\mathbf{f}}(\mathbf{r},\omega).} \tag{3.3.5}$$

3.3.2 Addressing harmonic excitations

Having the quantized annihilation/creation operators $\widehat{\mathbf{f}}(\mathbf{r},\omega), \widehat{\mathbf{f}}^\dagger(\mathbf{r},\omega)$, we make the connection with the spherically layered medium depicted in fig. 3.5, and the expression of the dynamical variable expansion (3.2.32). The results of this section have been published in ref. [99]. We expand the annihilation operator as:

$$\widehat{\mathbf{f}}(\mathbf{r},\omega) = \sum_{\mathbf{K}} \sum_{p=e,o} \sum_{n=0}^{+\infty} \sum_{m=0}^{n} \int_0^{+\infty} \mathrm{d}q \frac{1}{\sqrt{Q_{nm}^{(\mathbf{K})}(q)}} \mathbf{K}_{nmp}(\mathbf{r},q) \widehat{F}_{\mathbf{K}}^{(nmp)}(\omega,q), \tag{3.3.6}$$

where $\mathbf{K} = \mathbf{M}, \mathbf{N}, \mathbf{L}$ and $\widehat{F}_{\mathbf{K}}^{(nmp)}(\omega,q)$ are the mode-selective annihilation operators associated with the vector spherical harmonics. The normalization constants $Q_{nm}^{(\mathbf{K})}(q)$ are defined as:

$$Q_{nm}^{(\mathbf{K})}(q) = \begin{cases} \frac{\pi^2 n(n+1)(n+m)!(1+\delta_{m0})}{q^2(2n+1)(n-m)!} & \mathbf{K} = \mathbf{M}, \mathbf{N} \\ \frac{\pi^2 (n+m)!(1+\delta_{m0})}{q^2(2n+1)(n-m)!} & \mathbf{K} = \mathbf{L} \end{cases}. \tag{3.3.7}$$

Writing this decomposition, the spatial dependence and the polarization component are contained in the vector harmonics $\mathbf{K}_{nmp}(\mathbf{r},q)$, and the quantization is scalar. Operators $\widehat{F}_{\mathbf{K}}^{(nmp)}(\omega,q)$ span a one-dimensional single excitation Fock space associated with the vector spherical harmonics $\mathbf{K}_{nmp}(\mathbf{r},q)$:

$$\widehat{F}_{\mathbf{K}}^{(nmp)\dagger}(\omega,q)|\mathbf{0}\rangle = \left|1_{\mathbf{K}}^{(nmp)}(\omega,q)\right\rangle. \tag{3.3.8}$$

The parameters $\{q,n,m\}$ can be interpreted as coordinates in a spherical reciprocal space, analogous to $\{k_x,k_y,k_z\}$ of the reciprocal space in a Cartesian frame of reference.
We can establish the commutation relations of the mode-selective operators, recalling the orthogonality relations (3.2.20), and we invert expression (3.3.6):

$$\widehat{F}_{\mathbf{K}}^{(nmp)} = \frac{1}{\sqrt{Q_{nm}^{(\mathbf{K})}(q)}} \int \mathrm{d}^3 r\, \widehat{\mathbf{f}}(\mathbf{r},\omega) \cdot \mathbf{K}_{nmp}(\mathbf{r},q). \tag{3.3.9}$$

Subsequently, we the commutation relation are:

$$\left[\widehat{F}_{\mathbf{K}}^{(\bar{n})}(\omega,q), \widehat{F}_{\mathbf{K}'}^{(\bar{n}')\dagger}(\omega',q')\right] = \delta_{\bar{n}\bar{n}'}\delta_{\mathbf{K}\mathbf{K}'}\delta(\omega-\omega')\delta(q-q') \tag{3.3.10a}$$

$$\left[\widehat{F}_{\mathbf{K}}^{(\bar{n})}(\omega,q), \widehat{F}_{\mathbf{K}'}^{(\bar{n}')}(\omega',q')\right] = \left[\widehat{F}_{\mathbf{K}}^{(\bar{n})\dagger}(\omega,q), \widehat{F}_{\mathbf{K}'}^{(\bar{n}')\dagger}(\omega',q')\right] = 0, \tag{3.3.10b}$$

where we used the compact index notation $\bar{n} = n,m,p$. We have thus specified creation and annihilation operators associated with the spherical harmonic orders. The Hamiltonian (3.3.5) is rewritten in the following form, assuming the new decomposition:

$$\widehat{H}_F = \sum_{\mathbf{K}} \sum_{\bar{n}} \int_0^{+\infty} \mathrm{d}q \int_0^{+\infty} \mathrm{d}\omega\, \hbar\omega\, \widehat{F}_{\mathbf{K}}^{(\bar{n})\dagger}(\omega,q) \widehat{F}_{\mathbf{K}}^{(\bar{n})}(\omega,q). \tag{3.3.11}$$

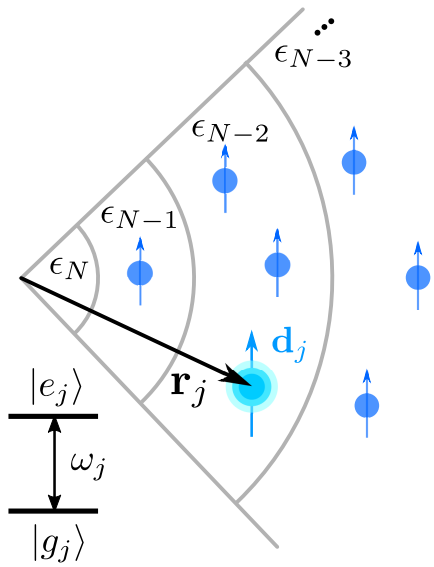

Figure 3.6: Two-level emitters embedded in a spherically layered medium. The layers are piecewise homogeneous with relative electric permittivity ϵ_i, $i = 1...N$. The emitters are located at point $\mathbf{r}_j$, and their transition dipole moment is $\mathbf{d}_j$.

3.3.3 Spherical mode-structured field and quantum emitters

Having derived the mode-selective field Hamiltonian, we now look at the situation where N_e two-level quantum emitters interact with the mode structure of the spherically layered medium (see fig. 3.6). The system under consideration is described by the following RWA Hamiltonian [21]:

$$\widehat{H} = \sum_{j=1}^{N_e} \hbar\omega_j \widehat{\sigma}_+^{(j)}\widehat{\sigma}_-^{(j)} + \widehat{H}_F - \sum_{j=1}^{N_e} \int_0^{+\infty} \mathrm{d}\omega \left(\mathbf{d}_j \cdot \widehat{\mathbf{E}}(\mathbf{r}_j,\omega)\widehat{\sigma}_+^{(j)} + \text{h.c.}\right), \tag{3.3.12}$$

where $\widehat{H}_F$ is given by (3.3.5), ω_j is the resonance frequency of the j-th emitter, $\widehat{\sigma}_+^{(j)} = |e_j\rangle\langle g_j| = \widehat{\sigma}_-^{(j)\dagger}$ is its raising fermionic operator, and $\mathbf{d}_j$ is its transition dipole moment. Combining (3.3.4), (3.3.5) and (3.3.6), we construct the mode-selective Hamiltonian, where the field operators address excitations associated with spherical harmonic orders:

$$\boxed{\begin{aligned}\widehat{H} = &\sum_{j=1}^{N_e} \hbar\omega_j \widehat{\sigma}_+^{(j)}\widehat{\sigma}_-^{(j)} + \sum_{\mathbf{K}}\sum_{\bar{n}} \int_0^{+\infty}\mathrm{d}q \int_0^{+\infty}\mathrm{d}\omega\, \hbar\omega\, \widehat{F}_{\mathbf{K}}^{(\bar{n})\dagger}(\omega,q)\widehat{F}_{\mathbf{K}}^{(\bar{n})}(\omega,q)\\ &- i\hbar \sum_{j=1}^{N_e}\sum_{\mathbf{K}}\sum_{\bar{n}} \int_0^{+\infty}\mathrm{d}q \int_0^{+\infty}\mathrm{d}\omega \left(V_{\mathbf{K}}^{(\bar{n})}(\mathbf{r}_j,\omega,q)\widehat{\sigma}_+^{(j)}\widehat{F}_{\mathbf{K}}^{(\bar{n})}(\omega,q) - \text{h.c.}\right),\end{aligned}} \tag{3.3.13}$$

with the spherical harmonic coupling strength:

$$V_{\mathbf{K}}^{(\bar{n})}(\mathbf{r}_j,\omega,q) = \frac{1}{\sqrt{\hbar\pi\epsilon_0 Q_{nm}^{\mathbf{K}}(q)}}\frac{\omega^2}{c^2}\int \mathrm{d}^3r \sqrt{\epsilon''(\mathbf{r},\omega)}\, \mathbf{d}_j \cdot \bar{\bar{\mathbf{G}}}_{\bar{n}}(\mathbf{r}_j,\mathbf{r},\omega)\mathbf{K}_{\bar{n}}(\mathbf{r},q). \tag{3.3.14}$$

Summary

We have constructed a theoretical framework that allows for addressing harmonic orders individually. Is is also consistent with previous, established methods of quantization. The general spherically layered system is rather complicated as a description, but can be directly applied to simpler systems, such as nanoparticles or core-shell spherical systems. Quantizing the excitation in such a way, starting from a microscopic model fulfilling the macroscopic equations, provides a basis for the derivation of simpler models, such as the effective Hamiltonians that we present in the next chapter.

Appendix

3.A Green's tensor in a spherically layered medium

The Green's tensor of a spherically layered system can be calculated following [96–98]. Constructing the Green's tensor of a layered, piecewise homogeneous medium involves two major steps: the expansion in the tensor-product basis of the eigenfunctions for the homogeneous medium, and the determination of the expansion coefficients by imposing boundary conditions at the layer interfaces. The general dyadic Green's function of a multilayered medium is:

$$\bar{\bar{\mathbf{G}}}(\mathbf{r},\mathbf{r}',\omega) = \bar{\bar{\mathbf{G}}}_0(\mathbf{r},\mathbf{r}',\omega)\delta_{fs} + \bar{\bar{\mathbf{G}}}_S(\mathbf{r},\mathbf{r}',\omega), \tag{3.A.1}$$

where the field point $\mathbf{r}$ and the source point $\mathbf{r}'$ are in the layers indexed with f and s, respectively. If $f = s$, a term appears in the Green's tensor that represents direct propagation from $\mathbf{r}'$ to $\mathbf{r}$. $\bar{\bar{\mathbf{G}}}_S$ accounts for propagation between $\mathbf{r}'$ and $\mathbf{r}$ due to the scattering of radiation on the surrounding layers. In the basis of vector spherical harmonics, the direct electric Green's tensor term assumes the form:

$$\begin{aligned}\bar{\bar{\mathbf{G}}}_0(\mathbf{r},\mathbf{r}',\omega) = {} & \frac{\delta(\mathbf{r}-\mathbf{r}')}{k_s^2}\hat{\boldsymbol{r}}\otimes\hat{\boldsymbol{r}} + i\frac{k_s}{4\pi}\sum_{p=e,o}\sum_{n=0}^{+\infty}\sum_{m=0}^{n}\frac{(2n+1)(n-m)!}{n(n+1)(n+m)!} \\ & \times\begin{cases}\mathbf{M}^{(1)}_{nmp}(\mathbf{r},k_s)\otimes\mathbf{M}^{(0)}_{nmp}(\mathbf{r}',k_s) + \mathbf{N}^{(1)}_{nmp}(\mathbf{r},k_s)\otimes\mathbf{N}^{(0)}_{nmp}(\mathbf{r}',k_s) & r \geqslant r' \\ \mathbf{M}^{(0)}_{nmp}(\mathbf{r},k_s)\otimes\mathbf{M}^{(1)}_{nmp}(\mathbf{r}',k_s) + \mathbf{N}^{(0)}_{nmp}(\mathbf{r},k_s)\otimes\mathbf{N}^{(1)}_{nmp}(\mathbf{r}',k_s) & r \leqslant r'\end{cases},\end{aligned} \tag{3.A.2}$$

where, depending on whether the field or the source point is closer to the origin, one has to choose a spherical Bessel or a spherical Hankel function of the first kind (upper indices 0 and 1, respectively) for the radial part $z_n(qr)$ of the vector harmonics. This ensures that $\bar{\bar{\mathbf{G}}}_0$ is regularized as its spatial arguments tend to the origin or infinity. The scattered term of the Green's tensor reads:

$$\begin{aligned}\bar{\bar{\mathbf{G}}}_S(\mathbf{r},\mathbf{r}',\omega) = {} & i\frac{k_s}{4\pi}\sum_{p=e,o}\sum_{n=0}^{+\infty}\sum_{m=0}^{n}(2-\delta_{0m})\frac{(2n+1)(n-m)!}{n(n+1)(n+m)!} \\ & \times\Big\{(1-\delta_{fN})\mathbf{M}^{(1)}_{nmp}(\mathbf{r},k_f)\otimes\Big((1-\delta_{s1})A^{fs}_{\mathbf{M}}\mathbf{M}^{(0)}_{nmp}(\mathbf{r}',k_s) + (1-\delta_{sN})B^{fs}_{\mathbf{M}}\mathbf{M}^{(1)}_{nmp}(\mathbf{r}',k_s)\Big) \\ & + (1-\delta_{fN})\mathbf{N}^{(1)}_{nmp}(\mathbf{r},k_f)\otimes\Big((1-\delta_{s1})A^{fs}_{\mathbf{N}}\mathbf{N}^{(0)}_{nmp}(\mathbf{r}',k_s) + (1-\delta_{sN})B^{fs}_{\mathbf{N}}\mathbf{N}^{(1)}_{nmp}(\mathbf{r}',k_s)\Big) \\ & + (1-\delta_{f1})\mathbf{M}^{(0)}_{nmp}(\mathbf{r},k_f)\otimes\Big((1-\delta_{s1})C^{fs}_{\mathbf{M}}\mathbf{M}^{(0)}_{nmp}(\mathbf{r}',k_s) + (1-\delta_{sN})D^{fs}_{\mathbf{M}}\mathbf{M}^{(1)}_{nmp}(\mathbf{r}',k_s)\Big) \\ & + (1-\delta_{f1})\mathbf{N}^{(0)}_{nmp}(\mathbf{r},k_f)\otimes\Big((1-\delta_{s1})C^{fs}_{\mathbf{N}}\mathbf{N}^{(0)}_{nmp}(\mathbf{r}',k_s) + (1-\delta_{sN})D^{fs}_{\mathbf{N}}\mathbf{N}^{(1)}_{nmp}(\mathbf{r}',k_s)\Big)\Big\},\end{aligned} \tag{3.A.3}$$

where the field and source wave numbers are:

$$k_{f,s} = \frac{\omega}{c}\sqrt{\mu_{f,s}\epsilon_{f,s}}, \tag{3.A.4}$$

$\mu_{f,s}$ and $\epsilon_{f,s}$ being the relative magnetic permeability and electric permittivity of the layers considered. The coefficients $A^{fs}_{\mathbf{M},\mathbf{N}}, B^{fs}_{\mathbf{M},\mathbf{N}}, C^{fs}_{\mathbf{M},\mathbf{N}}, D^{fs}_{\mathbf{M},\mathbf{N}}$ are found by imposing the boundary conditions:

$$\lim_{\delta r\to 0^+} \hat{\boldsymbol{r}} \times \bar{\bar{\mathbf{G}}}(\mathbf{r},\mathbf{r}',\omega)\Big|_{r=R_j-\delta r} = \lim_{\delta r\to 0^+} \hat{\boldsymbol{r}} \times \bar{\bar{\mathbf{G}}}(\mathbf{r},\mathbf{r}',\omega)\Big|_{r=R_j+\delta r}$$
$$\frac{1}{\mu_j}\lim_{\delta r\to 0^+} \hat{\boldsymbol{r}} \times \boldsymbol{\nabla} \times \bar{\bar{\mathbf{G}}}(\mathbf{r},\mathbf{r}',\omega)\Big|_{r=R_j-\delta r} = \frac{1}{\mu_{j+1}}\lim_{\delta r\to 0^+} \hat{\boldsymbol{r}} \times \boldsymbol{\nabla} \times \bar{\bar{\mathbf{G}}}(\mathbf{r},\mathbf{r}',\omega)\Big|_{r=R_j+\delta r}, \tag{3.A.5}$$

meaning that the tangential components of the electric and magnetic fields are continuous as we approach the boundary between two layers j and $j+1$ with the field point $\mathbf{r}$ from two sides of the interface, located at distance R_j from the origin. Solving for each boundary, we obtain the coefficients in $\bar{\bar{\mathbf{G}}}_S$ and thus the total Green's tensor.
In the expression (3.A.2), the singular term involving a Dirac delta function must also be expanded in the vector spherical harmonics basis. To do so we expand the total unit operator, choosing spherical Bessel function for the radial parts, i.e. $z_n = j_n$. Because of the completeness of the basis, we can express the delta operator as:

$$\bar{\bar{\delta}}(\mathbf{r}-\mathbf{r}') = \sum_{nmp}\int_0^{+\infty} \mathrm{d}q\Big[C^{(nmp)}_{\mathbf{M}}(q)\mathbf{M}^{(0)}_{nmp}(\mathbf{r},q)\otimes\mathbf{M}^{(0)}_{nmp}(\mathbf{r}',q)$$
$$+ C^{(nmp)}_{\mathbf{N}}(q)\mathbf{N}^{(0)}_{nmp}(\mathbf{r},q)\otimes\mathbf{N}^{(0)}_{nmp}(\mathbf{r}',q) + C^{(nmp)}_{\mathbf{L}}(q)\mathbf{L}^{(0)}_{nmp}(\mathbf{r},q)\otimes\mathbf{L}^{(0)}_{nmp}(\mathbf{r}',q)\Big], \tag{3.A.6}$$

which, taking the notation (3.2.17), is the position representation of the unit operator expansion:

$$\bar{\bar{\mathbb{1}}} = \sum_{nmp}\int_0^{+\infty} \mathrm{d}q\Big[C^{(nmp)}_{\mathbf{M}}(q)|\mathbf{M}^{(0)}_{nmp}(q)\rangle\langle\mathbf{M}^{(0)}_{nmp}(q)|$$
$$+ C^{(nmp)}_{\mathbf{N}}(q)|\mathbf{N}^{(0)}_{nmp}(q)\rangle\langle\mathbf{N}^{(0)}_{nmp}(q)| + C^{(nmp)}_{\mathbf{L}}(q)|\mathbf{L}^{(0)}_{nmp}(q)\rangle\langle\mathbf{L}^{(0)}_{nmp}(q)|\Big]. \tag{3.A.7}$$

In order to find the coefficients $C^{(nmp)}_{\mathbf{K}}(q)$, where $\mathbf{K} = \mathbf{M},\mathbf{N},\mathbf{L}$, we multiply both sides with the eigenfunctions $\langle\mathbf{K}|, |\mathbf{K}\rangle$, and using the orthogonality relations (3.2.20), we find:

$$C^{(nm^e_o)}_{\mathbf{M}}(q) = C^{(nm^e_o)}_{\mathbf{N}}(q) = \frac{q^2(2n+1)(n-m)!}{\pi^2 n(n+1)(n+m)!(1\pm\delta_{m0})} \tag{3.A.8a}$$
$$C^{(nm^e_o)}_{\mathbf{L}}(q) = n(n+1)C^{(nm^e_o)}_{\mathbf{M}}(q), \tag{3.A.8b}$$

where the upper sign refers to $p=e$ and the lower one to $p=o$. For the odd components, it seems that there is a divergence in the coefficients for $m=0$. It is easy to check that:

$$\mathbf{M}_{n0o}(\mathbf{r},q) = \mathbf{N}_{n0o}(\mathbf{r},q) = \mathbf{L}_{n0o}(\mathbf{r},q) = \mathbf{0}, \tag{3.A.9}$$

hence for $p=o$ and $m=0$ we do not need a coefficient in the expansion, and the divergence is not a problem. Finally we write the Dirac delta expansion:

$$\bar{\bar{\delta}}(\mathbf{r}-\mathbf{r}') = \sum_{nmp}\int_0^{+\infty} \mathrm{d}q\frac{q^2(2n+1)(n-m)!}{\pi^2 n(n+1)(n+m)!(1+\delta_{m0})}\Big[\mathbf{M}^{(0)}_{nmp}(\mathbf{r},q)\otimes\mathbf{M}^{(0)}_{nmp}(\mathbf{r}',q)$$
$$+ \mathbf{N}^{(0)}_{nmp}(\mathbf{r},q)\otimes\mathbf{N}^{(0)}_{nmp}(\mathbf{r}',q) + n(n+1)\mathbf{L}^{(0)}_{nmp}(\mathbf{r},q)\otimes\mathbf{L}^{(0)}_{nmp}(\mathbf{r}',q)\Big]. \tag{3.A.10}$$

To expand the singular term in $\bar{\bar{\mathbf{G}}}_0$ we take the $\hat{\boldsymbol{r}}\otimes\hat{\boldsymbol{r}}$ component of the latter.

Chapter 4

Effective models for quantum plasmonics

Chapter overview

Objectives: This chapter exploits the general field quantization for absorbing and dispersing media for the derivation of effective models, which are applicable to the quantum dynamics of spherically layered systems at the nanoscale.

Guideline:

- Derivation of a general mode-selective continuous Hamiltonian for the plasmonic modes.
- Derivation of a general mode-selective discrete Hamiltonian.
- Application for two emitters near a metal nanosphere.
- **keywords:** *Local density of states (LDOS), effective operators, dark/bright operators, continuous model, discrete model, overlap function, Gram-Schmidt orthogonalization.*

Results/novelty: Mode-selective quantization and multimodal effective models for spherically layered systems.

In the preceding chapter, we have derived a modal field quantization procedure for a spherically layered medium. The set of creation and annihilation operators defined in this quantization scheme allows to selectively toggle excitations associated with the separate spherical harmonic modes. In turn, it is possible to transpose cQED concepts to describe a range of systems where quantum emitters interact with eigenmodes, with a special regard to the field of nano-optics and plasmonics.
We focus on the effective models that are built from the quantization of the eigenmodes, following a derivation that is analogous to section 2.2, where it is done for a single atom in a cavity. The effective models are derived in two steps:

- A continuous model describing the interaction between emitters and the field, leading to a Hermitian Hamiltonian.
- A discrete model constructed from the preceding one, where all continuous degrees of freedom are integrated in the complex plane and the effective Hamiltonian is non-Hermitian.

In a last section, we derive both the continuous and effective models for two quantum emitters in the vicinity of a metal nanosphere.

4.1 Continuous model with multiple emitters

Resonances of the spherically layered system are structured with respect to the spherical harmonic orders. As an example, we can compute the local density of states (LDOS) of a metallic nanoparticle, which is defined as:

$$\rho_{\mathbf{n}}(\mathbf{r},\omega) = \frac{6\omega}{\pi c^2}\mathbf{n}\cdot\mathfrak{Im}\left\{\bar{\bar{\mathbf{G}}}(\mathbf{r},\mathbf{r},\omega)\right\}\mathbf{n}, \tag{4.1.1}$$

with $\mathbf{n}$ being the unit vector corresponding to the polarization direction on which the field is measured. In the case of a quantum emitter located in the vicinity of a sphere, the Green's tensor is of the form:

$$\bar{\bar{\mathbf{G}}}(\mathbf{r},\mathbf{r}',\omega) = \bar{\bar{\mathbf{G}}}_0(\mathbf{r},\mathbf{r}',\omega) + \bar{\bar{\mathbf{G}}}_S(\mathbf{r},\mathbf{r}',\omega), \tag{4.1.2}$$

since $r > R$, R being the radius of the sphere. Thus, the LDOS is decomposed into two terms corresponding to the vacuum and scattered parts of the Green's tensor. It is shown in refs [21,88] that:

$$\mathbf{n}\cdot\mathfrak{Im}\left\{\bar{\bar{\mathbf{G}}}_0(\mathbf{r},\mathbf{r},\omega)\right\}\mathbf{n} = \frac{\omega}{6\pi c}, \tag{4.1.3}$$

hence this term leads to a quadratic behaviour of the LDOS in free space. The scattered contribution $\bar{\bar{\mathbf{G}}}_S$ contains the properties of the metallic nanoparticle, and if the emitter is located very close to it, it is dominant. Using (3.2.24), we can decompose the Green's tensor into a sum, each term corresponding to a spherical harmonic index n:

$$\bar{\bar{\mathbf{G}}}(\mathbf{r},\mathbf{r}',\omega) = \sum_n \bar{\bar{\mathbf{G}}}_n(\mathbf{r},\mathbf{r}',\omega). \tag{4.1.4}$$

Fig. 4.1 shows the local density of states at position $\mathbf{r}_1$ close to a silver sphere of radius $R = 8$

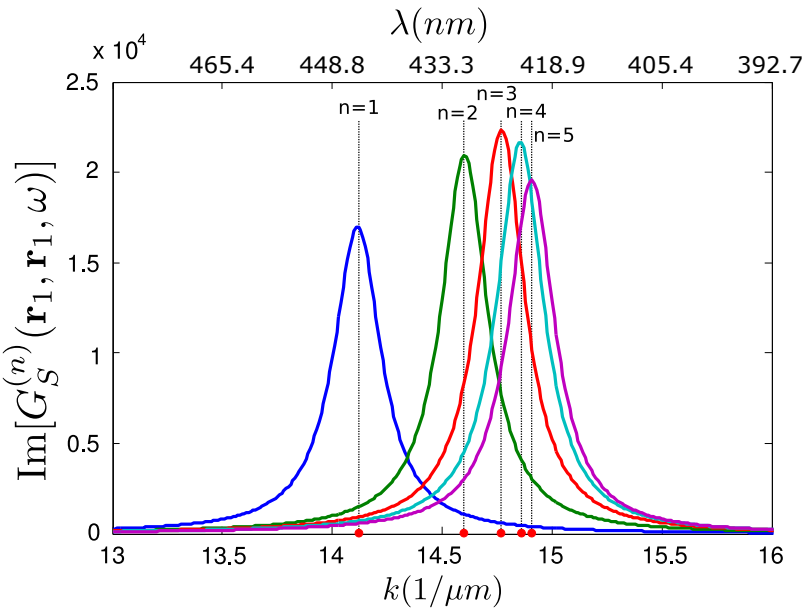

Figure 4.1: Scattered radial orders close to a silver nanosphere of 8 nm radius ($r_1 = 10$ nm), for an emitter polarized in the radial direction, i.e. $\mathbf{n} = \hat{\boldsymbol{r}}$. Each harmonic order contribution contains a single resonance peak.

nm, associated with the scattered part of the Green's tensor and the harmonic indices n. Each resonance peak corresponds to a particular mode labelled by the index n. As a consequence, it is convenient to derive cQED models from the Hamiltonian (3.3.13), with field operators associated with harmonic indices. In the following, we construct cQED Hamiltonians where field operators no longer depend on $\mathbf{r}$ as a continuous variable, and only contain harmonic indices that are relevant for a specific configuration.

4.1.1 Single emitter - dark and bright operators

Effective operators

Let us consider a single quantum emitter at position $\mathbf{r}_A$ interacting with the mode structure of a spherically layered, nonmagnetic medium, i.e. $N_e = 1$ in (3.3.12). Based on the interaction part of the Hamiltonian, we define the effective field operators driving the dynamics of the field-atom system:

$$\boxed{\widehat{a}_{\bar{n}}(\omega) := \frac{1}{\sqrt{\hbar\pi\epsilon_0}\kappa_{\bar{n}}(\omega)}\frac{\omega^2}{c^2}\int \mathrm{d}^3r\sqrt{\epsilon''(\mathbf{r},\omega)}\mathbf{d}\cdot\overline{\overline{\mathbf{G}}}_{\bar{n}}(\mathbf{r}_A,\mathbf{r},\omega)\,\widehat{\mathbf{f}}(\mathbf{r},\omega),} \tag{4.1.5}$$

with $\bar{n} = n, m, p$ and $\kappa_{\bar{n}}(\omega)$ is the emitter-field coupling. Writing this definition in terms of the mode-selective operators and looking at the orthogonality relations (3.2.20) of the vector spherical harmonics, it is indeed seen that $\widehat{a}_{\bar{n}}(\omega)$ annihilates excitations associated with the

harmonic term n, m and the parity p:

$$\widehat{a}_{\bar{n}}(\omega) = \sum_{\mathbf{K}} \int_0^{+\infty} \mathrm{d}q \frac{1}{\sqrt{\hbar\pi\epsilon_0 Q^{\mathbf{K}}_{nm}(q)}\kappa_{\bar{n}}(\omega)} \frac{\omega^2}{c^2} \int \mathrm{d}^3 r \sqrt{\epsilon''(\mathbf{r},\omega)} \mathbf{d} \cdot \bar{\bar{\mathbf{G}}}_{\bar{n}}(\mathbf{r}_A, \mathbf{r}, \omega)\, \mathbf{K}_{\bar{n}}(\mathbf{r}, q) \widehat{F}^{(\bar{n})}_{\mathbf{K}}(\omega, q). \tag{4.1.6}$$

The interaction Hamiltonian in (3.3.12) assumes then the form:

$$\widehat{H}_{\mathrm{int}} = -i\hbar \sum_{\bar{n}} \int_0^{+\infty} \mathrm{d}\omega \Big(\kappa_{\bar{n}}(\omega) \widehat{\sigma}_+ \widehat{a}_{\bar{n}}(\omega) - \kappa^*_{\bar{n}}(\omega) \widehat{a}^\dagger_{\bar{n}}(\omega) \widehat{\sigma}_- \Big). \tag{4.1.7}$$

We notice that this expression has the same form as (2.2.10a). We derive the commutation relation for the operators $\widehat{a}_{\bar{n}}(\omega), \widehat{a}^\dagger_{\bar{n}'}(\omega')$, using the commutation relations (3.3.3) and the Green's tensor identity for nonmagnetic materials [68]:

$$\int \mathrm{d}^3 r \frac{\omega^2}{c^2} \epsilon''(\mathbf{r},\omega) \bar{\bar{\mathbf{G}}}_{\bar{n}}(\mathbf{r}_1, \mathbf{r}, \omega) \bar{\bar{\mathbf{G}}}^*_{\bar{n}}(\mathbf{r}, \mathbf{r}_2, \omega) = \mathfrak{Im} \left\{ \bar{\bar{\mathbf{G}}}_{\bar{n}}(\mathbf{r}_1, \mathbf{r}_2, \omega) \right\}. \tag{4.1.8}$$

For the excitations to be normalized, we introduced the emitter-field coupling $\kappa_{\bar{n}}(\omega)$, which should take the form:

$$|\kappa_{\bar{n}}(\omega)|^2 = \frac{1}{\hbar\pi\epsilon_0} \frac{\omega^2}{c^2} \mathbf{d} \cdot \mathfrak{Im} \left\{ \bar{\bar{\mathbf{G}}}_{\bar{n}}(\mathbf{r}_A, \mathbf{r}_A, \omega) \right\} \mathbf{d}^*, \tag{4.1.9}$$

and the commutation relations read:

$$\left[\widehat{a}_{\bar{n}}(\omega), \widehat{a}^\dagger_{\bar{n}'}(\omega') \right] = \delta_{\bar{n}\bar{n}'} \delta(\omega - \omega') \tag{4.1.10a}$$

$$\left[\widehat{a}_{\bar{n}}(\omega), \widehat{a}_{\bar{n}'}(\omega') \right] = \left[\widehat{a}^\dagger_{\bar{n}}(\omega), \widehat{a}^\dagger_{\bar{n}'}(\omega') \right] = 0. \tag{4.1.10b}$$

We underline that the definition of these operators depends on the position $\mathbf{r}_A$ of the emitter. For different positions and frequencies, the emitter-field coupling varies and provides a structured continuum. The case where we consider several emitters will be derived later in this chapter.

Separation of dark and bright subspaces

We still have to express the field Hamiltonian $\widehat{H}_F$ in terms of the effective operators $\widehat{a}_{\bar{n}}(\omega), \widehat{a}^\dagger_{\bar{n}}(\omega)$. In order to achieve this, we make the following consideration: since $\widehat{a}_{\bar{n}}(\omega)$ is a particular linear combination of operators $\widehat{F}^{(\bar{n})}_{\mathbf{K}}(\omega, q)$ (as well as $\widehat{\mathbf{f}}(\mathbf{r}, \omega)$), the field-atom dynamics driven by it involves only a certain subspace of the total Hilbert space. States belonging to the rest of the Hilbert space will be decoupled from the dynamics. Thus, we separate the original Hilbert space into orthogonal *bright* and *dark* subspaces in order to construct an effective model by keeping the first and ignoring the latter.
This procedure is similar to the Gram-Schmidt orthogonalization, and consists in building the set of the dark field operators, and writing the total field Hamiltonian in a split form, as is done in section 2.2. In the following, we use the condensed definition:

$$\widehat{a}_{\bar{n}}(\omega) = \sum_{\mathbf{K}} \int_0^{+\infty} \mathrm{d}q\, \alpha^{(\bar{n})}_{\mathbf{K}}(\omega, q) \widehat{F}^{(\bar{n})}_{\mathbf{K}}(\omega, q), \tag{4.1.11}$$

which is identical to (4.1.6), with the coefficients:

$$\alpha_{\mathbf{K}}^{(\bar{n})}(\omega,q) = \frac{1}{\sqrt{\hbar\pi\epsilon_0 Q_{nm}^{\mathbf{K}}(q)}\kappa_{\bar{n}}(\omega)}\frac{\omega^2}{c^2}\int \mathrm{d}^3r\sqrt{\epsilon''(\mathbf{r},\omega)}\mathbf{d}\cdot\overline{\overline{\mathbf{G}}}_{\bar{n}}(\mathbf{r}_A,\mathbf{r},\omega)\,\mathbf{K}_{\bar{n}}(\mathbf{r},q). \tag{4.1.12}$$

Now, we define a set of operators in a way that, by construction, the Fock subspace generated by their action on the vacuum is orthogonal to the Fock subspace generated by the bright operators $\widehat{a}_{\bar{n}}(\omega)$:

$$\begin{aligned}\widehat{\mathtt{d}}_{\mathbf{K}}^{(\bar{n})}(\omega,q) &= \widehat{F}_{\mathbf{K}}^{(\bar{n})}(\omega,q) - \int_0^{+\infty}\mathrm{d}\omega'\left[\widehat{F}_{\mathbf{K}}^{(\bar{n})}(\omega,q),\widehat{a}_{\bar{n}}^{\dagger}(\omega')\right]\widehat{a}_{\bar{n}}(\omega')\\ &= \widehat{F}_{\mathbf{K}}^{(\bar{n})}(\omega,q) - \alpha_{\mathbf{K}}^{(\bar{n})*}(\omega,q)\widehat{a}_{\bar{n}}(\omega).\end{aligned} \tag{4.1.13}$$

From this definition, it is easy to check that the commutators between bright and dark operators are always zero:

$$\left[\widehat{\mathtt{d}}_{\mathbf{K}}^{(\bar{n})}(\omega,q),\widehat{a}_{\bar{n}'}^{\dagger}(\omega')\right] = \left[\widehat{\mathtt{d}}_{\mathbf{K}}^{(\bar{n})}(\omega,q),\widehat{a}_{\bar{n}'}(\omega')\right] = \left[\widehat{\mathtt{d}}_{\mathbf{K}}^{(\bar{n})\dagger}(\omega,q),\widehat{a}_{\bar{n}'}^{\dagger}(\omega')\right] = 0. \tag{4.1.14}$$

As a final step, we use the commutation relations (4.1.10) and the expression of the expansion coefficients $\alpha_{\mathbf{K}}^{(\bar{n})}(\omega,q)$ to derive the property:

$$\sum_{\mathbf{K}}\int_0^{+\infty}\mathrm{d}q\,\alpha_{\mathbf{K}}^{(\bar{n})}(\omega,q)\alpha_{\mathbf{K}}^{(\bar{n})*}(\omega,q) = 1, \tag{4.1.15}$$

that we invoke to obtain the expression of $\widehat{H}_F$ in terms of the bright and dark operators:

$$\sum_{\mathbf{K}}\int_0^{+\infty}\mathrm{d}q\,\widehat{F}_{\mathbf{K}}^{(\bar{n})\dagger}(\omega,q)\widehat{F}_{\mathbf{K}}^{(\bar{n})}(\omega,q) = \widehat{a}_{\bar{n}}^{\dagger}(\omega)\widehat{a}_{\bar{n}}(\omega) + \sum_{\mathbf{K}}\int_0^{+\infty}\mathrm{d}q\,\widehat{\mathtt{d}}_{\mathbf{K}}^{(\bar{n})\dagger}(\omega,q)\widehat{\mathtt{d}}_{\mathbf{K}}^{(\bar{n})}(\omega,q). \tag{4.1.16}$$

Having successfully separated the dark and bright subspaces, we write the single emitter effective Hamiltonian restricted to the bright subspace:

$$\boxed{\begin{aligned}\widehat{H}_{\mathrm{eff}} &= \hbar\omega_0\widehat{\sigma}_+\widehat{\sigma}_- + \sum_{\bar{n}}\int_0^{+\infty}\mathrm{d}\omega\,\widehat{a}_{\bar{n}}^{\dagger}(\omega)\widehat{a}_{\bar{n}}(\omega)\\ &\quad - i\hbar\sum_{\bar{n}}\int_0^{+\infty}\mathrm{d}\omega\Big(\kappa_{\bar{n}}(\omega)\widehat{\sigma}_+\widehat{a}_{\bar{n}}(\omega) - \kappa_{\bar{n}}^*(\omega)\widehat{a}_{\bar{n}}^{\dagger}(\omega)\widehat{\sigma}_-\Big),\end{aligned}} \tag{4.1.17}$$

where ω_0 is the transition frequency of the two-level emitter. We note that the dark/bright separation is feasible only if the spectrum of the non-interacting Hamiltonian (here $\hbar\omega$) does not depend on the eliminated variables. In our case, the eigenvalues do not depend on $\mathbf{K}, q, n, m, p$ hence we could construct effective models eliminating all of these parameters.

Eliminating indices

The mode-selective quantization procedure allows to access degrees of freedom from the vector spherical harmonics, i.e. indices associated with each eigenfunction. In practice, not all

harmonic indices are always relevant depending on the degree of specificity we want to reach. In the case of plasmon resonances with a metallic nanoparticle, for example, we can label the plasmonic modes with index n, leading to a set of normal modes, with different spatial patterns (dipolar for $n = 1$, quadrupolar for $n = 2$, etc...). However, both the parity and the m harmonics are summed over, and we do not need to specify them.
The described method for dark/bright separation of the Hilbert space enables us to eliminate some of the harmonic indices in case they are not relevant for the current investigation. In the following, we construct an effective model where n is the only index present, and m, p are summed over. To do so, we define the field operator:

$$\widehat{a}_n(\omega) = \frac{1}{\kappa_n(\omega)} \sum_{p=e,o} \sum_{m=0}^{n} \kappa_{nmp}(\omega) \widehat{a}_{nmp}(\omega), \tag{4.1.18}$$

where we have expanded the compact notation $\bar{n} = n, m, p$ back in its explicit form. Using (4.1.7), we express the interaction Hamiltonian as:

$$\widehat{H}_{\text{int}} = -i\hbar \sum_{n=0}^{+\infty} \int_0^{+\infty} \mathrm{d}\omega \Big(\kappa_n(\omega) \widehat{\sigma}_+ \widehat{a}_n(\omega) - \kappa_n^*(\omega) \widehat{a}_n^\dagger(\omega) \widehat{\sigma}_- \Big). \tag{4.1.19}$$

Again, we define the value of the emitter-field coupling $\kappa_n(\omega)$ by the normalization of the field operator, whose commutation relations are:

$$\Big[\widehat{a}_n(\omega), \widehat{a}_{n'}^\dagger(\omega') \Big] = \delta_{nn'} \delta(\omega - \omega') \tag{4.1.20a}$$

$$\Big[\widehat{a}_n(\omega), \widehat{a}_{n'}(\omega') \Big] = \Big[\widehat{a}_n^\dagger(\omega), \widehat{a}_{n'}^\dagger(\omega') \Big] = 0, \tag{4.1.20b}$$

and the emitter-field coupling is given by the relation:

$$\begin{aligned} |\kappa_n(\omega)|^2 &= \sum_{m,p} |\kappa_{nmp}(\omega)|^2 \\ &= \frac{1}{\hbar \pi \epsilon_0} \frac{\omega^2}{c^2} \mathbf{d} \cdot \mathfrak{Im} \left\{ \bar{\bar{\mathbf{G}}}_n(\mathbf{r}_A, \mathbf{r}_A, \omega) \right\} \mathbf{d}^*. \end{aligned} \tag{4.1.21}$$

To construct the full effective Hamiltonian, we perform the dark/bright subspace separation and define:

$$\widehat{\mathtt{d}}_{nmp}(\omega) = \widehat{a}_{nmp}(\omega) - \int_0^{+\infty} \mathrm{d}\omega \Big[\widehat{a}_{nmp}(\omega), \widehat{a}_n^\dagger(\omega') \Big] \widehat{a}_n(\omega'), \tag{4.1.22}$$

and the integrand of $\widehat{H}_F$ becomes:

$$\sum_{m,p} \widehat{a}_{nmp}^\dagger(\omega) \widehat{a}_{nmp}(\omega) = \widehat{a}_n^\dagger(\omega) \widehat{a}_n(\omega) + \sum_{m,p} \widehat{\mathtt{d}}_{nmp}^\dagger(\omega) \widehat{\mathtt{d}}_{nmp}(\omega). \tag{4.1.23}$$

Based on this description, we rewrite the effective Hamiltonian:

$$\boxed{\begin{aligned} \widehat{H}_{\text{eff}} &= \hbar \omega_0 \widehat{\sigma}_+ \widehat{\sigma}_- + \sum_n \int_0^{+\infty} \mathrm{d}\omega\, \widehat{a}_n^\dagger(\omega) \widehat{a}_n(\omega) \\ &\quad - i\hbar \sum_n \int_0^{+\infty} \mathrm{d}\omega \Big(\kappa_n(\omega) \widehat{\sigma}_+ \widehat{a}_n(\omega) - \kappa_n^*(\omega) \widehat{a}_n^\dagger(\omega) \widehat{\sigma}_- \Big), \end{aligned}} \tag{4.1.24}$$

4.1.2 Multiple two-level emitters

Effective operators

We consider the case of N_e quantum emitters coupled to the structured field, as done in section 3.3.3 (see also fig. 3.6). We wish to connect the effective model to the quantization scheme derived earlier. Because each individual emitter interacts differently with the structured field (characterized by the Green's tensor), we need to define a coupling for each emitter. In the following, we use the compact index $\bar{n} = n, m, p$ for the mode structure, but we keep in mind that indices can be summed up. The interaction Hamiltonian for the multi-emitter system reads:

$$\widehat{H}_{\text{int}} = -i\hbar \sum_{j=1}^{N_e} \sum_{\bar{n}} \int_0^{+\infty} \mathrm{d}\omega \Big(\kappa_{\bar{n}}^{(j)}(\omega) \widehat{\sigma}_+^{(j)} \widehat{a}_{\bar{n}}^{(j)}(\omega) - \kappa_{\bar{n}}^{(j)*}(\omega) \widehat{a}_{\bar{n}}^{(j)\dagger}(\omega) \widehat{\sigma}_-^{(j)} \Big), \tag{4.1.25}$$

where we have a set of creation and annihilation operators for each atomic position $\mathbf{r}_j$:

$$\widehat{a}_{\bar{n}}^{(j)}(\omega) = \frac{1}{\kappa_{\bar{n}}^{(j)}(\omega)} \sum_{\mathbf{K}} \int_0^{+\infty} \mathrm{d}q \frac{1}{\sqrt{\hbar \pi \epsilon_0 Q_{nm}^{\mathbf{K}}(q)}} \times \int \mathrm{d}^3 r \sqrt{\epsilon''(\mathbf{r}, \omega)} \mathbf{d}_j \cdot \overline{\overline{\mathbf{G}}}_{\bar{n}}(\mathbf{r}_j, \mathbf{r}, \omega) \mathbf{K}_{\bar{n}}(\mathbf{r}, q) \widehat{F}_{\mathbf{K}}^{(\bar{n})}(\omega, q), \tag{4.1.26}$$

analogously with the single emitter case, and the atom-field $\kappa_{\bar{n}}^{(j)}(\omega)$ is defined as (4.1.9) for the respective emitter positions $\mathbf{r}_j$ and transition dipole moments $\mathbf{d}_j$. To derive the commutation relations, we use (3.3.10) and the following identity, resulting from the orthogonality of the vector harmonics $\mathbf{K}$:

$$\sum_{\ell=1}^{3} \int \mathrm{d}^3 r' G_{k\ell,\bar{n}}(\mathbf{r}, \mathbf{r}') K_{\ell,\bar{n}}(\mathbf{r}', q) = \sum_{\ell=1}^{3} \int \mathrm{d}^3 r' G_{k\ell,\bar{n}}(\mathbf{r}, \mathbf{r}') \sum_{\bar{n}'} K_{\ell,\bar{n}'}(\mathbf{r}', q), \tag{4.1.27}$$

where $G_{k\ell,\bar{n}}$ are matrix elements of $\overline{\overline{\mathbf{G}}}_{\bar{n}}$ and K_ℓ are spatial components of $\mathbf{K}$. Simplifying the resulting expression by aid of the Dirac delta expansion in terms of spherical harmonics (see appendix 3.A) it becomes apparent that the creation and annihilation operators cease to be orthogonal for different emitter positions:

$$\left[\widehat{a}_{\bar{n}}^{(j)}(\omega), \widehat{a}_{\bar{n}'}^{(k)\dagger}(\omega') \right] = \delta_{\bar{n}\bar{n}'} \delta(\omega - \omega') \mu_{\bar{n}}^{(jk)}(\omega) \tag{4.1.28a}$$

$$\left[\widehat{a}_{\bar{n}}^{(j)}(\omega), \widehat{a}_{\bar{n}'}^{(k)}(\omega') \right] = \left[\widehat{a}_{\bar{n}}^{(j)\dagger}(\omega), \widehat{a}_{\bar{n}'}^{(k)\dagger}(\omega') \right] = 0, \tag{4.1.28b}$$

where we introduced the *mode overlap* function:

$$\boxed{\mu_{\bar{n}}^{(jk)}(\omega) = \frac{1}{\hbar \pi \epsilon_0} \frac{\omega^2}{c^2} \frac{\mathbf{d}_j \cdot \mathfrak{Im} \left\{ \overline{\overline{\mathbf{G}}}_{\bar{n}}(\mathbf{r}_j, \mathbf{r}_k, \omega) \right\} \mathbf{d}_k^*}{\kappa_{\bar{n}}^{(j)}(\omega) \kappa_{\bar{n}}^{(k)*}(\omega)}.} \tag{4.1.29}$$

An illustration of the non-orthogonality of the modes due to different atomic positions is shown in fig. 4.2. Using (4.1.9) it is seen that the N_e-emitter model returns the single emitter commutation for $N_e = 1$, as $\mu_{\bar{n}}^{(jj)}(\omega) = 1$.

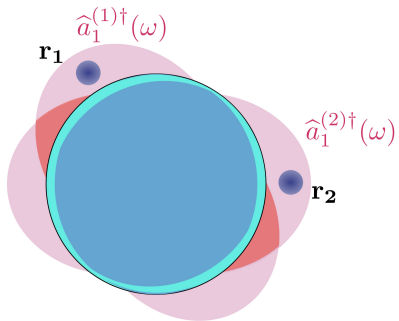

Figure 4.2: Dipolar modes ($n = 1$) of a single metallic sphere excited by emitters at $\mathbf{r}_1$ and $\mathbf{r}_2$. Although each emitter is directly coupled only to the field assigned to its position, the overlap between modes (red region) can induce a transfer of excitation between them.

Orthogonalization of the bright subspace and dark/bright decomposition

Following the procedure of dark/bright subspace separation, we should get the desired effective Hamiltonian. However, the presence of non-unity mode overlap poses a problem: since, for different j parameters, the bright operators $\widehat{a}_{\bar{n}}^{(j)}(\omega)$ are not necessarily orthogonal, trying to construct the dark operators similarly to (4.1.13) will not result in a set of operators commuting with the bright ones. In other words, the Hilbert space does no longer separate into two orthogonal subspaces if we follow this procedure.
Instead, one must include an intermediate step: the orthogonalization of the bright operator manifold with respect to the emitter position parameter. In a first step, we reduce the set of the original bright operators to linearly independent ones. If, for a given pair of position indices j, k associated with the emitters' positions $\mathbf{r}_j, \mathbf{r}_k$ we have:

$$|\mu_{\bar{n}}^{(jk)}(\omega)| = 1, \tag{4.1.30}$$

then it means that $\widehat{a}_{\bar{n}}^{(j)}(\omega)$ and $\widehat{a}_{\bar{n}}^{(k)}(\omega)$ are not linearly independent. This is apparent when multiplying the commutation relation (4.1.28) by $\mu_{\bar{n}'}^{(jk)*}(\omega')$:

$$\left[\widehat{a}_{\bar{n}}^{(j)}(\omega), \left[\mu_{\bar{n}'}^{(jk)}(\omega')\widehat{a}_{\bar{n}'}^{(k)}(\omega')\right]^\dagger\right] = \delta_{\bar{n}\bar{n}'}\delta(\omega - \omega'), \tag{4.1.31}$$

which is the same as the commutation relation for a single emitter (4.1.10). As a consequence, we have a linear relation between the two operators:

$$\widehat{a}_{\bar{n}}^{(j)} = \mu_{\bar{n}}^{(jk)}(\omega)\widehat{a}_{\bar{n}}^{(k)}(\omega). \tag{4.1.32}$$

Listing all the pairs $j > k$ for which (4.1.30) is satisfied and making the above assignment, reducing the number of field operators, we end up with a reduced dimensionality $N_r \leqslant N_e$ where N_r is the number of linearly independent field operators. We rewrite the Hamiltonian (4.1.25) in the form:

$$\widehat{H}_{\text{int}} = -i\hbar \sum_{j=1}^{N_r}\sum_{k=1}^{N_e}\sum_{\bar{n}} \int_0^{+\infty} \mathrm{d}\omega \left(\kappa_{\bar{n}}^{(jk)}(\omega)\widehat{\sigma}_+^{(k)}\widehat{a}_{\bar{n}}^{(j)}(\omega) - \kappa_{\bar{n}}^{(jk)*}(\omega)\widehat{a}_{\bar{n}}^{(j)\dagger}(\omega)\widehat{\sigma}_-^{(k)}\right), \tag{4.1.33}$$

where

$$\kappa_{\bar{n}}^{(jk)}(\omega) = \begin{cases} \mu_{\bar{n}}^{kj}(\omega)\kappa_{\bar{n}}^{(k)}(\omega) & j \leqslant k \text{ and } |\mu_{\bar{n}}^{(kj)}(\omega)| = 1 \\ 0 & \text{otherwise} \end{cases}. \tag{4.1.34}$$

At this stage, we have just written Hamiltonian (4.1.25) in a more detailed way, where we include the possibility of linearly dependent field operators, and labelled them with the same indices. Indeed, for the general case where all field operators are linearly independent, i.e. if $|\mu_{\bar{n}}^{(jk)}(\omega)| < 1$, only $j = k$ terms remain in (4.1.34), yielding $\kappa_{\bar{n}}^{(jj)}(\omega) \equiv \kappa_{\bar{n}}^{(j)}(\omega)$. The sum over j in (4.1.33) is dropped as it corresponds, in that case, to the sum over the number of emitters, and we find that (4.1.33) takes the form (4.1.25).

Having obtained a set of linearly independent operators, we can orthogonalize them. The orthogonalization procedure is not unique, and depending on our convenience, we can choose different methods. For example, with a Gram-Schmidt orthogonalization we can construct a set of orthogonal, normalized operators:

$$\begin{aligned}
\widehat{b}_{\bar{n}}^{(1)}(\omega) &= \widehat{a}_{\bar{n}}^{(1)}(\omega) \\
\widehat{b}_{\bar{n}}^{(2)}(\omega) &= \frac{1}{\beta_n^{(21)}}\left(\widehat{a}_{\bar{n}}^{(2)}(\omega) - \int_0^{+\infty} \mathrm{d}\omega' \left[\widehat{a}_{\bar{n}}^{(2)}(\omega), \widehat{b}_{\bar{n}}^{(1)\dagger}(\omega')\right] \widehat{b}_{\bar{n}}^{(1)}(\omega')\right) \\
&\vdots \\
\widehat{b}_{\bar{n}}^{(N_r)}(\omega) &= \frac{1}{\beta_{N_r}}\left(\widehat{a}_{\bar{n}}^{(N_r)}(\omega) - \sum_{j=1}^{N_r} \int_0^{+\infty} \mathrm{d}\omega' \left[\widehat{a}_{\bar{n}}^{(N_r)}(\omega), \widehat{b}_{\bar{n}}^{(j)\dagger}(\omega')\right] \widehat{b}_{\bar{n}}^{(j)}(\omega')\right),
\end{aligned} \tag{4.1.35}$$

where β_j are normalization factors. Other methods, such as the Householder reflection, can be chosen. The latter one, for example, preserves the symmetry of the original basis. In general, we represent the orthogonalized operators in the form:

$$\widehat{b}_{\bar{n}}^{(i)}(\omega) = \sum_{j=1}^{N_r} B_{\bar{n}}^{(ij)}(\omega)\widehat{a}_{\bar{n}}^{(j)}(\omega), \tag{4.1.36}$$

where, since the operators $\widehat{a}_{\bar{n}}^{(j)}(\omega)$ are linearly independent, the matrix made up by the elements $B_{\bar{n}}^{(ij)}(\omega)$ is non-singular. Taking the inverse of the latter, we write:

$$\widehat{a}_{\bar{n}}^{(j)}(\omega) = \sum_{i=1}^{N_r} A_{\bar{n}}^{(ji)}(\omega)\widehat{b}_{\bar{n}}^{(i)}(\omega). \tag{4.1.37}$$

The orthogonality being constructed, the commutation relations for the new operators are:

$$\left[\widehat{b}_{\bar{n}}^{(i)}(\omega), \widehat{b}_{\bar{n}'}^{(j)\dagger}(\omega')\right] = \delta_{ij}\delta_{\bar{n}\bar{n}'}\delta(\omega - \omega') \tag{4.1.38a}$$

$$\left[\widehat{b}_{\bar{n}}^{(i)}(\omega), \widehat{b}_{\bar{n}'}^{(j)}(\omega')\right] = \left[\widehat{b}_{\bar{n}}^{(i)\dagger}(\omega), \widehat{b}_{\bar{n}'}^{(j)\dagger}(\omega')\right] = 0, \tag{4.1.38b}$$

and thus we perform the dark/bright subspace separation described above, the only difference being that we use the new basis of operators $\{\widehat{b}_{\bar{n}}^{(j)}(\omega)\}$ instead of the original field operator basis. The dark operators read:

$$\widehat{\mathtt{d}}_{\mathbf{K}}^{(\bar{n})}(\omega, q) = \widehat{F}_{\mathbf{K}}^{(\bar{n})}(\omega, q) - \sum_{j=1}^{N_r} \int_0^{+\infty} \mathrm{d}\omega' \left[\widehat{F}_{\mathbf{K}}^{(\bar{n})}(\omega, q), \widehat{b}_{\bar{n}}^{(j)\dagger}(\omega')\right] \widehat{b}_{\bar{n}}^{(j)}(\omega'), \tag{4.1.39}$$

and we choose to represent operators $\widehat{b}_{\bar{n}}^{(j)}(\omega)$ in the compact form:

$$\widehat{b}_{\bar{n}}^{(j)}(\omega) = \sum_{\mathbf{K}} \int_0^{+\infty} \mathrm{d}q\, \beta_{\mathbf{K},j}^{(\bar{n})}(\omega, q) \widehat{F}_{\mathbf{K}}^{(\bar{n})}(\omega, q). \tag{4.1.40}$$

The commutation relations (3.3.10) and (4.1.38) together with the latter definition bring the property:

$$\sum_{\mathbf{K}} \int_0^{+\infty} \mathrm{d}q\, \beta_{\mathbf{K},j}^{(\bar{n})}(\omega, q) \beta_{\mathbf{K},j}^{(\bar{n})*}(\omega, q) = 1. \tag{4.1.41}$$

Writing the integrand of H_F, we get the expression in terms of the bright and dark modes:

$$\sum_{\mathbf{K}} \int_0^{+\infty} \mathrm{d}q \widehat{F}_{\mathbf{K}}^{(\bar{n})\dagger}(\omega, q) \widehat{F}_{\mathbf{K}}^{(\bar{n})}(\omega, q) = \widehat{b}_{\bar{n}}^{(j)\dagger}(\omega) \widehat{b}_{\bar{n}}^{(j)}(\omega) + \sum_{\mathbf{K}} \int_0^{+\infty} \mathrm{d}q\, \widehat{\mathtt{d}}_{\mathbf{K}}^{(\bar{n})\dagger}(\omega, q) \widehat{\mathtt{d}}_{\mathbf{K}}^{(\bar{n})}(\omega, q), \tag{4.1.42}$$

and we finally write the effective Hamiltonian for multiple emitters coupled to the spherical mode structure:

$$\boxed{\begin{aligned} \widehat{H}_{\mathrm{eff}} = &\sum_{k=1}^{N_e} \hbar\omega_k \widehat{\sigma}_+^{(k)} \widehat{\sigma}_-^{(k)} + \sum_{j=1}^{N_r} \sum_{\bar{n}} \int_0^{+\infty} \mathrm{d}\omega \hbar\omega\, \widehat{b}_{\bar{n}}^{(j)\dagger}(\omega) \widehat{b}_{\bar{n}}^{(j)}(\omega) \\ &- i\hbar \sum_{j=1}^{N_r} \sum_{k=1}^{N_e} \sum_{\bar{n}} \int_0^{+\infty} \mathrm{d}\omega \Big(\widetilde{\kappa}_{\bar{n}}^{(jk)}(\omega) \widehat{\sigma}_+^{(k)} \widehat{b}_{\bar{n}}^{(j)}(\omega) - \widetilde{\kappa}_{\bar{n}}^{(jk)*}(\omega) \widehat{b}_{\bar{n}}^{(j)\dagger}(\omega) \widehat{\sigma}_-^{(k)} \Big), \end{aligned}} \tag{4.1.43}$$

where each atom interacts with all the othogonalized field modes with atom-field couplings:

$$\widetilde{\kappa}_{\bar{n}}^{(jk)}(\omega) = \sum_{i=1}^{N_r} A_{\bar{n}}^{(ij)}(\omega) \kappa_{\bar{n}}^{(ik)}(\omega). \tag{4.1.44}$$

4.2 Discrete model

We proceed, in this section, with the last step of the effective model construction. We have previously successfully derived effective continuous models for quantum emitters interacting with a spherically layered, non-magnetic and absorbing medium, and those models can be used directly to compute the quantum dynamics of emitters coupled to the mode structure. However, when the continuum has a structure, it is possible to simplify the model even further by integrating the continuous degrees of freedom, leading to a discrete effective model. This reduces the size of the computation, and no discretization of the continuum is required.
In the following derivation, we will get rid of the frequency dependence and construct discrete field operators, each labelled by the index group $\bar{n}$. Thus, in case of a metallic system, we have an effective model where each plasmonic resonance peak has a single, discrete creation/annihilation pair of operators associated to it. The section is structured in an analogous way as the previous one, that is we derive the model for one single emitter, and extend it to multiple emitters interacting with the field.

4.2.1 Single emitter

For simplicity, we start with a system where a single quantum emitter interacts with its environment and so the effective Hamiltonian is given by (4.1.17). Eliminating ω from the interaction part naturally suggests the interaction Hamiltonian:

$$\widehat{H}_{\text{int}}^{(d)} = -i\hbar \sum_{\bar{n}} \Big(g_{\bar{n}} \widehat{\sigma}_+ \widehat{a}_{\bar{n}} - g_{\bar{n}}^* \widehat{a}_{\bar{n}}^\dagger \widehat{\sigma}_- \Big), \tag{4.2.1}$$

where we used the superscript (d) to note that the model is discrete, and the field operator relates to the previously established set as:

$$\widehat{a}_{\bar{n}} = \frac{1}{g_{\bar{n}}} \int_0^{+\infty} \mathrm{d}\omega \, \kappa_{\bar{n}}(\omega) \widehat{a}_{\bar{n}}(\omega). \tag{4.2.2}$$

However, the variable that we eliminate being ω, it is present in the eigenvalues of the non-interacting Hamiltonian. Thus, a dark/bright separation is no longer possible in the way previously discussed. In order to construct a discrete model, we follow a different path, analogous to the last part of section 2.2 for a single atom in a cavity.
We write explicitly the dynamics of the continuous effective model, using the Hamiltonian (4.1.17) and the Schrödinger equation:

$$i\hbar \frac{\mathrm{d}|\psi\rangle}{\mathrm{d}t} = \widehat{H}_{\text{eff}} |\psi(t)\rangle. \tag{4.2.3}$$

The single emitter having a two-level structure, it is reasonable to work in the single excitation subspace of the field, and thus we expand the wavefunction in the product basis and in the interaction picture:

$$|\psi(t)\rangle = c_{e,\mathbf{0}}(t) \mathrm{e}^{-i\omega_0 t} |e, \mathbf{0}\rangle + \sum_{\bar{n}} \int_0^{+\infty} \mathrm{d}\omega \, c_{g,1}^{(\bar{n})}(\omega, t) \mathrm{e}^{-i\omega t} |g, 1_\omega^{(\bar{n})}\rangle, \tag{4.2.4}$$

where the system is described only by one excitation in the field and the emitter in its ground state, or the field is in the vacuum state and the emitter is excited (see fig. 4.3). The single excitation state is given by the action of the creation operator on the vacuum state:

$$|1_\omega^{(\bar{n})}\rangle = \widehat{a}_{\bar{n}}^\dagger(\omega) |\mathbf{0}\rangle. \tag{4.2.5}$$

The equations of motion for the probability amplitudes read:

$$\dot{c}_{e,\mathbf{0}} = -\sum_{\bar{n}} \int_0^{+\infty} \mathrm{d}\omega \, \kappa_{\bar{n}} \mathrm{e}^{-i(\omega-\omega_0)t} c_{g,1}^{(\bar{n})}(\omega, t) \tag{4.2.6a}$$

$$\dot{c}_{g,1}^{(\bar{n})}(\omega) = \kappa_{\bar{n}}^*(\omega) \mathrm{e}^{i(\omega-\omega_0)t} c_{e,\mathbf{0}}(t). \tag{4.2.6b}$$

In order to proceed, we require an important feature of the atom-field coupling, namely, that it has a Lorentzian profile:

$$\kappa_{\bar{n}}(\omega) = g_{\bar{n}} L_{\bar{n}}(\omega) \text{ with } L_{\bar{n}}(\omega) = \sqrt{\frac{\gamma_{\bar{n}}}{2\pi}} \frac{1}{\omega - \omega_{\bar{n}} + i\frac{\gamma_{\bar{n}}}{2}}, \tag{4.2.7}$$

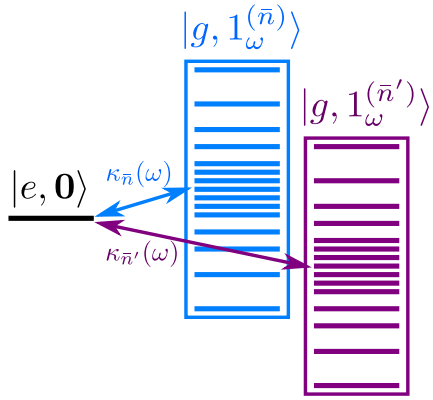

Figure 4.3: Single excitation subspace: the discrete state $|e, \mathbf{0}\rangle$ couples to several continua, where the atom is in its ground state and the field has one excitation $|1_\omega^{(\bar{n})}\rangle$. To underline the multiplicity of the continua, two manifolds are shown, corresponding to index $\bar{n}$ for the first and index $\bar{n}'$ for the second. Each of them is coupled to the discrete state with couplings $\kappa_{\bar{n}}(\omega)$ and $\kappa_{\bar{n}'}(\omega)$, respectively.

the parameters $\gamma_{\bar{n}}$ and $\omega_{\bar{n}}$ being the width and the center of the peak associated with mode $\bar{n}$, respectively. For a spherical system, examining the structure of the Green's tensor in more detail (see for instance appendix 3.A), one finds that the resonance-like behavior of the LDOS is possible due to the presence of the reflection and transmission coefficients in (3.A.3). The only other terms with frequency dependence are the radial terms of the vector spherical harmonics: these superimpose oscillations onto the resonance peak. Consequently, if the period of these oscillations is larger than the inverse of the peak's width $\gamma_{\bar{n}}$ (provided by the reflection coefficients), then the Lorentzian lineshape is a good approximation for the LDOS. We state that the condition for the applicability of this approximation is:

$$\gamma_{\bar{n}} \ll \frac{2\pi c}{\sqrt{\epsilon_f} r_A}, \tag{4.2.8}$$

where r_A is the radial coordinate of the atomic position and ϵ_f is the electric permittivity of the layer in which the emitter is located. This typically leads to $\gamma_{\bar{n}} \ll 2\pi \times (6 \times 10^{16}\ \mathrm{s}^{-1})$ (for $\epsilon_f = 1$ and $r_A = 5$ nm), and is generally available as $\gamma_{\bar{n}} \sim 2\pi \times (10^{13}\ \mathrm{s}^{-1})$. We note that there is no need of a numerical fitting procedure in order to determine the center and the width of the resonances. Instead, one can construct the so-called mode equation [105,106] by requiring a non-trivial solution of the boundary conditions equations. The solutions of the mode equation are complex numbers, the real part and the imaginary part being the central frequency and the width of the given resonance, respectively.
To derive the discrete model, we define the collective probability amplitude:

$$\boxed{c_{g,1}^{(\bar{n})}(t) = \int_0^{+\infty} \mathrm{d}\omega\, L_{\bar{n}}(\omega) \mathrm{e}^{-i(\omega-\omega_0)t} c_{g,1}^{(\bar{n})}(\omega, t).} \tag{4.2.9}$$

We differentiate the above equation with respect to time, and using equations (4.2.6) we get the equation of motion for the collective probability amplitude:

$$\begin{aligned}\dot{c}_{g,1}^{(\bar{n})} = \dot{c}_{g,1}^{(\bar{n},0)} + g_{\bar{n}}^* \int_0^{+\infty} \mathrm{d}\omega |L_{\bar{n}}(\omega)|^2 c_{e,\mathbf{0}}(t) \\ - i g_{\bar{n}}^* \int_0^t \mathrm{d}t' c_{e,\mathbf{0}}(t') \int_0^{+\infty} \mathrm{d}\omega (\omega - \omega_0) |L_{\bar{n}}(\omega)|^2 \mathrm{e}^{-i(\omega-\omega_0)(t-t')},\end{aligned} \tag{4.2.10}$$

where we have defined:

$$c_{g,1}^{(\bar{n},0)}(t) = \int_0^{+\infty} \mathrm{d}\omega\, L_{\bar{n}}(\omega) \mathrm{e}^{-i(\omega-\omega_0)t} c_{g,1}^{(\bar{n})}(\omega, 0). \tag{4.2.11}$$

The construction of the effective model is done in appendix 2.C, as the equations of motion are completely analogous to the one-dimensional cavity problem. After the complex plane integration, the above equation of motion becomes:

$$\dot{c}_{g,1}^{(\bar{n})} = \dot{c}_{g,1}^{(\bar{n},0)} + g_{\bar{n}}^* c_{e,\mathbf{0}}(t) - i g_{\bar{n}}^* \Big(\Delta_{\bar{n}} - i\frac{\gamma_{\bar{n}}}{2}\Big) \int_0^t \mathrm{d}t' c_{e,\mathbf{0}}(t') \mathrm{e}^{-i\left(\Delta_{\bar{n}} - i\frac{\gamma_{\bar{n}}}{2}\right)(t-t')}, \tag{4.2.12}$$

where $\Delta_{\bar{n}} = \omega_{\bar{n}} - \omega_0$ is the detuning between the atomic frequency and the peak frequency of a given mode associated with the triplet $\bar{n} = n, m, p$. We further simplify the equation of motion of the collective probability amplitude by integrating the second equation of (4.2.6), inserting it in the definition (4.2.9) and identifying the last term of the right hand side of (4.2.12), leading to:

$$\dot{c}_{g,1}^{(\bar{n})} = \dot{c}_{g,1}^{(\bar{n},0)} + g_{\bar{n}}^* c_{e,\mathbf{0}}(t) - i\Big(\Delta_{\bar{n}} - i\frac{\gamma_{\bar{n}}}{2}\Big)\big(c_{g,1}^{(\bar{n})}(t) - c_{g,1}^{(\bar{n},0)}(t)\big). \tag{4.2.13}$$

We take the initial condition of the wavefunction being the vacuum state for the field, and the excited state for the emitter:

$$|\psi(0)\rangle = |e, \mathbf{0}\rangle, \tag{4.2.14}$$

which nullifies both $c_{g,1}^{(\bar{n},0)}(t)$ and $\dot{c}_{g,1}^{(\bar{n},0)}$, and rewriting the system of equations (4.2.6) we get:

$$\boxed{\begin{aligned}\dot{c}_{e,\mathbf{0}} &= -\sum_{\bar{n}} g_{\bar{n}} c_{g,1}^{(\bar{n})}(t) && \text{(4.2.15a)}\\ \dot{c}_{g,1}^{(\bar{n})} &= g_{\bar{n}}^* c_{e,\mathbf{0}}(t) - i\Big(\Delta_{\bar{n}} - i\frac{\gamma_{\bar{n}}}{2}\Big) c_{g,1}^{(\bar{n})}(t). && \text{(4.2.15b)}\end{aligned}}$$

The dynamics is happening in a discrete system where each Lorentzian coupling leads to a specific mode, and the quantum emitter couples to each of them with couplings $g_{\bar{n}}$, thereby getting rid of the continuous frequency dependence. The wavefunction of the discrete basis is represented, in the Schrödinger picture, as:

$$|\psi(t)\rangle = c_{e,\mathbf{0}}(t)|e, \mathbf{0}\rangle + \sum_{\bar{n}} c_{g,1}^{(\bar{n})}(t)|g, 1_{\bar{n}}\rangle, \tag{4.2.16}$$

and the corresponding Hamiltonian is:

$$\widehat{H}_{\text{eff}}^{(d)} = \sum_{\bar{n}} \hbar\Big(\Delta_{\bar{n}} - i\frac{\gamma_{\bar{n}}}{2}\Big)\widehat{a}_{\bar{n}}^\dagger \widehat{a}_{\bar{n}} - i\hbar \sum_{\bar{n}} \Big(g_{\bar{n}} \widehat{\sigma}_+ \widehat{a}_{\bar{n}} - g_{\bar{n}}^* \widehat{a}_{\bar{n}} \widehat{\sigma}_-\Big). \tag{4.2.17}$$

Without influencing the dynamics, we renormalize the zero point energy by applying the unitary transformation:

$$\widehat{\mathcal{R}}(t) = \mathrm{e}^{i\omega_0 t}\widehat{\mathbb{1}} = \mathrm{e}^{i\omega_0 t}\Big(\widehat{\sigma}_+\widehat{\sigma}_- + \sum_{\bar{n}} \widehat{a}^\dagger_{\bar{n}}\widehat{a}_{\bar{n}}\Big), \tag{4.2.18}$$

leading to the effective Hamiltonian:

$$\boxed{\begin{aligned}\widehat{H}^{(d)}_{\text{eff}} &= \hbar\omega_0\widehat{\sigma}_+\widehat{\sigma}_- + \sum_{\bar{n}} \hbar\Big(\omega_{\bar{n}} - i\frac{\gamma_{\bar{n}}}{2}\Big)\widehat{a}^\dagger_{\bar{n}}\widehat{a}_{\bar{n}} \\ &\quad - i\hbar\sum_{\bar{n}}\Big(g_{\bar{n}}\widehat{\sigma}_+\widehat{a}_{\bar{n}} - g^*_{\bar{n}}\widehat{a}_{\bar{n}}\widehat{\sigma}_-\Big).\end{aligned}} \tag{4.2.19}$$

The operators $\widehat{a}_{\bar{n}}, \widehat{a}^\dagger_{\bar{n}}$ are defined through (4.2.2) and, using the commutation relations of the frequency-dependent $\widehat{a}_{\bar{n}}(\omega), \widehat{a}^\dagger_{\bar{n}}(\omega)$ (4.1.10) and the identity:

$$\int_0^{+\infty} \mathrm{d}\omega\, |L_{\bar{n}}(\omega)|^2 = 1, \tag{4.2.20}$$

which is valid for $\omega_{\bar{n}} \gg \gamma_{\bar{n}}$, we find the expected commutation relations:

$$\big[\widehat{a}_{\bar{n}}, \widehat{a}^\dagger_{\bar{n}'}\big] = \delta_{\bar{n}\bar{n}'} \tag{4.2.21a}$$

$$\big[\widehat{a}_{\bar{n}}, \widehat{a}_{\bar{n}'}\big] = \big[\widehat{a}^\dagger_{\bar{n}}, \widehat{a}^\dagger_{\bar{n}'}\big] = 0. \tag{4.2.21b}$$

We note that the structure requirements for the density of states can be less strict upon deriving the discrete model: resonances with general Fano profiles [107] also yield a similar Hamiltonian. A remark we can make about building the discrete effective model is the information loss aspect: with the dark/bright subspace separation, we find the subspace of bright operators participating in the dynamics, while the dark operators all remain decoupled. In this procedure, all the information about the system is kept, and is rearranged in a more efficient manner to eliminate unnecessary subspaces. The information about the energy distribution in the continuum is also accessible. The discrete model results from an integration over the frequency parameter, and to each peak in the structured reservoir is associated a resonance frequency $\omega_{\bar{n}}$ and a width $\gamma_{\bar{n}}$. Due to the contour integration, the structure of the discrete Hamiltonian is non-Hermitian, and the information about the energy distribution within a given mode in the continuum is lost.

4.2.2 Multiple emitters

To construct a discrete effective Hamiltonian in case of several emitters interacting with their environment, we apply a procedure analogous to the one described above. However, having had to orthogonalize the original set of modes with respect to emitter positions, the atom-field couplings $\widetilde{\kappa}^{(jk)}_{\bar{n}}(\omega)$ (4.1.44) in the effective continuous Hamiltonian (4.1.43) are different from the original, single-index couplings. It is essential to ascertain whether they inherited the Lorentzian resonance profile from the original $\kappa^{(j)}_{\bar{n}}(\omega)$ couplings if we want to construct a discrete effective model for multiple emitters.
According to definition (4.1.44), the possibly non-Lorentzian frequency dependence can only

come from the coefficients $A_{\bar{n}}^{(ij)}(\omega)$. These, in turn, originate from the construction (4.1.35) derived from the Gram-Schmidt orthogonalization procedure, and so they contain combinations of the mode overlap $\mu_{\bar{n}}^{(jk)}(\omega)$, as defined in (4.1.29).
According to the reasoning in the previous section, if the following condition is fulfilled:

$$\gamma_{\bar{n}} \ll \frac{2\pi c}{\max(\sqrt{\epsilon_{f_j}} r_j, \sqrt{\epsilon_{f_k}} r_k)}, \tag{4.2.22}$$

where ϵ_{f_j} is the electric permittivity of the layer in which the emitter j is located, then we can make the slow-varying approximation:

$$\mathbf{d}_j \cdot \mathfrak{Im}\left\{\bar{\bar{\mathbf{G}}}_{\bar{n}}(\mathbf{r}_j, \mathbf{r}_k, \omega)\right\} \mathbf{d}_k^* \approx \Omega_{\bar{n}}^{(jk)} |L_{\bar{n}}(\omega)|^2 \tag{4.2.23a}$$

$$\mathbf{d}_j \cdot \mathfrak{Im}\left\{\bar{\bar{\mathbf{G}}}_{\bar{n}}(\mathbf{r}_j, \mathbf{r}_j, \omega)\right\} \mathbf{d}_j^* \approx \Omega_{\bar{n}}^{(j)} |L_{\bar{n}}(\omega)|^2, \tag{4.2.23b}$$

where $L_{\bar{n}}(\omega)$ is the complex Lorentzian function defined in (4.2.7). Compared to it, the other position-dependent terms vary so slowly in frequency that they can be regarded as constants over the width of the Lorentzian peak:

$$\Omega_{\bar{n}}^{(jk)} = \frac{2\pi}{\gamma_{\bar{n}}} \mathbf{d}_j \cdot \mathfrak{Im}\left\{\bar{\bar{\mathbf{G}}}_{\bar{n}}(\mathbf{r}_j, \mathbf{r}_k, \omega_{\bar{n}})\right\} \mathbf{d}_k^* \tag{4.2.24a}$$

$$\Omega_{\bar{n}}^{(j)} = \frac{2\pi}{\gamma_{\bar{n}}} \mathbf{d}_j \cdot \mathfrak{Im}\left\{\bar{\bar{\mathbf{G}}}_{\bar{n}}(\mathbf{r}_j, \mathbf{r}_j, \omega_{\bar{n}})\right\} \mathbf{d}_j^*. \tag{4.2.24b}$$

Thus, the mode overlap function can be expressed as:

$$\mu_{\bar{n}}^{(jk)}(\omega) \approx \mu_{\bar{n}}^{(jk)} = \frac{\Omega_{\bar{n}}^{(jk)}}{\sqrt{\Omega_{\bar{n}}^{(j)} \Omega_{\bar{n}}^{(k)*}}}. \tag{4.2.25}$$

Since, compared to $L_{\bar{n}}(\omega)$, $\mu_{\bar{n}}^{(jk)}$ can be regarded as constant in frequency, the atom-field couplings between the emitters and the orthogonalized field operators will have the same Lorentzian dependence as the original couplings, only with a modified amplitude. Therefore, based on equations (4.1.34), (4.1.44) and (4.2.7), we write:

$$\tilde{\kappa}_{\bar{n}}^{(jk)}(\omega) \approx \sum_{i=1}^{N_r} A_{\bar{n}}^{(ij)}(\omega_{\bar{n}}) g_{\bar{n}}^{(ik)} L_{\bar{n}}(\omega) = \tilde{g}_{\bar{n}}^{(jk)} L_{\bar{n}}(\omega). \tag{4.2.26}$$

With the latter equation, the same procedure can be applied as for the single emitter case. Also, starting from Hamiltonian (4.1.43), the derived model is the same. We obtain the discrete, effective Hamiltonian for N_e emitters interacting with their environment:

$$\boxed{\begin{aligned} \widehat{H}_{\text{eff}} = &\sum_{k=1}^{N_e} \hbar\omega_k \widehat{\sigma}_+^{(k)} \widehat{\sigma}_-^{(k)} + \sum_{j=1}^{N_r} \sum_{\bar{n}} \hbar\Big(\omega_{\bar{n}} - i\frac{\gamma_{\bar{n}}}{2}\Big) \widehat{b}_{\bar{n}}^{(j)\dagger} \widehat{b}_{\bar{n}}^{(j)} \\ &- i\hbar \sum_{j=1}^{N_r} \sum_{k=1}^{N_e} \sum_{\bar{n}} \Big(\tilde{g}_{\bar{n}}^{(jk)} \widehat{\sigma}_+^{(k)} \widehat{b}_{\bar{n}}^{(j)} - \tilde{g}_{\bar{n}}^{(jk)*} \widehat{b}_{\bar{n}}^{(j)\dagger} \widehat{\sigma}_-^{(k)}\Big), \end{aligned}} \tag{4.2.27}$$

where we have now discrete, lossy modes interacting with the emitters, and the field operators are connected to those with continuous dependence as:

$$\widehat{b}_{\bar{n}}^{(j)} = \int_0^{+\infty} \mathrm{d}\omega\, L_{\bar{n}}(\omega)\widehat{b}_{\bar{n}}^{(j)}(\omega). \tag{4.2.28}$$

The use of the commutation relations (4.1.38) allows us to find the expected commutators for the discrete operators:

$$\left[\widehat{b}_{\bar{n}}^{(i)}, \widehat{b}_{\bar{n}'}^{(j)\dagger}\right] = \delta_{ij}\delta_{\bar{n}\bar{n}'} \tag{4.2.29a}$$

$$\left[\widehat{b}_{\bar{n}}^{(i)}, \widehat{b}_{\bar{n}'}^{(j)}\right] = \left[\widehat{b}_{\bar{n}}^{(i)\dagger}, \widehat{b}_{\bar{n}'}^{(j)\dagger}\right] = 0. \tag{4.2.29b}$$

4.3 Application: two emitters and a single metallic nanoparticle

In this section, we derive the general model describing two emitters at arbitrary positions around a metallic nanoparticle. This model is based on the general procedure developped in chapter 3 and the two preceding sections: the mode-selective quantization and effective models for spherically-layered media. We focus on the first harmonic index n mode decomposition, as was shown in fig. 4.1 at the beginning of the chapter. However, this derivation is also valid for more general mode decompositions, such as the general $\bar{n} = n, m, p$ mode.

4.3.1 Continuous model

The procedure includes an orthonormalization of field operators $\widehat{a}_n^{(j)}(\omega), \widehat{a}_n^{(j)\dagger}(\omega)$ that are associated with emitters positions $\mathbf{r}_j$. The new field operators $\widehat{b}_n^{(j)}(\omega), \widehat{b}_n^{(j)\dagger}(\omega)$, derived from the orthonormalization, describe the field-matter system in a frame where we can compute their couplings with individual emitters, as a function of the couplings between the field and single emitters. The continuous model Hamiltonian is given by:

$$\begin{aligned} H_{\text{eff}} = \sum_n \int_0^{+\infty} \mathrm{d}\omega \hbar\omega \Big(\widehat{b}_n^{(1)\dagger}(\omega)\widehat{b}_n^{(1)}(\omega) + \widehat{b}_n^{(2)\dagger}(\omega)\widehat{b}_n^{(2)}(\omega)\Big) + \hbar\omega_0\Big(\widehat{\sigma}_+^{(1)}\widehat{\sigma}_-^{(1)} + \widehat{\sigma}_+^{(2)}\widehat{\sigma}_-^{(2)}\Big) \\ - i\hbar \sum_n \int_0^{+\infty} \mathrm{d}\omega \Big(\widetilde{\kappa}_n^{(11)}(\omega)\widehat{b}_n^{(1)}(\omega)\widehat{\sigma}_+^{(1)} + \widetilde{\kappa}_n^{(12)}(\omega)\widehat{b}_n^{(1)}(\omega)\widehat{\sigma}_+^{(2)} \\ + \widetilde{\kappa}_n^{(22)}(\omega)\widehat{b}_n^{(2)}(\omega)\widehat{\sigma}_+^{(2)} + \widetilde{\kappa}_n^{(21)}(\omega)\widehat{b}_n^{(2)}(\omega)\widehat{\sigma}_+^{(1)} - \text{h.c.}\Big), \end{aligned} \tag{4.3.1}$$

where the $\widetilde{\kappa}_n^{(jk)}(\omega)$ are the field-emitter couplings. They are expressed as linear combination of the single emitter couplings (proportional to the LDOS):

$$|\kappa_n^{(j)}(\omega)|^2 = \frac{1}{\hbar\pi\epsilon_0}\frac{\omega^2}{c^2}\mathbf{d}_j \cdot \mathfrak{Im}\left\{\overline{\overline{\mathbf{G}}}_n(\mathbf{r}_j, \mathbf{r}_j, \omega)\right\}\mathbf{d}_j^*, \tag{4.3.2}$$

with proper coefficients that are found when performing the Gram-Schmidt orthogonalization procedure. The latter is done writing the linear relations:

$$\begin{cases} \widehat{b}_n^{(1)}(\omega) = \widehat{a}_n^{(1)}(\omega) \\ \widehat{b}_n^{(2)}(\omega) = \dfrac{1}{\beta_n^{(21)}} \left(\widehat{a}_n^{(2)} - \displaystyle\int_0^{+\infty} \mathrm{d}\omega' \left[\widehat{a}_n^{(2)}(\omega), \widehat{b}_n^{(1)\dagger}(\omega') \right] \widehat{b}_n^{(1)}(\omega') \right). \end{cases} \tag{4.3.3}$$

We recall the original operator basis commutation relations:

$$\left[\widehat{a}_n^{(2)}(\omega), \widehat{a}_{n'}^{(1)\dagger}(\omega') \right] = \delta_{nn'} \delta(\omega - \omega') \mu_n^{(21)}(\omega), \tag{4.3.4}$$

where $\mu_n^{(21)}(\omega)$ is the mode overlap function depending on the Green's tensor $\overline{\overline{\mathbf{G}}}(\mathbf{r}_2, \mathbf{r}_1, \omega)$. Using the commutation relation, the Gram-Schmidt decomposition reduces to:

$$\begin{cases} \widehat{b}_n^{(1)}(\omega) = \widehat{a}_n^{(1)}(\omega) \\ \widehat{b}_n^{(2)}(\omega) = \dfrac{1}{\beta_n^{(21)}} \left(\widehat{a}_n^{(2)} - \mu_n^{(21)}(\omega) \widehat{a}_n^{(1)}(\omega) \right). \end{cases} \tag{4.3.5}$$

Inverting the orthogonalization, we express the original operators as linear combination of the new ones:

$$\begin{cases} \widehat{a}_n^{(1)}(\omega) = \widehat{b}_n^{(1)}(\omega) \\ \widehat{a}_n^{(2)}(\omega) = \mu_n^{(21)}(\omega) \widehat{b}_n^{(1)}(\omega) + \beta_n^{(21)} \widehat{b}_n^{(2)}, \end{cases} \tag{4.3.6}$$

which, in a compact form, can be written as:

$$\widehat{a}_n^{(j)}(\omega) = A_{j1}^{(n)}(\omega) \widehat{b}_n^{(1)}(\omega) + A_{j2}^{(n)}(\omega) \widehat{b}_n^{(2)}(\omega). \tag{4.3.7}$$

The coefficients $A_{jk}^{(n)}(\omega)$ must be used to express the new couplings $\widetilde{\kappa}_n^{(jk)}(\omega)$ in terms of the $\kappa_n^{(k)}(\omega)$:

$$\widetilde{\kappa}_n^{(jk)} = \sum_{i=1}^{2} A_{ij}^{(n)}(\omega) \kappa_n^{(k)}(\omega). \tag{4.3.8}$$

We remark that in the case when some modes are overlapping completely, that is $|\mu_n^{(21)}(\omega)| = 1$, one has to construct intermediate couplings $\kappa_n^{(12)}(\omega) = \mu_n^{(21)}(\omega) \kappa_n^{(2)}(\omega)$. Unravelling the couplings, we write:

$$\begin{aligned} \widetilde{\kappa}_n^{(11)} &= A_{11}^{(n)}(\omega) \kappa_n^{(1)}(\omega) \\ \widetilde{\kappa}_n^{(22)} &= A_{22}^{(n)}(\omega) \kappa_n^{(2)}(\omega) \\ \widetilde{\kappa}_n^{(12)} &= A_{21}^{(n)}(\omega) \kappa_n^{(2)}(\omega) \\ \widetilde{\kappa}_n^{(21)} &= A_{12}^{(n)}(\omega) \kappa_n^{(1)}(\omega), \end{aligned} \tag{4.3.9}$$

and with the use of the linear relations (4.3.6), the A coefficients are found to be:

$$\boxed{\begin{aligned} A_{11}^{(n)}(\omega) &= 1 \\ A_{22}^{(n)}(\omega) &= \beta_n^{(21)} \\ A_{21}^{(n)}(\omega) &= \mu_n^{(21)}(\omega) \\ A_{12}^{(n)}(\omega) &= 0. \end{aligned}} \tag{4.3.10}$$

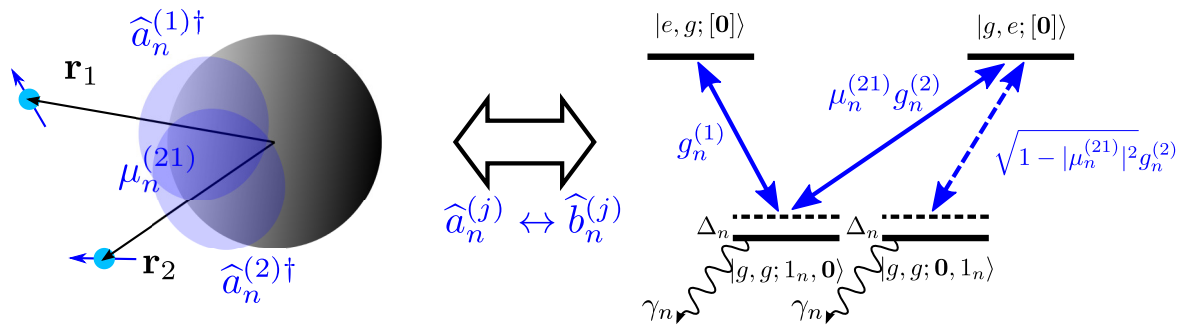

Figure 4.4: Left: Two emitter at arbitrary positions $\mathbf{r}_1, \mathbf{r}_2$ around a metallic nanosphere. Right: Effective linkage pattern in the orthogonalized basis.

One more request is the expression of the normalization coefficient $\beta_n^{(21)}$, which is found when writing the following commutation relation:

$$\left[\widehat{b}_n^{(2)}(\omega), \widehat{b}_{n'}^{(2)\dagger}(\omega')\right] = \delta_{nn'}\delta(\omega-\omega')\frac{1-|\mu_n^{(21)}(\omega)|^2}{\beta_n^{(21)2}}, \tag{4.3.11}$$

where we have used $\mu_n^{(12)}(\omega) = [\mu_n^{(21)}(\omega)]^*$ due to the fact that $\mathbf{d}_1 \cdot \mathfrak{Im}\{\overline{\overline{\mathbf{G}}}(\mathbf{r}_1, \mathbf{r}_2, \omega)\}\mathbf{d}_2^* = (\mathbf{d}_2 \cdot \mathfrak{Im}\{\overline{\overline{\mathbf{G}}}(\mathbf{r}_2, \mathbf{r}_1, \omega)\}\mathbf{d}_1^*)^*$. The orthonormalization is effective when:

$$\beta_n^{(21)} = \sqrt{1-|\mu_n^{(21)}(\omega)|^2}. \tag{4.3.12}$$

4.3.2 Discrete effective model

The discrete effective model associated with the precedingly detailed derivation is developed in section 4.2. The dependence in ω of the overlap function is ignored in the subwavelength limit, since the Lorentzian lineshape factorizes in the expression of the LDOS and the overlap term $\mathbf{d}_2 \cdot \mathfrak{Im}\{\overline{\overline{\mathbf{G}}}(\mathbf{r}_2, \mathbf{r}_1, \omega)\}\mathbf{d}_1^*$. The effective discrete Hamiltonian is given by:

$$\begin{aligned}\widehat{H}_{\text{eff}}^{(d)} = &\sum_n \hbar\left(\omega_n - i\frac{\gamma_n}{2}\right)\left(\widehat{b}_n^{(1)\dagger}\widehat{b}_n^{(1)} + \widehat{b}_n^{(2)\dagger}\widehat{b}_n^{(2)}\right) + \hbar\omega_0\left(\widehat{\sigma}_+^{(1)}\widehat{\sigma}_-^{(1)} + \widehat{\sigma}_+^{(2)}\widehat{\sigma}_-^{(2)}\right) \\ &- i\hbar\sum_n\left(\widetilde{g}_n^{(11)}\widehat{b}_n^{(1)}\widehat{\sigma}_+^{(1)} + \widetilde{g}_n^{(22)}\widehat{b}_n^{(2)}\widehat{\sigma}_+^{(2)} + \widetilde{g}_n^{(12)}\widehat{b}_n^{(1)}\widehat{\sigma}_+^{(2)} + \widetilde{g}_n^{(21)}\widehat{b}_n^{(2)}\widehat{\sigma}_+^{(1)} - \text{h.c.}\right),\end{aligned} \tag{4.3.13}$$

where:

$$\widetilde{g}_n^{(jk)} = \sum_{i=1}^{2} A_{ij}^{(n)}(\omega_n) g_n^{(k)}. \tag{4.3.14}$$

The coefficients $A_{ij}^{(n)}(\omega_n)$ are the same as derived before, with the difference that they are frequency independent (since $\mu_n^{(21)}(\omega_n) \equiv \mu_n^{(21)}$), due to the subwavelength regime. We expand

the couplings:

$$\boxed{\begin{aligned} \widetilde{g}_n^{(11)} &= g_n^{(1)} \\ \widetilde{g}_n^{(12)} &= \mu_n^{(21)} g_n^{(2)} \\ \widetilde{g}_n^{(22)} &= \sqrt{1-|\mu_n^{(21)}|^2} g_n^{(2)} \\ \widetilde{g}_n^{(21)} &= 0. \end{aligned}} \tag{4.3.15}$$

The Hamiltonian can be projected in a one-excitation basis:

$$\{|e,g;[\mathbf{0}]\rangle, ...|g,g;1_n,\mathbf{0}\rangle..., ...|g,g;\mathbf{0},1_n\rangle..., |g,e;[\mathbf{0}]\rangle\},$$

where $|i,j;n,m\rangle = |i\rangle_1 \otimes |j\rangle_2 \otimes |n\rangle_1 \otimes |m\rangle_2$ for $i,j = g,e$ and $n,m = \mathbf{0}, 1_n$ are product states of the atomic-field system ($|[\mathbf{0}]\rangle = |\mathbf{0}\rangle_1 \otimes |\mathbf{0}\rangle_2$). The matrix form of the Hamiltonian is then:

$$\widehat{H}_{\text{eff}}^{(d)} = \left(\begin{array}{c|ccc|ccc|c} 0 & \dots & \widetilde{g}_n^{(11)} & \dots & 0 & \dots & 0 & 0 \\ \hline \vdots & \ddots & & & 0 & \dots & 0 & \vdots \\ \widetilde{g}_n^{(11)*} & & \Delta_n - i\frac{\gamma_n}{2} & & \vdots & & \vdots & \widetilde{g}_n^{(12)*} \\ \vdots & & & \ddots & 0 & \dots & 0 & \vdots \\ \hline 0 & 0 & \dots & 0 & \ddots & & & \vdots \\ \vdots & \vdots & & \vdots & & \Delta_n - i\frac{\gamma_n}{2} & & \widetilde{g}_n^{(22)*} \\ 0 & 0 & \dots & 0 & & & \ddots & \vdots \\ \hline 0 & \dots & \widetilde{g}_n^{(12)} & \dots & \dots & \widetilde{g}_n^{(22)} & \dots & 0 \end{array}\right). \tag{4.3.16}$$

The effective linkage pattern corresponding to the discrete Hamiltonian is shown in fig. 4.4. In the limit where $|\mu_n^{(21)}| \to 1$, we see that the effective model corresponds to a single field operator $\widehat{b}_n^{(1)}$, coupled to both emitters.

Summary

We have derived effective models, in different stages: a continuous model where the Hamiltonian is projected on a subspace corresponding to the Lorentzian modes, and a discrete model where the reservoir population is modeled as losses through the decay rates $\gamma_{\bar{n}}$. The general mode structure of a spherical system can be expressed analytically, hence the calculation towards the different stages of the effective models is straightforward. In general, the mode structure of an arbitrary nanoscale system is complex, and is highly geometry-dependent. Therefore, this procedure is not applicable up to the discrete effective model for every system. Nonetheless, since all geometry-related information is contained in the Green's tensor, the construction of the effective models is done generally with the study of the LDOS, which is calculated from the Green's tensor associated with the structure. One can isolate resonances and study their interaction with nearly resonant quantum emitters, but as soon as resonances overlap, one has to check whether they form an orthogonal basis or not.
The derivations and results gathered in chapters 3 and 4 are an expansion of reference [99]. In the next chapter, we will apply the discrete effective model for the study of one and two emitters close to a spherical nanoparticle. We also provide a comparison between the continuous and the discrete models for the dynamics, and demonstrate their equivalence.

Appendix

4.A Single Lorentzian model - continuous and discrete Hamiltonian

In this appendix, we show numerical results obtained with Hamiltonians (4.1.24) and (4.2.19) with $n = 1$, i.e. we consider only one Lorentzian-structured mode in the field continuum, and the field is coupled to a two-level atom. We show the equivalence of the two models. The continuous effective Hamiltonian is:

$$\widehat{H} = \hbar\omega_0\widehat{\sigma}_+\widehat{\sigma}_- + \int_0^{+\infty} \mathrm{d}\omega\hbar\omega\, \widehat{a}^\dagger(\omega)\widehat{a}(\omega) - i\hbar\int_0^{+\infty}\mathrm{d}\omega\Big(\kappa(\omega)\widehat{\sigma}_+\widehat{a}(\omega) - \kappa^*(\omega)\widehat{a}^\dagger(\omega)\widehat{\sigma}_-\Big), \tag{4.A.1}$$

and the discrete non-Hermitian Hamiltonian corresponding to the latter is:

$$\widehat{H}^{(d)} = \hbar\omega_0\widehat{\sigma}_+\widehat{\sigma}_- + \hbar\Big(\omega_r - i\frac{\gamma}{2}\Big)\widehat{a}^\dagger\widehat{a} - i\hbar\Big(g\widehat{\sigma}_+\widehat{a} - g^*\widehat{a}^\dagger\widehat{\sigma}_-\Big). \tag{4.A.2}$$

Both Hamiltonians corresponds to each other in terms of dynamics when the atom-field coupling has the Lorentzian profile:

$$\kappa(\omega) = \sqrt{\frac{\gamma}{2\pi}}\frac{g}{\omega - \omega_r + i\frac{\gamma}{2}}, \tag{4.A.3}$$

where ω_r is the resonance frequency, γ is the full width at half maximum (FWHM), and g is a scaling corresponding to the effective Rabi frequency coupling in the discrete Hamiltonian.

4.A.1 Discretization

To solve the Schödinger equation numerically, we discretize the Hamiltonian $\widehat{H}$. For a simpler notation, we write it in the rotating frame $\widehat{\mathcal{R}}(t) = \mathrm{e}^{-i\omega_0 t}\widehat{\mathbb{1}}$, and discretizing the frequency continuum in N steps of length $\varepsilon \ll 1$, the discretized version of (4.A.1) reads:

$$\widehat{H}/\hbar = \sum_{k=-\frac{N}{2}}^{\frac{N}{2}} \Big(\Delta_k\widehat{a}_k^\dagger\widehat{a}_k - i\sqrt{\varepsilon}\big(\kappa_k\widehat{\sigma}_+\widehat{a}_k - \kappa_k^*\widehat{a}_k^\dagger\widehat{\sigma}_-\big)\Big), \tag{4.A.4}$$

where $\Delta_k = \omega_k - \omega_0 = k\varepsilon$ and $\kappa_k \equiv \kappa(\omega_k)$. In matrix form, we write:

$$\widehat{H}/\hbar \equiv \begin{pmatrix} 0 & i\sqrt{\varepsilon}\kappa^*_{-\frac{N}{2}} & i\sqrt{\varepsilon}\kappa^*_{-\frac{N-1}{2}} & \dots & i\sqrt{\varepsilon}\kappa^*_{\frac{N}{2}} \\ -i\sqrt{\varepsilon}\kappa_{-\frac{N}{2}} & -\frac{N}{2}\varepsilon & 0 & \dots & 0 \\ -i\sqrt{\varepsilon}\kappa_{-\frac{N-1}{2}} & 0 & -\frac{N-1}{2}\varepsilon & \ddots & \vdots \\ \vdots & \vdots & \ddots & \ddots & 0 \\ -i\sqrt{\varepsilon}\kappa_{\frac{N}{2}} & 0 & \dots & 0 & \frac{N}{2}\varepsilon \end{pmatrix}. \tag{4.A.5}$$

The wavefunction is also discretized:

$$|\psi(t)\rangle = c_{e,\mathbf{0}}(t)|e,\mathbf{0}\rangle + \sum_{k=-\frac{N}{2}}^{\frac{N}{2}} c_{g,1_k}(t)|g,1_k\rangle, \tag{4.A.6}$$

where $|1_k\rangle = \widehat{a}_k^\dagger|\mathbf{0}\rangle$.

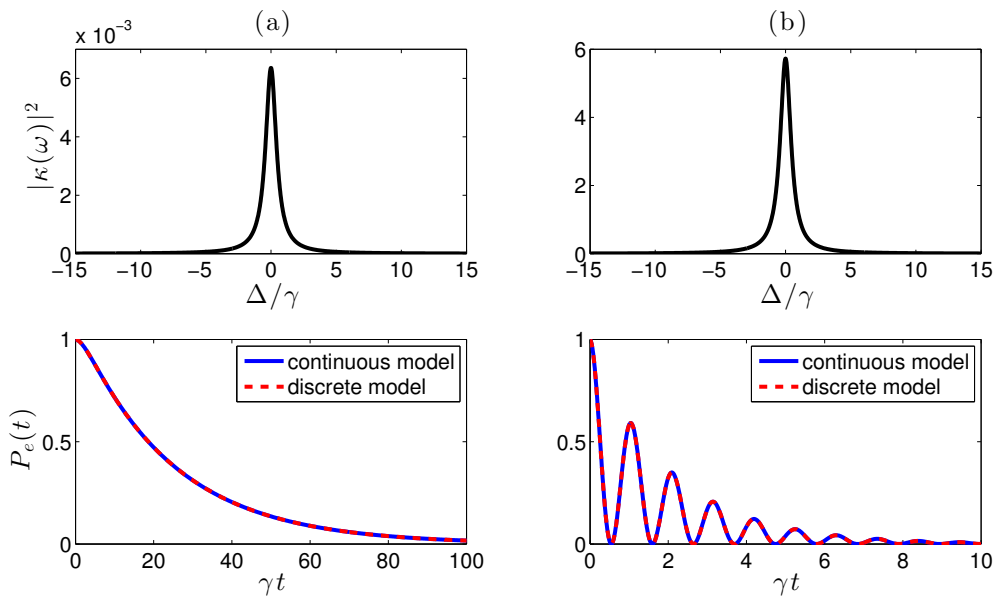

Figure 4.5: Dynamics of a two-level system interacting with a Lorentzian-structured continuum. Upper panels: square modulus of the emitter-field coupling. Lower panels: excitation probability versus time for the continuous Hamiltonian (blue line) and the discrete one (red dashed line). The chosen parameters are normalized with respect to the width γ. (a) $g = 0.1\gamma$. (b) $g = 3\gamma$.

4.A.2 Dynamics

We compute the dynamics of the emitter-field system, using the initial wavefunction:

$$|\psi(0)\rangle = |e, \mathbf{0}\rangle, \tag{4.A.7}$$

and we show the equivalence between the continuous and the discrete Hamiltonians, for the probability of excitation $P_e(t) = |c_{e,\mathbf{0}}(t)|^2$, shown in fig. 4.5. To do so, we run a program where the solution of the Schrödinger equation is found using the discretized continuum Hamiltonian, and in parallel, the effective non-Hermitian Hamiltonian in the matrix form:

$$\widehat{H}^{(d)}/\hbar = \begin{pmatrix} 0 & ig^* \\ -ig & \Delta_r - i\frac{\gamma}{2} \end{pmatrix}, \tag{4.A.8}$$

where $\Delta_r = \omega_r - \omega_0$ (here we chose $\Delta_r = 0$). From the results we get, we distinguish two regimes:

- **the weak coupling regime** ($g \ll \gamma$), where the excitation probability follows an exponential decrease, as seen in section 3.1.2 for the Purcell factor. The effective decay rate is:

$$\Gamma = \frac{|g|^2\gamma}{(\omega_0 - \omega_r)^2 + \left(\frac{\gamma}{2}\right)^2}. \tag{4.A.9}$$

- **the strong coupling regime** ($g \gtrsim \gamma$), where the excitation probability is a combination of Rabi oscillations corresponding to a coherent coupling between the emitter and the field, and an exponential decay of the order of γ.

Chapter 5

Quantum plasmonics with metallic nanoparticles

Chapter overview

Objectives: In this last chapter, we apply the effective models derived from the mode-selective quantization to the interaction of emitters with a spherical nanosphere. We show the quantum dynamics of a single emitter, and two emitters coupled to the plasmon modes. Lastly, we show the feasibility of the stimulated Raman adiabatic passage (STIRAP) for two three-level emitters coupled to a nanosphere and addressed by laser pulses.

Guideline:

- Single emitter coupled to a nanosphere: strong coupling regime and quantum dynamics.
- Two emitter model: population transfer using the STIRAP.
- Two emitter model: entanglement using fractional STIRAP.
- Discussion about the STIRAP feasibility.
- **keywords:** *quantum emitter, metallic nanoparticle, local density of states (LDOS), Drude model, strong coupling regime, quantum dynamics, STIRAP, population transfer, entanglement.*

Results/novelty:

- Dressed states of a quantum emitter strongly coupled to a metal nanoparticle.
- Adiabatic passage mediated by plasmons: A route towards a decoherence-free quantum plasmonic platform.

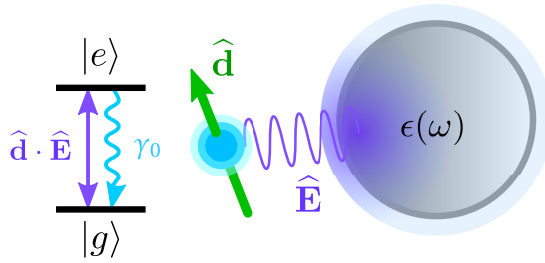

Figure 5.1: Single two-level quantum emitter coupled to a MNP, whose relative dielectric permittivity is $\epsilon(\omega)$. The transition $|e\rangle \leftrightarrow |g\rangle$ of the emitter is nearly resonant with the plasmonic modes. The quantized electric field $\widehat{\mathbf{E}}$ couples to the dipole $\widehat{\mathbf{d}}$ of the emitter, and the intrinsic vacuum decay rate of the transition is γ_0.

The effective models derived in the preceding chapter are applied to quantum plasmonic systems, where quantum emitters interact with spherical metallic nanoparticles (MNP). We expand in the plasmonic modes of a single MNP interacting with one emitter, and compute the dynamics of the excitation probability [108]. We also demonstrate the feasability of the STIRAP process introduced in section 1.1.3 for two three-level quantum emitters coupled to a metal nanoparticle [109]. This application paves the way to decoherence-free quantum control at the nanoscale, since the lossy plasmonic excitations are avoided during the process.

5.1 Quantum emitter coupled to a metallic nanoparticle

5.1.1 Local density of states

We study the interaction of a single, two-level quantum emitter with a MNP of radius R (see fig. 5.1) [21]. The emitter is located at position $\mathbf{r}_A$, the origin being the center of the spherical MNP. We consider a silver MNP, and its dielectric constant is modeled by the Drude formula:

$$\epsilon(\omega) = \epsilon_\infty - \frac{\omega_p^2}{\omega^2 + i\gamma_e\omega}, \tag{5.1.1}$$

where ϵ_∞ is the high-frequency limit of the dielectric function, ω_p is the bulk plasmon frequency, and γ_e is the Landau damping constant. We note that tabulated data can also be used assuming that they obey the Kramers-Kronig relations.The quantum emitter is modeled with a two-level structure $\{|g\rangle, |e\rangle\}$, where $|g\rangle$ is the emitter's ground state and $|e\rangle$ is the excited state. The transition frequency is ω_0, and the vacuum decay rate is given by the Wigner-Weisskopf formula:

$$\gamma_0 = \frac{\omega_0^3 d^2}{3\hbar\pi\epsilon_0 c^3}, \tag{5.1.2}$$

where $d = |\langle e|\widehat{\mathbf{d}}|g\rangle|$ is the norm of the transition dipole moment. We see from expressions (4.1.1) and (4.1.3) that the vacuum decay rate can be expressed with the LDOS in the vacuum $\rho_{\mathbf{n},0}(\mathbf{r}_A, \omega_0)$:

$$\gamma_0 = \frac{2d^2}{\hbar\epsilon_0}\frac{\omega_0^2}{c^2}\rho_{\mathbf{n},0}(\mathbf{r}_A, \omega_0) = \frac{2}{\hbar\epsilon_0}\frac{\omega_0^2}{c^2}\mathbf{d} \cdot \mathfrak{Im}\left\{\overline{\overline{\mathbf{G}}}_0(\mathbf{r}_A, \mathbf{r}_A, \omega_0)\right\}\mathbf{d}^*. \tag{5.1.3}$$

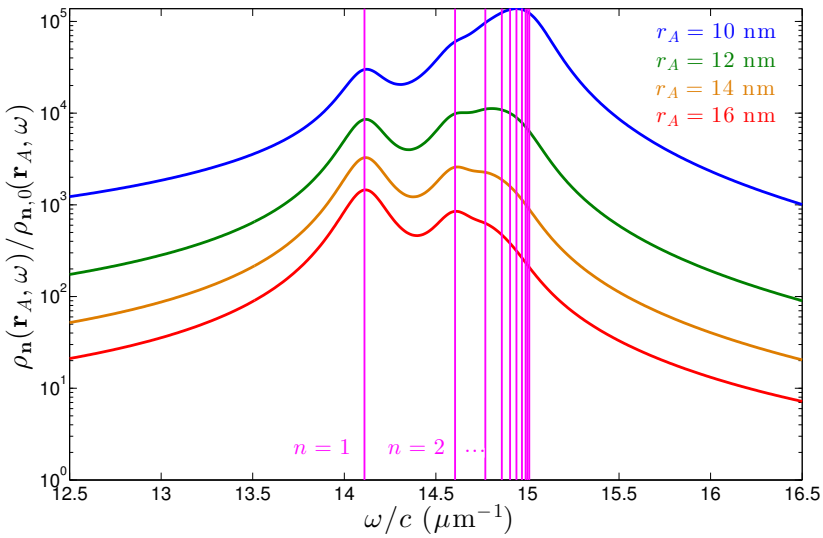

Figure 5.2: Local density of states scaled by the vacuum LDOS for a sphere of radius $R = 8$ nm and a quantum emitter located at various distances r_A from the center of the sphere, as a function of ω/c. The emitter has a radial polarization $\mathbf{n} = \hat{\boldsymbol{r}}$. The n-mode resonance positions are located with vertical lines.

The Hamiltonian of the single emitter-MNP system is given by (4.1.24), where the mode structure is labelled with the index n. Indeed, the symmetry of the system is independent of the angular part, hence we sum over the parity and the m indices. The emitter-field coupling has the form (4.1.21):

$$|\kappa_n(\omega)|^2 = \frac{1}{\hbar\pi\epsilon_0}\frac{\omega^2}{c^2}\mathbf{d}\cdot\mathfrak{Im}\left\{\bar{\bar{\mathbf{G}}}_n(\mathbf{r}_A, \mathbf{r}_A, \omega)\right\}\mathbf{d}^*, \tag{5.1.4}$$

where $\bar{\bar{\mathbf{G}}}_n(\mathbf{r}_A, \mathbf{r}_A, \omega)$ is the Green's tensor associated with the mode n. The full Green's tensor is obtained by summing all the mode-selective components:

$$\bar{\bar{\mathbf{G}}}(\mathbf{r}, \mathbf{r}', \omega) = \sum_{n=1}^{+\infty}\bar{\bar{\mathbf{G}}}_n(\mathbf{r}, \mathbf{r}', \omega) = \bar{\bar{\mathbf{G}}}_0(\mathbf{r}, \mathbf{r}', \omega) + \bar{\bar{\mathbf{G}}}_S(\mathbf{r}, \mathbf{r}', \omega), \tag{5.1.5}$$

with $\bar{\bar{\mathbf{G}}}_0$ being the direct contribution part and $\bar{\bar{\mathbf{G}}}_S$ the scattered part. The calculation of the Green's tensor is detailed in appendix 3.A of chapter 3.
The coupling constant (5.1.4) depends on the partial LDOS along the transition dipole moment (see also equation (4.1.1)). It is remarkable that, as the emitter is closer to the MNP (2 nm from the surface), the LDOS exceeds 10^5 times the vacuum LDOS and we can reach the strong coupling regime, as discussed in the next paragraph. This originates from the highly confined high order modes [108].

5.1.2 Dynamics and strong coupling regime

We investigate the dynamics of the emitter-MNP system using the effective Hamiltonian (4.2.19) derived in chapter 4. The discrete non-Hermitian Hamiltonian of the system is

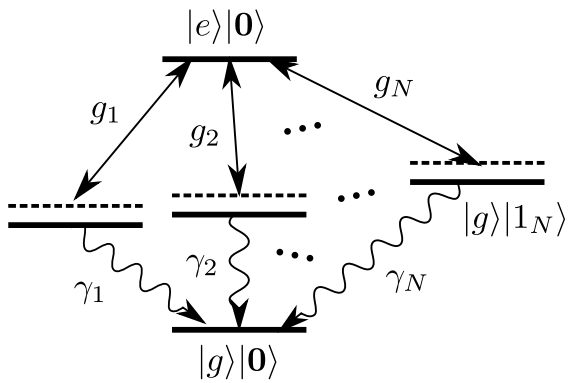

Figure 5.3: Linkage pattern of the emitter dressed by the plasmonic modes corresponding to Hamiltonian (5.1.6). The dissipation of each plasmon leads to the state $|g, \mathbf{0}\rangle$.

expressed in matrix form:

$$\widehat{H}^{(d)}/\hbar = \begin{pmatrix} 0 & ig_1 & ig_2 & \dots & ig_N \\ -ig_1 & \Delta_1 - i\frac{\gamma_1}{2} & 0 & \dots & 0 \\ -ig_2 & 0 & \Delta_2 - i\frac{\gamma_2}{2} & \ddots & \vdots \\ \vdots & \vdots & \ddots & \ddots & 0 \\ -ig_N & 0 & \dots & 0 & \Delta_N - i\frac{\gamma_N}{2} \end{pmatrix}, \tag{5.1.6}$$

$\Delta_n = \omega_n - \omega_0$ being the detuning between the emitter transition and the n-th LSP resonance, and g_n being given by:

$$g_n = \left(\gamma_n \frac{\omega_n^2}{2\hbar\epsilon_0 c^2} \mathbf{d} \cdot \mathfrak{Im} \left\{ \bar{\bar{\mathbf{G}}}_n(\mathbf{r}_A, \mathbf{r}_A, \omega_n) \right\} \mathbf{d}^* \right)^{1/2}, \tag{5.1.7}$$

where we replaced ω by ω_n since the evolution of ω^2 is slow-varying with respect to the Lorentzian lineshape of the original continuous model: $\gamma_n \ll \omega_n$. The poles of the Lorentzian functions are found using the mode equation, and then both the continuous and discrete couplings are constructed using (5.1.7). This effective model corresponds to the linkage pattern shown in fig. 5.3. The dynamics with a quantum emitter initially in $|e, \mathbf{0}\rangle$ is shown in fig. 5.4 for two nanospheres of radii $R = 8$ and $R = 20$ nm. We check that the convergence is achieved using the 25 first LSP modes. We show that, although the excitation probability decays over a few dozens of femtoseconds, it oscillates as well and the dynamics is non-Markovian. For first understanding of the strong coupling regime, we define the average decay rate and coupling:

$$\bar{\gamma} = \frac{1}{N} \sum_{n=1}^{N} \gamma_n, \quad \bar{g} = \sqrt{N} \left(\frac{1}{N} \sum_{n=1}^{N} g_n \right), \tag{5.1.8}$$

and computing the ratio $\bar{g}/\bar{\gamma}$, we find 1.05 and 1.23 for $R = 8$ and $R = 20$ nm, respectively. This fulfills the strong coupling condition, that is $\bar{g} \gtrsim \bar{\gamma}$. Lastly, we plot the excitation probability for a two level model using the Hamiltonian:

$$\widehat{H}_{\text{tls}}/\hbar = \begin{pmatrix} 0 & i\bar{g} \\ -i\bar{g} & \bar{\Delta} - i\frac{\bar{\gamma}}{2} \end{pmatrix}, \tag{5.1.9}$$

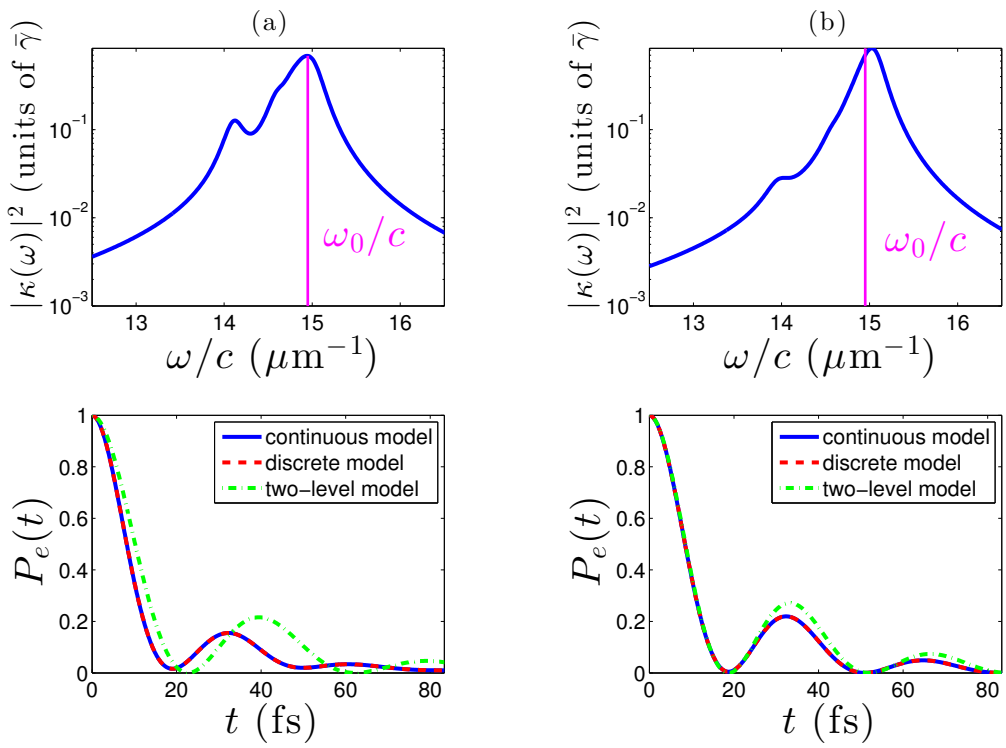

Figure 5.4: Dynamics of a single quantum emitter initially in $|e, \mathbf{0}\rangle$, 2 nm away from the surface of a MNP of radius (a) $R = 8$ and (b) $R = 20$ nm. The calculation is done using $N = 25$ plasmonic modes. Upper panel: continuous emitter-field coupling $|\kappa(\omega)|^2 = \sum_n |\kappa_n(\omega)|^2$ (in units of the average mode width $\bar{\gamma}$) versus $k = \omega/c$ in μm^{-1}. The position of the transition frequency ω_0 is shown by a vertical line. Lower panel: excitation probability $P_e(t)$ of the emitter versus time (in fs). The continuous and discrete models are shown to be equivalent and an approximative two-level model is compared to them.

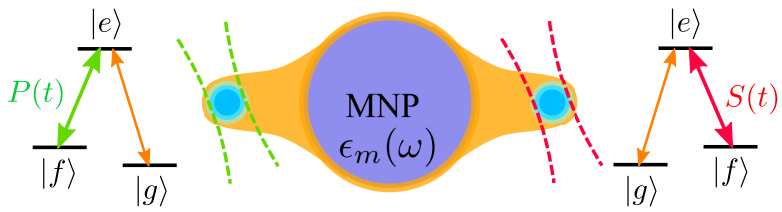

Figure 5.5: Two three-level emitters in the vicinity of a metal nanoparticle of permittivity $\epsilon_m(\omega)$. Transitions $|e\rangle \leftrightarrow |f\rangle$ are addressed with laser beams $P(t)$ and $S(t)$, while transitions $|e\rangle \leftrightarrow |g\rangle$ are nearly resonant with the plasmonic modes of the MNP.

with $\bar{\Delta} = \bar{\omega} - \omega_0$ being the average mode frequency detuning. This model qualitatively reproduces the dynamics with Rabi oscillations characterizing the energy exchange between the emitter and the MNP. However, the exact behavior of the dynamics can be understood solely from the discrete Hamiltonian (5.1.6), and leads to the definition of atomic states dressed by all the LSP modes [108]. We see in fig. 5.4 that this model works better for $R = 20$ nm because the lineshape of the full LDOS has an overall Lorentzian behavior.
It is important to note that the strong coupling regime is reached due to a mode accumulation phenomenon. The emitter being coupled to a large number of modes, the effective coupling $\bar{g}$ increases with a factor $\sqrt{N}$. However, the individual modes have small g_n values compared to $\bar{\gamma}$: between 0.15 and 0.30 for $R = 20$ nm. Therefore, the strong coupling regime arises from the accumulation effect, associated with the closeness of the emitter to the surface of the sphere.

5.2 Adiabatic passage mediated by plasmons

Surface plasmon polaritons provide a strong mode confinement, allowing control below the diffraction limit. The plasmon field is strongly confined and enhanced, but the modes are very lossy. In the following, we present adiabatic techniques to couple two quantum emitters together, circumventing the lossy nature of the modes of a metallic nanoparticle (MNP).
Having already built effective models in chapters 3 and 4, we derive a configuration that allows an efficient coupling between the emitters, mediated by the plasmon modes. We show that in the strong coupling regime, we can do a complete population transfer between two emitters using the STIRAP technique. In a last section, we use a fractional STIRAP leading to the entanglement between the emitters.

5.2.1 Population transfer: STIRAP

We consider two three-level quantum emitters that are located close to a MNP (see fig. 5.5). The emitters are both coupled to the plasmon modes through their $|e\rangle \leftrightarrow |g\rangle$ transitions. They are also individually driven by control laser pulses, referred to as pump for emitter 1 and Stokes pulses for emitter 2, through transitions $|e\rangle \leftrightarrow |f\rangle$. The Rabi frequencies associated with the control pulses are denoted $P(t)$ and $S(t) = |S(t)|\mathrm{e}^{i\phi}$, and their resonant frequencies are ω_P and ω_S, respectively.

Effective model: simplest structure

We use the previously derived discrete effective model (4.2.27) where we sum over the parity and the m indices so that $\bar{n} \to n$, to model the emitter-plasmon field interaction. The structure of this Hamiltonian is complex, in general, because one has to write the original model with the field operators (4.1.26), and compute the mode overlap function (4.1.29) constructed from the Green's tensor of the spherically layered system, to see whether we can reduce the span of the field operators, leading to the effective $\widehat{b}_n^{(j)}, \widehat{b}_n^{(j)\dagger}$. We suggest the reader to go through sections 4.1.2 and 4.2.2 for a detailed description of this construction, as well as section 4.3 for the construction of the effective model for two emitters close to a nanosphere. Because of the spatial properties of the plasmon modes, the simplest effective model corresponds to the case where the emitters are very close to each other. We recall the mode overlap function for two emitters:

$$\mu_n^{(12)}(\omega) = \frac{1}{\hbar\pi\epsilon_0}\frac{\omega^2}{c^2}\frac{\mathbf{d}_1 \cdot \mathfrak{Im}\left\{\bar{\bar{\mathbf{G}}}_n(\mathbf{r}_1, \mathbf{r}_2, \omega)\right\}\mathbf{d}_2^*}{\kappa_n^{(1)}(\omega)\kappa_n^{(2)*}(\omega)}, \tag{5.2.1}$$

where here $\mathbf{d}_j = \langle e|\widehat{\mathbf{d}}_j|g\rangle$, and the single emitter-field couplings are:

$$|\kappa_n^{(j)}(\omega)|^2 = \frac{1}{\hbar\pi\epsilon_0}\frac{\omega^2}{c^2}\mathbf{d}_j \cdot \mathfrak{Im}\left\{\bar{\bar{\mathbf{G}}}_n(\mathbf{r}_j, \mathbf{r}_j, \omega)\right\}\mathbf{d}_j^*. \tag{5.2.2}$$

Choosing the emitters to be located close to each other on the same side of the MNP, that is $\mathbf{r}_2 \to \mathbf{r}_1$, and having identical dipole polarization (chosen radial as it leads to better energy exchange), we get:

$$\mu_n^{(12)}(\omega) = 1 \tag{5.2.3a}$$

$$\mathbf{r}_2 \to \mathbf{r}_1. \tag{5.2.3b}$$

Later, we also investigate the case where the two emitters are placed symmetrically on each side of the MNP, that is $\mathbf{r}_2 = -\mathbf{r}_1$ and $\mu_n^{(21)} = (-1)^n$. The absolute value of $\mu_n^{(12)}$ being 1, the field operators associated with each atomic position $\widehat{a}_n^{(1)}(\omega)$ and $\widehat{a}_n^{(2)}(\omega)$ are linearly dependent. Hence, $N_r = 1$ in (4.2.27), and the Hamiltonian of the emitter-field system reduces to:

$$\boxed{\begin{aligned}\widehat{H}^{(d)} = &\sum_{j=1}^{2}\left(\hbar\left(\omega_{eg} - i\frac{\gamma_0}{2}\right)\widehat{\sigma}_{ee}^{(j)} + \hbar\omega_{fg}\widehat{\sigma}_{ff}^{(j)}\right) + \sum_n \hbar\left(\omega_n - i\frac{\gamma_n}{2}\right)\widehat{a}_n^\dagger\widehat{a}_n \\ &- i\hbar\sum_{j=1}^{2}\sum_n\left(g_n^{(j)}\widehat{\sigma}_{eg}^{(j)}\widehat{a}_n - g_n^{(j)*}\widehat{a}_n^\dagger\widehat{\sigma}_{ge}^{(j)}\right) \\ &+ \left(\hbar P(t)\mathrm{e}^{-i\omega_P t}\widehat{\sigma}_{ef}^{(1)} + \hbar|S(t)|\mathrm{e}^{-i(\omega_S t - \phi)}\widehat{\sigma}_{ef}^{(2)} + \text{h.c.}\right).\end{aligned}} \tag{5.2.4}$$

The state of the full system is expressed in a tensor product basis featuring the two ground states $|g\rangle, |f\rangle$ and the excited state $|e\rangle$ of the emitters, and those of the plasmonic modes. We assume initially the emitter state $|f, g\rangle$ and the empty plasmonic modes $|\mathbf{0}\rangle = |0_1, 0_2, ..., 0_N\rangle$ for the field. Considering N modes, we can thus construct the complete tensor basis as depicted in fig. 5.6.

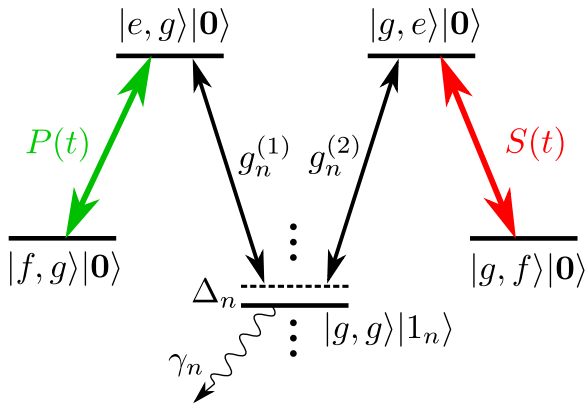

Figure 5.6: Linkage pattern of the two emitters dressed by the plasmonic modes with $|1_n\rangle = |0_1, ..., 1_n, ..., 0_N\rangle$. Each single plasmon of mode n and loss rate γ_n couples the atomic transition (frequency ω_{eg}) with the Rabi frequency $g_n^{(j)}$ and the detuning Δ_n.

Writing the Hamiltonian in the basis $\{|f,g,\mathbf{0}\rangle, |e,g,\mathbf{0}\rangle, ..., |g,g,1_n\rangle, ..., |g,e,\mathbf{0}\rangle, |g,f,\mathbf{0}\rangle\}$, and moving to the proper rotating frame, we get the matrix form:

$$\widehat{H}^{(d)} = \begin{pmatrix} 0 & P(t) & 0 & 0 & \dots & 0 & 0 & 0 \\ P(t) & -i\frac{\gamma_0}{2} & ig_1^{(1)} & ig_2^{(1)} & \dots & ig_N^{(1)} & 0 & 0 \\ 0 & -ig_1^{(1)} & \Delta_1 - i\frac{\gamma_1}{2} & 0 & \dots & 0 & ig_1^{(2)} & 0 \\ 0 & -ig_2^{(1)} & 0 & \Delta_2 - i\frac{\gamma_2}{2} & \ddots & \vdots & ig_2^{(2)} & 0 \\ \vdots & \vdots & \vdots & \ddots & \ddots & 0 & \vdots & \vdots \\ 0 & -ig_N^{(1)} & 0 & \dots & 0 & \Delta_N - i\frac{\gamma_n}{2} & ig_N^{(2)} & 0 \\ 0 & 0 & -ig_1^{(2)} & -ig_2^{(2)} & \dots & -ig_N^{(2)} & -i\frac{\gamma_0}{2} & S(t) \\ 0 & 0 & 0 & 0 & \dots & 0 & S^*(t) & 0 \end{pmatrix}, \tag{5.2.5}$$

where $\Delta_n = \omega_n - \omega_{eg}$, and for simplicity we set the laser frequencies equal to the transition frequency: $\omega_P = \omega_S = \omega_{ef}$. We recall condition (5.2.3) to express the couplings:

$$g_n^{(2)} = g_n^{(1)}. \tag{5.2.6}$$

All the parameters $\omega_n, \gamma_n, g_n^{(j)}$ are found by solving the mode equation and calculating the LDOS at the resonance frequencies, as shown in (5.1.7). This effective Hamiltonian shows that one can manipulate coherently, by laser fields, the states of the emitter, coupled by the SPP. This formulation shows clearly that all the modes are involved and we can anticipate a relatively broad frequency range where the coherent accumulation of all of them enhances the coupling, even if one mode is weakly interacting (for instance, the dipolar mode at very small distance). This is confirmed in the numerics below. The resulting strong coupling allows one to fully exploit the tools developed in quantum control [42].

Numerics

STIRAP-type processes between the states $|f,g,\mathbf{0}\rangle$ and $|g,f,\mathbf{0}\rangle$ can be achieved via Hamiltonian (5.2.5) under strong coupling $g_n \gtrsim \gamma_n$. For this purpose, we use a sequence of two

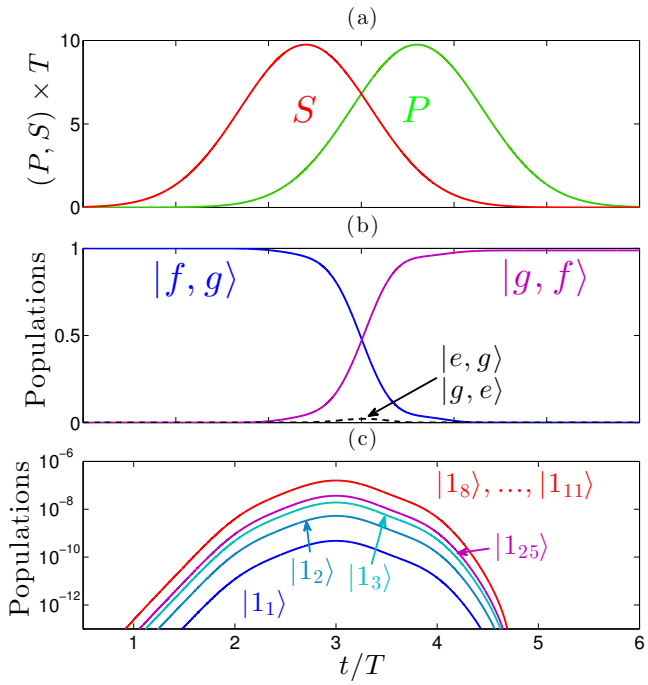

Figure 5.7: Dynamics of the STIRAP process for two emitters located 2 nm away from the surface of a MNP ($R = 20$ nm and emitters on the same side [see (5.2.3)]). (a) Counterintuitive pulse sequence. (b) Population history with complete transfer from $|f, g, \mathbf{0}\rangle$ to $|g, f, \mathbf{0}\rangle$ and low population of $|e, g, \mathbf{0}\rangle, |g, e, \mathbf{0}\rangle$. (c) Population dynamics for the single plasmon mode excitations. For better visibility only five curves are represented, as modes around $n = 10$ show very similar dynamics (red line). We used $\Omega_0 T = 10$ and $\tau/T = 0.6$. The number of modes taken into account is $N = 25$.

Gaussian pulses delayed by a time τ, of peak Rabi frequency Ω_0:

$$P(t) = \Omega_0 \mathrm{e}^{-(t-t_0-\tau)^2/T^2} \tag{5.2.7a}$$

$$|S(t)| = \Omega_0 \mathrm{e}^{-(t-t_0+\tau)^2/T^2}, \tag{5.2.7b}$$

such that a negative delay (resp. positive) corresponds to an intuitive sequence (resp. counterintuitive). The pulse duration T is set with respect to the average plasmon loss $\bar{\gamma}T = 7500$. Complete population transfer from $|f, g, \mathbf{0}\rangle$ to $|g, f, \mathbf{0}\rangle$ is achieved and shown in fig. 5.7, with pulse area $\Omega_0 T = 10$ and delay $\tau/T = 0.6$. We chose the MNP being made of silver, with radius $R = 20$ nm, and the emitters are located on the same side of the MNP, both distant 2 nm away from its surface. We show complete transfer, with negligible population of $|e, g, \mathbf{0}\rangle, |g, e, \mathbf{0}\rangle$ and of the plasmon modes $|g, g, 1_n\rangle$.

In fig. 5.8, we show a contour plot of the transfer efficiency from $|f, g, \mathbf{0}\rangle$ to $|g, f, \mathbf{0}\rangle$ as a function of the pulse delay and the peak Rabi amplitude. A non-robust, oscillating and low transfer efficiency for the intuitive sequence is observed, due to the strong population of the lossy plasmon excitation. On the other hand, the counterintuitive sequence results in a robust and efficient (above 95%) transfer due to low plasmon population during the process for a modest pulse area $\Omega_0 T$. The process has been found more efficient for an emitter whose transition frequency is resonant with higher-order modes, since there is an accumulation of strong resonances at high orders for emitters close to the sphere. For this reason, the choice

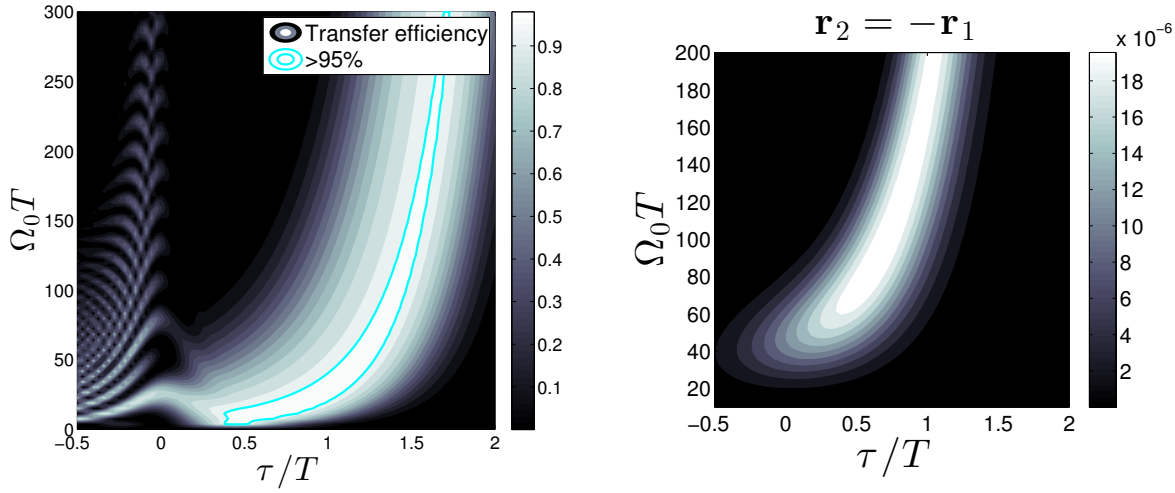

Figure 5.8: Left panel: Contour plot of the transfer efficiency to state $|g, f, \mathbf{0}\rangle$ at the end of the pulse sequence, as a function of the pulse delay τ and the peak Rabi frequency Ω_0 for $\bar{\gamma}T = 7500$. We chose a sphere radius $R = 20$ nm, and the emitters are located 2 nm away from the sphere, on the same side. Their transition frequency is set resonant to the 10th mode: $\omega_{eg} = \omega_{10}$, their dipole moment is taken to be $d_{eg}^{(1)} = d_{eg}^{(2)} = 10$ D, and $N = 25$ plasmon modes have been taken into account. Right panel: same calculation for $\mathbf{r}_2 = -\mathbf{r}_1$ (emitters on opposite sides) and $\mu_n^{(21)} = (-1)^n$.

of frequency is not required to be very precise, as long as it belongs to the plasmon polariton bandwidth. In addition, we show that the population transfer fails when the emitters are placed on each side of the sphere, symmetrically ($\mathbf{r}_2 = -\mathbf{r}_1$, right panel in fig. 5.8). This is due to the presence of a mode-wise phase factor corresponding to $\mu_n^{(21)} = (-1)^n$ in the coupling of the second emitter: $g_n^{(2)} = (-1)^n g_n^{(1)}$. The transfer efficiency obtained for this configuration is shown to be below 10^{-5}. In reference [109], we mistakenly wrote that the population transfer was effective for the case $\mathbf{r}_2 = -\mathbf{r}_1$, while we presented figures for the case $\mathbf{r}_2 \to \mathbf{r}_1$, as shown on the left panel in fig. 5.8. We plan to correct this mistake in an erratum.

5.2.2 Entanglement: fractional STIRAP

The interest in the entanglement of emitters close to a plasmonic structure is motivated by the possibility of creating mixed states that cannot be factorized in a product of states belonging to the basis [17, 102, 110]. This is essential for quantum information and computing, relying on the superposition states and entanglement properties of quantum mechanics.
In our system, the following state can be achieved:

$$|f, g, \mathbf{0}\rangle \mapsto \frac{1}{\sqrt{2}}\Big(|g, f\rangle + \mathrm{e}^{-i\phi}|f, g\rangle\Big)|\mathbf{0}\rangle, \tag{5.2.8}$$

by shaping the laser pulses such that they start in a counterintuitive way and they are switched off simultaneously. This sequence is known as fractional STIRAP (or f-STIRAP) since it leads, in principle, to a partial population transfer corresponding to a final coherent superposition of the initial and target state [111, 112]. We show the fully deterministic process of entanglement

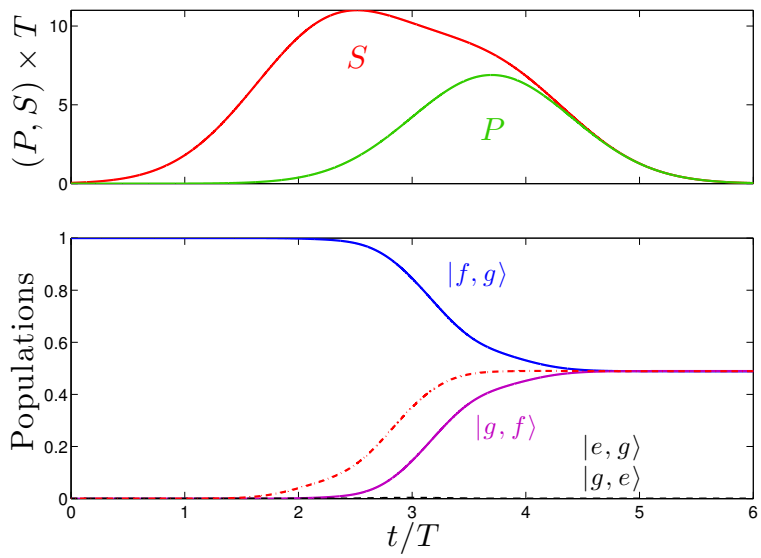

Figure 5.9: Dynamics leading to the entangled state in the same conditions as in fig. 5.7 except for the pulse shaping (pump: green line; Stokes: red line) starting in a counterintuitive way and ending simultaneously. The populations of state $|f,g,\mathbf{0}\rangle$ (blue line) and state $|g,f,\mathbf{0}\rangle$ (purple line) converge to 1/2 in a coherent way (the absolute value of their coherence is shown as a red dash-dotted line). The populations of $|e,g,\mathbf{0}\rangle$ and $|g,e,\mathbf{0}\rangle$ are not distinguishable at the scale of the figure.

creation between the two emitters in fig. 5.9. We have designed the pulses using:

$$P(t) = \sin\theta_0\Omega_0 \mathrm{e}^{-(t-t_0-\tau)^2/T^2} \tag{5.2.9a}$$

$$|S(t)| = \Omega_0 \mathrm{e}^{-(t-t_0+\tau)^2/T^2} + \cos\theta_0\Omega_0 \mathrm{e}^{-(t-t_0-\tau)^2/T^2}, \tag{5.2.9b}$$

where we chose $\theta_0 = \pi/4$. The coherence between $|f,g\rangle$ and $|g,f\rangle$ is shown to increase and reaches 0.5, demonstrating deterministic entanglement.
In the next sections, we provide a simplified model to understand the dynamics of the STIRAP process, and discuss its limits. Finally, perspectives for the study of more general configurations will be presented.

5.2.3 Simplified model and discussion

To interpret and determine the practical limitations of the above results by complete or fractional STIRAP, it is useful to consider a simplified effective Hamiltonian with a resonant ($\Delta_1 = 0$) single mode $N = 1$:

$$\widehat{H}^{(d)} = \begin{pmatrix} 0 & P & 0 & 0 & 0 \\ P & 0 & g & 0 & 0 \\ 0 & g & -i\frac{\gamma}{2} & g & 0 \\ 0 & 0 & g & 0 & S \\ 0 & 0 & 0 & S & 0 \end{pmatrix}. \tag{5.2.10}$$

We consider the transformation which diagonalizes the excited plasmonic and emitter parts:

$$\widehat{T} = \begin{pmatrix} 1 & \mathbf{0}_{13} & 0 \\ \mathbf{0}_{31} & \widehat{T}_3 & \mathbf{0}_{31} \\ 0 & \mathbf{0}_{13} & 1 \end{pmatrix},$$
$$\widehat{T}_3^\dagger \begin{pmatrix} 0 & g & 0 \\ g & -i\frac{\gamma}{2} & g \\ 0 & g & 0 \end{pmatrix} \widehat{T}_3 = \begin{pmatrix} \lambda_- & 0 & 0 \\ 0 & 0 & 0 \\ 0 & 0 & \lambda_+ \end{pmatrix}, \tag{5.2.11}$$

with the lossy eigenvalues:

$$\lambda_\pm = \frac{1}{2}\left(-i\frac{\gamma}{2} \pm \sqrt{8g^2 - \left(\frac{\gamma}{2}\right)^2}\right). \tag{5.2.12}$$

and the non-lossy eigenvalue 0 associated with the dark state $|\mathbf{\Phi}_0^{(ge)}\rangle = \frac{1}{\sqrt{2}}(|e,g\rangle - |g,e\rangle)|\mathbf{0}\rangle$. It is convenient to choose the normalization of the transformation $\widehat{T}_3$ via a complex mixing angle (see e.g. ref. [113] for a lossy two-state Hamiltonian). The application of the transformation on the full Hamiltonian leads to:

$$\widehat{T}^\dagger \widehat{H}^{(d)} \widehat{T} = \frac{1}{\sqrt{2}} \begin{pmatrix} 0 & Pc & P & Ps & 0 \\ Pc & \sqrt{2}\lambda_+ & 0 & 0 & Sc \\ P & 0 & 0 & 0 & -S \\ Ps & 0 & 0 & \sqrt{2}\lambda_- & Ss \\ 0 & Sc & -S & Ss & 0 \end{pmatrix} \tag{5.2.13a}$$

$$c = \frac{\sqrt{2}g}{\sqrt{\lambda_+(\lambda_+ - \lambda_-)}} \tag{5.2.13b}$$

$$s = \sqrt{\frac{\lambda_+}{\lambda_+ - \lambda_-}}. \tag{5.2.13c}$$

This shows that the adiabatic passage will be immune to loss when $\mathfrak{Re}(\lambda_\pm) \gg P, |S|$, that is:

$$g \gg P, |S|. \tag{5.2.14}$$

At the lowest order, this leads to the effective Hamiltonian in the basis $\{|f,g,\mathbf{0}\rangle, |\mathbf{\Phi}_0^{(eg)}\rangle, |g,f,\mathbf{0}\rangle\}$:

$$\widehat{T}^\dagger \widehat{H}^{(d)} \widehat{T} \approx \frac{1}{\sqrt{2}} \begin{pmatrix} 0 & P & 0 \\ P & 0 & -S \\ 0 & -S & 0 \end{pmatrix}. \tag{5.2.15}$$

Adiabatic passage is achieved along the eigenstate:

$$|\mathbf{\Phi}_0^{(fg)}\rangle = \Big(\cos\theta|f,g\rangle + \sin\theta|g,f\rangle\Big)|\mathbf{0}\rangle, \tag{5.2.16}$$

corresponding remarkably to the same state in the original basis: $\widehat{T}|\mathbf{\Phi}_0^{(fg)}\rangle = |\mathbf{\Phi}_0^{(fg)}\rangle$, with the mixing angle $\tan\theta = P/|S|$, which connects the initial state when $P = 0$, i.e. $\theta = 0$, and the

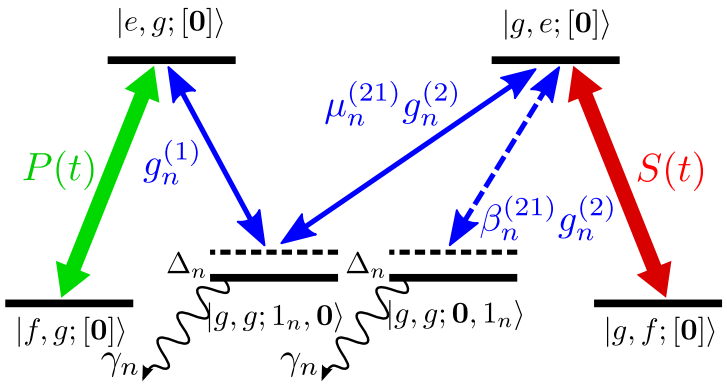

Figure 5.10: Effective discrete linkage pattern of a system of two three-level emitters at arbitrary positions $\mathbf{r}_1, \mathbf{r}_2$ around a metallic nanosphere. The basis corresponds to the product between atomic states $\{|g\rangle, |e\rangle, |f\rangle\}$ and the Gram-Schmidt orthogonalized Fock spaces of the plasmonic excitations. Laser pulses $P(t)$ ans $S(t)$ drive the $|e\rangle \leftrightarrow |f\rangle$ transitions of each emitter, respectively.

final state when $S = 0$, i.e. $\theta = \pi/2$. This corresponds to the counterintuitive pulse sequence. The requirement is a relatively large pulse area:

$$\Omega_0 T \gg 1, \tag{5.2.17}$$

as confirmed in fig. 5.8. The strong coupling regime corresponds to to $g \sim \gamma$ with the typical width in this system $\gamma \sim 7.5 \times 10^{13}$ s^{-1}, hence a duration for the pulse of the order of 100 ps corresponds to $\gamma T = 7500$, with which figs. 5.7 and 5.8 have been produced. A modest pulse area of the laser pulse $\Omega_0 T \sim 10$ gives already a high efficiency, and this corresponds to peak Rabi frequency of the order of 100 GHz, i.e. of peak intensity 10 GW/cm^2 for a 1 debye dipole. Shorter pulse durations can be considered, but they would need stronger pulse intensities for the same pulse area to achieve adiabatic passage.

5.2.4 General model and perspectives

To close this chapter, we provide an overview of the general system formed by two three-level emitters close to a nanosphere, as well as future prospects for the achievement of adiabatic passage in this system.

The effective two-emitter model presented for the STIRAP has been limited to the close emitters case (5.2.3) for simplicity. This allows us to use a simplified version of the more general model, which is useful to investigate and discuss the properties of the STIRAP mediated by LSPs. However, the simplified model does not provide a realistic description of the system, since emitters cannot be at the same position. The general model implies that the emitters are located such that $\mathbf{r}_1$ and $\mathbf{r}_2$ are arbitrary. This is shown in section 4.3, where we considered two-level emitters coupled to a nanosphere.

Adiabatic passage in the general linkage pattern, corresponding to arbitrary subwavelength positions (i.e. considering distances below 100 nm), can be envisioned. The linkage pattern of the effective discrete model is shown in fig. 5.10 (see preceding sections and section 4.3). It is seen that this pattern is more complicated than the one of the $\mathbf{r}_2 \to \mathbf{r}_1$ case shown in fig. 5.6: the plasmonic excitation basis splits into two Fock spaces, each associated with

an excitation $\widehat{b}_n^{(j)}, \widehat{b}_n^{(j)\dagger}$ created by emitter j. The emitter-field coupling also becomes more complicated, since emitter 2 couples to both field subspaces with $\mu_n^{(21)} g_n^{(2)}$ and $\beta_n^{(21)} g_n^{(2)}$, with $\beta_n^{(21)}$ being the Gram-Schmidt normalization factor. The asymmetry of the coupling structure comes from the Gram-Schmidt orthogonalization procedure. We underline that the dynamics of the $\mathbf{r}_2 \to \mathbf{r}_1$ case is recovered by this pattern since this yields $\mu_n^{(21)} = 1$ and $\beta_n^{(21)} = 0$.
The general study of the dynamics of such a system is not done yet. However, we identified the structural obstacles of the linkage pattern in the case of population transfer from state $|f, g; [\mathbf{0}]\rangle$ to state $|g, f; [\mathbf{0}]\rangle$:

1. As the middle block, corresponding to $\{|e, g; [\mathbf{0}]\rangle, |g, g; 1_n, \mathbf{0}\rangle, |g, g; \mathbf{0}, 1_n\rangle, |g, e; [\mathbf{0}]\rangle\}$, embed the plasmon dynamics, we see that the transition $|g, g; \mathbf{0}, 1_n\rangle \leftrightarrow |e, g; [\mathbf{0}]\rangle$ is an obstacle to the population transfer. Therefore, if $\beta_n^{(21)}$ is large (i.e. close to 1), those two states couple and the plasmons will strongly decay.

2. Moreover, if $\beta_n^{(21)}$ is large, then $\mu_n^{(21)}$ is small and this induces an asymmetry in the coupling, which is also preventing the population transfer.

3. Finally, when the overlap function $\mu_n^{(21)}$ varies from one mode to another, this induces an interference effect as the high-order modes of the nanospheres overlap in frequency. Therefore the collective effect of the modes is a blockade for the population transfer when $\mu_n^{(21)}$ varies, that is when the emitters are not aligned on the same side of the sphere. This happens for example when considering the case $\mathbf{r}_2 = -\mathbf{r}_1$ (the emitters located symmetrically at two poles of the sphere), where the overlap function flips sign from a mode to another: $\mu_n^{(21)} = (-1)^n$.

We project to use an adiabatic elimination in order to solve points 1 and 2. Indeed, if Δ_n is chosen such that:

$$\Delta_n \gg g_n^{(j)}, \tag{5.2.18}$$

then we adiabatically eliminate the plasmonic excitation states $|g, g; 1_n, \mathbf{0}\rangle$ and $|g, g; \mathbf{0}, 1_n\rangle$. Consequently, the transition $|g, g; \mathbf{0}, 1_n\rangle \leftrightarrow |e, g; [\mathbf{0}]\rangle$ is blocked while the V-shaped block transition $|g, e; [\mathbf{0}]\rangle \leftrightarrow |g, g; 1_n, \mathbf{0}\rangle \leftrightarrow |e, g; [\mathbf{0}]\rangle$ is allowed since there is no two-photon detuning. The last point can be addressed by designing plasmonic systems with well-resolved resonances, so that the interference effects are small. In the case of the sphere, the mode accumulation can be exploited by placing the emitters on the same side of the sphere, therefore allowing a bigger mode overlap, hence a better coupling.

Part IV

Conclusion

Summary of the thesis

In this manuscript, we have addressed different aspects of quantum control, stated its current development and extended it to further applications in quantum technologies at the nanoscale. The challenges brought by quantum information and computation play, nowadays, an important role in the fields of quantum light-matter interactions, like cQED and ion trapping. Optical cavities and ion traps provide interesting features for the control of atoms, molecules, quantum dots, and quantum light. They are quantum systems where applications of strong coupling, quantum computation using gates, and quantum communication can be achieved provided that the decoherence processes are avoided. This presents strong technical requirements, such as the control of very low temperatures in the system environment.
In this thesis, we have considered applications of adiabatic techniques, such as the stimulated Raman adiabatic passage (STIRAP), or the adiabatic elimination, to bypass lossy states that are detrimental to population transfer between two metastable states. These techniques were used for different systems: trapped ions, atoms in a cavity, emitters close to plasmonic structures. Moreover, they are also necessary for the design of the fast qudit quantum gate presented in chapter 1.
We have also extended the quantization procedures necessary for the understanding of quantum optics, both in the fields of cQED and quantum plasmonics. These extensions lead to effective models, that we derive in detail and are shown to be similar both for cQED and quantum plasmonics: the rotating wave approximation Hamiltonians derived have the structure of multilevel systems, each cavity or plasmonic mode corresponding to a particular family of quantum states. The effective Hamiltonians were derived in two steps: a first one leading to an effective continuous system, where the atom-field coupling has a Lorentzian structure, and a second one where the structure of the Hamiltonian is discrete and non-Hermitian, the losses being modeled by imaginary terms on the diagonal.
The effective models were used to describe the dynamics of quantum systems composed of emitters coupled to either a cavity field or the plasmonic modes of a single metallic nanosphere. In the case of the cavity system, we studied the output field derived from the Poynting vector, and described the nature of the leaking photonic quantum state. As for the plasmonic system, we studied the dynamics of a quantum emitter placed very close to the surface of the nanoparticle, in the strong coupling regime. We also computed the dynamics of two emitters coupled to the modes of a nanoparticle, and showed the feasibility of STIRAP at the nanoscale, allowing the coupling of emitters mediated by plasmons. This opens the door to ultrafast quantum control at the nanoscale in the field of quantum plasmonics.

Perspectives

The detailed work of this manuscript has lead to some future prospects and further questions. In view of the recent developments in quantum plasmonics, and its analogies with cQED, the quantum mechanical approach of plasmons that we presented in this manuscript is of particular interest.
We have expanded a quantization procedure based on the Green's tensor for spherically layered media, and applied it to the study of emitters coupled to a single spherical nanoparticle. In the end of chapter 5, we detailed the prospects concerning the STIRAP applied to two

emitters near a metallic nanoparticle: we plan to analyze the full description of this system, where the emitters are placed at arbitrary positions around the sphere.
One could also apply such a formalism to core-shell structures, such as spherical nanoparticles with a coating (e.g. a gain medium as in the study of SPASER systems), or other spherical systems. In addition, the full quantization, the effective models, and therefore the adiabatic processes can be further studied with different geometries, since the Green's tensor can be expanded in a basis of electromagnetic eigenfunctions, or calculated numerically when the geometry is complex. Some experiments, e.g. with ellipsoid nanoparticles, nanoprisms, bow-tie systems or plasmonic waveguides present interesting optical properties and are still not well understood theoretically. The quantization procedure using the Green's tensor may provide the basis of a quantum mechanical study of such systems.
Finally, the description of quantum measurement processes in quantum optics has been addressed, in the manuscript, for cQED systems. The quantum Poynting vector is the observable which allows to understand the absorption of a photon by a photodetector. The study of light scattered by nanoparticles contributes to the development of single photon generation at the nanoscale, therefore the description of the Poynting vector in the far field is required to understand the quantum nature of light for plasmonics experiments. One could also think of developing input-output relations at the nanoscale, which would correspond to relations between near-field and far-field observables. This would also be consistent with the cQED analogy, and establish an even stronger link between the fields of quantum optics and plasmonics.

Publications

- B. Rousseaux, S. Guérin and N. V. Vitanov, "Arbitrary qudit gates by adiabatic passage", Phys. Rev. A **87**, 032328 (2013).
- B. Rousseaux, Z. Kis, G. Colas des Francs, A. Gogyan, H.-R. Jauslin and S. Guérin, "Production of photon states from Λ-atoms in a cavity" (preprint).
- B. Rousseaux, D. Dzsotjan, G. Colas des Francs, H.-R. Jauslin, C. Couteau and S. Guérin, "Adiabatic passage mediated by plasmons: A route towards a decoherence-free quantum plasmonic platform" Phys. Rev. B **93**, 045422 (2016).
- D. Dzsotjan, B. Rousseaux, H.-R. Jauslin, G. Colas des Francs, C. Couteau and S. Guérin, "Mode-selective quantization and multimodal effective models for spherically layered systems", Phys. Rev. A **94**, 023818 (2016).
- H. Varguet, B. Rousseaux, D. Dzsotjan, H.-R. Jauslin, S. Guérin and G. Colas des Francs, "Dressed states of a strongly coupled metal nanoparticle-quantum emitter system" Opt. Lett. (accepted).

Bibliography

[1] M. Šašura and V. Bužek, "Quantum information processing using an ion trap system", J. Mod. Opt. **49**, 1593 (2002).

[2] U. Gaubatz, P. Rudecki, S. Schiemann and K. Bergmann, "Population transfer between molecular vibrational levels by stimulated Raman scattering with partially overlapping laser fields. A new concept and experimental results", J. Chem. Phys. **92**, 5363 (1990).

[3] N. V. Vitanov, M. Fleischhauer, B.W. Shore, and K. Bergmann, "Coherent manipulation of atoms molecules by sequential laser pulses", Adv. At. Mol. Opt. Phys. **46**, 55 (2001).

[4] N. V. Vitanov, T. Halfmann, B. W. Shore, and K. Bergmann, "Laser-induced population transfer by adiabatic passage techniques", Annu. Rev. Phys. Chem. **52**, 763 (2001).

[5] S. Guérin and H. R. Jauslin, "Control of quantum dynamics by laser pulses: adiabatic Floquet theory", Adv. Chem. Phys. **125**, 147 (2003).

[6] I. Thanopulos, P. Kràl, and M. Shapiro, "Complete control of population transfer between clusters of degenerate states", Phys. Rev. Lett. **92**, 113003 (2004).

[7] K. Bergmann, N. V. Vitanov and B. W. Shore, "Perspectives: stimulated Raman adiabatic passage: the status after 25 years", J. Chem. Phys. **142**, 170901 (2015).

[8] N. Gisin, G. Ribordy, W. Tittel and H. Zbinden, "Quantum Cryptography", Rev. Mod. Phys. **74**, 145 (2002).

[9] A. Reiserer and G. Rempe, "Cavity-based quantum networks with single atoms and optical photons", Rev. Mod. Phys. **87**, 1379 (2015).

[10] D. E. Chang, A. S. Sørensen, P. R. Hemmer and M. D. Lukin, "Quantum optics with surface plasmons", Phys. Rev. Lett. **97**, 053002 (2006).

[11] D. E. Chang, A. S. Sørensen, E. A. Demler and M. D. Lukin, "A single-photon transistor using nanoscale surface plasmons", Nat. Phys. **3**, 807 (2007).

[12] *Plasmonics, from Basics to Advanced Topics*, edited by S. Enoch and E. Bonod, Springer Series in Optical Sciences Vol. 167 (Springer, New York, 2012).

[13] M. Tame, K. McEnery, S. Ozdemir, J. Lee, S. Maier, and M. Kim, "Quantum plasmonics", Nat. Phys. **9**, 329 (2013).

[14] J. Bellessa, C. Bonnand, J. C. Plenet and J. Mugnier, "Strong coupling between surface plasmons and excitons in an organic semiconductor", Phys. Rev. Lett. **93**, 036404 (2004).

[15] A. González-Tudela, F. J. Rodríguez, L. Quiroga, and C. Tejedor, "Dissipative dynamics of a solid-state qubit coupled to surface plasmons: From non-Markov to Markov regimes", Phys. Rev. B **82**, 115334 (2010).

[16] E. Waks and D. Sridharan, "Cavity QED treatment of interactions between a metal nanoparticle and a dipole emitter", Phys. Rev. A **82**, 043845 (2010).

[17] A. González-Tudela, D. Martín-Cano, E. Moreno, L. Martín-Moreno, C. Tejedor and F. J. García-Vidal, "Entanglement of two qubits mediated by one-dimensional plasmonic waveguides", Phys. Rev. Lett. **106**, 020501 (2011).

[18] C. Van Vlack, P. T. Kristensen and S. Hughes, "Spontaneous emission spectra and quantum light-matter interactions from a strongly coupled quantum dot metal-nanoparticle system", Phys. Rev. B **85**, 075303 (2012).

[19] T. Hümmer, F. J. García-Vidal, L. Martín-Moreno and D. Zueco, "Weak and strong coupling regimes in plasmonic QED", Phys. Rev. B **87**, 115419 (2013).

[20] A. González-Tudela, P. A. Huidobro, L. Martín-Moreno, C. Tejedor and F. J. García-Vidal, "Theory of strong coupling between quantum emitters and propagating surface palsmons", Phys. Rev. Lett. **110**, 126801 (2013).

[21] J. Hakami, L. Wang, and M. S. Zubairy, "Spectral properties of a strongly coupled quantum-dot-metal-nanoparticle system", Phys. Rev.A **89**, 053835 (2014).

[22] A. Delga, J. Feist, J. Bravo-Abad and F. J. García-Vidal, "Quantum Emitters Near a Metal Nanoparticle: Strong Coupling and Quenching", Phys. Rev. Lett. **112**, 253601 (2014)

[23] A. Delga, J. Feist, J. Bravo-Abad and F. J. García-Vidal, "Theory of strong coupling between quantum emitters and localized surface plasmons", J. Opt. **16**, 114018 (2014).

[24] K. V. Nerkararyan and S. I. Bozhevolnyi, "Relaxation dynamics of a quantum emitter resonantly coupled to a metal nanoparticle", Opt. Lett. **39**, 1617 (2014).

[25] E. Sanchez-Burillo, D. Zueco, J. J. Garcia-Ripoll, and L. Martín-Moreno, "Scattering in the ultrastrong regime: Nonlinear optics with one photon", Phys. Rev. Lett. **113**, 263604 (2014).

[26] G. Zengin, M. Wersäll, A. Nilsson, T. J. Antosiewicz, M. Käll and T. Shegai, "Realizing Strong Light-Matter Interactions between Single-Nanoparticle Plasmons and Molecular Excitons at Ambient Conditions", Phys. Rev. Lett. **114**, 157401 (2015).

[27] E. Sánchez-Burillo, J. García-Ripoll, L. Martín-Moreno and D. Zueco, "Nonlinear quantum optics in the (ultra) strong light-matter coupling", Faraday Discuss. **178**, 335-356 (2015).

[28] M. A. Nielsen and I. L. Chuang, "Quantum computation and quantum information", Cambridge Univ. Press, 2000.

[29] M. Le Bellac, "A short introduction to quantum information and quantum computation", Cambridge Univ. press, 2006.

[30] P. W. Shor, "Algorithms for quantum computation: discrete logarithms and factoring", in *Proceedings of the 35th annual symposium on foundations of computer science*, IEEE Press, CA, 1994.

[31] P. W. Shor, "Polynomial-time algorithms for prime factorisation and discrete logarithms on a quantum computer", SIAM J. Comp. **26**, 1484 (1997).

[32] L. K. Grover, "Quantum mechanics helps in searching for a needle in a haystack", Phys. Rev. Lett. **79**, 325 (1997).

[33] A. Messiah, "Quantum mechanics", Dover Publications, 1961.

[34] M. Born and V. Fock, "Beweis des Adiabatensatzes", Z. Phys. **51**, 165 (1928).

[35] T. Kato, "On the adiabatic theorem of quantum mechanics", Phys. Soc. Jap. **5**, 435 (1958).

[36] G. Nenciu, "On the adiabatic theorem of quantum mechanics", J. Phys. A **13**, L15 (1980).

[37] J. E. Avron, R. Seiler and L. G. Yaffe, "Adiabatic theorem and applications to the quantum Hall effect", Commun. Math. Phys. **110**, 33 (1987).

[38] G. Hagedorn, "Adiabatic expansions near eigenvalue crossings", Ann. Phys. **196**, 278 (1989).

[39] J. E. Avron, J. Howland and B. Simon, "Adiabatic theorems for dense point spectra", Commun. Math. Phys. **128**, 497 (1990).

[40] J. E. Avron and A. Elgart, "Adiabatic theorem without a gap condition: two-level system coupled to quantized radiation field", Phys. Rev. A **58**, 4300 (1998).

[41] J. E. Avron and A. Elgart, "Adiabatic theorem without a gap condition", Commun. Math. Phys. **203**, 445 (1999).

[42] B. W. Shore, "Manipulating quantum structures using laser pulses", Cambridge Univ. Press, 2011.

[43] N.V. Vitanov and S. Stenholm, "Non-adiabatic effects in population transfer in three-level systems", Opt. Commun. **127**, 215 (1996).

[44] K. Bergmann, H. Theuer and B. W. Shore, "Coherent population transfer among quantum states of atoms and molecules", Rev. Mod. Phys. **70**, 1003 (1998).

[45] P. A. Ivanov, E. S. Kyoseva, and N. V. Vitanov, "Engineering of arbitrary U(N) transformations by quantum Householder reflections", Phys. Rev. A **74**, 022323 (2006).

[46] N. V. Vitanov, "Synthesis of arbitrary SU(3) transformations of atomic qutrits", Phys. Rev. A **85**, 032331 (2012).

[47] E. S. Kyoseva and N. V. Vitanov, "Coherent pulsed excitation of degenerate multistate systems: Exact analytic solutions", Phys. Rev. A **73**, 023420 (2006).

[48] P. A. Ivanov and N. V. Vitanov, "Synthesis of arbitrary unitary transformations of collective states of trapped ions by quantum Householder reflections", Phys. Rev. A **77**, 012335 (2008).

[49] S. S. Ivanov, P. A. Ivanov, and N. V. Vitanov, "Simple implementation of a quantum search with trapped ions ", Phys. Rev. A **78**, 030301 (2008).

[50] S. S. Ivanov, H. S. Tonchev, and N. V. Vitanov, "Time-efficient implementation of quantum search with qudits", Phys. Rev. A **85**, 062321 (2012).

[51] Z. Kis and F. Renzoni, "Qubit rotation by stimulated Raman adiabatic passage", Phys. Rev. A **65**, 032318 (2002).

[52] H. Goto and K. Ichimura, "Multiqubit controlled unitary gate by adiabatic passage with an optical cavity", Phys. Rev. A **70**, 012305 (2004).

[53] N. Sangouard, X. Lacour, S. Guérin, and H. R. Jauslin, "Fast SWAP gate by adiabatic passage", Phys. Rev. A **72**, 062309 (2005).

[54] X. Lacour, N. Sangouard, S. Guérin, and H. R. Jauslin, "Arbitrary state controlled-unitary gate by adiabatic passage", Phys. Rev. A **73**, 042321 (2006).

[55] D. Daems and S. Guérin, "Adiabatic quantum search scheme with atoms in a cavity driven by lasers", Phys. Rev. Lett. **99**, 170503 (2007).

[56] D. Daems and S. Guérin, "Analog Grover search by adiabatic passage in a cavity-laser-atom system", Phys. Rev. A **78**, 022330 (2008).

[57] D. Daems, S. Guérin, and N. J. Cerf, "Quantum search by parallel eigenvalue adiabatic passage", Phys. Rev. A **78**, 042322 (2008).

[58] H. Sagawa and N. Yoshida, "Fundamentals of quantum information", World Scientific Publishing, Singapore, 2011.

[59] B. T. Torosov, E. Kyoseva and N. V. Vitanov, "Fault-tolerant composite Householder reflection", J. Phys. B: At. Mol. Opt. Phys. **48**, 135502 (2015).

[60] M. J. Collett and C. W. Gardiner, "Squeezing of intracavity and traveling-wave light fields produced in parametric amplification", Phys. Rev. A **30**, 1386 (1984).

[61] C. W. Gardiner and M. J. Collett, "Input and output in damped quantum systems: quantum stochastic differential equations and the master equation", Phys. Rev. A **31**, 3761 (1985).

[62] S. M. Dutra and G. Nienhuis, "Derivation of a Hamiltonian for photon decay in a cavity", J. Opt. B: Quantum Semiclass. Opt. **2**, 584 (2000).

[63] S. M. Dutra and G. Nienhuis, "A Hamiltonian for photon decay in a cavity", Act. Phys. Slov. **50** vol. 3, 275-284 (2000).

[64] B. R. Hunt, R. Brian, T. Sauer and J. A. Yorke, "Prevalence: a translation-invariant "almost every" on infinite-dimensional spaces", Am. Math. Soc. **27**, 217238 (1992).

[65] R. J. Glauber and M. Lewenstein, "Quantum optics of dielectric media", Phys. Rev. A **43**, 467 (1991).

[66] M. Wubs, L. G. Suttorp and A. Lagendijk, "Multipole interaction between atoms and their photonic environment", Phys. Rev. A **68**, 013822 (2003).

[67] S. M. Dutra, "Cavity quantum electrodynamics: the strange theory of light in a box", Wiley, 2005.

[68] W. Vogel and D. G. Welsch, "Quantum optics", Wiley-VCH, 2006.

[69] P. Nisbet-Jones, J. Dilley, D. Ljunggren and A. Kuhn, "Highly efficient source for indistinguishable single photons of controlled shape", New J. Phys. **13**, 103036 (2011).

[70] K. M. Gheri, K. Ellinger, T. Pellizzari and P. Zoller, "Photon-wavepackets as flying quantum bits", Fortschr. Phys. **46**, 401-415 (1998).

[71] G. S. Vasilev, D. Ljunggren and A. Kuhn, "Single photons made-to-measure", New J. Phys. **12**, 063024 (2010).

[72] A. Gogyan, S. Guérin, H.-R. Jauslin, and Yu. Malakyan, "Deterministic production of N-photon states from a single atom-cavity system", Phys. Rev. A **82**, 023821 (2010).

[73] B. Rousseaux, Z. Kis, G. Colas des Francs, A. Gogyan, H.-R. Jauslin and S. Guérin, "Production of photon states from Λ-atoms in a cavity" (preprint).

[74] M. Keller, B. Lange, K. Hayasaka, W. Lange and H. Walther, "A calcium ion in a cavity as a controlled single-photon source", New J. Phys. 6, 95 (2004).

[75] C. W. Gardiner and P. Zoller, "Quantum noise" 3rd edition, Springer-Verlag, Berlin, 2004.

[76] K. J. Blow, R. Loudon, S. J. D. Phoenix and T. J. Shepherd, "Continuum fields in quantum optics", Phys. Rev. A **42**, 4102 (1990).

[77] B. J. Smith and M. G. Raymer, "Photon wave functions, wave-packet quantization of light, and coherence theory", New J. Phys. **9**, 414 (2007).

[78] R. Loudon, "The quantum theory of light" 3rd edition, Oxford Univ. Press, Oxford, 2000.

[79] G. Grynberg, A. Aspect and C. Fabre, "Introduction to quantum optics: from the semi-classical approach to quantized light", Cambridge University Press, 2010.

[80] W. H. Louisell, "Quantum statistical properties of radiation", Wiley, 1973.

[81] H. J. Carmichael, "Statistical methods in quantum optics", Springer-Verlag, Berlin Heidelberg, 1999.

[82] H. P. Breuer and F. Petruccione, "The theory of open quantum systems", Oxford university press, New York, 2002.

[83] A. Kuhn, M. Hennrich, T. Bondo and G. Rempe, "Controlled generation of single photons from a strongly coupled atom-cavity system", Appl. Phys. B **69**, 373 (1999).

[84] Z. Y. Ou, "Temporal distinguishability of an N-photon state and its characterization by quantum interference", Phys. Rev. A **74**, 063808 (2006).

[85] P. P. Rohde, W. Mauerer and C. Silberhorn, "Spectral structure and decompositions of optical states and their applications", New J. Phys. **9**, 91 (2007).

[86] J. Keeling, "Light-matter interactions and quantum optics", http://www.standrews.ac.uk/jmjk/keeling/teaching/quantumoptics.pdf.

[87] E. C. Titchmarsh, "Introduction to the theory of Fourier integrals" 2nd edition, Oxford University Press, 1948.

[88] L. Novotny and B. Hecht, "Principles of nano-optics", Cambridge Univ. Press, 2006.

[89] R. Carminati, J.-J. Greffet, C. Henkel and J. M. Vigoureux, "Radiative and non-radiative decay of a single molecule close to a metallic nanoparticle", Opt. Com. **261**, 368 (2006).

[90] C. Sauvan, J. P. Hugonin, I. S. Maksymov and P. Lalanne, "Theory of the spontaneous optical emission of nanosize photonic and plasmon resonators", Phys. Rev. Lett. **110**, 237401 (2013).

[91] G. Colas des Francs, J. Barthes, A. Bouhelier, J.-C. Weeber, A. Dereux, A. Cuche and C. Girard, "Plasmonic Purcell factor and coupling efficiency to surface plasmons. Implications for addressing and controlling optical nanosources" J. of Optics **18**, 094005 (2016).

[92] L. Piatkowski, N. Accanto and N. F. van Hulst, "Ultrafast meets ultrasmall: Controlling nanoantennas and molecules", Am. Chem. Soc. Phot. **3**, 1401 (2016).

[93] S. M. Dutra and P. L. Knight, "Spontaneous emission in a planar Fabry-Pérot micro-cavity", Phys. Rev. A **53**, 3587 (1996).

[94] H. T. Dung, L. Knöll and D.-G. Welsch, "Three-dimensional quantization of the electromagnetic field in dispersive and absorbing inhomogeneous dielectrics", Phys. Rev. A **57**, 3931 (1998).

[95] L. Knöll, S. Scheel and D.-G. Welsch, "QED in dispersing and absorbing media", in *Coherence and Statistics of Photons and Atoms*, Wiley, New York, 2001.

[96] L.-W. Li, P.-S. Kooi, M.-S. Leong and T.-S. Yeo, "Electromagnetic dyadic Green's function in spherically multilayered media", IEEE Trans. Microw. Theory Techn.**42**, 2302 (1994).

[97] C.-T. Tai, "Dyadic Green functions in electromagnetic theory", IEEE Press, New York, 1996.

[98] W.-C. Chew, "Waves and Fields in Inhomogeneous Media", IEEE Press, New York, 1995.

[99] D. Dzsotjan, B. Rousseaux, H.-R. Jauslin, G. Colas des Francs, C. Couteau and S. Guérin, "Mode-selective quantization and multimodal effective models for spherically layered systems", Phys. Rev. A **94**, 023818 (2016).

[100] T. G. Philbin, "Canonical quantization of macroscopic electromagnetism", New J. Phys. **12**, 123008 (2010).

[101] D. Dzsotjan, A. S. Sørensen and M. Fleishhauer, "Quantum emitters coupled to surface plasmons of a nanowire: A Green?s function approach", Phys. Rev. B **82**, 075427 (2010).

[102] D. Martín-Cano, A. González-Tudela, L. Martín-Moreno, F. J. García-Vidal, C. Tejedor and E. Moreno, "Dissipation-driven generation of two-qubit entanglement mediated by plasmonic waveguides", Phys. Rev. B **84**, 235306 (2011).

[103] G. Colas des Francs, "Molecule non-radiative coupling to a metallic nanosphere: An optical theorem treatment", Int. J. Mol. Sci. **10**, 3931 (2009).

[104] S. Savasta, R. Saija, A. Ridolfo, O. Di Stefano, P. Denti and F. Borghese "Nanopolaritons: Vacuum Rabi splitting with a single quantum dot in the center of a dimer nanoantenna", Am. Chem. Soc. Nano **11**, 6369 (2010).

[105] S. Derom, R. Vincent, A. Bouhelier and G. Colas des Francs, "Resonance quality, radiative/ohmic losses and modal volume of Mie plasmons", Eur. Phys. Lett. **98**, 4 (2012).

[106] D. E. Chang, A. S. Sørensen, P. R. Hemmer and M. D. Lukin, "Strong coupling of single emitters to surface plasmons", Phys. Rev. B **76**, 035420 (2007).

[107] B. J. Dalton, S. M. Barnett and B. M. Garraway, "Theory of pseudomodes in quantum optical processes" Phys. Rev. A **64**, 053813 (2001).

[108] H. Varguet, B. Rousseaux, D. Dzsotjan, H.-R. Jauslin, S. Guérin and G. Colas des Francs, "Dressed states of a strongly coupled metal nanoparticle-quantum emitter system" Opt. Lett. (accepted).

[109] B. Rousseaux, D. Dzsotjan, G. Colas des Francs, H.-R. Jauslin, C. Couteau and S. Guérin, "Adiabatic passage mediated by plasmons: A route towards a decoherence-free quantum plasmonic platform" Phys. Rev. B **93**, 045422 (2016).

[110] K. V. Nerkararyan and S. I. Bozhevolnyi, "Entanglement of two qubits mediated by a localized surface plasmon", Phys. Rev. B **92**, 045410 (2015).

[111] N. V. Vitanov, K.-A. Suominen and B. W. Shore, "Creation of coherent atomic superpositions by fractional stimulated Raman adiabatic passage", J. Phys. B **32**, 4535 (1999).

[112] L. P. Yatsenko, S. Guérin and H.-R. Jauslin, "Pulse-driven near-resonant quantum adiabatic dynamics: lifting of quasidegeneracy" Phys. Rev. A **70**, 043402 (2004).

[113] G. Dridi, S. Guérin, H.-R. Jauslin, D. Viennot and G. Jolicard, "Adiabatic approximation for quantum dissipative systems: formulation, topology, and superadiabatic tracking", Phys. Rev. A **82**, 022109 (2010).